PB 171030
Price $3.00

UNITED STATES
DEPARTMENT OF THE INTERIOR

A STUDY AND DEVELOPMENT OF THE HICKMAN SEA-WATER STILL

OFFICE OF SALINE WATER

RESEARCH AND DEVELOPMENT PROGRESS REPORT NO. 43

For sale by the U.S. Department of Commerce, Office of Technical Services,
Washington, D.C., 20230

UNITED STATES

DEPARTMENT OF THE INTERIOR

FRED A. SEATON, SECRETARY

FRED. G. AANDAHL, ASSISTANT SECRETARY
FOR WATER AND POWER DEVELOPMENT

RESEARCH AND DEVELOPMENT PROGRESS REPORT NO. 43

A STUDY AND DEVELOPMENT OF THE HICKMAN SEA-WATER STILL

By

W. L. Buckel, W.D. Beck, J. R. Irwin, A. A. Putnam,
and J. A. Eibling

of the

BATTELLE MEMORIAL INSTITUTE

FOR

OFFICE OF SALINE WATER

A. L. Miller, M.D., Director

J. J. Strobel, Chief, Processes Development Division

E. A. Cadwallader, Chemical Engineer

September 1960

FOREWORD

This is the forty third of a series of reports designed to present accounts of progress on saline water conversion with the expectation that the exchange of such data will contribute to the long-range development of economical processes applicable to large-scale, low-cost demineralization of sea or other saline water.

Except for minor editing, the data herein are as contained in the report submitted by the Battelle Memorial Institute of Columbus, Ohio, under Contract No. 14-01-001-104 covering research carried out through June 1960. The data and conclusions given in this report are essentially those of the Contractor and are not necessarily endorsed by the Department of the Interior.

The report culminates a series of studies on the research and development of the Hickman still. A new program may be initiated to study corrosion and rotor life as recommended by the report, depending upon availability of funds.

TABLE OF CONTENTS

TABLE OF CONTENTS FOR APPENDIX A

TABLE OF CONTENTS
(Continued)

A STUDY AND DEVELOPMENT OF THE HICKMAN SEA-WATER STILL

INTRODUCTION

This summary report describes the research work performed on the Hickman still by Battelle during the period November 15, 1957, through April 30, 1960. The general objective of this research program has been to develop the Hickman process further and to determine the economic potential of the Hickman vapor-compression still in application to sea-water distillation. The scope of the work leading toward this objective has included the field testing of a pilot-plant still, the fundamental study of the rotating heat-transfer surface, and the preparation of estimates of the total cost of producing fresh water with the process.

A 17,000-gallons-per-day pilot-plant still known as the Badger-Hickman No. 5 still was field tested by Battelle on raw sea water during 1958 at Wrightsville Beach, North Carolina. Effort in this program was directed toward determining and improving the performance characteristics of the still. The experimental work associated with the fundamental heat-transfer study was performed in the Battelle laboratories at Columbus, Ohio, using a laboratory-size unit called the No. 4 still.

The report is organized into three major sections and three appendixes. In the first major section are presented a brief historical account of the work done by other organizations prior to November, 1957, and a detailed description of the experiments conducted by Battelle with the No. 4 and No. 5 stills. The second major section summarizes the results of cost studies. The third major section gives data, calculations, and derivations pertaining to the heat-transfer aspects of the Hickman still. The three appendixes contain further details on the heat-transfer, operational, and economic aspects of the Hickman process.

SUMMARY

Perhaps the most important phases of the Battelle program have been the fundamental studies of heat transfer on the rotor and the economic analysis. The fundamental studies were especially necessary because evaporation and condensation on a rotating heat-transfer surface is a new art; it was particularly desirable to determine (1) the conditions under which rotating disks could be wetted with the thinnest possible films, and (2) the maximum heat-transfer coefficients that could be obtained with rotating disks. As a corollary of this study, the factors governing the economic potential of the distillation process have been reasonably well defined.

During the field test of the 17,000 gallons-per-day pilot plant (No. 5 still) at Wrightsville Beach, N. C., the performance characteristics of the unit were determined, various minor modifications were evaluated, and one continuous 72-hour run was made. Also, of course, practical experience was gained in the field operation of a rotary evaporator.

Heat-transfer coefficients obtained with the field-test unit were about 2150 Btu/(hr)(ft^2)(F), whereas a value of 3500 had been expected on the basis of tests conducted earlier by the Badger Manufacturing Company. Attempts to increase the heat transfer in the No. 5 still were unsuccessful, for reasons that were not fully understood until the results of the fundamental studies became available. However, at that time, the need to place emphasis on the fundamental studies was recognized and for this reason the No. 5 still was placed in stand-by status in December, 1958.

Early in the laboratory program it was determined, by visual observation, that the feed water or evaporating film on the conical rotor of the No. 4 still was breaking into little streams or rivulets, leaving sections of the rotor surface near the rim unwetted. Accordingly, the first problem dealt with in the fundamental study was that of maintaining a continuous feed film. Utilization of a smooth, flat rotor instead of the conical configuration eliminated the formation of rivulets. It was also shown experimentally that both the top side and the under side of the flat rotor could be wetted. Because of the advantage of compactness gained by the use of flat (or nearly flat) rotors, subsequent work was restricted to studies of flat rotors. However, it is possible that properly designed conical rotors might also be completely wetted; accordingly these should not be disregarded in future investigations.

Using the flat-rotor configuration and an improved purging arrangement, an overall heat-transfer coefficient of over 5000 Btu/(hr)(ft^2)(F) was obtained with the No. 4 still operating at a rotor speed of 600 rpm. To obtain this value a multiple-nozzle feed system was used and it is believed that dropwise condensation existed. This unusually high coefficient was obtained under ideal laboratory conditions with fresh water feed. For production-size stills, which may operate with lower rotor speeds, a conservative design heat-transfer coefficient of 3000 Btu/(hr)(ft^2)(F) is suggested.

A drawing of a possible 20-rotor evaporator, which incorporates flat rotors and improved purging, is contained in the report. This unit would differ from the No. 5 still in many details, but the most significant differences would result from the use of nearly flat rotors and the application of the feed water on the outside surfaces of the rotors. However, the operating conditions, that is, evaporating temperature, ΔT, and rotor speed of the 20-rotor unit would be quite similar to those that had been selected by the Badger Manufacturing Company for the No. 5 still.

Analytical studies of the heat transfer of a rotating surface showed that the best experimental results obtained with the No. 4 still are only about 15 per cent below the theoretical maximum. Analytical studies also showed that the heat-transfer coefficient does not vary with rotor size when a multiple-nozzle feed system is used. That is, regardless of rotor size, all other conditions being constant, the heat-transfer coefficient of geometrically similar rotors should be the same. It is theorized that this relationship holds regardless of the feed system.

Results of the cost analysis indicate that the cost of producing water with a Hickman 100,000-gallons-per-day still is about $1.00 per 1000 gallons, if the life of the evaporator is assumed to be 20 years, or $1.30 per 1000 gallons if a 5-year evaporator life is

assumed. The most economical rotor speed for a 100,000-gallons-per-day still with 8-foot-diameter rotors was found to be in the range of 400 to 600 rpm. The maximum practical number of 8-foot-diameter rotors in a 400-rpm still was found to be approximately 60 because of the critical-speed limitation of the one-foot diameter rotor shaft. The cost study shows that the most economical operating conditions for a 60-rotor still would be 150 F evaporating temperature, 8 degrees F apparent ΔT, and 400-rpm rotor speed. The resulting capacity of the still would be about 330,000 gallons per day. Product water cost for this capacity would be $1.07 per 1000 gallons and capital costs would be $1.21 per gallon per day, assuming a useful rotor life of 5 years.

Although a 330,000-gallons-per-day single-rotor-column still appears theoretically possible and, thus, is useful for cost-study purposes, such a unit may not be a practical still due to the high pressure difference required at 8 degrees F ΔT and the possibility that the cursory critical-speed calculation may be slightly in error. At the present time the largest practical still is considered to be a 50-rotor unit which would operate at an evaporating temperature of 120 F and with an apparent ΔT of 6 degrees F. The capacity of this unit would be about 175,000 gallons per day. Thus, for larger capacity plants, multiple units would be required.

In order to obtain realistic data on the useful life of the evaporator and in turn a closer estimate of product water cost, it will be necessary in future work to place emphasis on corrosion studies.

CONCLUSIONS

On the basis of the results of the studies made both by Battelle and by previous investigators, the following conclusions were derived:

(1) Cost of product water for the Hickman process have been estimated to range from $1.30 per 1000 gallons for 100,000-gallons-per-day capacity to $1.07 per 1000 gallons for 330,000-gallons-per-day capacity, based on an assumed rotor life of 5 years. A rotor life of 20 years would reduce these costs to $1.03 and $0.94, respectively. These estimates were obtained using the standardized cost procedure recommended by the Office of Saline Water. The installed evaporated cost was taken as $18 to $23 per sq ft of surface, depending on the number of rotors. Further study of fabrication techniques may show that lower evaporator costs can be assumed.

(2) The over-all heat-transfer coefficients that may be expected with the rotating surface have been fairly well defined. Although further increases in heat-transfer rates undoubtedly could be obtained, the magnitudes of the gain are likely to be small.

(3) As presently conceived, the design of future rotary evaporators will differ markedly from the rotor assembly of the No. 5 still. Accordingly, the No. 5 rotor assembly can be considered obsolete.

(4) It may be inferred from data obtained on the No. 4 laboratory still that an 8-foot-diameter rotor could be wetted properly with an outside feed system. However, it should be emphasized this has not been demonstrated by tests of an actual 8-foot-diameter rotor, but rather only inferred from data obtained with a 4-1/2-foot-diameter rotor.

(5) Data on the expected life of a rotor and evaporator are not available. Accordingly, in the economic studies it is necessary to assume rather wide limits for evaporator life. The evaporator life is an important factor in the economic feasibility of the Hickman process. Thus, realistic data on evaporator life are urgently needed.

(6) The two items which contribute most of the cost of product water are power and evaporator amortization; these being about 30 per cent and 26 per cent, respectively. The most promising areas for reducing the total cost of product water with the Hickman process are those associated with increasing evaporator life and with cost reductions in the fabrication of the evaporator.

(7) Scaling of the evaporator surface may not be a serious problem considering that bubble formation does not occur in the evaporating film. With completely wetted surfaces, scale deposition may be slight or nonexistent, but as yet there is little direct experimental evidence available to support this premise.

RECOMMENDATIONS

The cost estimates that have been prepared in this research program appear to substantiate that further development of the Hickman still is warranted. The cost estimates place the Hickman process within the range of cost estimates published for other distillation processes in the output range of 50,000 to 200,000 gallons per day.

A 2-foot-diameter, 10-rotor still should be fabricated for the specific purposes of investigating scaling and corrosion characteristics of various materials. The still should be automatic in operation and, therefore, well suited to a long-term testing program. The unit should be used first for studying the scaling-control requirements. For all tests, the unit should be operated on raw sea-water feed. After the scale-control requirements are determined, the unit should be used for a study of the corrosion rates of different rotor materials and rotor coatings including a study of the possibility of using mild scale formation as a protective coating for the evaporator surface. As presently conceived, the blower, degasser and pumps of the No. 4 still could be used in the construction of this new still. A diameter of 2 feet is suggested for the rotor of the new still, primarily because plating baths for applying the various metal coatings and furnaces for baking possible chemical coatings are readily available for this size. Also, equipment of this size should be relatively inexpensive to fabricate and transport. It is believed that through this experimental approach, supplemented with analytical studies, the fabrication of a more inexpensive rotor design may be attained.

If the results of the corrosion studies indicate that a reasonable rotor life can be expected, then consideration should be given to the construction of a demonstration plant. However, prior to preparing a detailed design of a demonstration-size Hickman still, it is suggested that conceptual design studies of rotor assemblies be undertaken and that the practicality of using a peripheral feed system with an 8-foot-diameter rotor be determined experimentally. Also, it may be necessary to make an experimental stress analysis of different rotor-mounting methods.

DEVELOPMENT PROGRAM OF THE HICKMAN STILL

An account of the development of the Hickman still is presented in this section of the report. The first subsection outlines the work done prior to 1958. In the second and third subsections, the programs conducted by Battelle are described.

Historical Account of the Development of the Hickman Still

The first model of a rotary-surface vapor-compression still was fabricated in 1952 by Dr. K. C. D. Hickman, the inventor, with the financial support of G. D. Dickason, a professional heat engineer. The evaporator-condenser of this unit consisted of a single conical aluminum disk 15 inches in diameter. A second, more versatile model (No. 2 still) was built in 1953. Its heat-transfer surface consisted of one rotor made of two opposed 18-inch-diameter conical aluminum disks. Feed water was supplied to the inside surfaces of the rotor and vapor condensed on the outside surfaces. The No. 3 still, a refined version of the No. 2 still, was built in 1954 by the Badger Manufacturing Company of Cambridge, Massachusetts, under contract with the Office of Saline Water. Throughout this program and the Battelle program which followed, Dr. Hickman served as consultant. The No. 3 unit used an 18-inch-diameter conical copper rotor. All units built subsequently had the more corrosion-resistant copper rotors. The heat-transfer coefficients, U, obtained with Stills Nos. 1, 2, and 3 were in the order of 3500 Btu/(hr)(ft^2)(F) at an operating temper ature of 120 F and a rotor speed of 1000 rpm.[1]* Using the relationship between rotor speed, N, and heat-transfer coefficient, U, of

$$\frac{\sqrt{N_1}}{\sqrt{N_2}} = \frac{U_1}{U_2} ,$$

which has been determined to be descriptive of rotating surfaces, the U of 3500 Btu/(hr)(ft^2)(F) at 1000 rpm becomes 2200 Btu/(hr)(ft^2)(F) at 400 rpm. For purposes of performance comparison, these operating conditions, i.e., 120 F condensing temperature and 400-rpm rotor speed, will be considered standard conditions throughout this section of the report.

On the basis of the experience gained with the No. 3 still, the No. 4 and No. 5 stills were built by the Badger Manufacturing Company under OSW sponsorship. The original No. 4 still housed a 4-1/2-foot-diameter conical rotor. This unit was in operation by early 1956. As with the No. 2 and No. 3 stills, feed water was evaporated from the inside surface of the rotor and condensation occurred on the outside surface. The residue was removed from the inside of the rotor by a stationary scoop positioned near the rim of the rotor. The U obtained with this unit at 400 rpm and 120 F evaporating temperature was 2300 to 2550 Btu/(hr)(ft^2)(F).[2] Higher values of U were reported but, as will be explained later, these data are now believed to be in error.

*References appear on page 58.

In early 1957, testing of the No. 5 still was started at Cambridge, Massachusetts, by Badger. This unit had eight conical rotors 8 ft in diameter, giving a total evaporating surface of about 600 square feet. The basic configuration of this unit was the same as that of the No. 4 still except that, in addition to the difference in size, the No. 5 had a rotor column rather than a single rotor and the residue was removed from this rotor column by two downspouts mounted at the rim of the rotors and rotating with the column. The compressor of the No. 5 still was an integral part of the evaporator. The data presented later in this report show that a typical U for the No. 5 still operating at 400 rpm and 120 F evaporating temperature is 2250 Btu/(hr)(ft^2)(F) with freshwater feed.

During the early experimental programs with the Nos. 2, 3, and 4 stills, the following relationships affecting heat transfer were formulated: U varies as the square root of rotor speed, U increases with increasing operating temperature, and the U's which can be expected from geometrically similar but different-sized rotors are related to the mean centrifugal force of the rotors. The last of these items now seems to be invalid. Subsequent studies at Battelle have indicated that U is independent of rotor size for geometrically similar rotors.

As the experimental program continued, the rotating heat-transfer surface showed promise of even better performance than had been achieved previously but no theoretical expression had been derived. In November, 1957, the Office of Saline Water placed a project at Battelle to field test and, if possible, to improve the performance of the No. 5 still, and also to supplement the field tests with a fundamental heat-transfer study. In preparation for this program, the No. 5 still was moved from Cambridge, Massachusetts, to the Atlantic Coast at the International Nickel Company's corrosion-test site located near Wrightsville Beach, North Carolina. The No. 4 still was shipped to the Battelle laboratories at Columbus, Ohio, to be used in conjunction with the fundamental study.

Field Testing of the No. 5 Badger-Hickman Still

On December 17, 1957, Battelle assumed responsibility for the No. 5 still. After additional instrumentation had been installed and some minor mechanical difficulties that developed during preliminary runs had been corrected, the experimental program was started in April, 1958. A description of the significant mechanical troubles encountered during the No. 5 experimental program is given in Appendix B.

Figures 1 through 4 show several views of the No. 5 still. The photograph of the rotor column, shown in Figure 1, was taken while the still was located at the Badger Manufacturing Company. Figures 2 through 4 show the No. 5 still at the North Carolina test site.

Figure 5 is a process flow diagram of the No. 5 still. The thermometers are so located that an energy balance can be made for the still and for each of its accessories. Before the experimental program began, all thermometers, vacuum gages, and electric meters were calibrated. Intermittent recalibration of critical thermometers continued throughout the program.

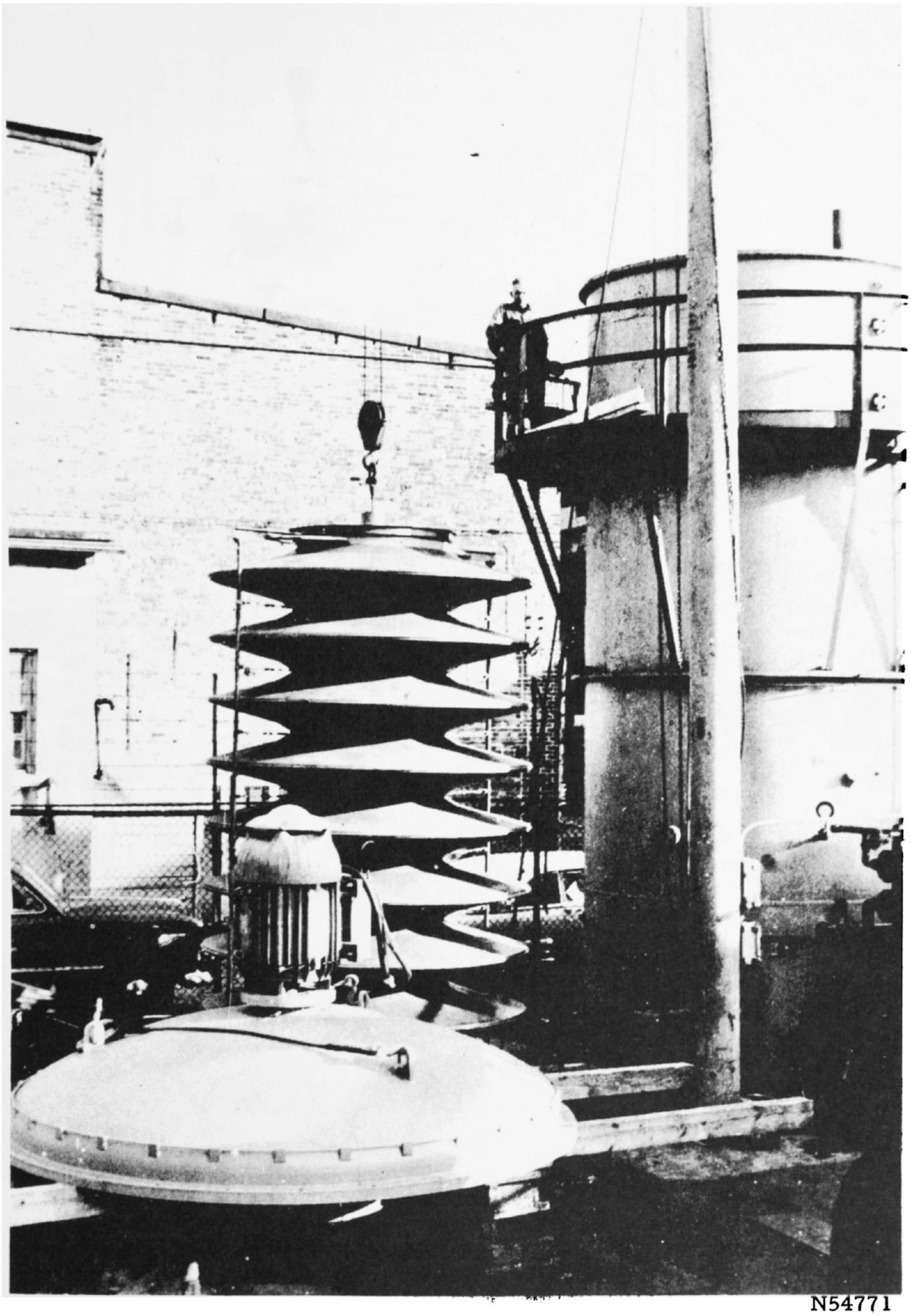

N54771

FIGURE 1. PHOTOGRAPH TAKEN AT CAMBRIDGE, MASSACHUSETTS, OF THE COMPRESSOR HOUSING OR LID, THE ROTOR COLUMN, AND THE SHELL OF THE NO. 5 BADGER-HICKMAN STILL

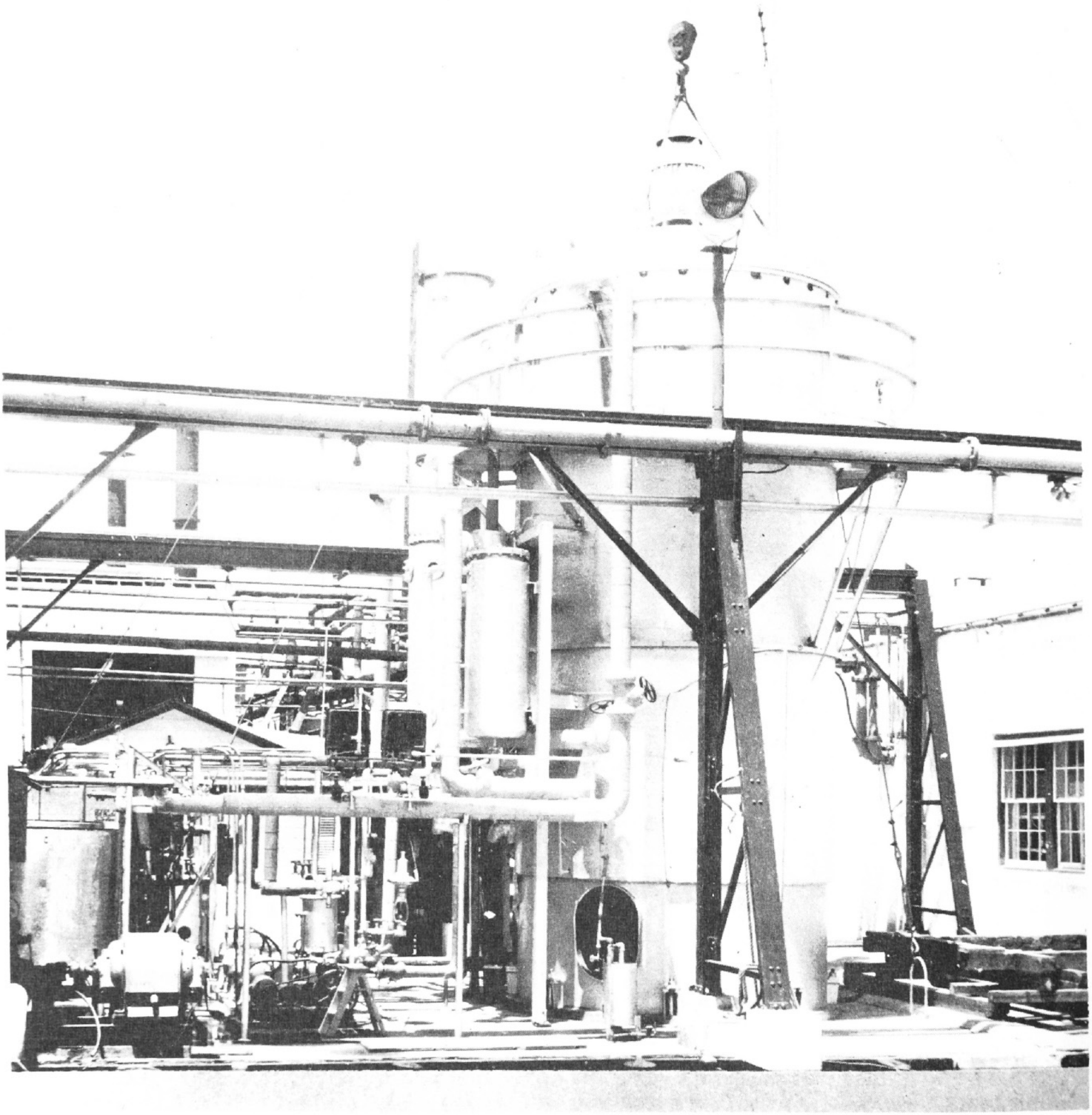

FIGURE 2. EASTERN VIEW OF THE NO. 5 BADGER-HICKMAN STILL ON TEST AT WRIGHTSVILLE BEACH, NORTH CAROLINA

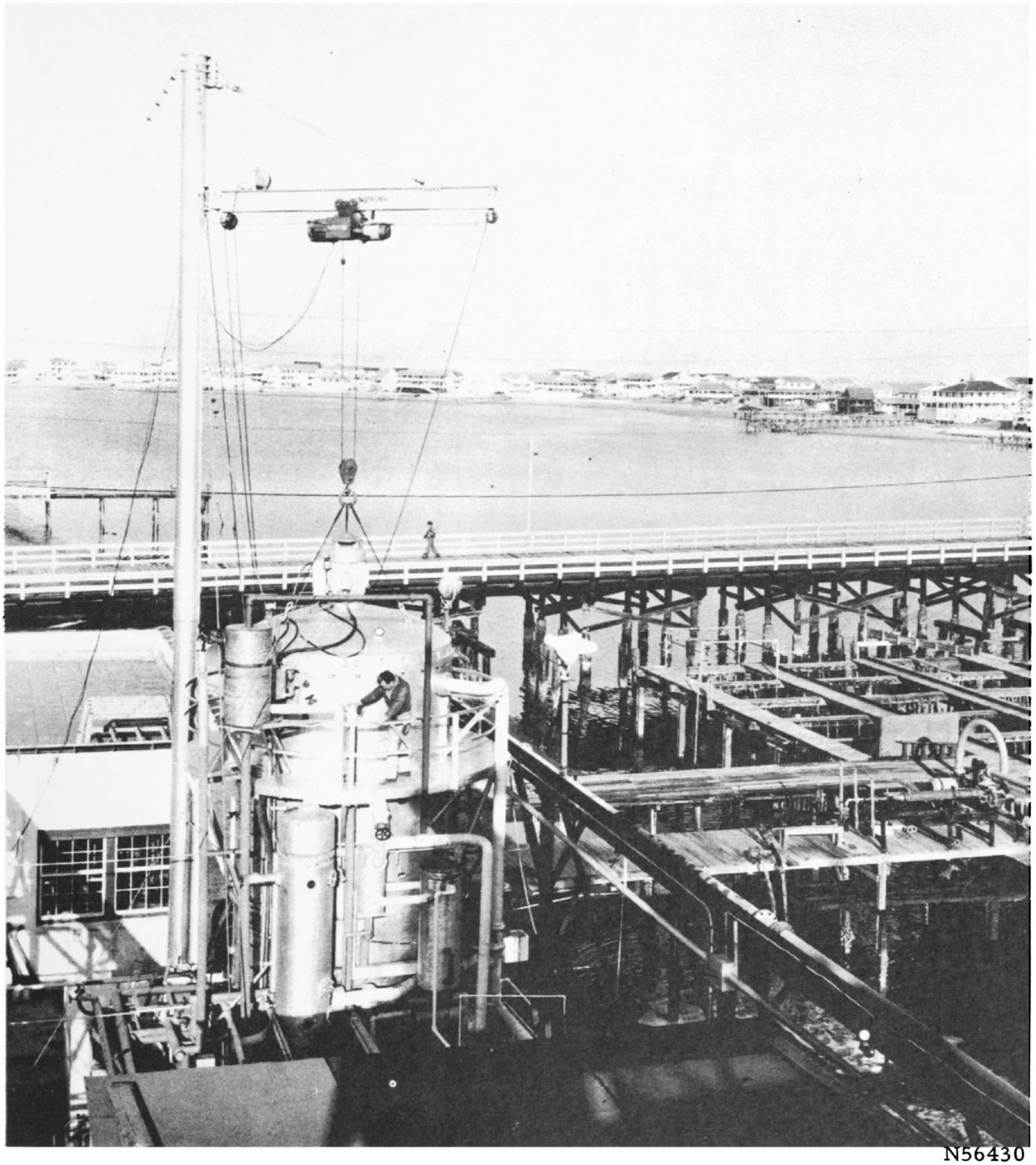

N56430

FIGURE 3. NORTHERN VIEW OF THE NO. 5 BADGER-HICKMAN STILL ON TEST AT WRIGHTSVILLE BEACH, NORTH CAROLINA

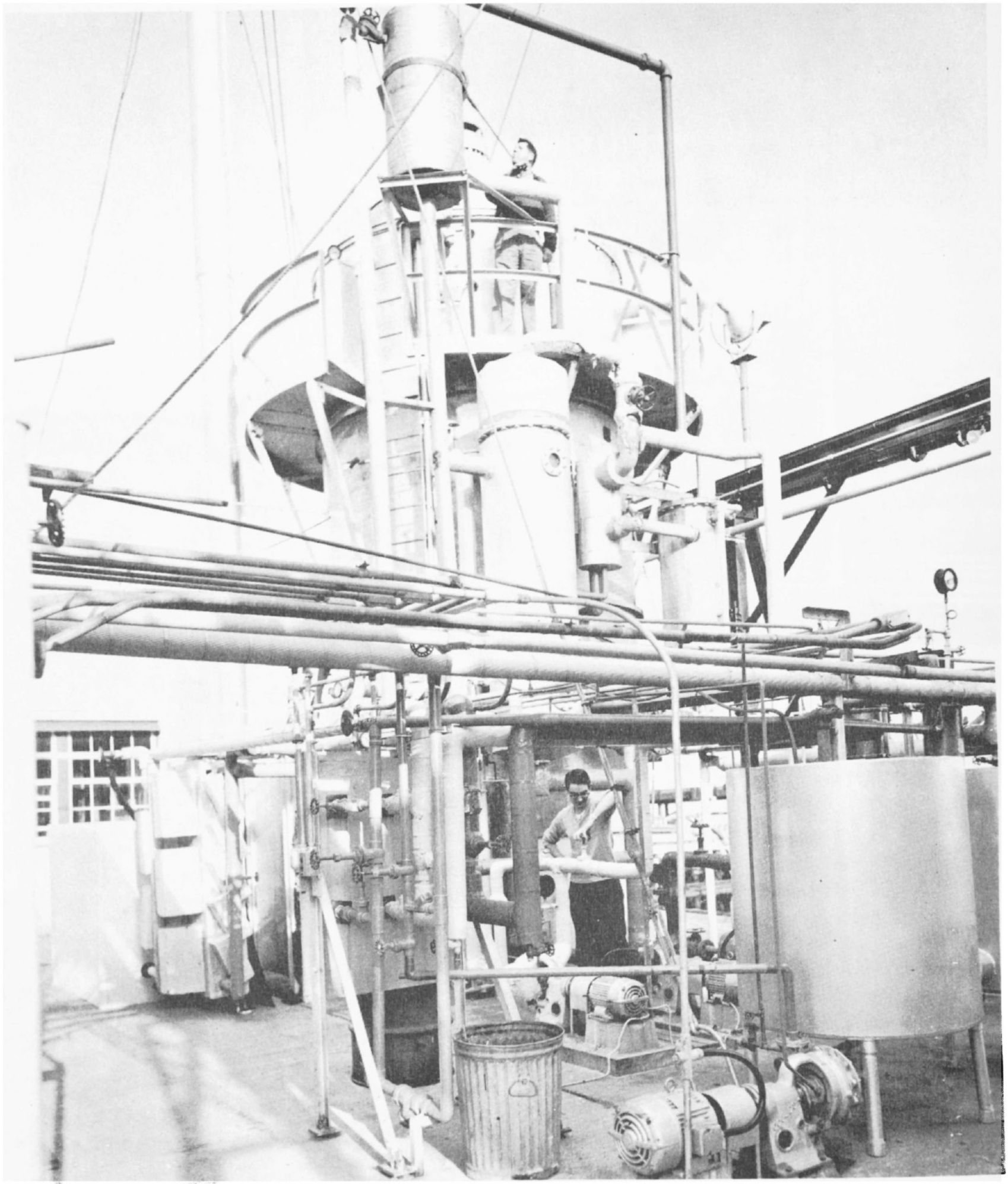

N56429

FIGURE 4. CLOSE-UP VIEW OF THE NO. 5 BADGER-HICKMAN STILL AT WRIGHTSVILLE BEACH, NORTH CAROLINA

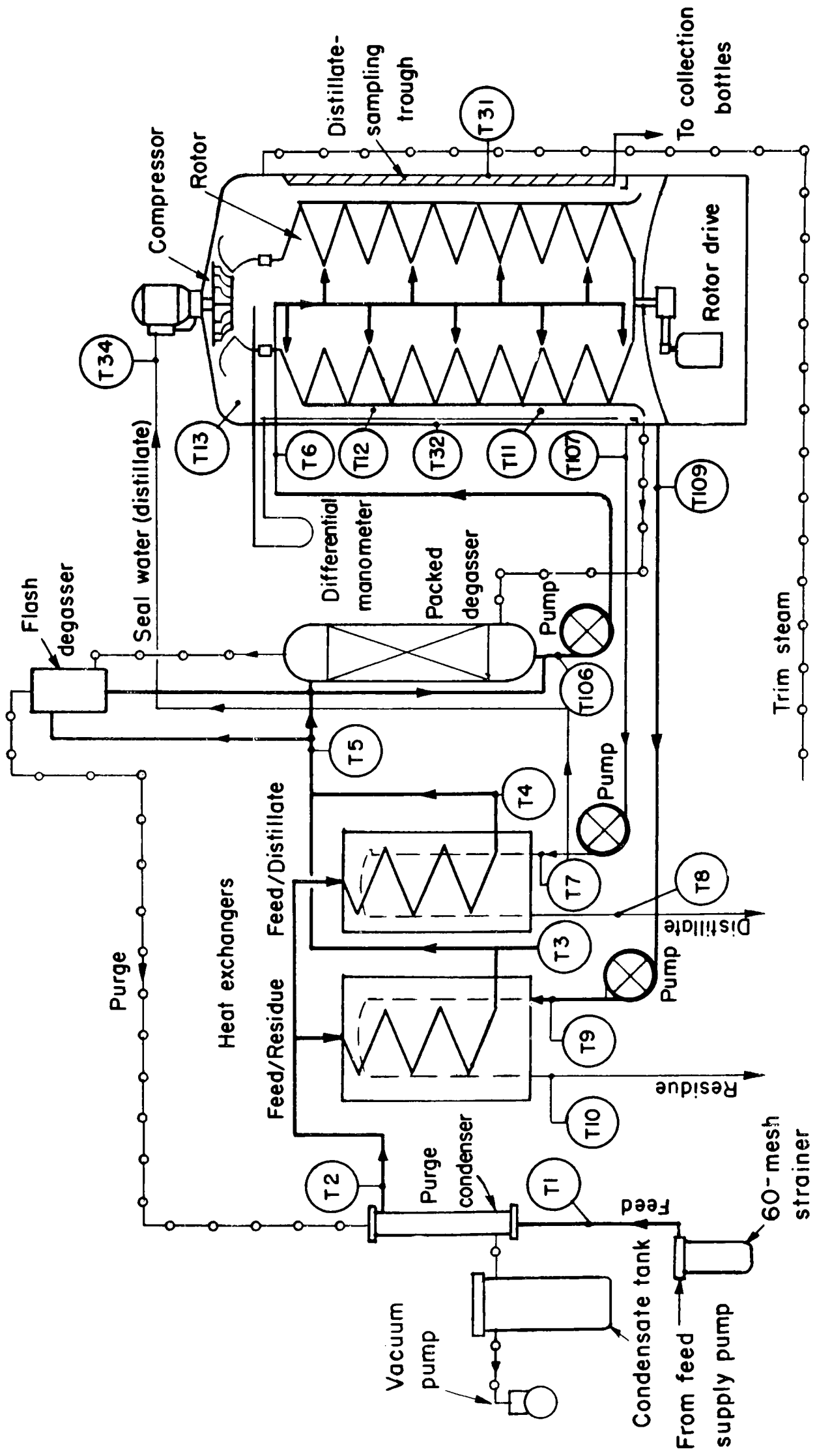

FIGURE 5. PROCESS FLOW DIAGRAM FOR THE NO. 5 STILL

On April 10, 1958, a U of 2010 Btu/(hr)(ft^2)(F) with sea-water feed at 120 F condensing temperature and a rotor speed of 400 rpm was recorded. In an effort to improve this value, several different feed arrangements were evaluated. The evaluations were made possible through the use of a distillate sampler. This sampler consisted of a partitioned vertical trough which collected a proportional quantity of distillate from each of the top seven rotors. The distillate collected in each section of the trough passed through tubes to measuring containers located outside the still. These containers were maintained in pressure equilibrium with the condensing pressure by a manifold system. The results of the evaluation of different feed methods are explained in detail in Appendix B. Although the accuracy of the data obtained may be in question, the over-all heat-transfer coefficient of the No. 5 still measured during the 72-hr run started on September 8, 1958, was about 2250 Btu/(hr)(ft^2)(F) for sea-water feed. The data obtained from several of the many runs made during the program are also presented in Appendix B.

Figure 6 shows the reproducibility of the No. 5 still under different conditions. As may be seen in Figure 6a, the day-to-day reproducibility of the still was rather poor. The reproducibility under what might be termed normal continuous operation, that is, the 72-hour run, appears to be within ±2 per cent. Figure 6c shows the reproducibility of the No. 5 still under what must be termed ideal conditions.

As testing continued, it became apparent that the No. 5 still was not a good research tool, particularly for evaluating minor changes with short-duration tests. For example, the total down time required to make a minor change on the interior of the still was about 2 days. In addition, the time required to warm up and stabilize the operation of the still prior to each day's testing was between 3 and 4 hours, assuming trouble-free operation. Also, the day-to-day reproducibility of the unit was poor enough that minor changes in performance could not be detected.

Concurrently with the No. 5 program, the No. 4 laboratory still in Columbus was being used to determine whether, in fact, it was possible to achieve heat-transfer coefficients higher than those already obtained. From this study it was found that the feed-water film on the outer portions of the rotor was breaking into small streams or rivulets with the result that large sections of the evaporating surface were operating dry. Consequently, it was concluded that improvements in heat transfer, if possible, could only result from a fundamental study. Due to its small size and versatility, the No. 4 still was best suited for this study. Therefore, a decision was made to place the No. 5 still in stand-by status and concentrate all effort on solving the feed distribution problem using the No. 4 still.

Laboratory Study With the No. 4 Hickman Still

The No. 4 still in its "as-delivered" condition was put into operation in the Battelle laboratories on March 25, 1958. The heat-transfer coefficients obtained in April, when converted to standard conditions, were in the range of 1900 to 2100 Btu/(hr)(ft^2)(F).

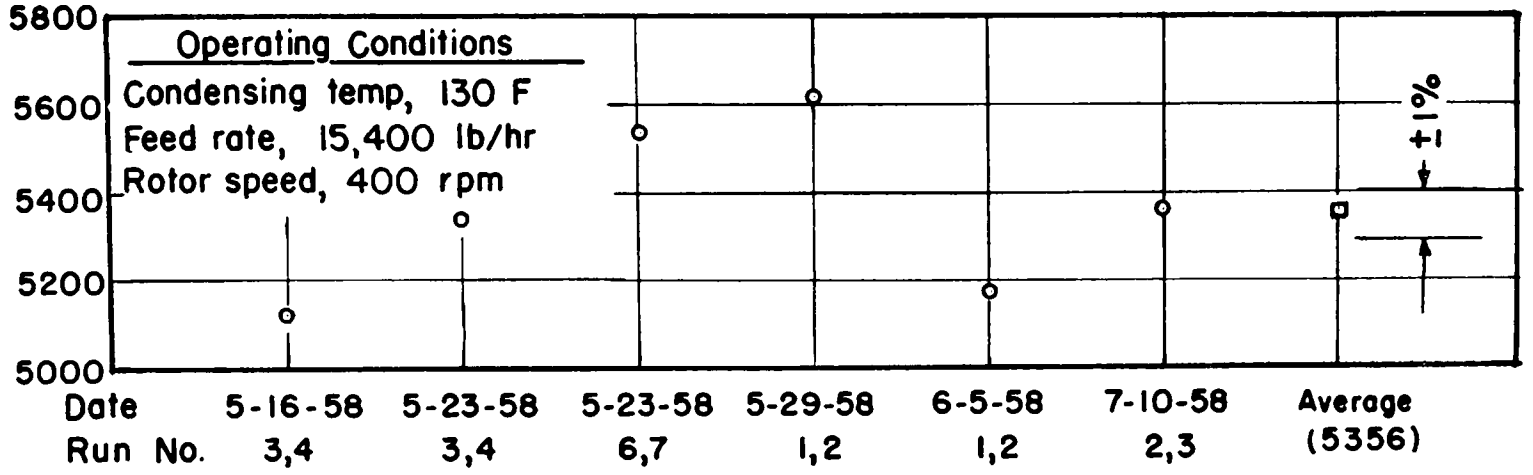

(a) Runs of Near-Identical Operating Conditions

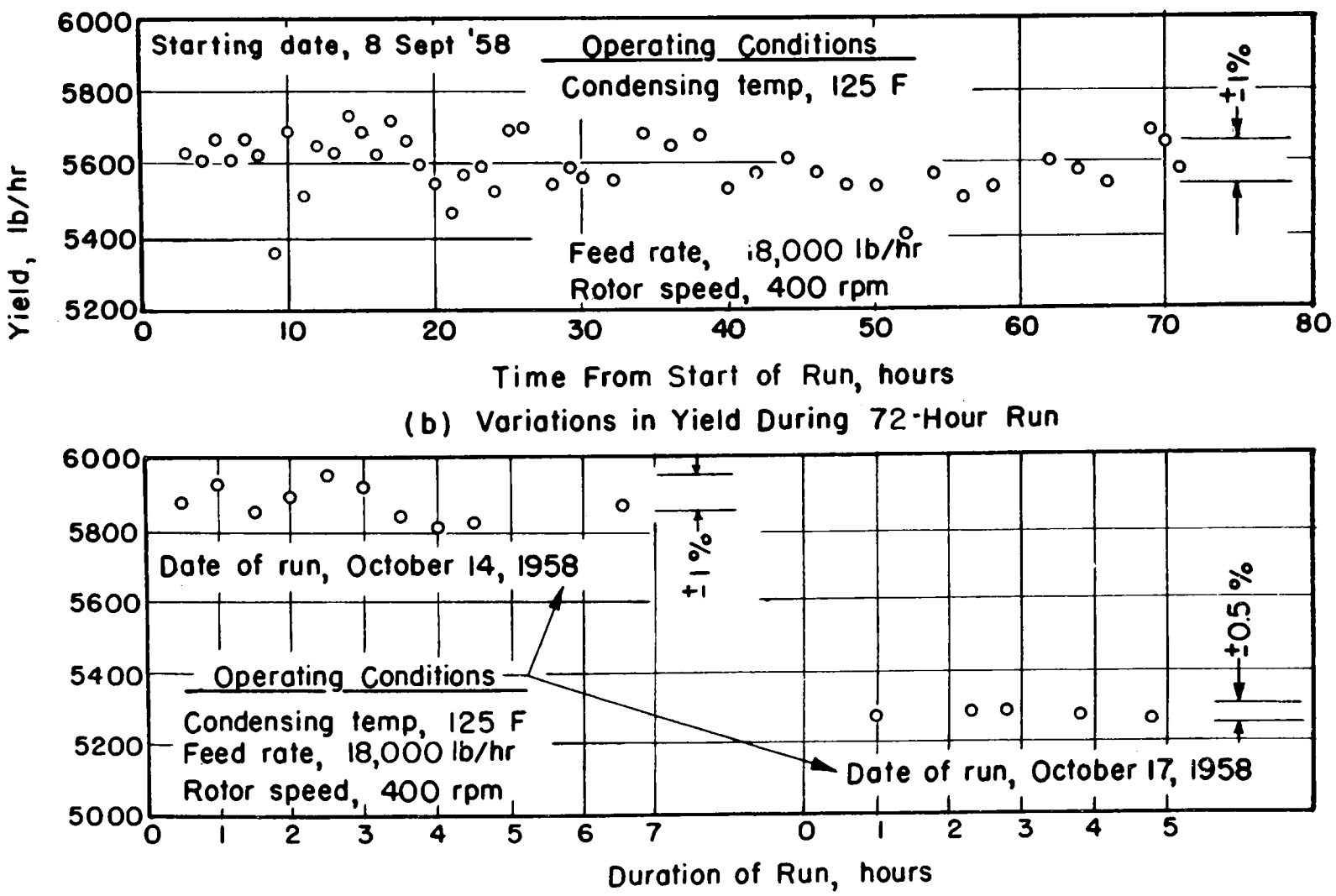

(b) Variations in Yield During 72-Hour Run

(c) Variations in Yield During Reproducibility Study

G 6022-A

FIGURE 6. REPRODUCIBILITY OF TESTS OF THE NO. 5 BADGER-HICKMAN STILL

Figures 7 and 8 show a flow diagram of the original No. 4 still and a picture of the still as it was set up in Columbus.* Of particular interest, as is shown in Figure 7, is the manner in which residue is scooped from the inside rim of the rotor by a stationary tube. This scoop, by causing splash, aided in the wetting of the rotor surface. In July, 1958, the rotor was modified when two vertical tubes were soldered into the rim of the rotor. With this arrangement, residue passed down these tubes and was flung into a circular collection gutter. This residue removal system, the same as that used in the No. 5 still, eliminated the downspout splash. A typical U obtained under standard conditions with this arrangement was 1700 Btu/(hr)(ft^2)(F).

Feed Distribution

Figure 9 shows the feed distribution on the lower half of the rotor of the No. 4 still obtained with a two-nozzle central-type feed system. The photographs were taken with the aid of a strobe light. Each photograph covers an area of the rotor extending from the inner distributing ring to the rim. Water appears as light areas, and dry or sparsely wetted rotor surfaces appear as dark areas in the photographs. In general, the photographs show that water tends to spread uniformly in the distributing ring and in the central area of the rotor. When either the speed or the evaporation rate is increased, the wetted area is reduced in size. Briefly, water proceeds from the uniformly wetted area as petals, which subsequently merge into relatively thick streams. These streams are seen to follow a radial path to the rim of the rotor. This radial path indicates little or no tangential slippage between the rotor surface and the water.

The rotor surfaces were cleaned several times during the test period. Water patterns on the rotor appeared the same immediately after cleaning as after several hours of operation. Therefore, it is unlikely that a possible build-up of a contaminating agent on the rotor is a cause of the rivulet formation. Further, to learn whether reduced surface tension would improve the feed distribution, at one point during the testing period a commercial wetting agent, Aerosol O. T., was added to the feed water. Solutions of 0.1 to 1.0 per cent wetting agent brought about no apparent change in feed distribution.

Figure 10 illustrates "feed interchange", another factor entering into the feed distribution process of the conical rotor in the No. 4 still. The combined effects of the spray caused by the residue scoops and feed interchange make heat-transfer data obtained by "using" only the upper or lower rotor half very misleading.

Figure 11 shows an unusual difference between the heat-transfer coefficient for the upper and lower rotor halves of the No. 4 still. At increasing feed-water supply rates, the coefficient of heat transfer increases rapidly when either of the rotor halves is used; whereas, when feed is supplied to the two rotor halves simultaneously, the coefficient of heat transfer remains practically constant. Further, it is observed from Figure 11 that at feed rates approaching 900 lb/hr operation with only the upper rotor half appears to be approximately 50 per cent more efficient than operation with only the lower rotor half. This is a highly unlikely circumstance. Closer observation of these data reveals the heat-transfer coefficient of the upper rotor at a feed-supply rate of 878 lb/hr to be exactly twice the value at equivalent conditions with feed to both rotor halves. It can be deduced that this large increase in heat-transfer coefficient for the

*For more detailed information on the No. 4 still see "Research and Development Progress Report No. 15" of the Office of Saline Water, U. S. Department of the Interior.

upper rotor is attributable to drops of water being thrown from the upper rotor onto the bottom evaporating surface. Thus, the heat-transfer areas of both rotors are utilized. An identical situation probably exists with respect to the lower rotor half. However, because of natural gravity, less of the water detaching from the lower surface would reach the upper rotor. That an interchange of water between the two rotor halves did occur was confirmed by visual observation.

To provide for easy observation of the feed distribution, the vapor flow of the No. 4 still was reversed so that feed water could be evaporated from the outside of the rotor. Modifying the still for an "outside feed" arrangement also provided facilities for evaluating different rotor shapes.

Figure 12 shows the No. 4 still after it had been modified to permit evaporation to take place on the outside surface of the rotors. With this arrangement, the test-rotor section is supported at the rim by the original lower conical rotor half which now, in effect, is used as the turntable. The flat-rotor section which was used for most of the tests is indicated by the solid line in the figure. The slightly convex rotor was obtained by elevating the center of the flat rotor approximately 2 inches. It was found that a slope of approximately 5 degrees could be obtained in this way without distortion or warpage of the surface. The feed-water supply line enters through the top of the still, and for the flat rotor the water was supplied at the center for the majority of runs. Once-through fresh water was used rather than recirculated feed to reduce the possibility of contamination of the rotor surface by impurities that might exist in the system. Both distillate and noncondensable gas were removed from the rim of the test section. Distillate flowed through two 1/4-inch copper tubes to a collecting trough, and noncondensable gas was removed through stationary 1/2-inch copper lines as indicated.

Under standard conditions, a typical U obtained with the flat rotor and a central feed system was about 2500 Btu/(hr)(ft^2)(F). At feed rates which resulted in a feed-to-distillate ratio as low as 2:1, there was no rivulet formation on the evaporating surface.

Heat Transfer With a Flat Rotor

Once it became apparent that flat rotors could be wetted and offered the potential advantages of lower fabrication costs, and increased compactness, no further heat-transfer studies were made with conical surfaces. Although experimental data are not available which might explain why feed distribution on a flat surface was better than on the conical surface, several conjectures have been offered. As may be seen in Figure 12, the conical surface had a rather abrupt change in slope a few inches out from its inside diameter. It is possible that this slope change sets up instabilities which contribute to the breakup of the evaporating film further out on the rotor. Another possibility is that because the velocity of the film on a conical surface is slower than on a flat surface, the film on the conical surface is allowed a longer time in which to shift to the more stable rivulet condition. It is also possible that vibration or surface conditions influenced the results. In any event, the emphasis of the program was shifted from simply finding a way to obtain continuous evaporating film to exploring methods of obtaining the thinnest possible film. The search for a means whereby the evaporating-film thickness could be reduced was of course motivated by the fact that the thinner this film the less resistance it offers to heat flow.

Although some valuable preliminary work on flat surfaces was done with the No. 4 unit, as shown in Figures 7 and 12, it was decided to modify both the still and the auxiliary system. Incorporated in the modified No. 4 still was a more efficient purge system, a more stable rotor turntable, a mounting shaft capable of holding more than one rotor, a preferred method of adding trim heat to the still, and a means of accurately measuring the noncondensable gas that leaves the still.

Figures 13 and 14 show the No. 4 still as it appeared after being modified in early 1959. With this modified unit, the heat-transfer characteristics of a single flat rotor with central feed were studied in detail. In one instance, annular areas of the rotor starting at the rim were covered with an insulating layer of 1/8-inch-thick plastic to determine the variation in yield with rotor radius. These data are compared with analytical estimates in the heat-transfer section of this report. Briefly, the experimental data showed that the local heat-transfer coefficient increased with radius up to a point, then fell off sharply near the rim. It was theorized that this fall-off was caused by noncondensable-gas accumulation between purge points.

Figure 15 shows the heat-transfer coefficients that were obtained with a 4-1/2-foot-diameter flat rotor under about standard operating conditions. The U obtained with central feed was 2800 Btu/(hr)(ft^2)(F). With a multiple-nozzle feed system, the U was about 3300 Btu/(hr)(ft^2)(F). It should be noted that the relation between the square root of the rotor speed and U, which was determined by earlier investigators, still holds true. Although it had been proved that adding feed water at several different radii offers a heat-transfer advantage over applying all of the feed at the center of the rotor, data on both systems were obtained concurrently because it was not clear which feed system would be more practical in a production still.

Multiple-Rotor System

Figures 16 and 17 show the multiple-rotor No. 4 still. The multiple-rotor system was in operation by October, 1959. This unit incorporates three evaporating surfaces, an eight-nozzle-per-rotor surface feed system, and a further-developed purge system. This purge system, which is considered very effective, is described in the section of this report covering heat transfer.

The effectiveness of the improved purge system was demonstrated by the following experiment. The purge throttle valve was closed until the yield of the still dropped to 50 per cent of normal. Then the valve was set at the standard purge rate. After 90 seconds, the yield of the still was back to normal. Previously, the recovery time would have been at least 1 hour.

The primary purpose of installing the multiple rotors in the No. 4 still was to determine whether feed water could be supplied to the under surface of a rotor with the same success as was achieved with the upper surface. The U obtained shortly after the multiple-rotor system was placed in operation was about 3100 Btu/(hr)(ft^2)(F) under standard conditions. This value is approximately 6 per cent below that which was obtained on a single flat surface. Inspection of the feed nozzles showed that some nozzles had become plugged. It is possible that uneven feed distribution as well as experimental error contributed to this 6 per cent reduction. Therefore, it was concluded that the under surface of the top rotor had been adequately wetted. The U of the multiple rotors was increased to about 4000 Btu/(hr)(ft^2)(F) at 400 rpm by spraying

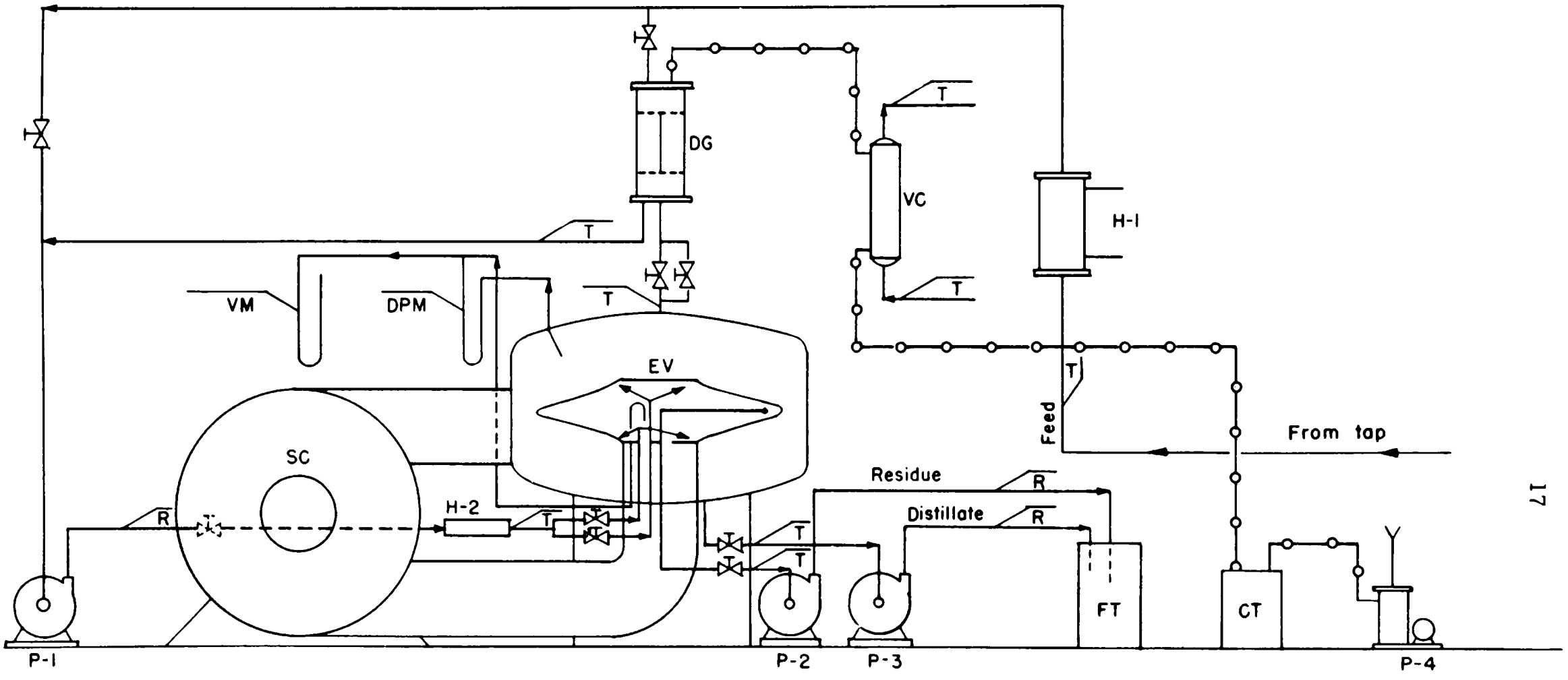

EV	Evaporator	CT	Condensate-collecting tank	P-1	Feed pump	T	Thermometer
SC	Steam compressor	H-1	Trim heater	P-2	Residue pump	R	Rotameter
DG	Feed water degasser	H-2	Trim heater	P-3	Distillate pump	DPM	Differential pressure manometer
VC	Vent condenser	FT	Feed tank	P-4	Vacuum pump	VM	Vacuum manometer

A 5550-A

FIGURE 7. FLOW DIAGRAM FOR THE NO. 4 HICKMAN STILL

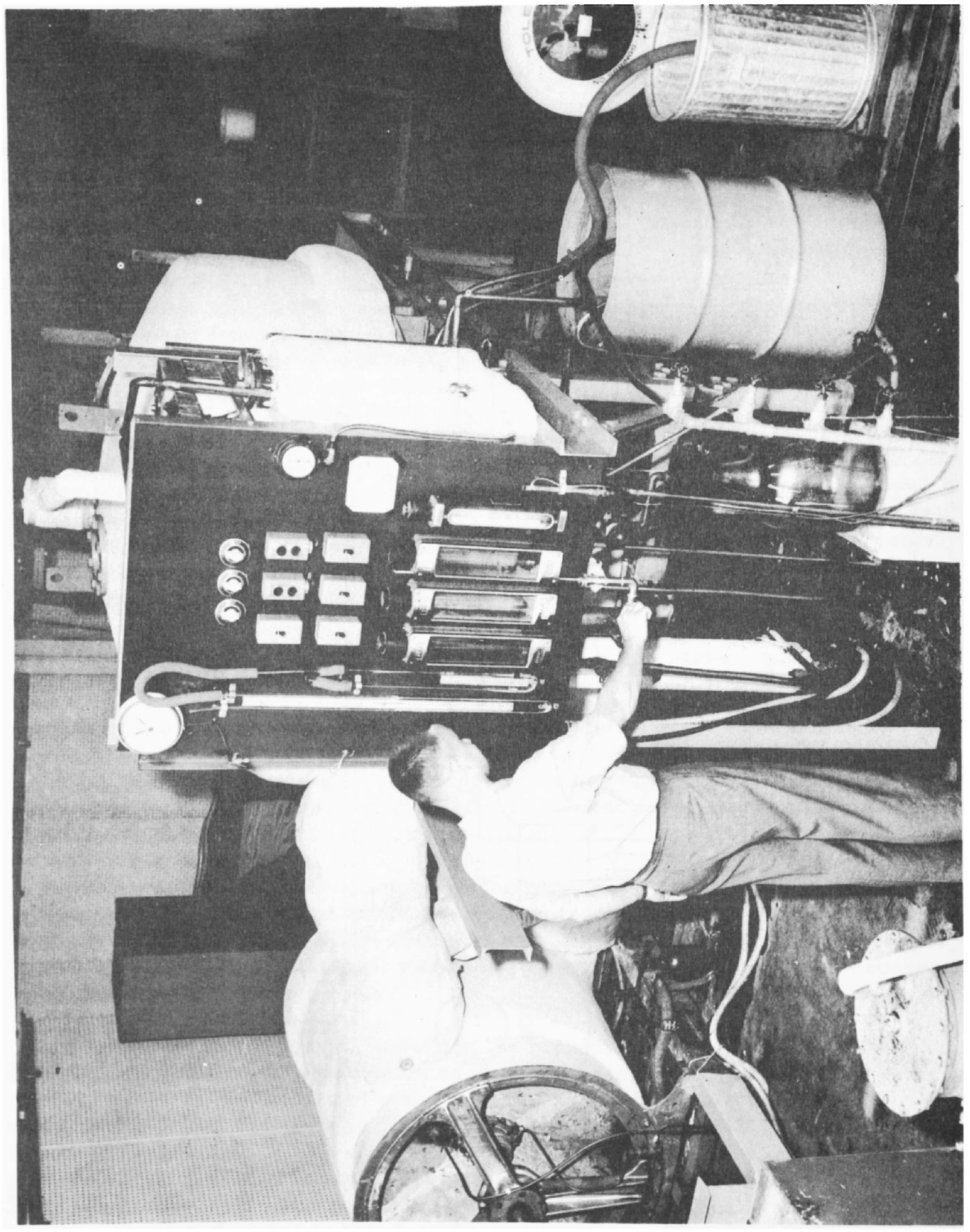

N50314

FIGURE 8. THE NO. 4 HICKMAN STILL AT COLUMBUS, OHIO

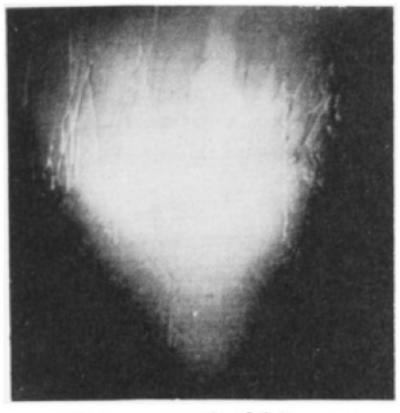

Rotor speed, 225 rpm
(Condensing temp, 75 F)

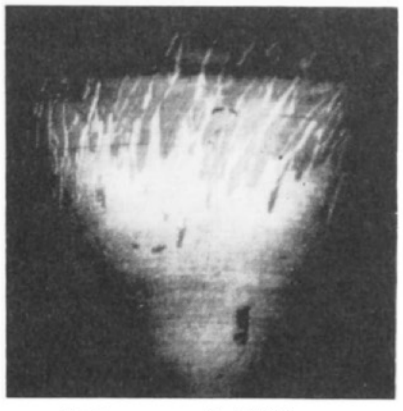

Rotor speed, 300 rpm

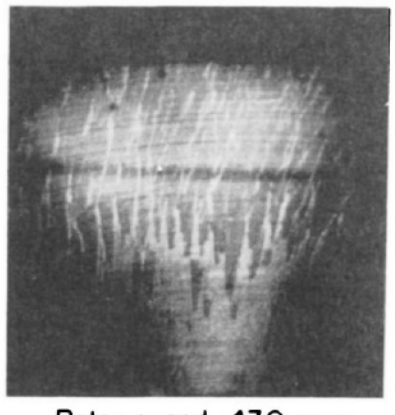

Rotor speed, 430 rpm

(a) Influence of Rotor Speed

Condensing temperature=110 F; Temperature difference=4 F; Feed supply rate=0.88 gpm

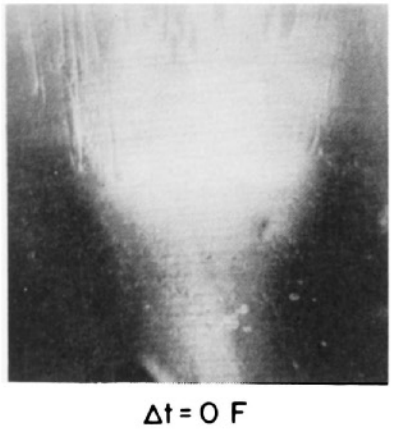

Δt = 0 F

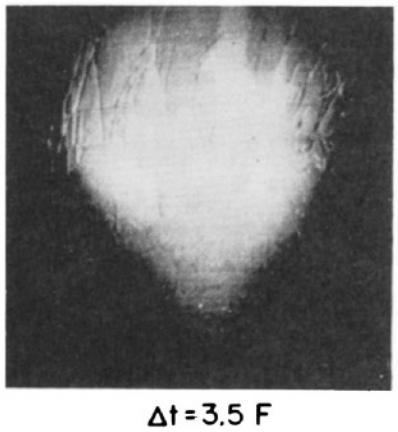

Δt = 3.5 F

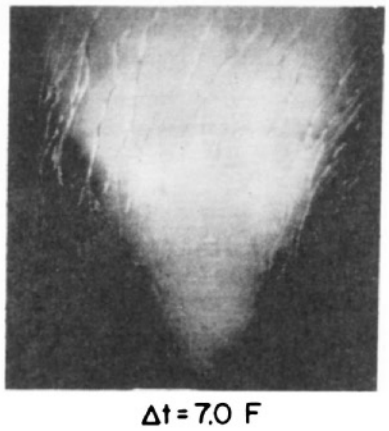

Δt = 7.0 F

(b) Influence of Temperature Difference

Condensing temperature = 75 F; Rotor speed = 225 rpm; Feed supply rate = 0.88 gpm

Feed=0.88 gpm

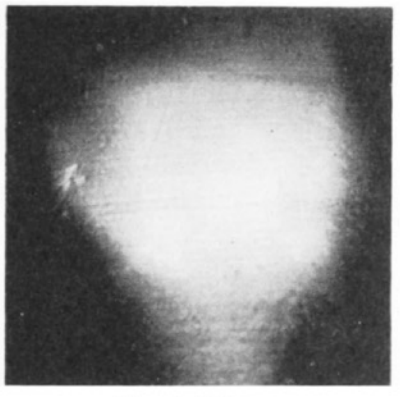

Feed=1.3 gpm

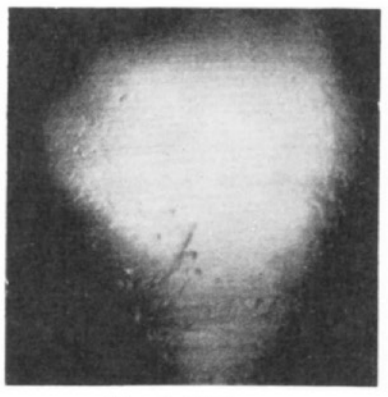

Feed=1.76 gpm

(c) Influence of Feed Supply Rate

Condensing temperature=120 F; Rotor speed=225 rpm; Temperature difference=1.5 F

N69272

FIGURE 9. FEED-WATER DISTRIBUTION ON THE LOWER ROTOR HALF OF THE NO. 4 STILL

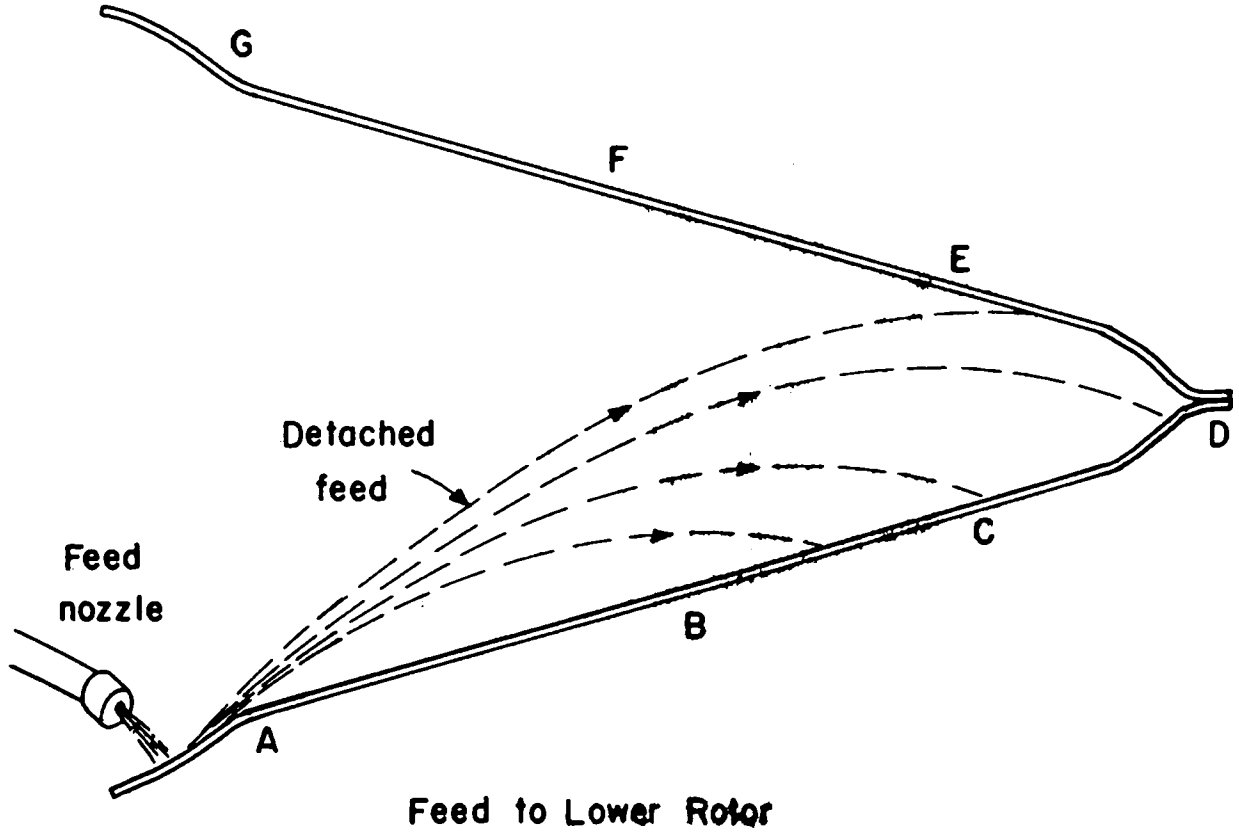

FIGURE 10. PATHS OF DETACHED FEED WITHIN ROTOR

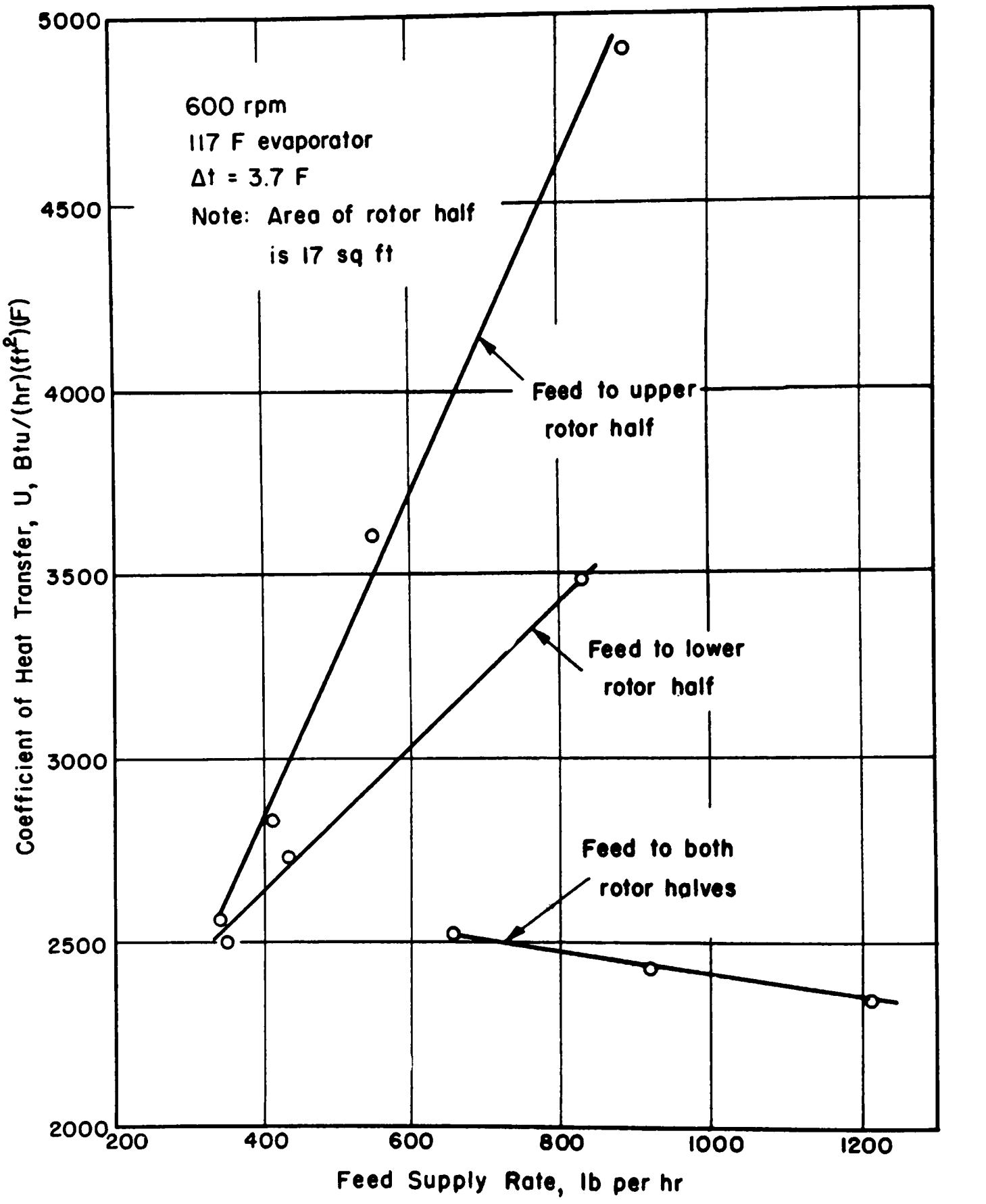

FIGURE 11. COEFFICIENTS OF HEAT TRANSFER FOR INDEPENDENT FEED TO UPPER AND LOWER ROTOR HALVES

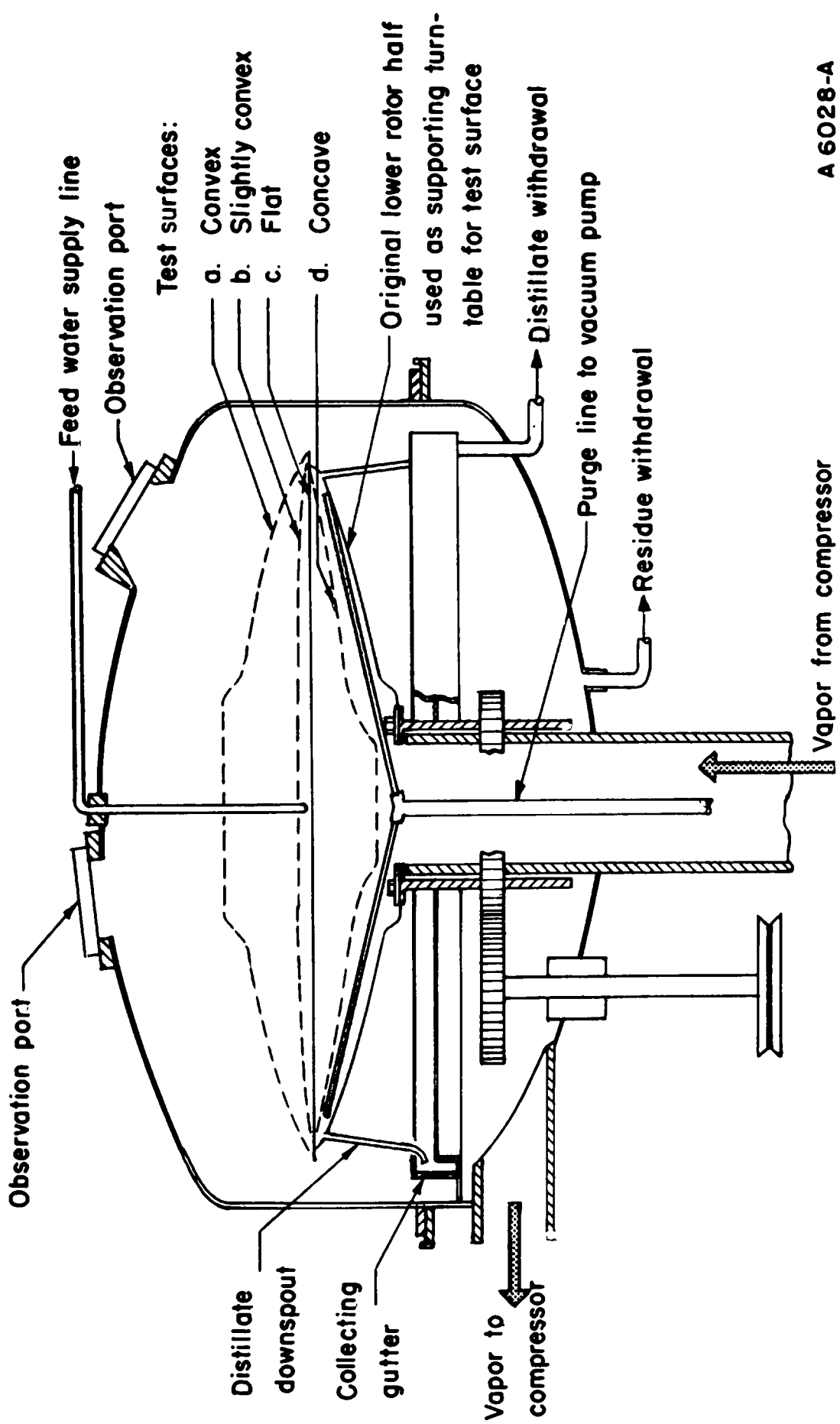

FIGURE 12. NO. 4 STILL ADAPTED FOR "OUTSIDE FEED" APPLICATION

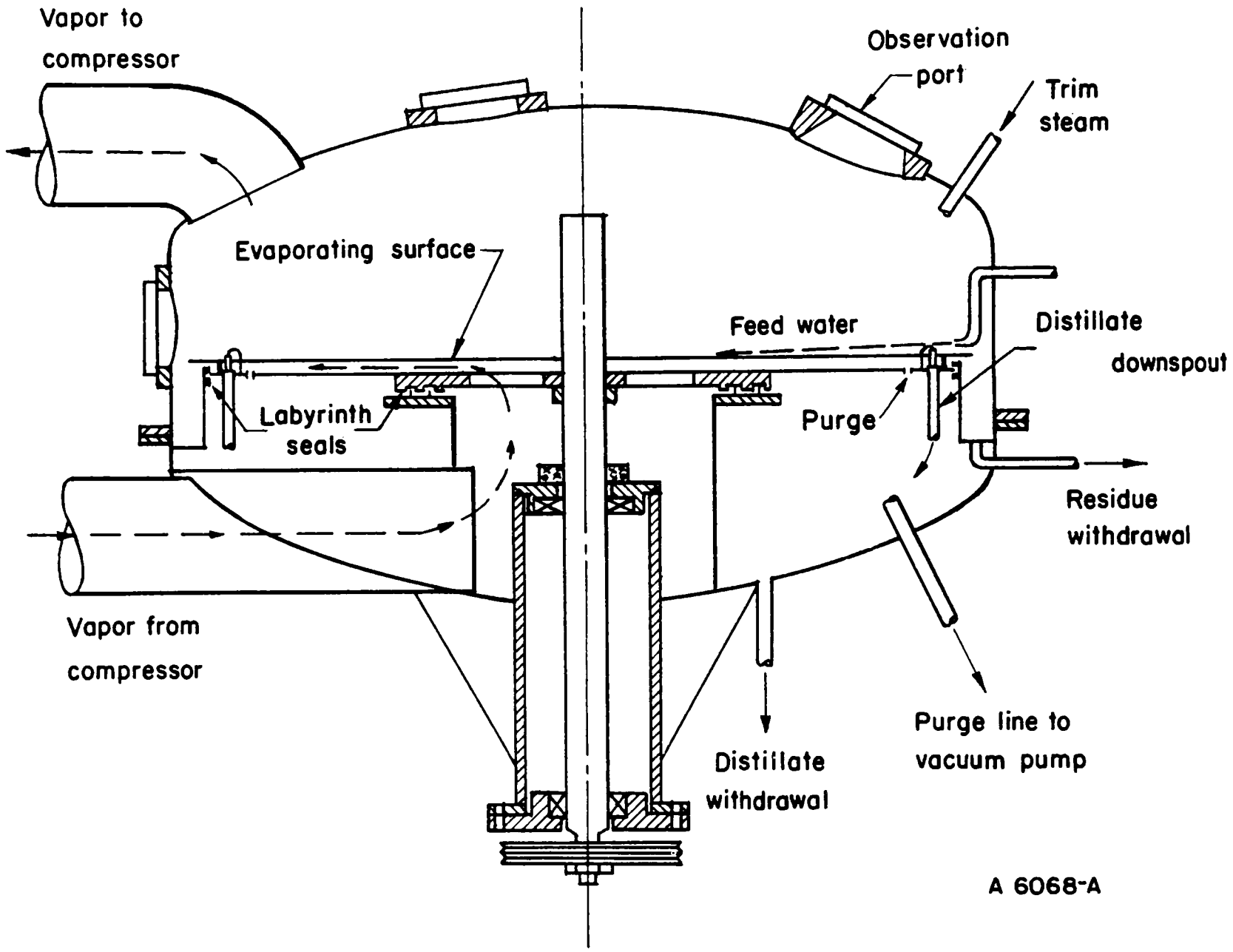

FIGURE 13. MODIFIED NO. 4 STILL ADAPTED TO ACCOMMODATE ONE OR MORE ROTORS

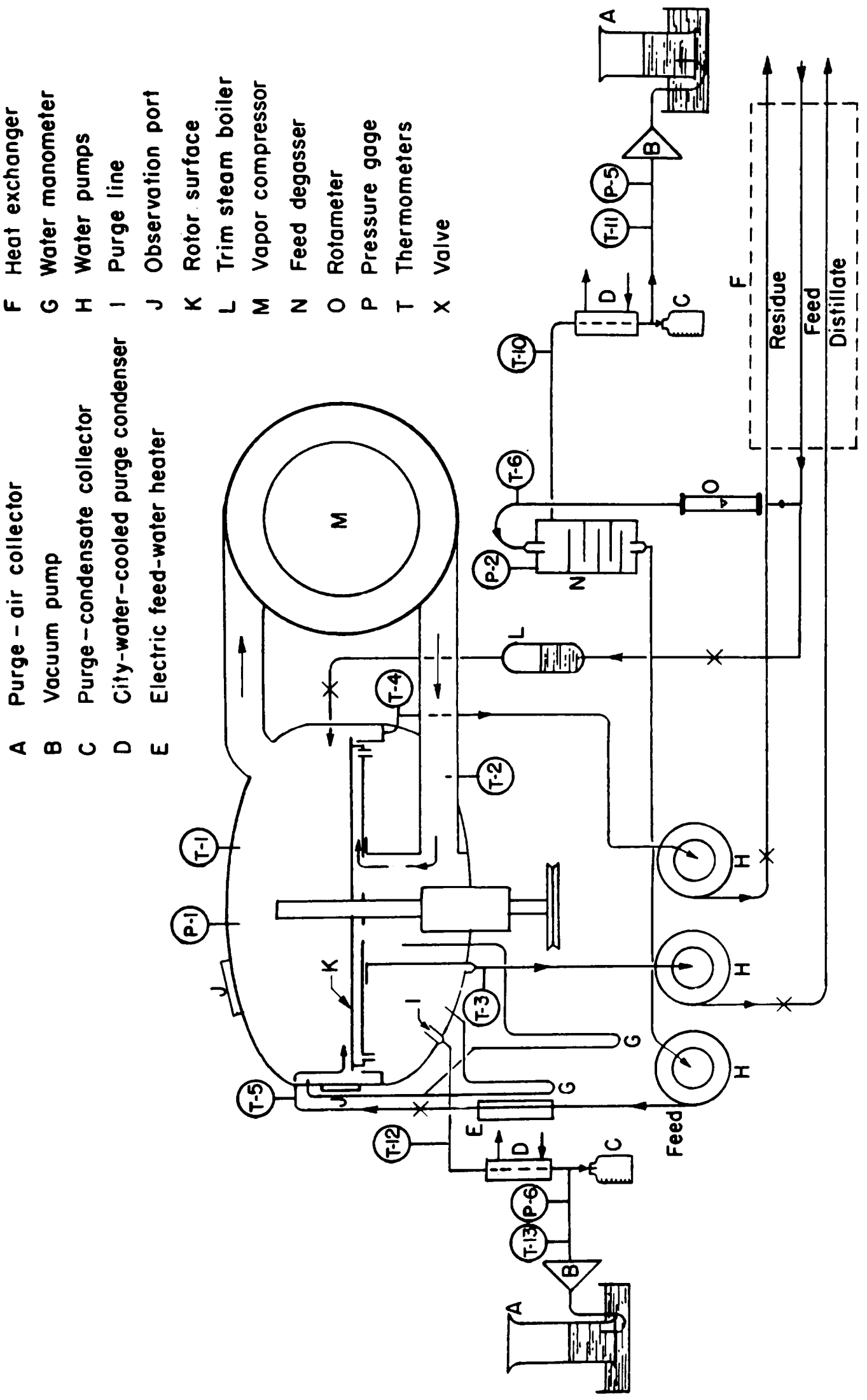

FIGURE 14. FLOW DIAGRAM FOR THE MODIFIED NO. 4 STILL

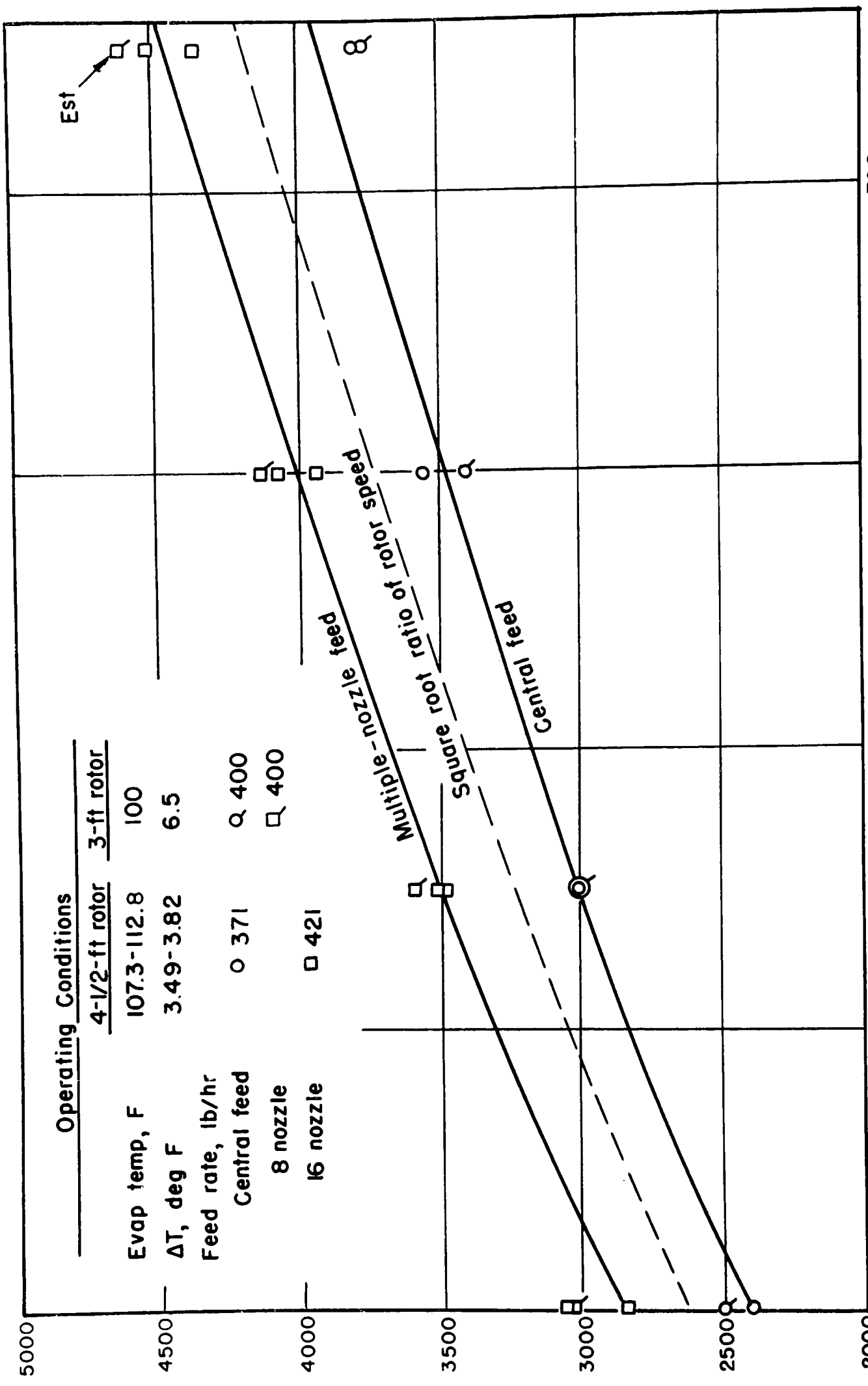

FIGURE 15. VARIATION OF HEAT-TRANSFER COEFFICIENT WITH ROTOR SPEED – NO. 4 STILL USING FRESH-WATER FEED

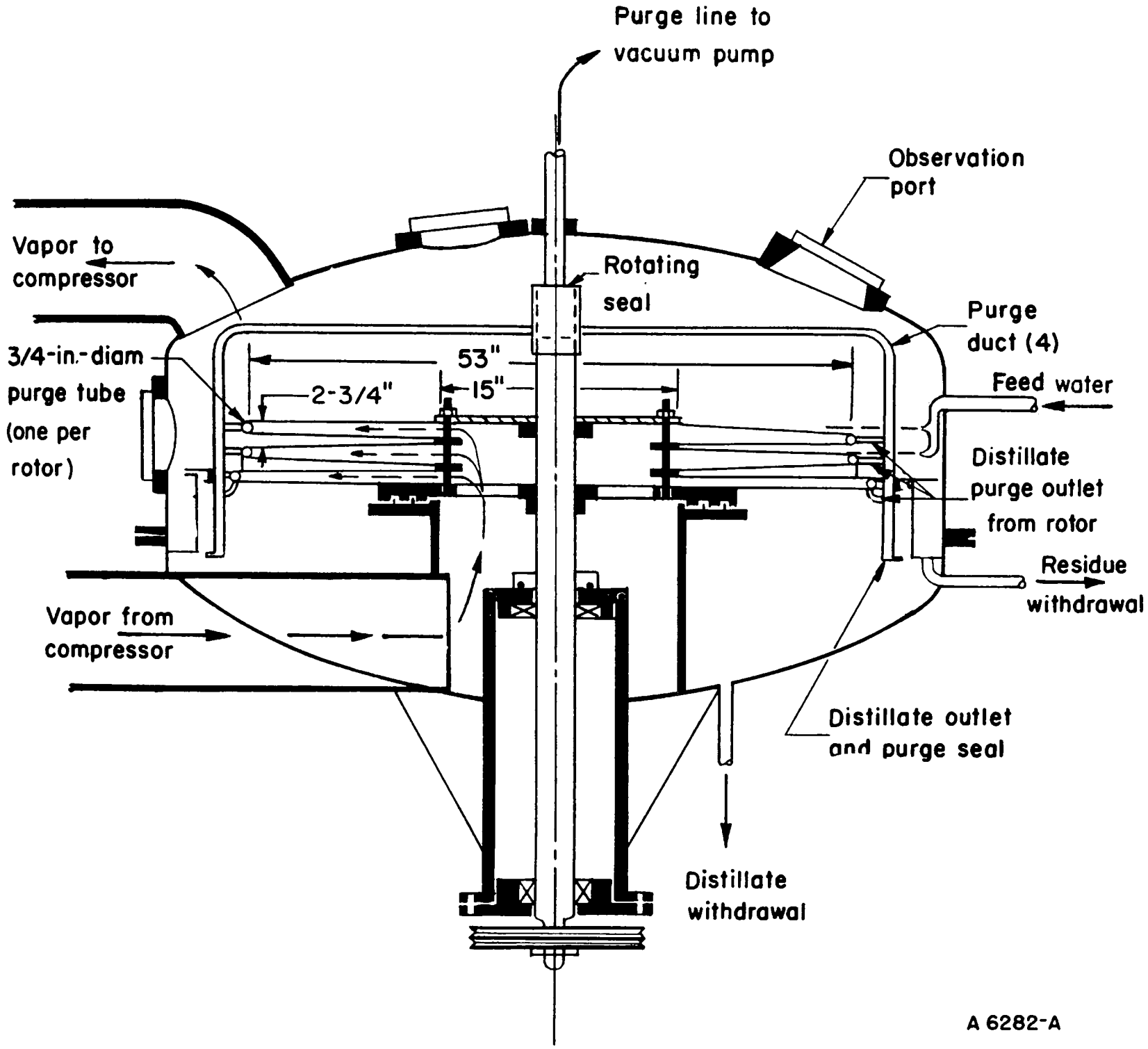

FIGURE 16. NO. 4 STILL ADAPTED TO ACCOMMODATE MULTIPLE ROTORS

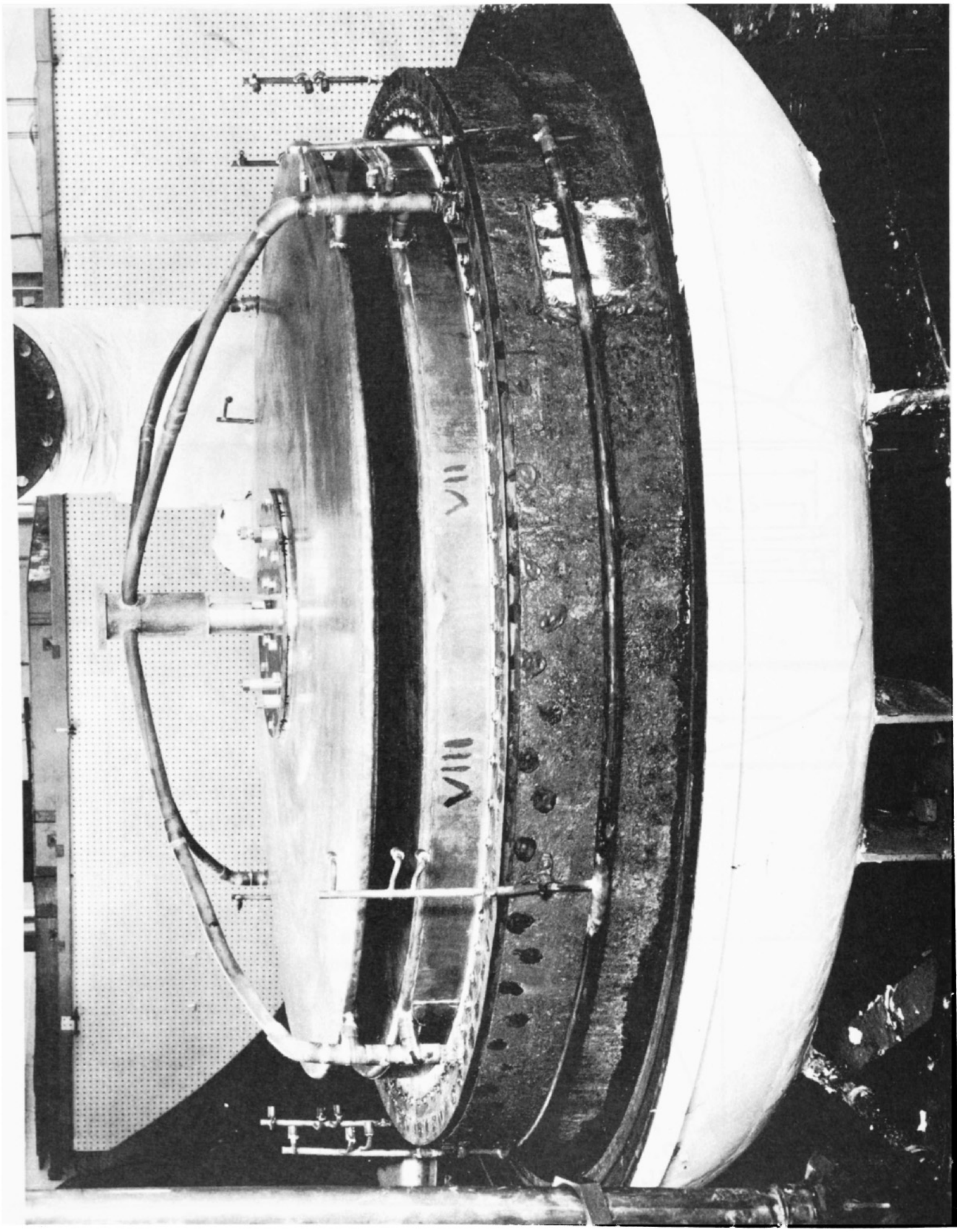

N64727

FIGURE 17. THE MULTIPLE ROTOR SYSTEM OF THE NO. 4 STILL

hot sulfamic acid into the condensing cavity while the still was in operation. The acid used was a product of Bull and Roberts, Inc., called H-400 Scale Solvent. It had been observed previously that the H-400 Scale Solvent, when applied hot, produced a non-wettable surface on copper. Presumably then, dropwise condensation occurred in the still, although this could not be confirmed by visual inspection. The U of 4000 Btu/(hr)(ft^2)(F) is approximately 15 per cent below the theoretical maximum expected with a multiple-nozzle feed system. This theoretical value is based upon conditions of fresh-water feed, ideal dropwise condensation, and a feed-to-distillate ratio of about 2:1.

Although a U of 4000 Btu/(hr)(ft^2)(F) has been achieved with fresh-water feed under laboratory conditions, it is not reasonable to assume that this value can be achieved in the field with sea-water feed and a more practical multiple-nozzle feed system. More practical, in this instance, means having fewer and thus larger, less easily plugged nozzles. The U expected under field conditions is about 3000 Btu/(hr)(ft^2)(F) at a condensing temperature of 110 F.

Figure 18 shows a comparison between fresh-water and salt-solution feeds. These data were obtained with a single flat rotor and with central feed. It will be noted that the heat-transfer coefficients obtained with 3.5 per cent salt-solution feed are about 7 per cent below those obtained with fresh-water feed. This difference is discussed in the report section on heat transfer. The fact that the fresh-water heat-transfer coefficients given in Figure 18 are below those shown in Figure 15 is attributed to an iron oxide film which was deposited on the condensing surface during the test program. Subsequent experiments have shown that the heat-transfer coefficients obtained with 3.5 per cent salt solution and with sea water are essentially the same. Accordingly, to reduce laboratory costs, a salt solution rather than sea water was used in most of the heat-transfer studies.

Although the multiple-nozzle feed systems offer a heat-transfer advantage in comparison with a central feed system, the use of many small feed nozzles introduces the problem of preventing nozzle plugging. This in turn increases the filtering requirements of the plant. Therefore, if heat transfer is not significantly reduced, it would be desirable to use a feed system which incorporates a few large nozzles rather than many small nozzles. For this reason the multiple-rotor No. 4 still was operated with a two-nozzle peripheral feed system. The two-nozzle feed system, with both nozzles directed toward only the innermost radius of each rotor, may be thought of as a central feed system for the multiple rotors. The results obtained using 3.5 per cent salt-solution feed with both the eight-nozzle and two-nozzle peripheral feed systems showed that the heat-transfer coefficients obtained with the eight-nozzle system were about 4 per cent higher than those obtained with the two-nozzle system. Earlier work with a single flat rotor and fresh-water feed had shown that heat-transfer coefficients obtained with a multiple-nozzle feed system were about 15 per cent above those obtained with a central feed system (Figure 15). This difference between 4 per cent in the case of salt-water runs and 15 per cent in the case of fresh-water runs is due to: (1) the hole in the center of the multiple rotors and (2) the boiling-point elevation of salt water.

In performing a cost analysis on a distillation plant which incorporates the Hickman principle, it is necessary to choose a U that can be expected under a given set of operating conditions. On the basis of results obtained during the No. 4 still experimental program, a U of 3000 Btu/(hr)(ft^2)(F) at a rotor speed of 400 rpm and an evaporating temperature of 110 F was considered reasonable. This value was arrived at as follows: A U of 3400 Btu/(hr)(ft^2)(F) was obtained with the multiple-rotor No. 4 still while operating at the following conditions:

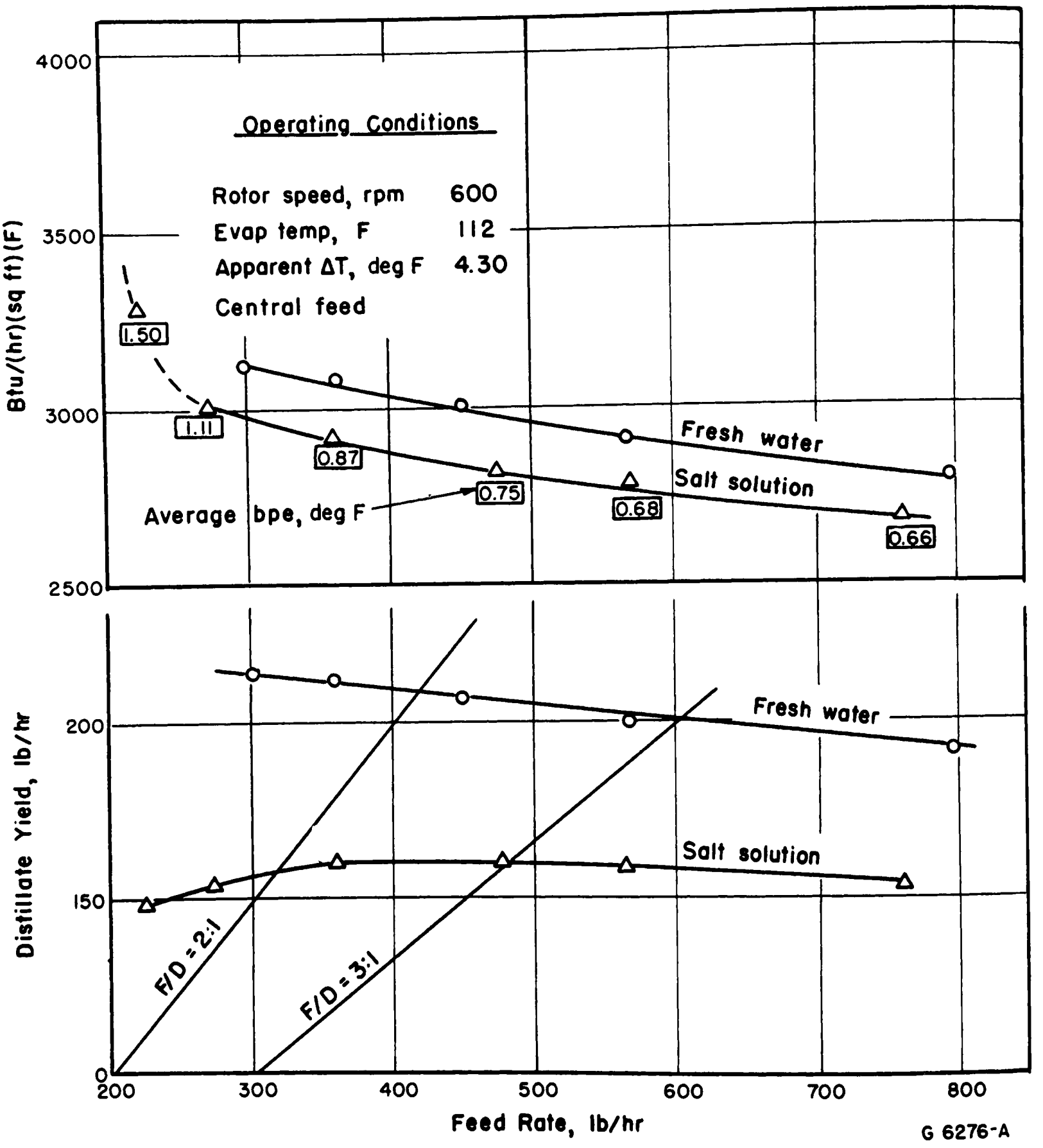

FIGURE 18. COMPARISON OF THE PERFORMANCE OF THE NO. 4 STILL WITH FRESH-WATER FEED AND 3.5 PER CENT SALT-SOLUTION FEED

5.7 degrees F apparent ΔT

400-rpm rotor speed

120 F evaporating temperature

Salt-water feed

Two-nozzle feed system.

The value of 3400 Btu/(hr)(ft^2)(F) has to be reduced by 5 per cent if the base operating temperature of 110 F used in the cost analysis is to be considered. The resulting U is 3220 Btu/(hr)(ft)(F). This value should be reduced further to make allowance for slight scaling that may occur in the field. Accordingly, a heat-transfer coefficient of 3000 Btu/(hr)(ft^2)(F) is considered to be practical and realistic.

COST STUDY

Operating costs have been estimated for Hickman stills utilizing a single rotor column of 100,000 gallons per day and greater capacity, following the procedure outlined in the Office of Saline Water publication "A Standardized Procedure for Estimating Costs of Saline Water Conversion". Variables considered in the estimates include capacity, operating temperature, temperature difference between evaporating and condensing media, and rotor speed. The results of the study indicate the operating conditions for a single rotor-column unit in the size of 100,000-gallons-per-day capacity should be: rotor speed = 400 rpm, evaporating temperature = about 120 F, and ΔT = about 7 degrees F. If a 20-year rotor life is assumed, then a ΔT of about 5.5 degrees is desirable. It is interesting to note that the No. 5 still, although smaller in capacity, was designed for operation very close to these conditions, namely at a rotor speed of 400 rpm, an evaporating temperature of 125 F, and a ΔT of 5.1 degrees F. The use of evaporating temperatures much higher than 120 F is not suggested at this time because of the resulting high pressure differences.

Figure 19 is a flow diagram of the plant arrangement which is used throughout this cost study. The arrangement differs from that of the No. 5 still in that the plant feed pump is eliminated, the purge condenser is eliminated, and the degasser is operated at ambient temperature. The plant feed pump is not required because the feed water is drawn to the degasser which operates under vacuum. With the rim purge method, only 0.1 per cent purge is required; consequently, the purge is not large enough to warrant installation of a separate condenser. As it is possible to degas adequately at any temperature, the lowest temperature was chosen in order to reduce heat loss and corrosion rate in the degasser.

Figure 20 shows an assembly drawing of a possible 8-foot-diameter, 20-rotor evaporator. Each rotor is 3-1/2 inches high. This design incorporates improved features resulting from the research program. A breakdown of estimated costs of an evaporator of this type is presented in Table C-1 of Appendix C. The costs used in the study are based on the use of a 1-foot-diameter rotor-support shaft rather than the 3-inch-diameter shaft shown in Figure 20.

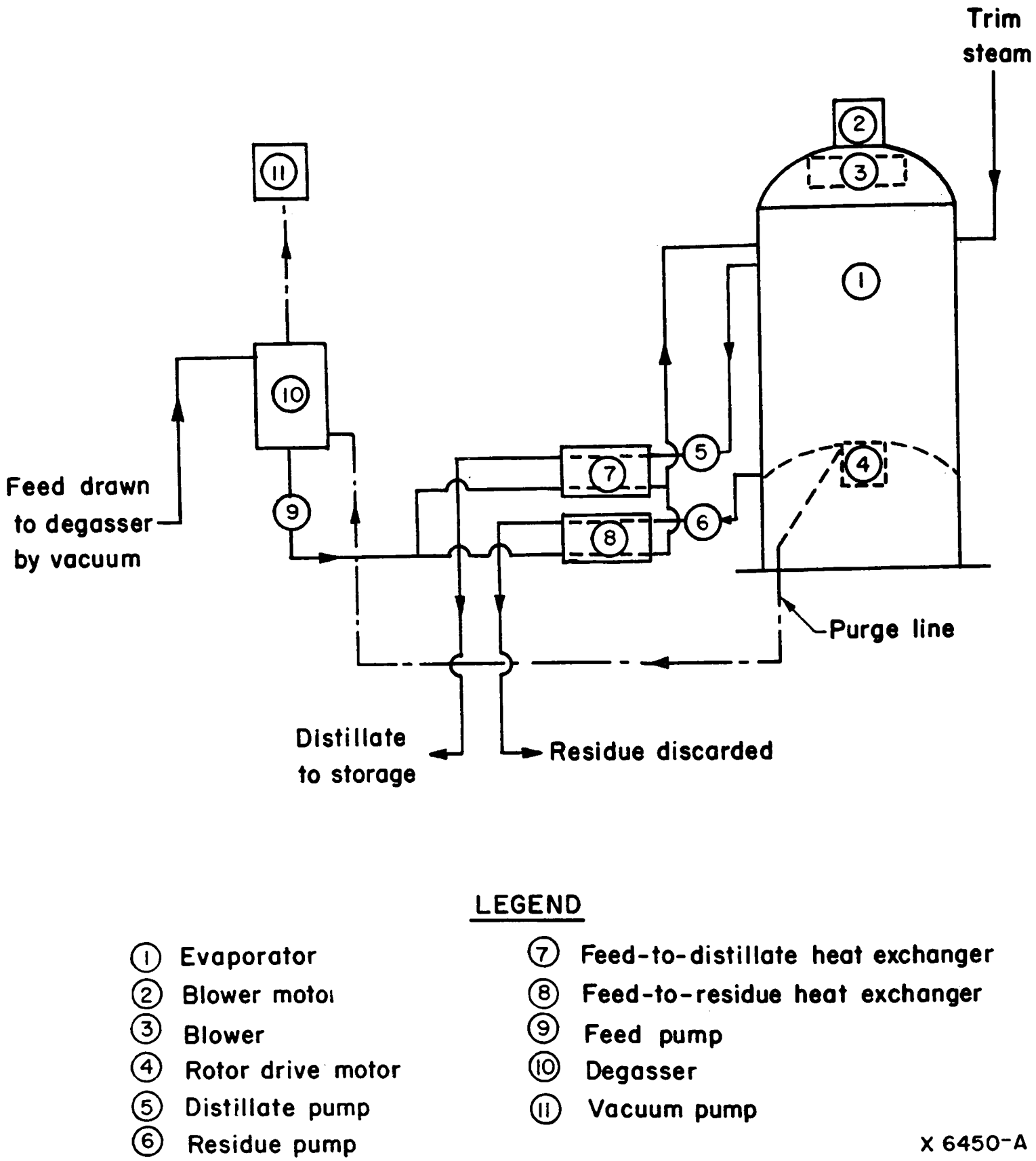

FIGURE 19. FLOW DIAGRAM OF HICKMAN STILL

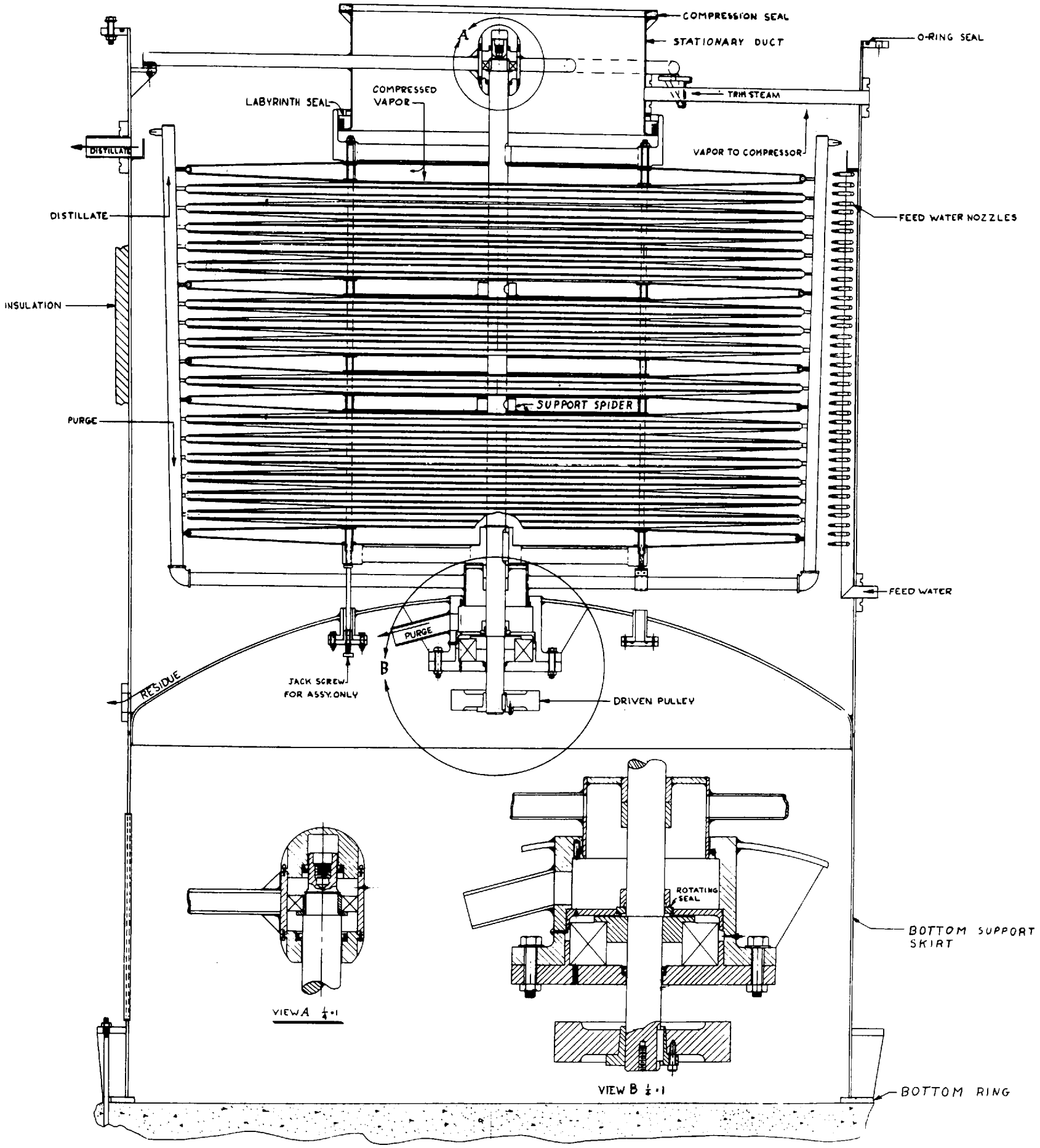

FIGURE 20. ASSEMBLY DRAWING OF A 20-ROTOR HICKMAN STILL

100,000-Gallons-Per-Day Still

Figure 21 summarizes the operating costs for a single "can" still of 100,000-gallons-per-day capacity, showing the influence of evaporating temperature and the temperature difference between the evaporating and condensing regions of the still. The lower curves, based on a life of 20 years for the entire still, indicate a minimum operating cost of $1.02, $1.03, and $1.07 per 1000 gallons for evaporating temperatures of 150 F, 120 F, and 90 F, respectively. The corresponding capital costs are $1.78, $1.85, and $1.78 per gallon per day of production. The upper curves, based on a life of 5 years for the rotating assembly and 20 years for the remainder of the still, show minimum operating costs of $1.28, $1.31, and $1.40 per 1000 gallons for evaporating temperatures of 150 F, 120 F, and 90 F, respectively. The capital costs are $1.70, $1.72, and $1.80 per gallon per day. The shift, shown in Figure 21, to lower optimum temperature differences for the longer evaporator life (20 years) is due to a change in the balance point between capital cost and compressor power cost. That is, for a fixed-capacity unit, as the capital amortization cost is reduced, the optimum power cost must be correspondingly reduced in order to obtain the point of most economical operation. Thus, both capital and power costs, and in turn product-water cost, depend to a large extent on the life of the evaporator.

The relatively higher costs of operating at 90 F are due to the increased velocity of the steam and the consequent friction losses associated with the relatively large specific volume of saturated steam at this temperature. The unusual slope of the 90 F curve is caused by a decrease in compressor efficiency due to the combination of large volume and high pressure ratio at the higher ΔT's. It appears that the best operating temperature is about 120 F as this temperature gives almost the minimum total cost while retaining the possible advantages of less scaling and lower corrosion rates than would result from operation at 150 F.

Cost Parameters

Figure 22 illustrates how lower operating costs can be obtained by increasing the capacity range of the still. If 8-foot-diameter rotors and a 12-inch-diameter rotor shaft are selected, critical-speed considerations limit the size of a still to about 60 rotors. With a 60-rotor still operating at an evaporating temperature of 150 F, maximum still capacity varies from 145,000 to 332,000 gallons per day at apparent temperature differences of 4 to 8 degrees F. The corresponding operating costs, assuming 5 years of useful life for the rotating assembly, reach a minimum of $1.07 per 1000 gallons at a capacity of 332,000 gallons per day. The capital cost for this condition is $1.21 per gallon per day. If useful rotor life is assumed to be 20 years, operating costs at the minimum point are reduced to $0.94 per 1000 gallons.

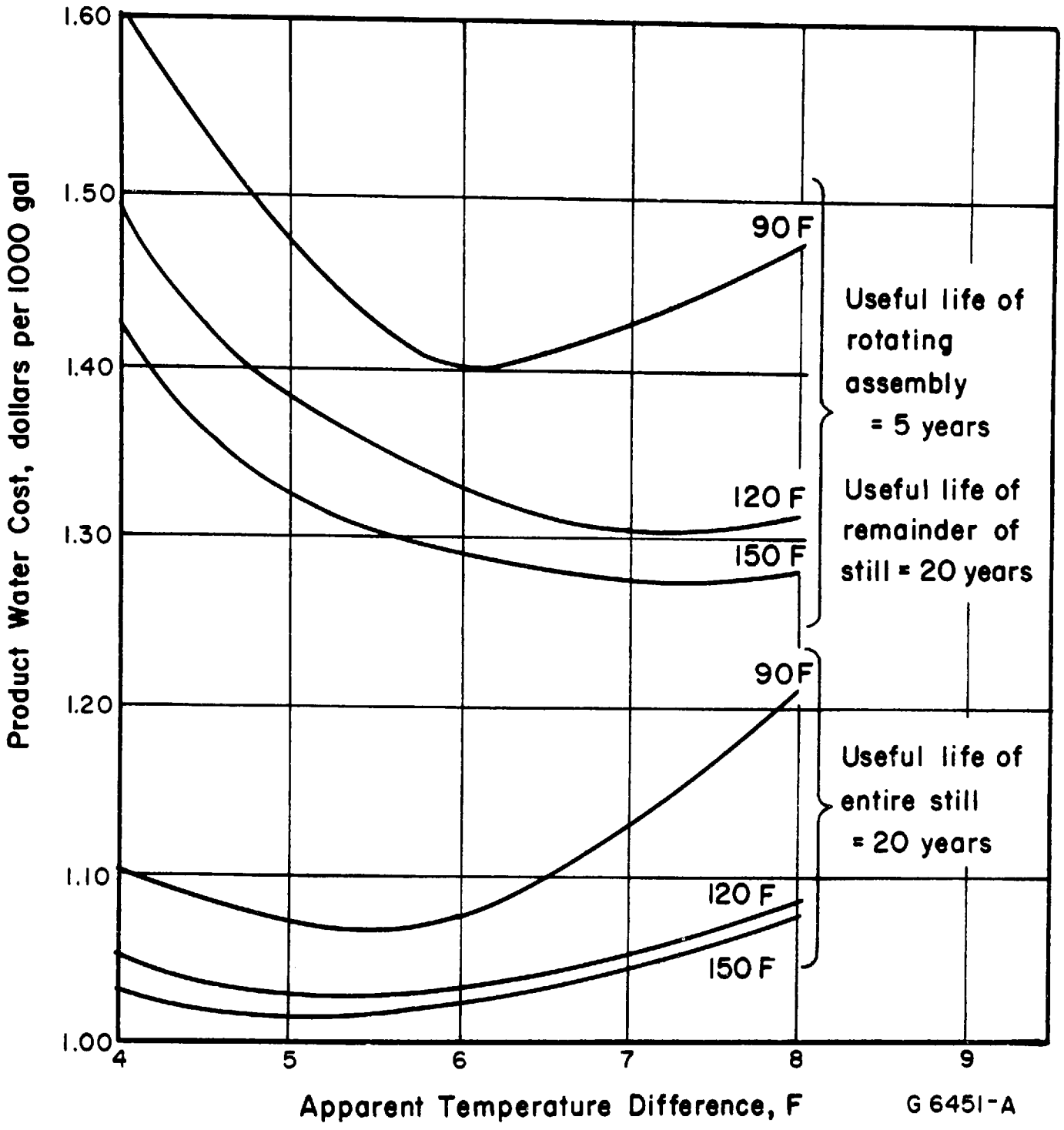

FIGURE 21. PRODUCT-WATER COST FROM A 100,000-GALLON-PER-DAY STILL AS A FUNCTION OF EVAPORATING TEMPERATURE AND TEMPERATURE DIFFERENCE

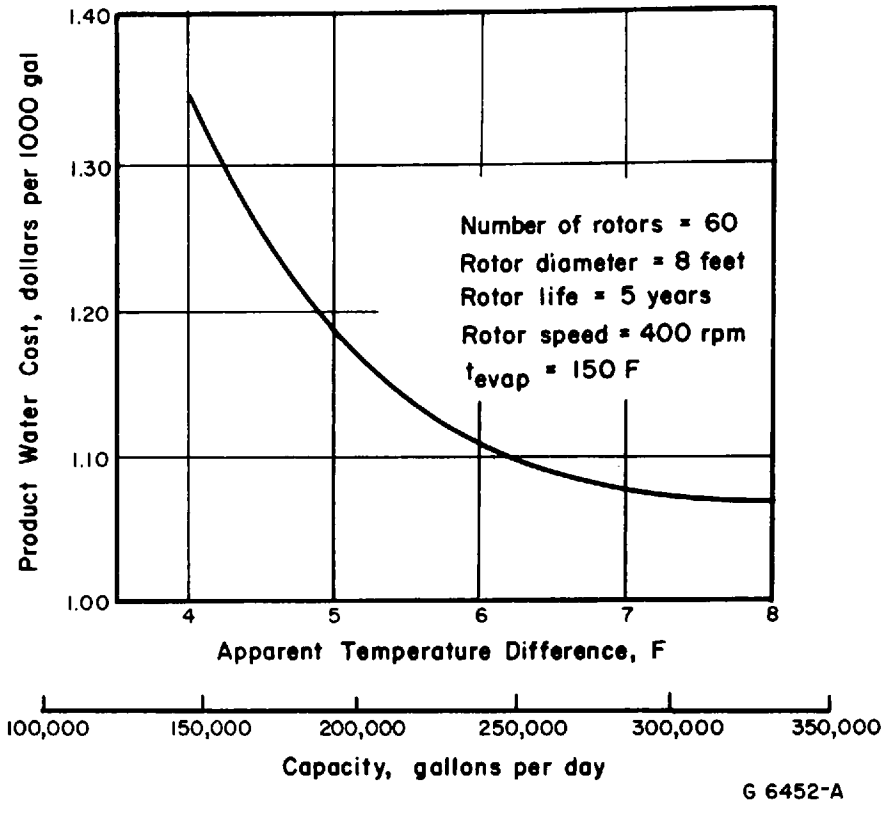

FIGURE 22. PRODUCT-WATER COST FOR A STILL OF MAXIMUM SIZE

Figure 23 shows the relative costs of the various items which would make up the total operating cost for a typical plant of 100,000-gallons-per-day capacity at 150 F and 332,000-gallons-per-day capacity at 150 F. Clearly, the two largest cost items are power and evaporator amortization. Both of these cost items are related to evaporator cost in that the lower the cost of the heat-transfer surface, the lower the optimum compressor power requirements.

However, it should be remembered that until a large still is built and tested it is only possible to estimate the critical shaft speed. Also, it may not be possible to operate an 8-foot-diameter rotor of the design shown in Figure 20 with temperature differences above 6 degrees F because of the resulting high pressure differences. Therefore, at this time, it appears reasonable to assign to a single rotor column an upper capacity limit of 175,000 gallons per day. Such a still would be a 50-rotor unit operating at a temperature difference of 6 degrees F and at an evaporating temperature of 120 F.

Figure 24 shows the influence of rotor speed on the operating costs of a 100,000-gallons-per-day still. The primary variables considered in this instance were the amount of power required to drive the rotor and the change in heat-transfer coefficient with rotor speed. The curves are based on operating at the optimum ΔT at each speed. It is interesting that the range of minimum cost is fairly wide, extending from 400 to 600 rpm. No correction was included for the change in cost of the rotating assembly as the speed, and consequently the stress in the rotating parts, varied. A correction of this type would make the lower speeds appear slightly more favorable. Thus it appears that the best operating speed is near 400 rpm.

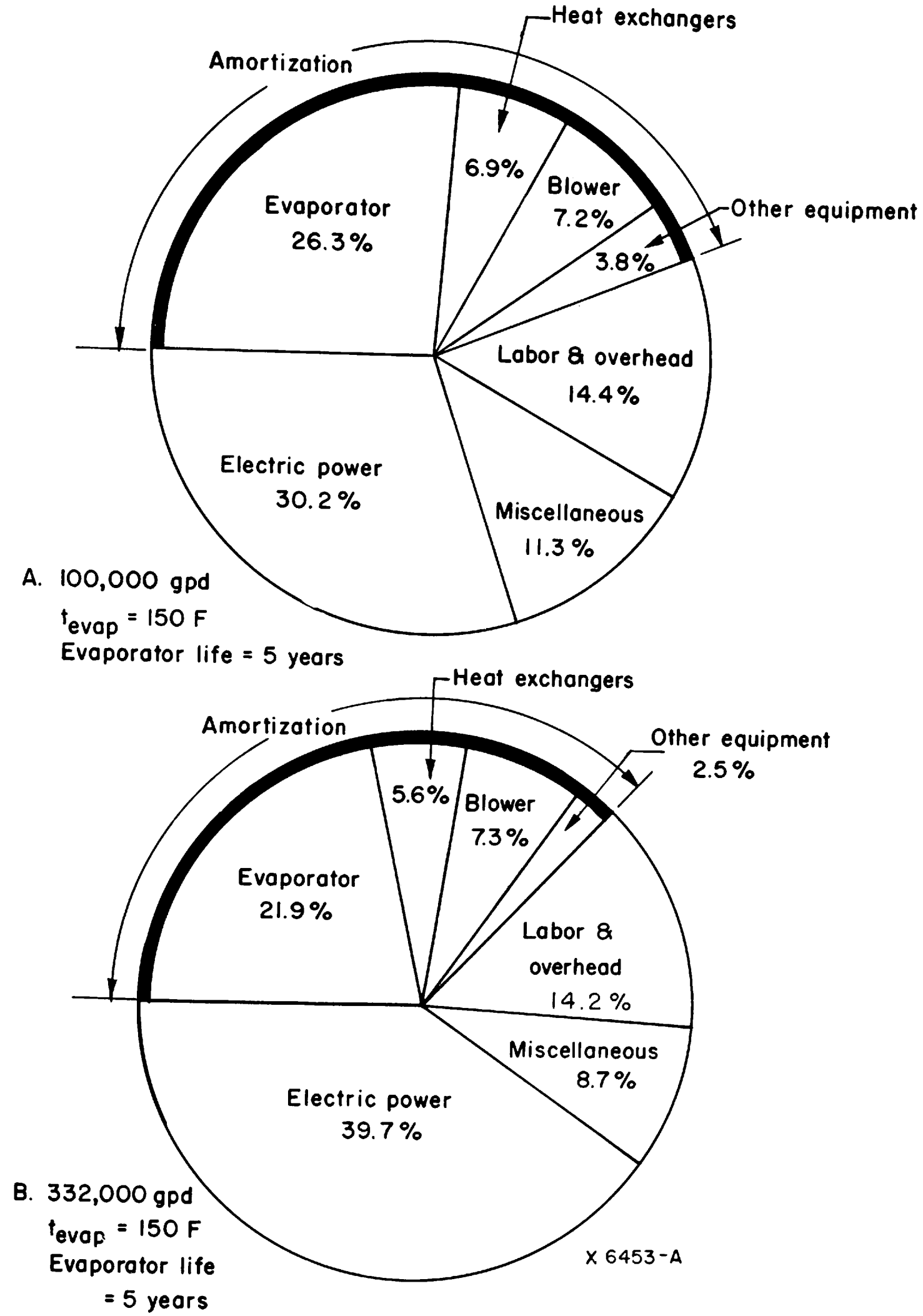

FIGURE 23. BREAKDOWN OF PRODUCT-WATER COST OF HICKMAN STILL

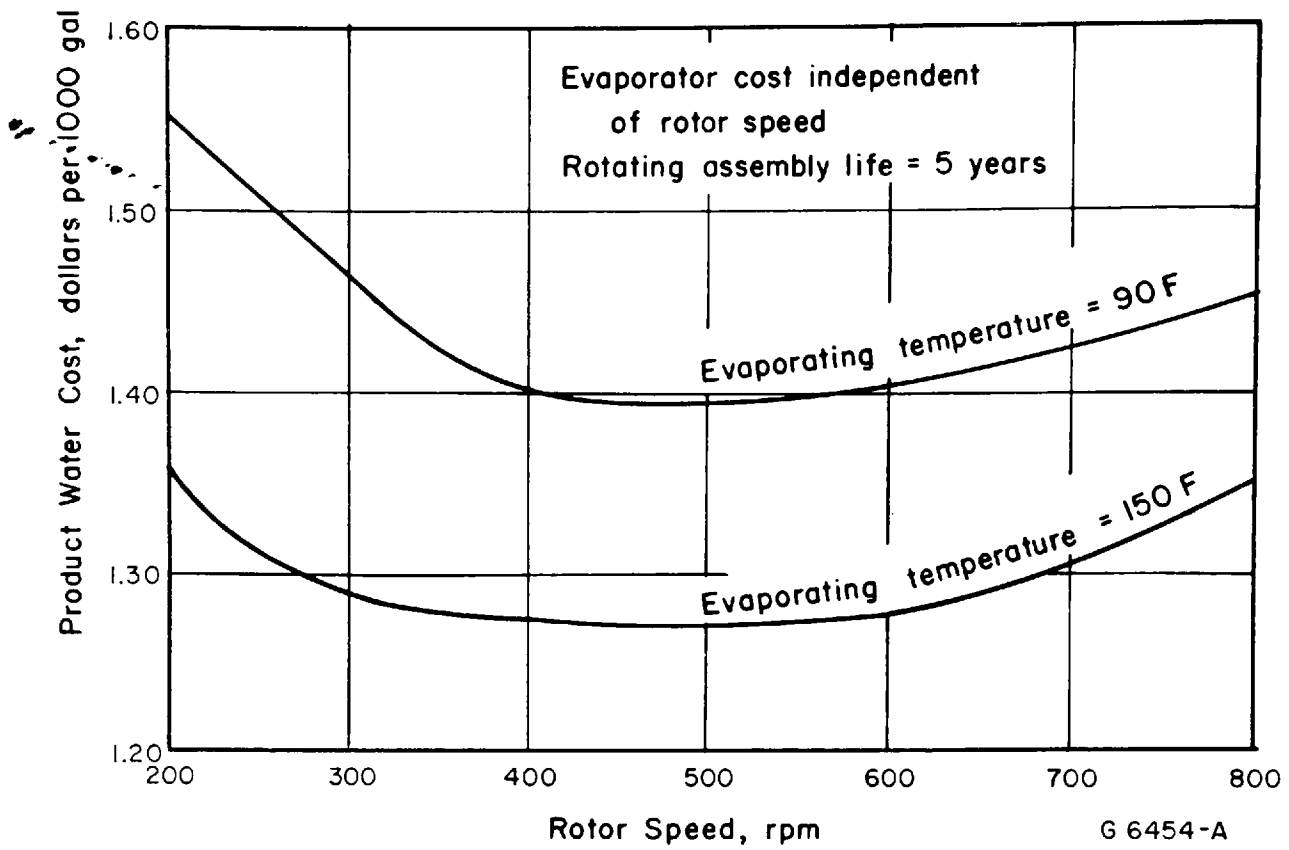

FIGURE 24. PRODUCT-WATER COST AS A FUNCTION OF ROTOR SPEED, FOR A 100,000-GALLONS-PER-DAY PLANT

The assumptions and method of calculation used for the costs presented in this section are described in Appendix C.

HEAT TRANSFER IN A HICKMAN EVAPORATOR

The following discussion of evaporation-condensation heat transfer across a rotating surface is divided into three subsections which deal with the fundamentals of heat transfer, heat-transfer characteristics of the entire rotor, and variations in heat transfer with changes in operating conditions.

Fundamentals of Heat Transfer of a Rotating Disk

In the Hickman evaporator, high heat-transfer coefficients are obtained through the use of a rotating heat-transfer surface. In principle, the spinning surface serves,

through the action of centrifugal force, to spread the condensing and evaporating liquids into thin films which offer relatively little resistance to heat flow. The overall thermal resistance of the system can be thought of as being distributed through a series of layers, each of which offers resistance to heat flow. Starting at the condensing side of the surface, these layers are:

(1) The noncondensable gas layer at the steam-condensate interface
(2) The condensate film on the rotor surface
(3) The contaminants on the condensing surface (oxides or foreign material carried over from the evaporating section)
(4) The metal rotor
(5) The contaminants on the evaporating surface, scale and corrosion products
(6) The film of feed water on the evaporating surface
(7) The substances dissolved in the feed water which influence its boiling-point elevation.

In the following subsections the passage of heat from the high-pressure or condensing side to the low-pressure or evaporating side of the still is discussed starting at the point where the compressed steam enters the condensing cavity. In practice, the steam leaving the compressor contains a very fine aerosol of sea-water carryover and some noncondensable gas. In this discussion, only the effects of noncondensable gas are considered.

Effect of Noncondensable Gas

The amount of noncondensable gas in the condensing steam in a fully developed still is expected to be in the order of 10 or less parts per million by weight. The source of this gas may be either mechanical air leaks or dissolved gas in the seawater feed.

The steam and noncondensable gas which pass from the compressor to the rotor column are assumed to be well mixed. The mixture flows through the center of the rotor column and then into each rotor cavity. As the mixture travels toward the rim of each rotor, the steam continues to condense, with the result that the average concentration of the noncondensable gas increases. Under conditions of laminar flow, the noncondensable gas does not stay freely mixed but rather tends to be trapped in a thin layer next to the condensing surface at the steam-condensate interface (Appendix A). The noncondensable gas in this layer may be pictured as having been deposited by the condensed steam. The growing layer of concentrated noncondensable gas, which travels outward with the remaining steam and resulting liquid film, hinders further condensation. Clearly, the best purge method would be the use of many points of gas removal at the rim of the rotor close to the condensing surface. The No. 4 still's rim-purge system, which is illustrated herein, was designed to accomplish this multiple-point purging. The rim-purge system offers an additional advantage in that some of the purge steam is condensed directly in the purge tube. This action allows part of the purge steam heat to be recovered at the highest possible temperature.

Figure 25, a cross-sectional view of the rim-purge tube that was used in the No. 4 still, shows the flow path of the purge steam and distillate. In operation, purge

steam and distillate entering the purge tube are withdrawn at a number of points around the periphery. In the No. 4 still, four vertical purge-distillate ducts were used. However, it is now felt that two ducts would have been adequate. Purge steam in the vertical ducts passes upward to a central housing, and the distillate is flung off at the bottom of the duct. At the central housing, which is located at the top of the rotor drive shaft in the No. 4 still, the purge steam enters a stationary pipe that leads to the purge condenser. If the sealing diameter at the rotating central housing is kept small, it is expected that this seal will be very effective. With this type of purge system, recirculation of noncondensable gas is reduced to a minimum.

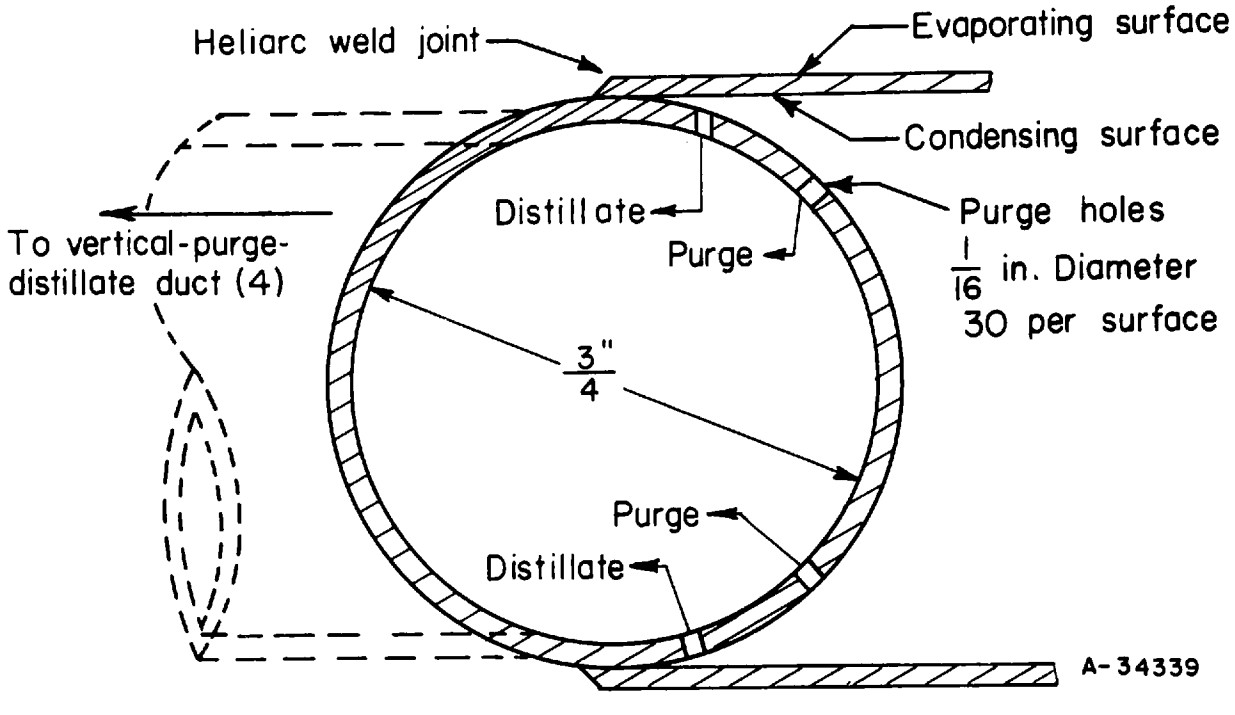

FIGURE 25. RIM-PURGE SYSTEM USED IN THE NO. 4 STILL

Figure 26 shows how the heat-transfer coefficient of the multiple-rotor No. 4 still was affected when varying amounts of nitrogen, a noncondensable gas, were introduced into the condensing cavity. From this figure it may be seen that the condensing rate is not appreciably influenced when the amount of noncondensable gas in the condensing steam is 30 ppm or less. On the basis of these data, a design noncondensable gas contamination level of 10 ppm has been derived. In general, the No. 5 still operated with a noncondensable-gas contamination of slightly less than 100 ppm (Appendix A). This leak rate is considered excessive. The No. 4 still, with an external compressor, operated with steam contamination levels of only 20 ppm. Again considering the data presented in Figure 26, it appears reasonable to assume that, with the level of noncondensable gas in the condensing steam held below 10 ppm, purge rates as low as 0.1 per cent of the steam entering the condensing cavity may be used without retarding condensation. Accordingly, the analytical studies of the evaporation-condensation heat transfer on a rotating surface do not take into account the effects of noncondensable gas on the condensing process. Also, it should be pointed out that a purge rate of 0.1 per cent of the steam entering the condensing cavity is used for calculating heat loss in the cost study.

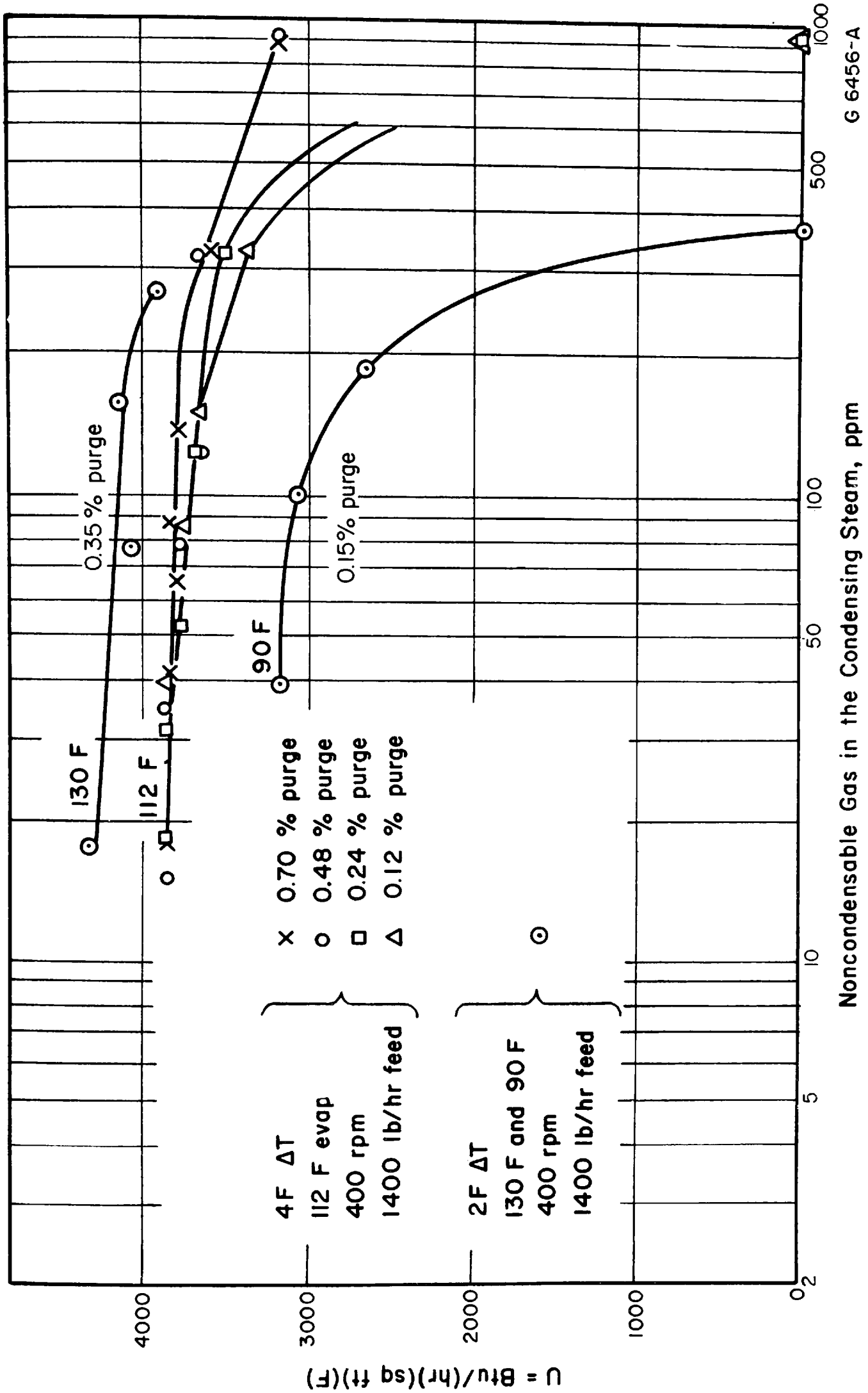

FIGURE 26. THE EFFECT OF NONCONDENSABLE GAS ON THE HEAT-TRANSFER COEFFICIENT OF THE MULTIPLE-ROTOR NO. 4 STILL

Condensate Film

Condensation of steam on the rotor surface may be filmwise, dropwise, or a combination of the two. In the analytical studies, both filmwise and dropwise condensation were considered. However, results of the experimental studies indicate that neither ideal dropwise nor ideal filmwise condensation was obtained in the laboratory. As expected, dropwise condensation gave higher heat-transfer coefficients.

Figure 27 shows the calculated thicknesses of the condensing and feed films on a flat rotor without a center hole. A detailed discussion of the method used in these calculations is presented in Appendix A. In Figure 27, the condensing film is shown as being smooth. After visual inspection of the condensing surface under operating conditions and a study of the flow patterns on the rotor surface during down time, it has been generally concluded that the condensing film does not form a smooth sheet but rather the film tends to break into rivulets. In addition, it is very likely that waves form on the film surface. However, to simplify mathematical calculations, the film resulting from filmwise condensation is assumed to be smooth and in laminar flow. Using these assumptions, the resistance to heat flow offered by the condensate film may be calculated, considering the film as a fixed layer of water. In calculations involving dropwise condensation, the condensing film is considered as having no thickness and thus no thermal resistance.

As is shown in Figure 27, almost half of the thermal resistance of the rotor is attributable to the condensing film. It is therefore logical, in attempting to improve the over-all heat transfer of a rotor, to consider ways of reducing the thickness of the condensing film. To do this, the use of dropwise condensation and condensate dams was evaluated experimentally.

Figure 28 shows the results of this evaluation. It is felt that dropwise condensation occurred on most of the rotor surface as a result of spraying warm sulfamic acid into the condensing cavity while the still was in operation. The sulfamic acid used was a product of Bull and Roberts, Inc., called H-400 Scale Solvent. The exact chemical reaction between the Scale Solvent and copper rotor is not known. However, through the use of test samples it was shown that a copper surface becomes noticeably hydrophobic when treated with warm H-400 Scale Solvent solution. The use of Scale Solvent for increasing heat-transfer coefficient was discovered by accident during an attempt to clean the condensing surface while the No. 4 still was in operation. The beneficial effects obtained with what is thought to be dropwise condensation indicate that over-all heat transfer of a clean rotor can be improved by at least 12 per cent at ΔT of 4 degrees F.

The experiments with the condensate dams were made with the condensate dams placed at several radii on the condensating surface. The condensate dams consisted of strips of copper soldered to the rotor surface. Eight of these strips formed an octagon. Each corner of the octagon was left open to allow the trapped liquid to escape, in a thick stream, to the rim of the rotor. In the tests conducted with the No. 4 still on a 4.5-foot-diameter rotor, five concentric octagons or sets of dams were used. The sets were numbered 1 to 5, starting with the inner set. The No. 1 set was formed around a circle of 10-3/4-inch radius. The radius of the layout circle for each progressively larger set was increased by 3-1/4 inches. During the experiment, the

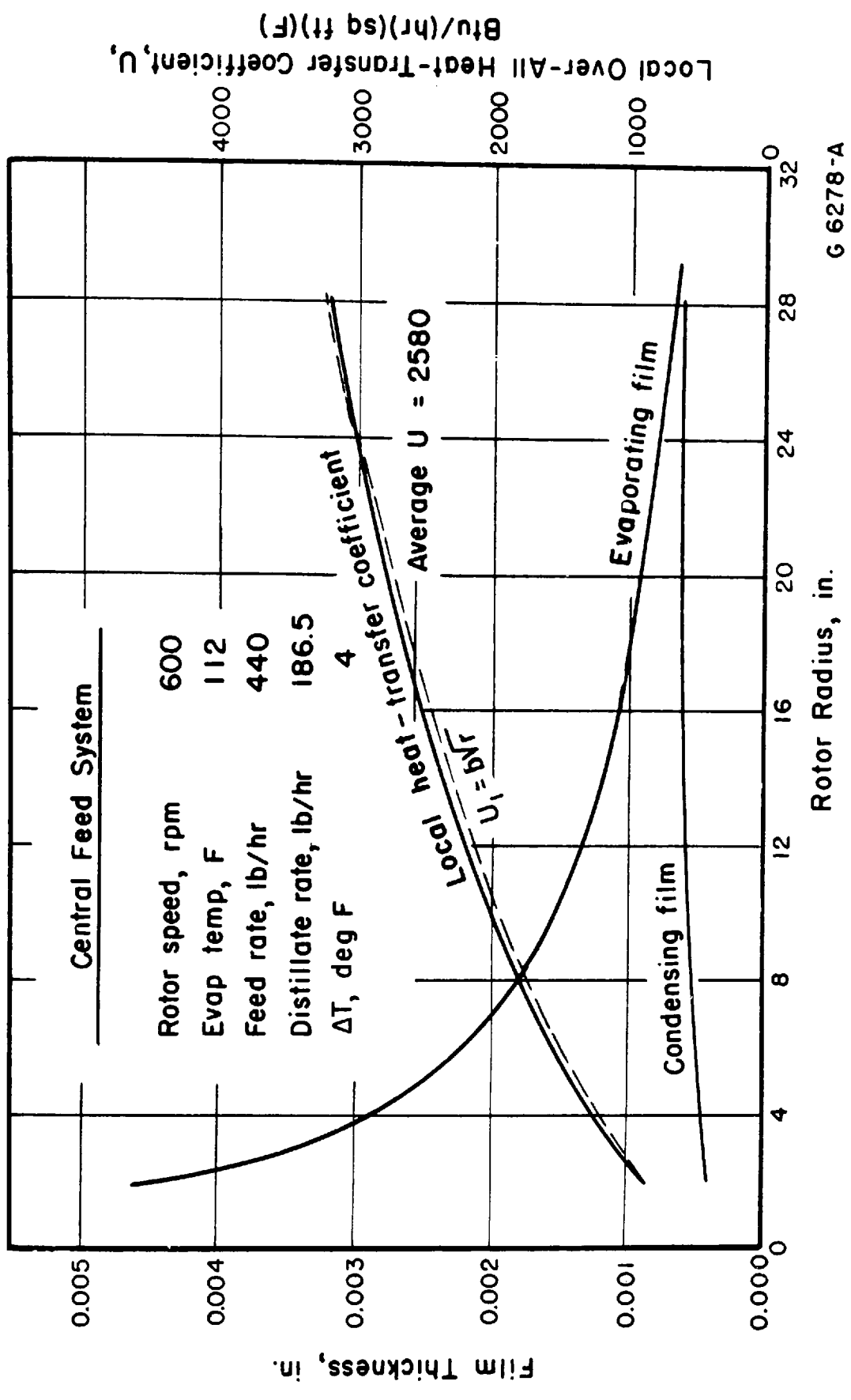

FIGURE 27. CALCULATED FILM THICKNESS AND LOCAL HEAT-TRANSFER COEFFICIENT AT DIFFERENT RADII ON THE ROTOR SURFACE WHEN CENTRAL FEED IS USED

No. 3 set was attached first. Then sets Nos. 1 and 5 were added. Finally, sets Nos. 2 and 4 were added. As shown in Figure 28, none of these arrangements resulted in an improvement in the over-all heat-transfer coefficient of the rotor.

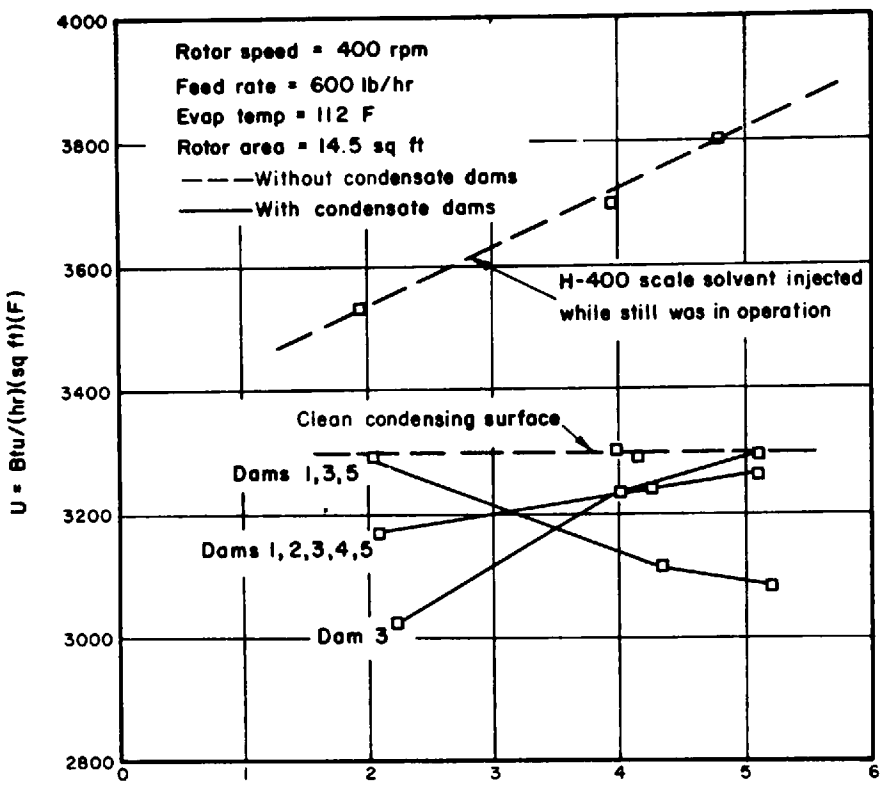

FIGURE 28. EFFECT OF CONDENSATE DAMS AND DROPWISE CONDENSATION

No clear-cut reason for this unexpected result was obtained from the experimental or analytical studies. However, it is believed that the condensate dams were ineffective because the rivulet formation which normally occurs on the condensing surface automatically does what the dams were designed to accomplish. A variation of the condensate dams would be a condensate detacher. This device may be thought of as a backward dam, in that the condensate is lifted from the surface and propelled to the rim. This method was not evaluated as it was felt that results obtained with a single rotor surface would be misleading because the effect of the condensate falling from the upper to the lower surface could not be measured.

Chemical Formations on the Rotor Condensing Surface

During the analytical study, the metal-distillate interface was considered as having no thermal resistance. This may be an oversimplification, particularly when a dropwise promoter is applied to the surface. There is, however, a good possibility that the resistance of this film would be small if a material which will form a tenacious monomolecular layer is found. Another possible source of thermal resistance, but again one which may in practice prove to be rather unimportant, is that attributable to the carry-over of solid substances from the evaporating side.

Figure 29 shows the condensing surface of the single rotor from the No. 4 still. The circular smears on the surface were made after the rotor was disassembled. The many minute radially orientated streaks of interest are the result of iron oxide deposits. It is assumed that this rust came from the blower. Although no specific data are available, the presence of this rust film appears to have retarded heat transfer by only a few per cent.

The Metal Rotor

The thermal resistance of the metal rotor is dependent upon the thickness and the thermal conductivity of the metal. The effective rotor thickness can be determined easily if the rotor surface is sufficiently smooth. The surface-roughness measurements obtained from a typical sample of copper rotor material indicate that the average deviation from a smooth surface is about ±0.000023 inch. The thickness of the feed and condensate films are in the order of 0.001 inch, about 40 times the surface roughness. Thus, for the purposes of the analytical study the metal surface of both the condensing and evaporating side were considered flat and smooth.

Figure 30 shows the effect of thermal conductivity and the thickness of the rotary barrier on the over-all heat-transfer coefficient for centrifugal evaporators. The curves in Figure 30 were plotted by first calculating the condensing and evaporating film coefficients for the present 1/16-inch copper rotor. These calculations were based on over-all coefficients of 1750, 3500, and 7000 Btu/(hr)(ft^2)(F). The film coefficients then were assumed to remain constant and were used to calculate new over-all coefficients using various conductivities and thicknesses for the barrier. The thermal conductivities of a number of corrosion-resistant metals and alloys are shown on the abscissa of Figure 30. These materials are representative of those now commercially available for use in marine equipment. It may be of interest to note that the thermal conductivity of aluminum, which has limited marine application, is about 120 Btu/(hr)(ft^2)(F)/ft. The highest thermal conductivity of the materials considered is much below that of copper.

Deposits on the Rotor Evaporating Surface

It is likely that in practice some thermal resistance will be added at the evaporating surface. Although it is expected that an excessive formation of scale can be controlled, the use of protective films, platings, or coatings to preserve the life of the rotor may reduce heat transfer somewhat. The expected useful life of the copper

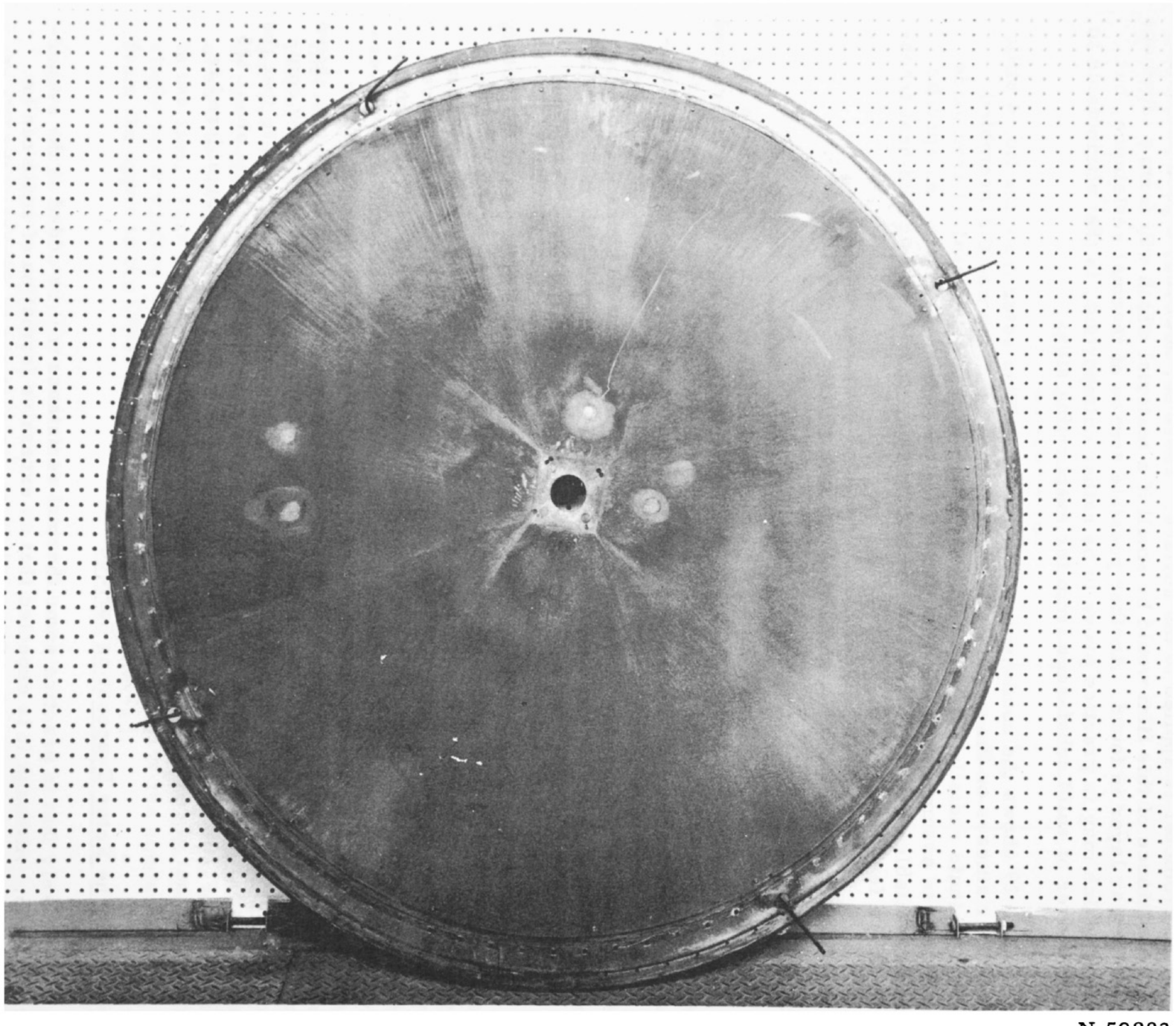

N 59883

FIGURE 29. "DIRT" DEPOSITS ON THE CONDENSING SURFACE OF THE SINGLE ROTOR OF THE NO. 4 STILL

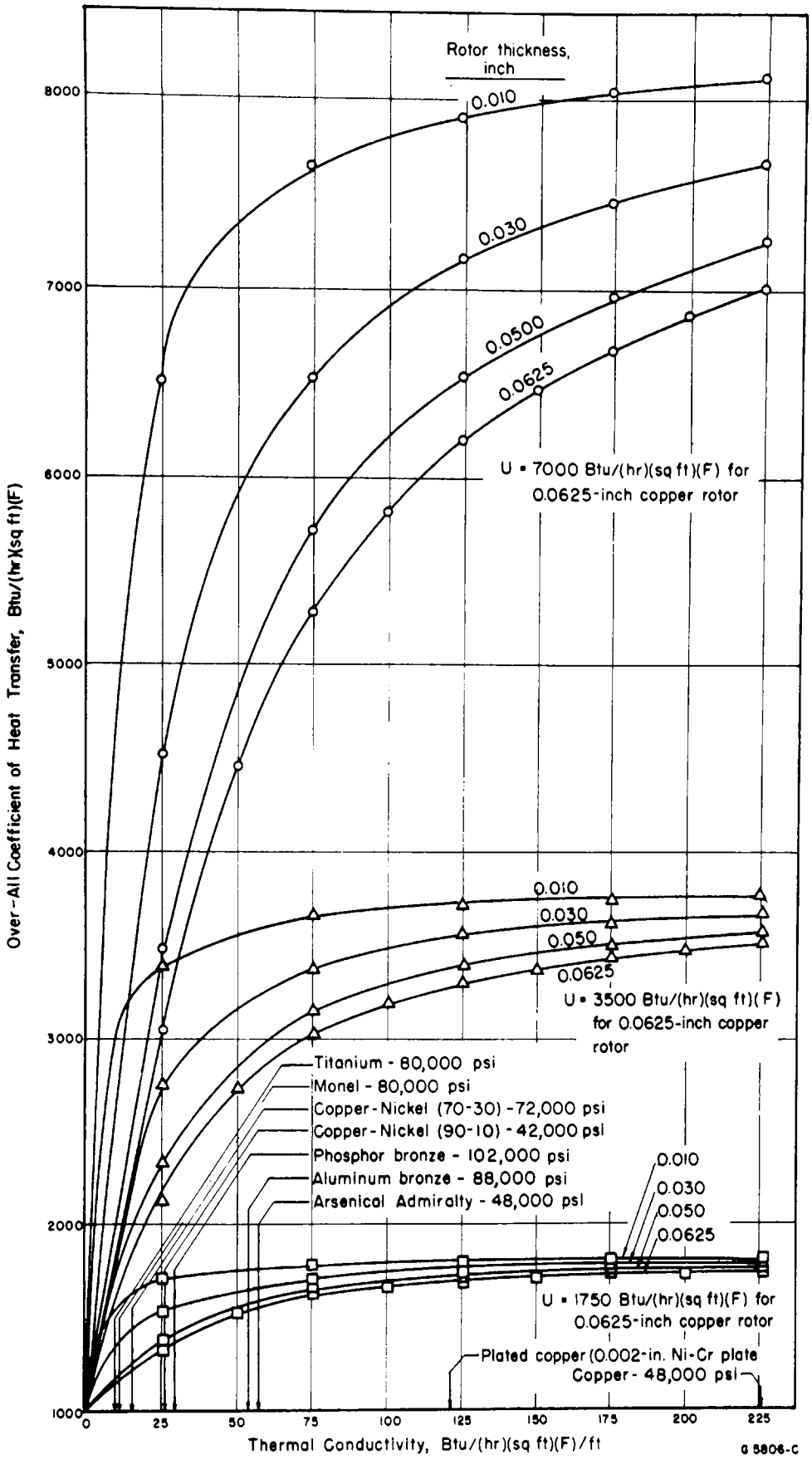

FIGURE 30. RELATION OF THERMAL CONDUCTIVITY AND THICKNESS OF ROTOR TO OVER-ALL COEFFICIENT OF HEAT TRANSFER

rotor and the general subject of corrosion and rotor materials are discussed in the Recommendations Section of this report. The formation of scale on the rotating heat-transfer surface has not been investigated to a significant extent. Figure 6b shows that, during the 72-hour run with sea water, the yield of the No. 5 still did not decrease significantly. Of course, in terms of the time that is generally considered necessary for obtaining realistic data on scaling, 72 hours would be little more than warm-up time. Early investigators have obtained data which indicate that scale will not form on a rotor surface which is completely covered with feed water. Although little is known about the magnitude of effects that can be expected from scale, corrosion products, or protective coatings on the metal surface, it is known that the data obtained with the No. 4 still were not influenced appreciably by these surface deposits. During the experimental program, the plain copper rotors were frequently cleaned with citric acid and steel wool. Accordingly, as during the study of the condensing side, the analytical study did not take into consideration thermal resistance resulting from deposits on the metal surface.

The Evaporating Film

As was mentioned previously, with a conical rotor it was found that the feed-water film broke into rivulets and that because of this rivulet formation areas of the rotor near the periphery were completely dry. Even though several different feed methods, such as using fog nozzles, radial spargers, and circumferential distribution, were tried, the rivulet condition persisted. Because of this, the evaporating film was considered to be the controlling factor in the performance of the Hickman evaporator. As experimental work with the 4-1/2-foot-diameter flat rotor progressed, it became apparent that a flat rotor could be wetted much more easily than a conical rotor in the speed range of interest. After this had been established, only the more compact flat rotors were studied. The studies showed that a 4-1/2-foot-diameter rotor could be completely wetted with a central feed system even at very low feed rates.

Figure 31 shows the calculated velocity and thickness of the feed film under nonevaporating conditions. If it is assumed that laminar flow exists within the liquid layer, that the direction of flow is practically radial, and that the film is free of waves, the feed-film thickness and mean radial velocity may be calculated.[4] However, through visual observation, it was determined that the feed flow, at least at the point of supply, is not laminar and radial. Also, it was observed that small or mild waves form on the film surface.

Even taking into consideration the fact that the actual film thickness differs somewhat from that shown in Figure 31, it is still apparent that the film is thicker at the center than at the rim of the rotor. One would expect that if the feed water were supplied at several different points rather than entirely at the center of the rotor, a more uniform evaporating film would result. Experimentally it was shown that, with fresh-water feed and a single flat rotor, the multiple-nozzle system gave heat-transfer coefficients about 15 per cent above those obtained with a central feed (Figure 15). Where the rotor has a large center hole, the heat-transfer advantage of the multiple-nozzle feed system over that of a system in which the feed is supplied only at the inter-most radius is not as pronounced as with the solid rotor. With the multiple-rotor system of the No. 4 still and salt-water feed, the difference between the central and multiple-nozzle feed systems was only about 4 per cent.

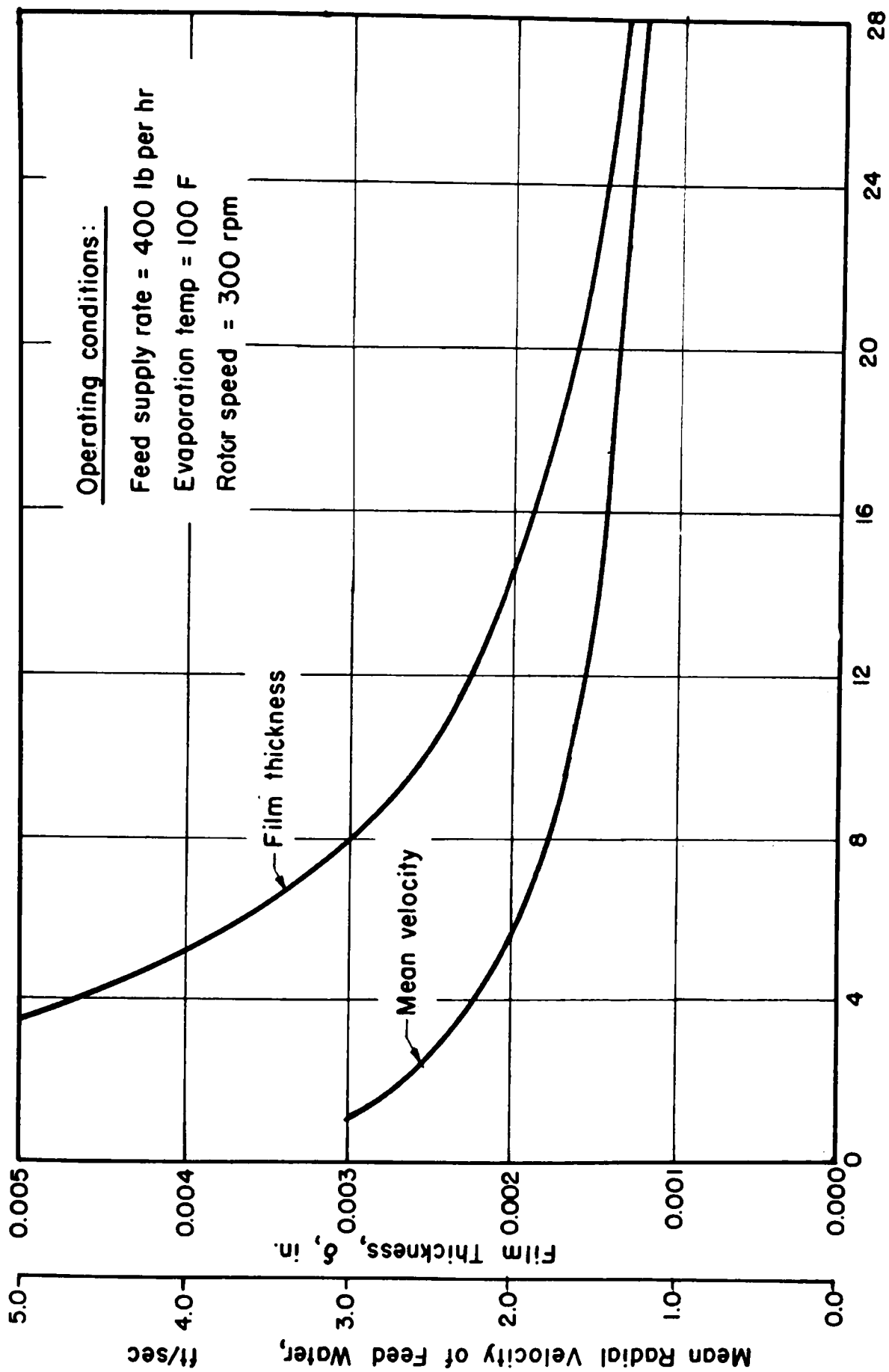

FIGURE 31. CALCULATED VALUES OF FILM THICKNESS AND MEAN LIQUID VELOCITY FOR A FLAT ROTOR

Boiling-Point Elevation of the Feed Liquid

At any given pressure, the boiling point of a salt solution is higher than the boiling point of pure water. This temperature increment is called the boiling-point elevation (bpe) of the solution. The more concentrated the salt solution, the higher the bpe. At 112 F, a 3.5 per cent salt solution has a bpe of 0.57 degrees F; whereas a 7.0 per cent solution has a bpe of 1.3 degrees F. In the case of a central feed system, the salt concentration of the feed water increases as the evaporating film travels outward across the rotor surface. Therefore, the over-all average bpe must be greater than that of the salt-water feed. In the past, this average bpe has been approximated by the arithmetical average of the bpe of the feed water and the bpe of the residue. In view of the apparent accuracy of available data, this approximation seems reasonable. Within limits, the average bpe can be controlled by increasing or decreasing the feed rate, thereby changing the concentration of the residue, that is, the higher the feed rate, the lower the average bpe.

Figure 32 compares the performance of the No. 5 still for fresh-water and sea-water feeds. The heat-transfer coefficients obtained with sea-water feed have been corrected for boiling-point elevation. Still, these values are consistently about 10 per cent below those obtained with fresh-water feed. Figure 18 shows how changes in fresh-water and salt-water feed rates affect the heat-transfer coefficient and distillate yield of the No. 4 still. The 3.5 per cent salt solution used for these tests was prepared by using distillate and chemically pure sodium chloride. This procedure was used in order to eliminate the possibility of side effects produced either by minerals in the city water or by impurities in ordinary salt. In general, heat-transfer coefficients for the 3.5 per cent salt-solution feed, corrected for bpe, were about 7 per cent below those obtained for fresh-water feed.

Data obtained earlier with the No. 5 still showed that heat-transfer coefficients for sea-water feed were about 10 per cent below those obtained for fresh-water feed. At the time the data from the No. 5 still were obtained, it was thought that the 10 per cent difference was due either to the presence of noncondensable gas in the system or to poor feed distribution. Both of these possibilities were eliminated in the series of runs of the No. 4 still shown in Figure 18. At present, the exact reason for the 7 per cent difference detected with the No. 4 still is not clear. However, three possible explanations have been suggested. Two of these involve questions relative to the validity of the method used for determining the over-all average bpe. In the following discussion, two salt-concentration gradients are considered; the first is the radial gradient and the second is the gradient perpendicular to the film surface. The present method of using an arithmetic average of the bpe of the feed water and residue may introduce an error because the bpe does not vary with evaporation rate, but rather with the concentration of the residue. Calculations show that under normal conditions use of the arithmetic average method introduces about a 1 per cent error. Another possibility is that a salt concentration gradient develops across the evaporating film. This gradient would result from the combined effects of a relatively high rate of evaporation and a relatively low diffusion rate of sodium chloride in the salt-water film. A gradient of this nature in the perpendicular direction would cause the actual bpe at a point on the surface of the film to be slightly higher than the bpe resulting from a film of uniform concentration.

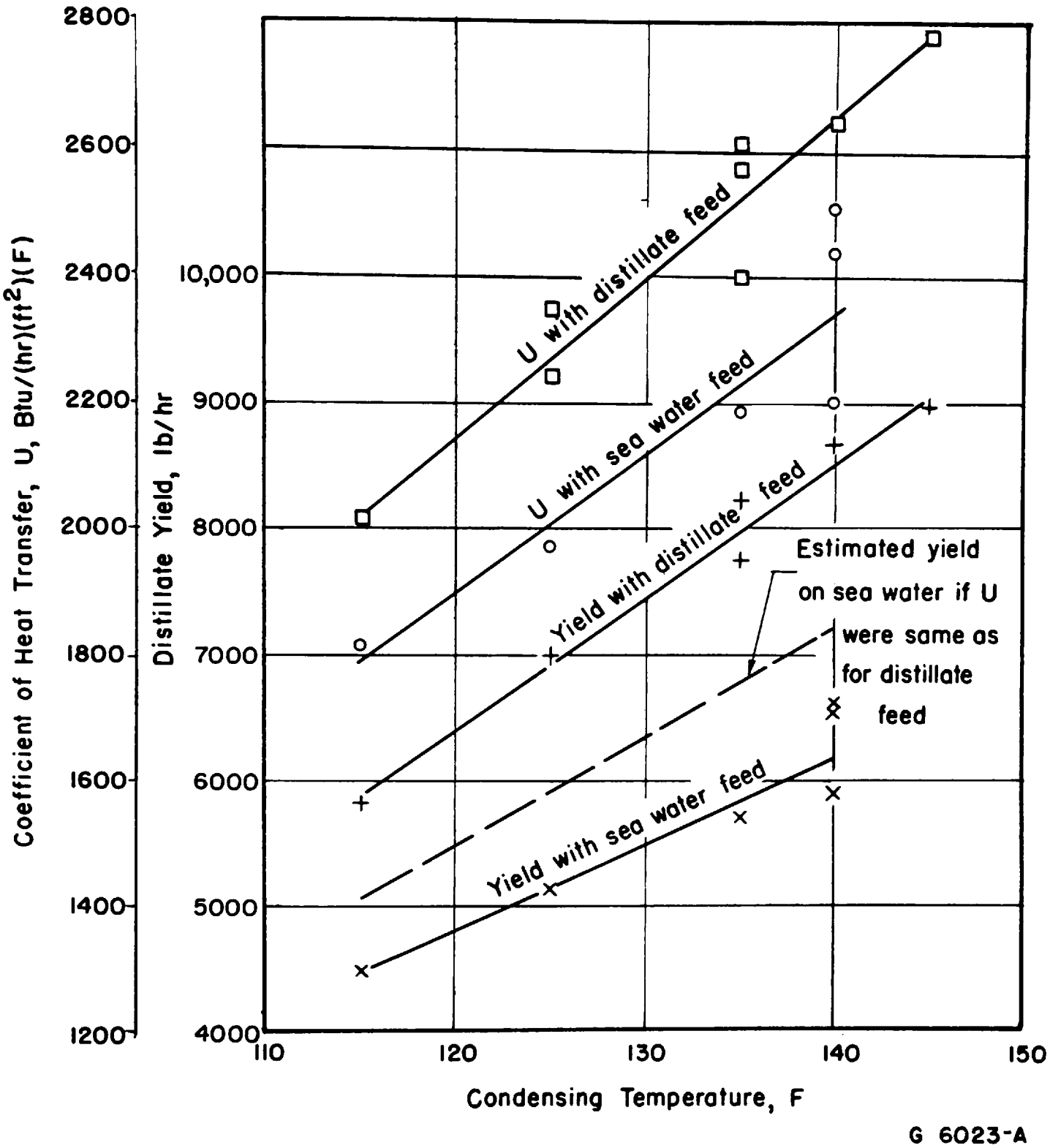

FIGURE 32. COMPARISON OF THE PERFORMANCE OF THE NO. 5 STILL WITH DISTILLATE FEED AND SEA-WATER FEED

The results of a preliminary study of the diffusion rate of sodium chloride in the evaporating film are presented in Appendix A.

Another factor related to the difference in heat transfer between salt-water and fresh-water feed may be the physical properties of the two different liquids. A discussion of this subject is also presented in Appendix A. From these two studies it was found that the combined effect of physical-property difference and salt-concentration gradient in the evaporating film may very well be responsible for the lower heat-transfer coefficients obtained with salt-water Feed. However, the calculations are not rigorous enough to constitute a proof.

Over-All Heat-Transfer Coefficient of a Rotating Disk

Both the No. 4 still and the No. 5 still programs have been in part directed toward improving the heat-transfer coefficient of the rotating surface. The experimental work, quite logically, was supported by an analytical study. Through the analytical study it was possible to develop expressions for predicting the over-all heat-transfer coefficient, U, under different operating conditions. Also, an expression was derived for use in estimating the maximum U that is possible with salt-water feed for a given set of operating conditions. The details of these derivations are presented in Appendix A.

Figure 33 shows how heat transfer varies with rotor radius. The experimental data were obtained in the No. 4 still. A detailed explanation of this experiment is also

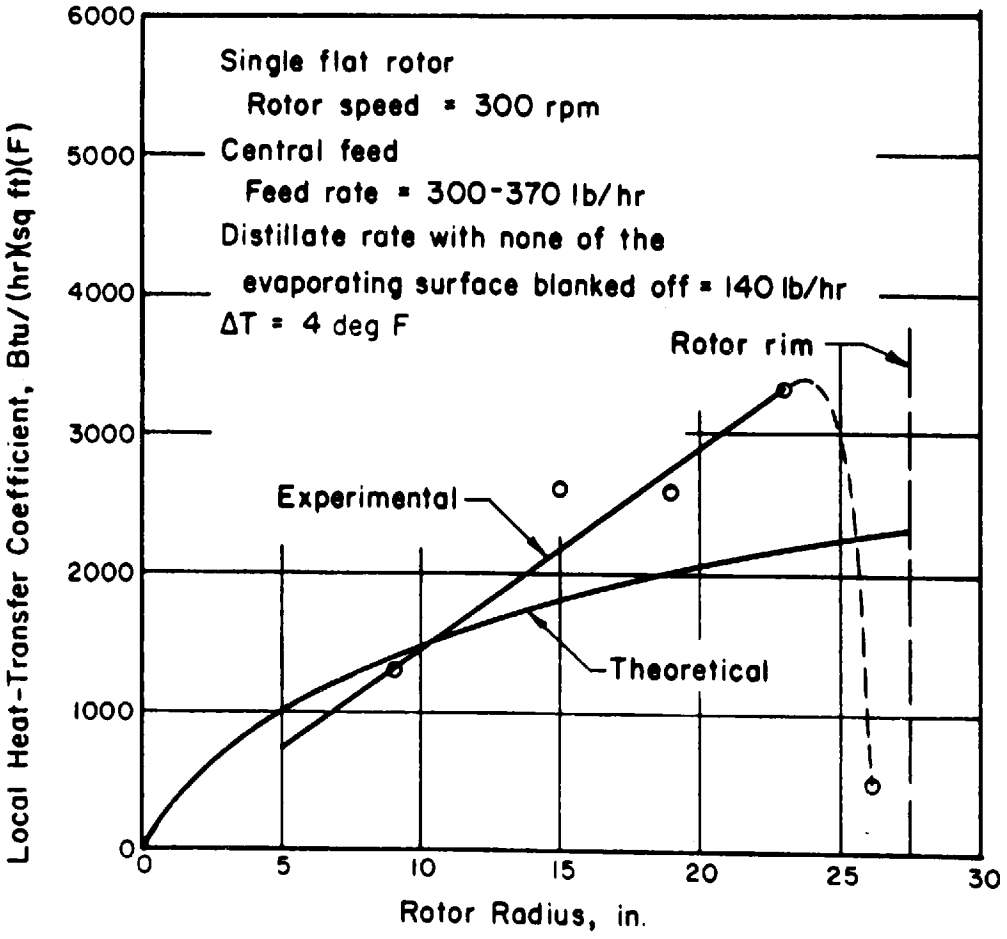

FIGURE 33. VARIATION IN HEAT-TRANSFER COEFFICIENT WITH ROTOR RADIUS

presented in Appendix A. It is felt that the rapid drop-off in heat transfer near the rim of the rotor was caused by an accumulation of noncondensable gas at the rim rather than to a sudden build-up of either the condensate or the feed films. To correct this condition, the rim-purge system was devised (Figure 25). Unfortunately, time did not permit determining the variation of U with rotor radius for a rotor which incorporates the rim-purge system. However, the effectiveness of the purge system was observed by noting the change in performance of the still when varing amounts of noncondensable gas were added. The results of this study are presented in Figure 26.

Effect of Operating Conditions on Heat-Transfer Coefficients

In obtaining data for use in design and cost studies, particularly optimization studies, it is necessary that changes in still performance resulting from variations in operating conditions be known. The following operating parameters have been considered in this research program: rotor speed, evaporating temperature, temperature difference (ΔT), feed rate, and rotor size.

Rotor Speed

Figure 34 shows the variation in theoretical maximum heat-transfer coefficient with changes in rotor speed. The figure, which is based upon a derivation presented in Appendix A, shows how closely the theoretical U_o follows the square root of rotor-speed ratio. The term U_o is a heat-transfer coefficient that is based upon the over-all ΔT minus the boiling-point elevation of raw sea water. In arriving at the values for U_o, dropwise condensation was assumed. The use of this rather unusual notation makes it possible to optimize yield by optimizing the heat-transfer coefficient. This can be done because the yield is related to U_o by a constant. Although the use of a larger center hole increases the α factor and thus appears to improve average U_o which is based on only the active heat-transfer area. This effect may be misleading unless it is remembered that, as far as cost is concerned, the metal removed to form the center hole must be thought of as metal purchased but not used.

Figure 15, presented in the first section of this report, shows how the U of a solid flat rotor varies with speed of rotation. In this instance, constant fresh-water feed was used and film-type condensation occurred. However, because the feed rate was not varied to obtain a constant feed-to-distillate ratio, the increase in U with increasing rotational speed is slightly exaggerated. However, for the present, the square root of rotor-speed ratio (0.5 power) is held to be satisfactory, even though the ratio of rotor speeds to the 0.46 power more closely fits the theoretical curve.

Evaporating Temperature

As the temperature of still operation changes, the physical properties of the evaporating and condensing streams change in the direction that results in an increase in over-all heat-transfer coefficient with increasing temperature.

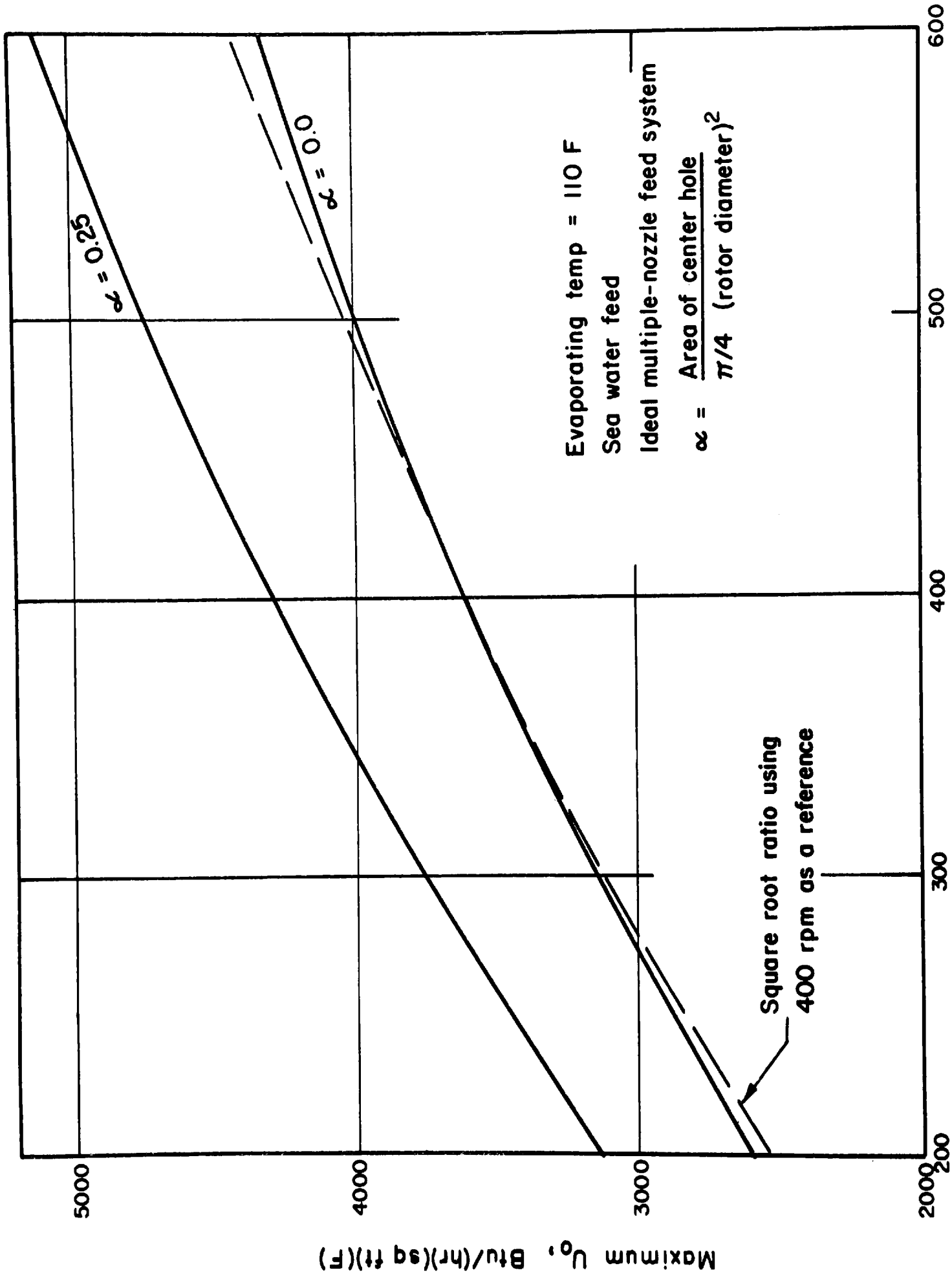

FIGURE 34. THEORETICAL MAXIMUM HEAT-TRANSFER COEFFICIENT VERSUS ROTOR SPEED

Figures 35 and 36 show the relation between operating temperature and heat-transfer coefficient. The data presented in Figure 35 were obtained using fresh-water feed with the multiple-rotor system of the No. 4 still. These data show that U increases about 10 per cent for each 10-degree-F increase in operating temperature. The theoretical curves based on salt-water feed show less than a 5 per cent increase in U_o per 10 degrees F. It is reasonably certain that the difference in increase between the experimental and theoretical trends is not due to the influence of noncondensable gas or physical properties. A more likely explanation for this difference stems from the fact that the theoretical "runs" were made at a variable feed rate, whereas the experimental runs were made at a constant feed rate. Thus, as the evaporation rate increased with temperature, the feed film became thinner; that is, it offered less resistance to heat flow. As a result, the experimental curve reflects not only the changes in physical properties due to temperature change of the feed water but also the changes in thickness of the evaporating film due to increased evaporation. The varying thickness of condensing "film" need not be considered significant in this instance because in both the theoretical and the experimental cases, dropwise condensation was used, and therefore the evaporating film was controlling.

Temperature Difference, ΔT

Figure 28, mentioned previously, shows variations in U with changes in ΔT for a constant fresh-water feed rate. The two curves labled "without condensate dams" describe dropwise and filmwise condensation. The dropwise curve indicates the expected trend of an increase in U with an increase of ΔT. Of course, this trend would continue only until sections of the evaporating surface became dry. The reason for the filmwise condensation curve showing almost no change of U with changes of ΔT is not clearly understood. Although it is certainly of interest to know how U changes with ΔT under conditions of a constant fresh-water feed rate, the more complicated condition of changes in U with changes in ΔT for sea-water feed and constant F/D ratio are of more practical importance. In this instance, the advantage of operating with a low F/D ratio is offset in part by the resulting high boiling-point elevation. No experimental data were obtained specifically for investigating this point. However, in deriving the expression for maximum heat transfer for a rotating surface using salt-water feed, it was found that U_o was independent of ΔT. U_o is defined as over-all heat-transfer coefficient based on apparent ΔT minus the boiling-point elevation of raw sea water. Accordingly, in the cost study the effect of ΔT on heat transfer was not considered as a variable.

Feed Rate

Logically, a higher feed rate, assuming complete coverage of the rotor in all instances, causes a thicker evaporating film; this in turn causes a lower heat-transfer rate. Distillation of fresh water with the highest U then calls for the lowest possible feed rate. In the case of sea-water feed, the situation is somewhat complicated due to boiling-point elevation. Figure 18, in the first section of this report, shows an example of how both yield and U vary with changes in feed rate when sea-water and fresh-water feeds are used. In this instance, the maximum yield from sea water was obtained at a F/D ratio of 2.5/1, whereas the U continued to increase as the feed rate

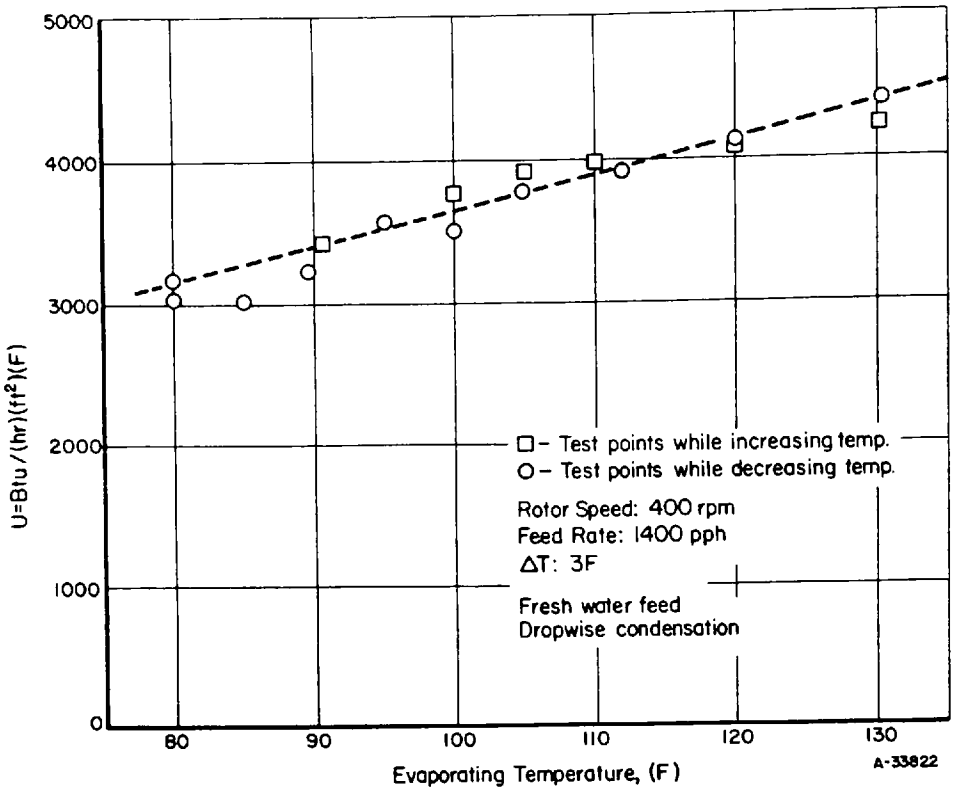

FIGURE 35. EXPERIMENTAL DETERMINATION OF VARIATION IN HEAT-TRANSFER COEFFICIENT WITH CHANGES IN EVAPORATING TEMPERATURE FOR THE MULTIPLE-ROTOR NO. 4 STILL

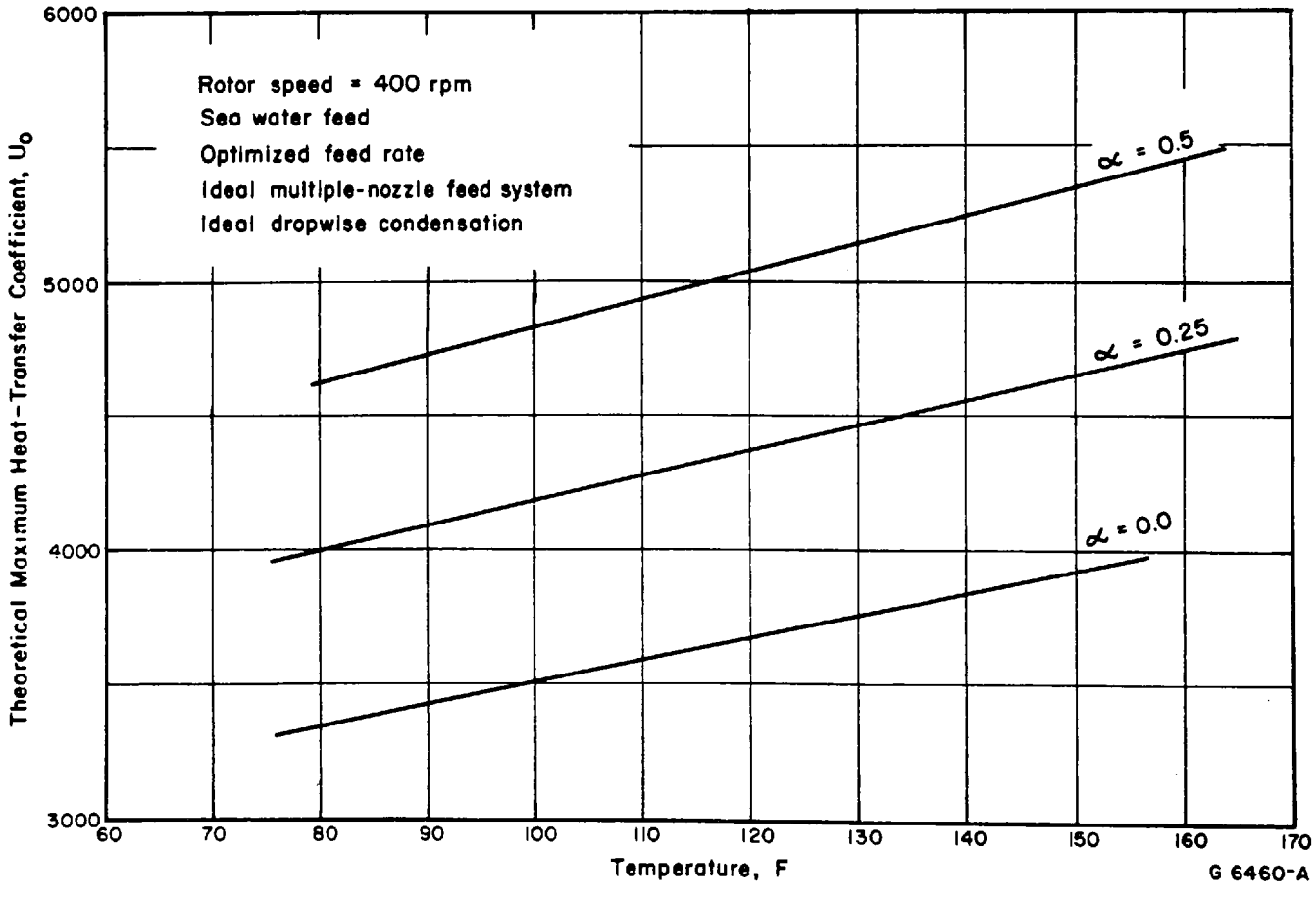

FIGURE 36. THEORETICALLY DETERMINED VARIATION IN HEAT-TRANSFER COEFFICIENT WITH CHANGES IN EVAPORATING TEMPERATURE AND ROTOR GEOMETRY

was further reduced. Theoretically, when sea-water feed is supplied with a multiple-nozzle feed system, the most favorable feed rate is one in which (ΔT-bpe) of the residue and (ΔT-bpe) of raw sea water have a ratio of about 3 to 4. For example, operation at 112 F evaporating temperature and with a ΔT of 4 degrees F calls for a F/D ratio of less than 2/1. For the purposes of the cost study, the more conservative F/D ratio of 2.5/1 was chosen. If, however, the hoped-for lower F/D ratios prove to be practical, a lower product-water cost will result.

In practice, supplying feed water to the evaporating surface is not merely a matter of directing the feed nozzles at the desired radius point on the rotor. If feed water is supplied to the inside of the rotor, as in the case of the No. 5 still, the feed-water jets are continally interrupted by the structural members of the rotor column. If outside feed is used, as in the case of the multiple-rotor No. 4 still, the feed-jet interruptions are caused by the distillate-purge downspouts. In both instances a feed-water "shadow" is left on the rotor surface. For this reason, obtaining a continuous evaporating film requires that the feed water be supplied to each rotor surface by at least two nozzles. A detailed discussion of feed-jet interruption is presented in Appendix B.

Rotor Size

On the basis of both experimental and theoretical studies, it has been concluded that for geometrically similar rotors operating at the same conditions and with identical feed-to-distillate ratios, the over-all average heat-transfer coefficients obtained will be independent of rotor size. At first glance, the data presented in Figure 33 may seem to indicate that larger rotors offer a heat-transfer advantage. However, the data presented in this figure were obtained at a nearly constant feed rate. As a result, the smaller central areas are overfed or flooded while the rotor areas located near the rim are operating under more optimum conditions. Therefore, this type of comparison is not realistic. In the historical section of this report, it was pointed out that the concical rotors in the No. 1 through No. 5 stills gave comparable heat-transfer coefficients even though the rotor diameters varied from 15 in. to 8 ft. Figure A-7 in Appendix A shows a plot of the dimensionless groups $W^{4/3}$ and β, where β is proportional to the heat-transfer coefficient and W is defined as $\left(\frac{kA_o\Delta T_t}{Q_o \lambda \rho}\right)^{3/4}$ times $\left(\frac{2 A_o \omega^2}{3 \nu Q_o}\right)^{1/4}$. If the rotor area, A_o, were doubled and the feed rate, Q_o, were correspondingly doubled to provide the necessary feed, then the increase in feed rate would, in effect, cancel the area increase, with the result, that $W^{4/3}$, and in turn β, would not be modified.

Perhaps the argument that U is independent of rotor size is supported by the basic equation for film thickness.[4] The equation $\delta = \left(\frac{3 Q_o \nu}{2\pi\omega^2 r^2 \cos\theta}\right)^{1/3}$ defines the thickness, δ, of the feed film under nonevaporating conditions. The only terms of interest here are Q and r, feed rate and rotor radius, respectively. When different sized rotor are compared geometricly similar radii (r) must be used. The other terms, which are held constant during this example, are described in the nomenclature of

Appendix A. As r is increased, for example by a factor of two, the area increases by a factor of four. In this example r equals the rotor radius r_o. However, 1/2 r_o, 1/3 r_o, or 15/16 r_o could have been used. To supply adequate feed water to the larger area, Q_o must also be increased by a factor of four. The result is that as Q_o/r_o^2 is changed to $4\,Q_o/(2\,r_o)^2$ and the film thickness at the rotor rim remains constant. This argument, of course, cannot be used if the two rotors under comparison are not geometrically similar. Also, it should be pointed out that this latter presentation does not constitute a proof. It is intended only to provide a means for visualizing possibilities as to why U is independent of rotor radius.

Experimental data on the No. 5 still program are recorded in Battelle Laboratory Record Books Numbers 14193, 14829, and 14829-A. Data and calculations pertaining to the No. 4 still fundamental study are recorded in Laboratory Record Books Numbers 14194, 15741, and 15741-A.

REFERENCES

(1) Office of Saline Water, U. S. Department of the Interior, Research and Development Progress Report No. 12, November, 1956, page 31.

(2) Office of Saline Water, U. S. Department of the Interior, Research and Development Progress Report No. 15, March, 1957, pages 9-10.

(3) "A Standardized Procedure for Estimating Costs of Saline Water Conversion", issued by the Office of Saline Water, U. S. Department of the Interior, March, 1956.

(4) Hinze, J. O., and Milborn, H., "Atomization of Liquids by Means of a Rotating Cup", Journal of Applied Mechanics, June, 1950, pp 145-153.

(5) Sparrow, E. M., and Gregg, J. L., "A Theory of Rotating Condensation", ASME Transactions, 81, Series C (Journal of Heat Transfer), No. 2, May, 1959, p 113.

(6) U. S. Atomic Energy Commission Report No. UCRL-3874 prepared under Contract No. W-7405-eng-48, "Prediction of Performance Characteristics of the Hickman-Badger Centrifugal Boiler Compression Still", LeRoy A. Bromley, July, 1957.

(7) Stepanoff, A. J., Turboblowers, John Wiley and Sons, Inc., New York (1955).

(8) Drew, T. B., Hottel, H. C., and McAdams, W. H., "Heat Transmission", Transactions of the American Institute of Chemical Engineering, 32, 1936, pp 271-305

(9) Koerig, Louis, "Economic Boundaries of Saline Water Conversion", Journal of American Water Works Association, 51, No. 7, July, 1959, pp 845-862.

ACKNOWLEDGMENT

The authors wish to acknowledge the support and cooperation of the staff of the Office of Saline Water, particularly E. A. Cadwallader who monitored the program. E. O. Bransford served as a project engineer during 1958. J. E. Teeter served as laboratory technician during field testing of the No. 5 still at Wrightsville Beach, North Carolina. The field testing of the No. 5 still was performed at the site of the International Nickel Company's Marine Corrosion Test Station which is under the direction of Dr. T. P. May. Dr. K. C. D. Hickman acted as consultant for the experimental studies conducted with both the No. 4 and No. 5 stills.

WLB:WDB:JRI:AAP:JAE/ims:ab:jvo:jdg

APPENDIX A

DERIVATIONS, CALCULATIONS, AND DATA PERTAINING TO THE ROTATING HEAT-TRANSFER SURFACE

The analytical studies have been directed toward determining the manner in which the evaporating and condensing films influence the over-all heat-transfer coefficient of the rotating heat-transfer surface. The ultimate objective is to provide a means whereby the heat-transfer characteristics of any proposed rotor system may be determined without resorting to costly experimental work. This appendix contains derivations of equations for predicting the heat-transfer characteristics of a rotating surface. In addition, calculations and data pertaining to the effect of noncondensable gas on the condensing coefficient are presented.

Experiments with the Hickman stills have shown that the heat-transfer coefficients obtained with sea-water feed are generally about 7 per cent below the coefficients obtained with fresh-water feed. Two factors which may have contributed to this condition, i.e., salt diffusion rate and differences in physical properties, are examined in this appendix.

The two basic fluid-flow equations[4]* which are referred to frequently in this appendix as well as in the text of the report are presented below for convenient reference:

$$\delta = \left(\frac{3 Q_o \nu}{2\pi\omega^2 r^2 \cos\phi} \right)^{1/3}$$

$$V_m = \left(\frac{\omega^2 Q_o^2 \cos\phi}{12\pi^2 \nu^2 r} \right)^{1/3} .$$

Approximate Method for Determining the Evaporation-Condensation Heat Transfer of a Spinning Surface

In an effort to obtain an insight into the flow and heat-transfer conditions on a rotating surface, two different approaches were used. In the first instance, the problem was somewhat oversimplified to facilitate arriving at a quick solution for one set of operating conditions. The second, more refined approach, gave a general solution.

In deriving the following expression, the rotating heat-transfer surface is assumed to present only three barriers to heat transfer: the condensate film (distilled water), the metal rotor (copper), and the evaporating film (distilled water assumed). In this analysis an equation for predicting the condensing-film thickness on a spinning surface is developed for cases in which the condensing rate is uniform[5]. Admittedly, this is not a case in which a central feed system is used on a flat rotor. In fact, in the final expression, the heat-transfer coefficient is considered to vary directly with the

*References appear on page 58.

square root of the rotor radius. However, it is felt that a fair approximation can be made by assuming the film thickness at any point to be dependent only upon the heat flux at that point. For the evaporating film, a somewhat similar assumption is made. In this case, the equations developed by Hinze and Milborn[4] are used without modification. That is, the film thickness at any point depends only on the flow past the point, and not on the upstream conditions.

Derivation

The heat-transfer barrier is considered as consisting of only three layers: the condensing film, the metal rotor, and the evaporating film. The total temperature drop through the barrier is:

$$\Delta T_t = \Delta T_c + \Delta T_m + \Delta T_e \, . \tag{A-1}$$

When fresh-water feed is used, $\Delta T_t = \Delta T_p$ (nomenclature of terms is given at the end of Appendix A).

The relation between heat transfer, temperature difference, and conductivity of each barrier is:

$$J = \frac{k \Delta T A_t}{\delta} \text{ or } q = \frac{k \Delta T}{\delta} \tag{A-2}$$

Then

$$\Delta T = \frac{q \delta}{k} \, . \tag{A-3}$$

The temperature difference across the condensing film may be expressed as:

$$\Delta T_c = \frac{q \delta_c}{k_c} \, . \tag{A-4}$$

From Sparrow and Gregg's work[5], the equation for the condensing-film thickness on a spinning flat rotor is:

$$\delta_c \left(\frac{\omega}{\nu} \right)^{1/2} = \left(3/2 \right)^{1/4} \left(\frac{c_p \Delta T_c}{N_{pr} h_{fg}} \right)^{1/4} . \tag{A-5}$$

Combining and rearranging Equations (A-4) and (A-5), δ_c is eliminated from the expression:

$$\Delta T_c = \left[\frac{q^4 \, 3 \mu}{k_c^{\,3} \omega^2 \rho^2 \, 2 h_{fg}} \right]^{1/3} . \tag{A-6}$$

The temperature drop across the metal rotor is expressed as:

$$\Delta T_m = \frac{q\,\delta_m}{k_m} . \tag{A-7}$$

Again, using Equation (A-3), the temperature drop across the evaporating film is:

$$\Delta T_e = \frac{q\,\delta_e}{k_e} . \tag{A-8}$$

From Hinze and Milborn[4], the evaporating-film thickness on a flat spinning rotor is:

$$\delta_e = \left(\frac{3Q\nu}{2\pi\omega^2 r^2} \right)^{1/3} . \tag{A-9}$$

The quantity of water in the evaporating film at any particular radius is equal to the feed rate minus the amount of water evaporated. If the amount of water evaporated is considered to be equal to the amount condensed, the following holds:

$$Q_e = Q_o - Q_c . \tag{A-10}$$

As may be seen in Figure 27 of this report, the local heat-transfer coefficient, U_l, varies almost directly with the square root of the rotor radius. Thus, U_l may be approximated by:

$$U_l = b\sqrt{r} ,$$

where b is a constant.

By definition:

$$q = \Delta T_t\, U_l \text{ or } q = (\Delta T_t)(b)\sqrt{r} . \tag{A-11}$$

When the q expression is integrated over the entire rotor, it becomes:

$$J_o = \int_o^{r_o} q\, dA = \int_o^{r_o} (\Delta T_t)(b)\sqrt{r}\,(2)\,(\pi)\,(r)\,(dr)$$

$$J_o = (4/5)\,(\pi)\,(b)\,(\Delta T_t)[r^{5/2}]_o^{r_o} . \tag{A-12}$$

The more general case is:

$$J = (4/5)\,(\pi)\,(b)\,(\Delta T_t)\,[r^{5/2}]_o^{r} . \tag{A-12a}$$

The constant b may be expressed in terms of the assumed conditions at the rim, r_o, of the rotor:

$$b = \frac{J_o\ (5)}{(4)\ (\pi)\ (\Delta T_t)\ (r_o^{5/2})} = \frac{(U_a)\ (A_t)\ (\Delta T_t)\ (5)}{(4)\ (\pi)\ (\Delta T_t)\ (r_o^{5/2})}$$

$$b = \frac{(U_a)\ (\pi)\ (r_o^2)(5)}{(4)\ (\pi)\ (r_o^{5/2})} = (U_a)\ (5/4)\ (r_o^{-1/2}). \qquad \text{(A-12b)}$$

Eliminating b from Equation (A-12a):

$$J = (U_a)\ (5/4)\ (r_o^{-1/2})\ (\Delta T_t)\ (4/5)\ (\pi)\ (r^{5/2})$$

$$J = (\pi)\ (\Delta T_t)\ (r_o^{-1/2})\ (U_a)\ (r^{5/2})\ . \qquad \text{(A-13)}$$

The volume flow of distillate at any radius on the rotor is:

$$Q_c = J/(h_{fg})\ (\rho)\ . \qquad \text{(A-14)}$$

Combining Equations (A-13) and (A-14), the flow at r is obtained:

$$Q_c = \frac{(\pi)\ (\Delta T_t)\ (U_a)\ (r^{5/2})}{(r_o^{1/2})\ (h_{fg})\ (\rho_c)}\ . \qquad \text{(A-15)}$$

Using (A-9), (A-10), and (A-15):

$$\delta_e = \left[\frac{(3)\ (\mu_e)\left(Q_o - \dfrac{(\Delta T_t)\ (\pi)\ (U_a)\ (r^{5/2})}{(r_o^{1/2})\ (h_{fg})\ (\rho_c)} \right)}{(2)\ (\pi)\ (\omega^2)\ (r^2)\ (\rho_e)} \right]^{1/3}\ . \qquad \text{(A-16)}$$

An expression that contains variables of only the local heat flux, q, and rotor radius, r, may be obtained by combining and rearranging Equations (A-1), (A-6), (A-7), (A-8), and (A-16):

$$\Delta T_t = \left[\frac{q}{k_e} \right] \left[\frac{(3)\ (\mu)\left(Q_o - \dfrac{(\Delta T_t)\ (\pi)\ (U_a)\ (r^{5/2})}{(r_o^{1/2})\ (h_{fg})\ (\rho)} \right)}{(2)\ (\pi)\ (\omega^2)\ (r^2)\ (\rho)} \right]^{1/3} +$$

$$\frac{(q)\ (\delta_m)}{(k_m)} + \left[\frac{(q^4)\ (\mu)\ (3)}{(k_c^3)\ (\omega^2)\ (\rho^2)\ (2)\ (h_{fg})} \right]^{1/3}\ . \qquad \text{(A-17)}$$

Example Problem

For this example a 56-inch-diameter flat rotor without a center hole will be used. The central feed rate will be considered 440 lb/hr and an evaporating temperature of 112 F will be assumed.

Design Parameters.

$c_p = 0.998$ Btu/(lb)(F)

$h_{fg} = 1029$ Btu/lb

$k_e = 0.366$ Btu/(hr)(ft^2)(F/ft)

$k_c = 0.366$ Btu/(hr)(ft^2)(F/ft)

$k_m = 224$ Btu/(hr)(ft^2)(F/ft)

$Q_o = (440 \text{ lb/hr})/(\rho) = 7.12 \text{ ft}^3/\text{hr} = 3.41 \text{ in.}^3/\text{sec}$

$r_o = 28/12 = 2.333$ ft

$\Delta T_p = 4F = \Delta T_t$

$\delta_m = 0.062$ in.

$\mu = 1.41$ lb/(hr)(ft)

$\rho = 61.8$ lb/ft^3

$\omega = 600$ rpm $= 20\ \pi$ radian/sec $= (7.2)(\pi)(10^4)$ radian/hr.

Analysis. For the first approximation, U_a is taken as 2800 Btu/(hr)(ft^2)(F) and U_l is assumed to vary with the square root of the rotor radius. The thickness of the evaporating film is determined by substituting into Equation (A-16):

$$\delta_e = \left[\frac{(3)\ (1.41) \left(7.12 - \dfrac{(4)\ (\pi)\ (2800)\ (r^{5/2})}{(2.33)\ (1029)\ (61.8)} \right)}{(2)\ (\pi)\ (7.2^2)\ (\pi^2)\ (10^8)\ (r^2)\ (61.8)} \right]^{1/3}$$

$$\delta_e = \frac{[1.517 - (0.0507)\ (r^{5/2})]^{1/3}}{(10^4)\ (r^{2/3})}$$

A plot of δ_e is shown in Figure 27 of the report. Substituting the above expression for δ_e into Equation (A-8), the following is obtained:

$$\Delta T_e = \frac{(q)\,[1.517 - (0.0507)\,(r^{5/2})]}{(0.366)\,(r^{2/3})\,(10^4)}^{1/3} ,$$

$$\Delta T_e = (q)\,(2.73)\,(10^{-4})\,(r^{-2/3})\,[1.517 - (0.0507)\,(r^{5/2})]^{1/3} .$$

Figure A-1 shows plots of ΔT_e versus q for several different radii. Also shown in Figure A-1 are curves for ΔT_m versus q and ΔT_c versus q. By using Equation (A-7), the following expression for ΔT_m versus q is obtained:

$$\Delta T_m = \frac{(q)\,(0.062)}{(12)\,(224)} = (2.30)\,(10^{-5})\,(q) .$$

An expression of ΔT_c in terms of q is obtained by substituting into Equation (A-6):

$$\Delta T_c = \left[\frac{(q^4)\,(1.41)\,(3)}{(0.366^3)\,(7.2^2)\,(\pi^2)\,(10^8)\,(61.8^2)\,(2)\,(1029)} \right]^{1/3}$$

$$= (q^{4/3})\,(0.599)\,(10^{-5}) .$$

Because

$$\Delta T_t = \Delta T_c + \Delta T_m + \Delta T_e , \qquad (A-1)$$

ΔT_e may be expressed by

$$\Delta T_e = \Delta T_t - (\Delta T_c + \Delta T_m) = 4 - (\Delta T_c + \Delta T_m) .$$

In Figure A-1, the points of intersection of the radius lines and the curve of ΔT_e versus q define the local heat flux at each particular radius. It is also possible to obtain ΔT_m, ΔT_c, and ΔT_e at the various radii of the sample rotor. The temperature difference across each film is shown in Figure A-2.

Figure A-2 shows to what degree each film and the rotor resist the transfer of heat. This figure presents essentially the same information as is shown in Figure 27, but with a more explanatory arrangement.

Figure A-3, a plot of local heat flux versus rotor area, is made from the graphic solution of the general heat-transfer equation presented in Figure A-1. The total heat flux for the rotor is found by integrating q over the entire rotor surface. The integration can be performed graphically by measuring the area under the curve in Figure A-3. Using this method, the total heat flux for the example rotor is measured at $(1.77)(10^5)$ Btu/hr. The average heat-transfer coefficient then is $U = J/(\Delta T_t)(A_t) = 2580$ Btu/(hr)(ft^2)(F). A plot of U_1 versus r is shown in Figure 27 in the Heat Transfer section of the text.

For the second approximate solution, a value of $U_a = 2580$ Btu/(hr)(ft^2)(F) would be used in determining the evaporating-film thickness. In deriving the second solution, it would be necessary to change only the radius lines in Figure A-1 and then continue as in the above example.

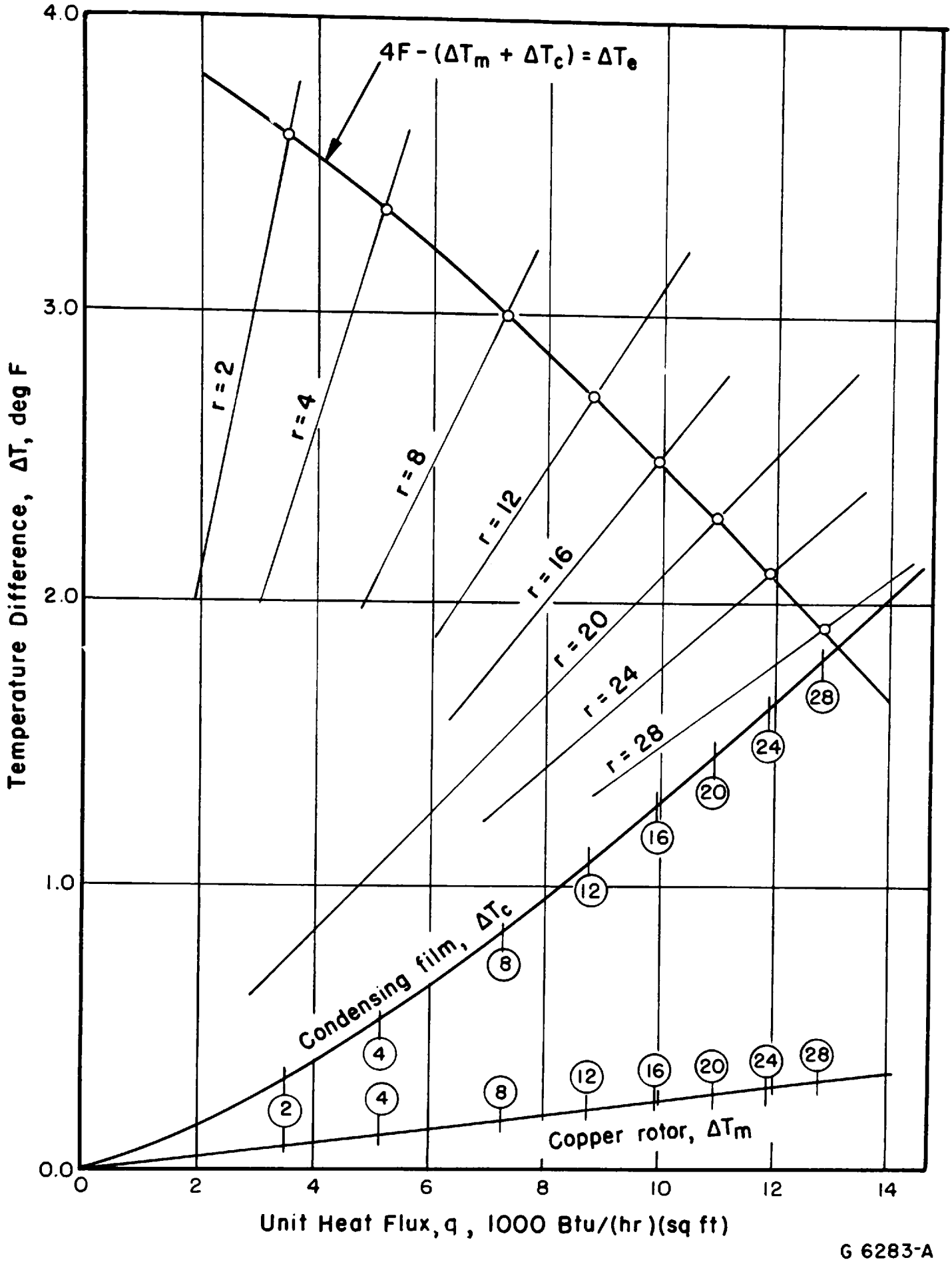

FIGURE A-1. GRAPHIC SOLUTION OF EQUATION A-17

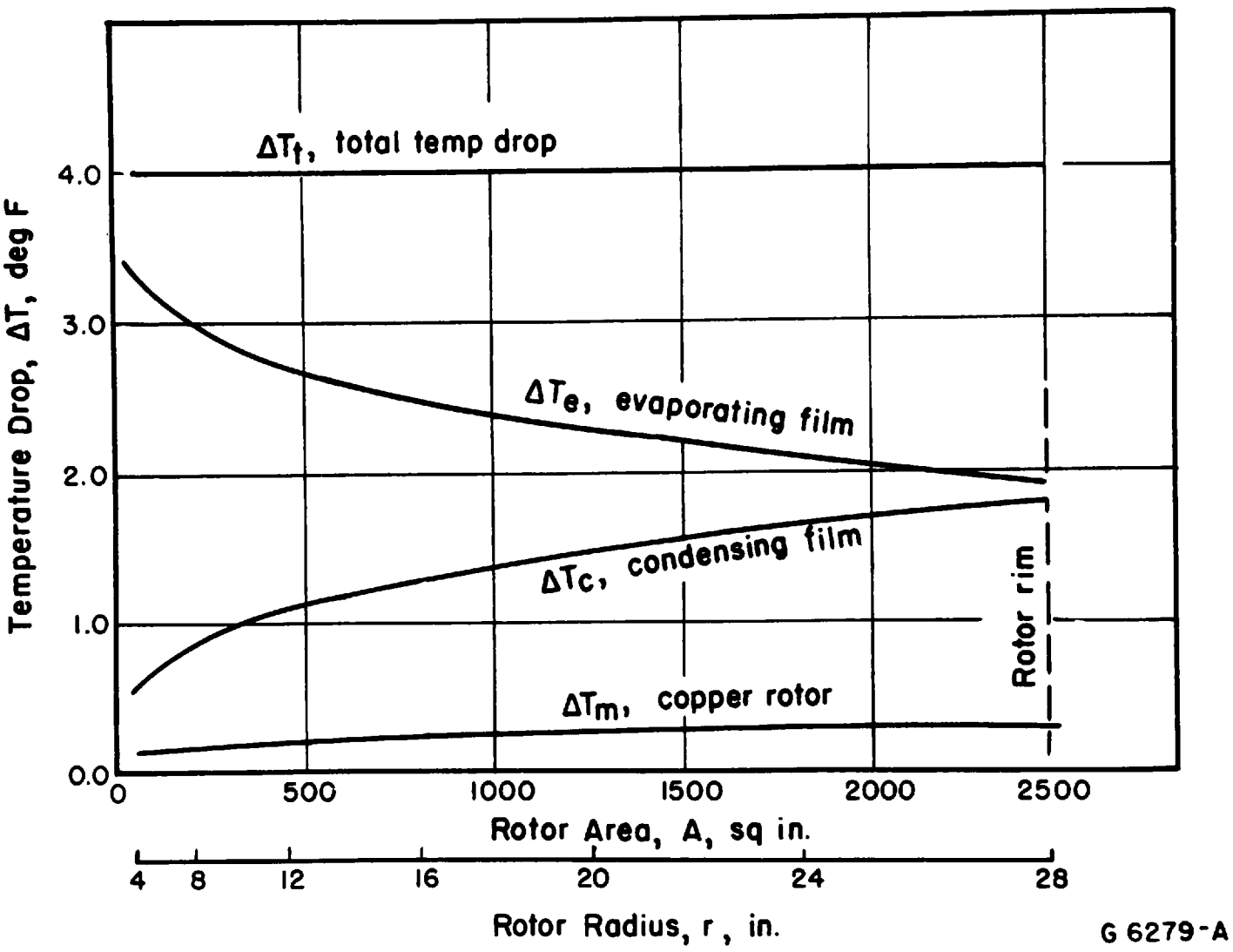

FIGURE A-2. CALCULATED TEMPERATURE DROPS ACROSS THE DIFFERENT HEAT-TRANSFER BARRIERS

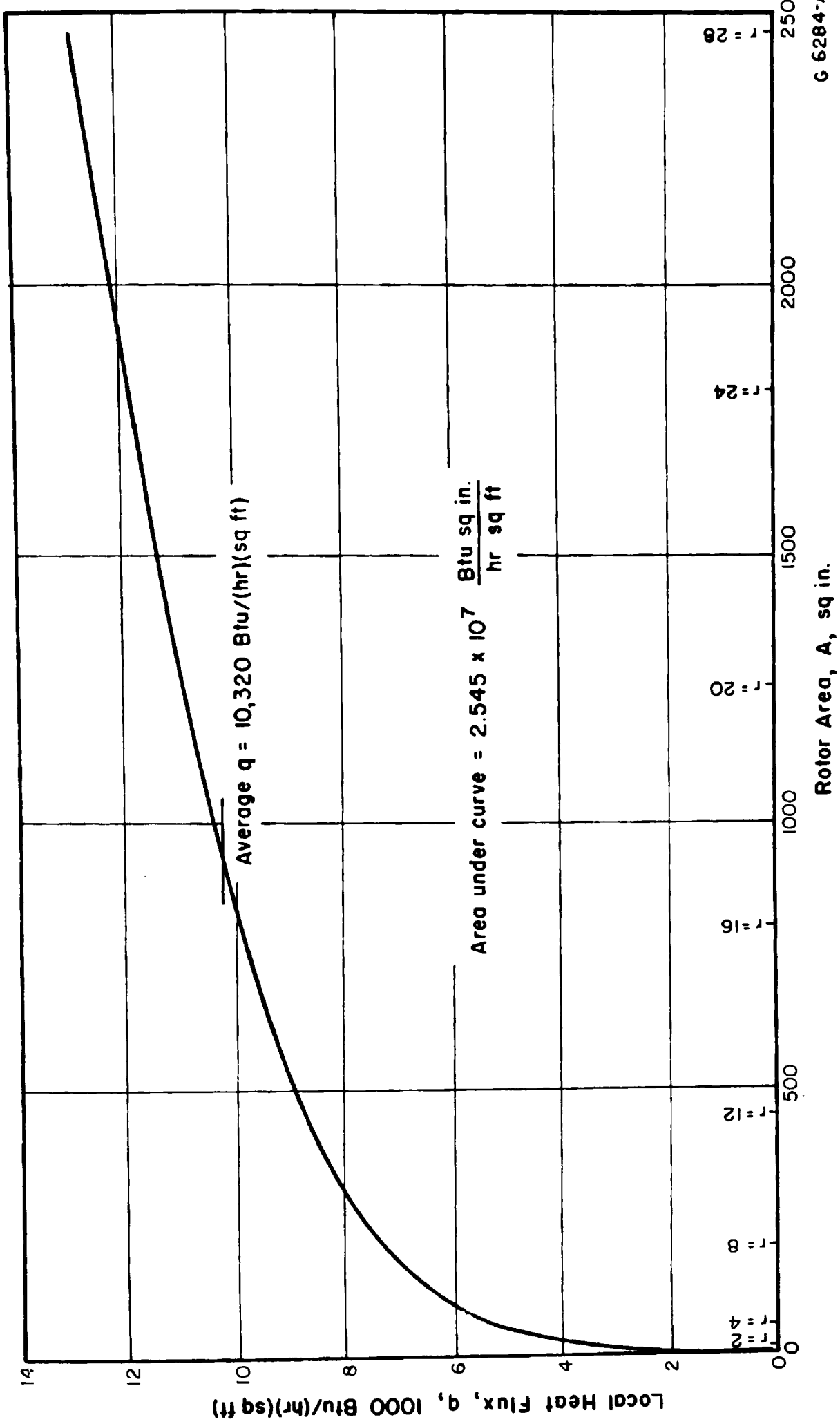

FIGURE A-3. VARIATION IN LOCAL HEAT FLUX ACROSS THE SURFACE OF THE EXAMPLE ROTOR

It may be noted that the curves describing heat transfer which were obtained by the above method do not agree exactly with values based upon the more refined derivation to follow. However, because the difference is small, about 5 per cent, the curves are presented in order to provide a general illustration.

Derivation of Equation for Heat-Transfer Coefficient

Evaporating and Condensing Film

The over-all rate of evaporation is equal to the integrated effect of heat transfer from the condensing to the evaporating side over the entire disk; therefore:

$$\beta Q_o = \int_{r_i}^{r_o} \left(\frac{2 \pi r q}{\lambda \rho} \right) dr = \int_{A_i}^{A_o} \left(\frac{q}{\lambda \rho} \right) d(\pi r^2) \quad , \tag{A-18}$$

or

$$\beta = \int_{A_i}^{A_o} \left(\frac{q}{Q_o \lambda \rho} \right) dA = \int_{\frac{A_i}{A_o}}^{1} \left(\frac{q A_o}{Q_o \lambda \rho} \right) d\left(\frac{A}{A_o} \right) \quad . \tag{A-19}$$

This relation indicates that there is an advantage to defining the following dimensionless operating variables:

$$X \equiv \pi r^2 / A_o \equiv A / A_o$$

$$Y \equiv q A_o / Q_o \lambda \rho$$

$$\alpha \equiv A_i / A_o \quad .$$

Using these dimensionless variables Equation (A-19) becomes:

$$\beta = \int_{\alpha}^{1} Y dX \quad . \tag{A-20}$$

Then, for a given value of α, when Y is known as a function of X, β can be determined.

The temperature drop across the rotor, from the condensing to the evaporating surfaces, is given by

$$\Delta T_t = \Delta T_c + \Delta T_m + \Delta T_e \quad . \tag{A-1}$$

The temperature drop through the metal disk is given by

$$\Delta T_m = q \delta_m / k_m = \left(\frac{Q_o \lambda \rho \delta_m}{A_o k_m} \right) Y \quad . \tag{A-21}$$

Assuming that the rate of change of film thickness is gradual so that the conventional relation between surface flow rate and thickness used in deriving the thickness relation for a nonevaporating laminar film may be used, that is, that

$$\overline{Q} = \frac{2 \pi r^2 \delta^3 \omega^2}{3 \nu} \quad , \tag{A-22}$$

the evaporating-film thickness is given by:

$$\delta_e = \left(\frac{3 \nu Q_o \left(1 - \int_\alpha^X Y \, dX \right)}{2 \pi r^2 \omega^2} \right)^{1/3} \tag{A-23}$$

and the condensing film thickness by:

$$\delta_c = \left(\frac{3 \nu Q_o \int_\alpha^X Y \, dX}{2 \pi r^2 \omega^2} \right)^{1/3} \quad . \tag{A-24}$$

Therefore:

$$\Delta T_c = q \, \delta_c / k = \left(\frac{Q_o \lambda \rho}{A_o k} \right) \left(\frac{3 Q_o \nu}{2 \omega^2 A_o} \right)^{1/3} Y \left(\frac{\int_\alpha^X Y \, dX}{X} \right)^{1/3} \quad , \tag{A-25}$$

and

$$\Delta T_e = q \, \delta_e / k = \left(\frac{Q_o \lambda \rho}{A_o k} \right) \left(\frac{3 \nu Q_o}{2 \omega^2 A_o} \right)^{1/3} Y \left(\frac{1 - \int_\alpha^X Y \, dX}{X} \right)^{1/3} \quad . \tag{A-26}$$

Substituting into Equation (A-1), and rearranging terms,

$$\left(\frac{k \pi r_o \Delta T_t}{Q_o \lambda \rho} \right) \left(\frac{2 \pi r_o^5 \omega^2}{3 \nu Q_o} \right)^{1/3} = Y \left(\frac{k \delta_m}{r_o k_m} \right) \left(\frac{2 \pi r_o^5 \omega^2}{3 \nu Q_o} \right)^{1/3} + Y \left(\frac{\int_\alpha^X Y \, dX}{X} \right)^{1/3} + Y \left(\frac{1 - \int_\alpha^X Y \, dX}{X} \right)^{1/3} \quad . \tag{A-27}$$

Using W, γ, Z, and K as defined in the nomenclature,

$$1 = Z \left[K + \left(\frac{\int_\gamma^W Z \, dW}{W} \right)^{1/3} + \left(\frac{1 - \int_\gamma^W Z \, dW}{W} \right)^{1/3} \right] . \tag{A-28}$$

For K = 0, which corresponds to zero disk thickness, it is easily shown by substituting $d\left(\int_{\gamma}^{W} Z\, dW\right) \Big/ dW$ for Z, separating variables, and integrating between limits that

$$1 + \left(\int_{\gamma}^{W} Z\, dW\right)^{4/3} - \left(1 - \int_{\gamma}^{W} Z\, dW\right)^{4/3} = W^{4/3} - \gamma^{4/3} \quad . \qquad \text{(A-29)}$$

Letting W be equal to the value of W at the rotor rim, that is, X = 1, using Equation (A-20), and substituting the definitions of W, Z, and γ:

$$1 + \beta^{4/3} - (1 - \beta)^{4/3} = \left(\frac{k\, \pi\, r_o\, \Delta T_t}{Q_o\, \lambda \rho}\right) \left(\frac{2\, \pi\, r_o^5\, \omega^2}{3\, \nu\, Q_o}\right)^{1/3} (1 - \alpha^{4/3}) \quad . \qquad \text{(A-30)}$$

This equation for the fractional distillation, β, corresponds to Equation 8 of Reference 6 (Bromley). In the region of β of interest, this is closely approximated by

$$\beta \cong \left(\frac{4}{5}^{\frac{2}{3}}\right) \left\{\left(\frac{k\, \pi\, r_o\, \Delta T_t}{Q_o\, \lambda \rho}\right) \left(\frac{2\, \pi\, r_o^5\, \omega^2}{3\, \nu\, Q_o}\right)^{1/3} (1 - \alpha^{4/3})\right\}^{\frac{15}{16}} \quad . \qquad \text{(A-31)}$$

Figure A-4 shows the exact solution of Equation (A-30) and the approximate solution of Equation (A-31) for β. It is clear that in the region of interest, below $\beta = 0.6$, the approximate solution may be used.

Putting this in terms of U,

$$\left(\frac{U\, r_o}{k}\right) \cong \left(\frac{4}{5}^{\frac{2}{3}}\right) \left\{\frac{Q_o\, \lambda \rho}{k\, r_o\, \pi\, \Delta T_t}\right\}^{1/16} \left\{\frac{2\, \pi\, r_o^5\, \omega^2}{3\, \nu\, Q_o}\right\}^{5/16} \frac{(1 - \alpha^{4/3})^{15/16}}{(1 - \alpha)} \quad . \qquad \text{(A-32)}$$

Eliminating the integral between Equations (A-28) and (A-29), the relation between Z and W becomes

$$W^{4/3} (1 - \alpha^{4/3}) = 1 \pm \frac{2}{3\sqrt{3}} \left(2 + \frac{W}{Z^3}\right) \left(\frac{Z}{W^{1/3}}\right)^{1/2} \left(1 - \frac{W}{4Z^3}\right)^{1/2} \quad . \qquad \text{(A-33)}$$

In the region of interest, the negative sign is used.

It will be noted that the term $\left(1 - \frac{W}{4\, Z^3}\right)^{1/2}$ determines an upper limiting value for W/Z^3 while equating $W^{4/3} (1 - \alpha^{4/3})$ to zero in Equation (A-32) determines a lower limiting value of W/Z^3, which is 1.

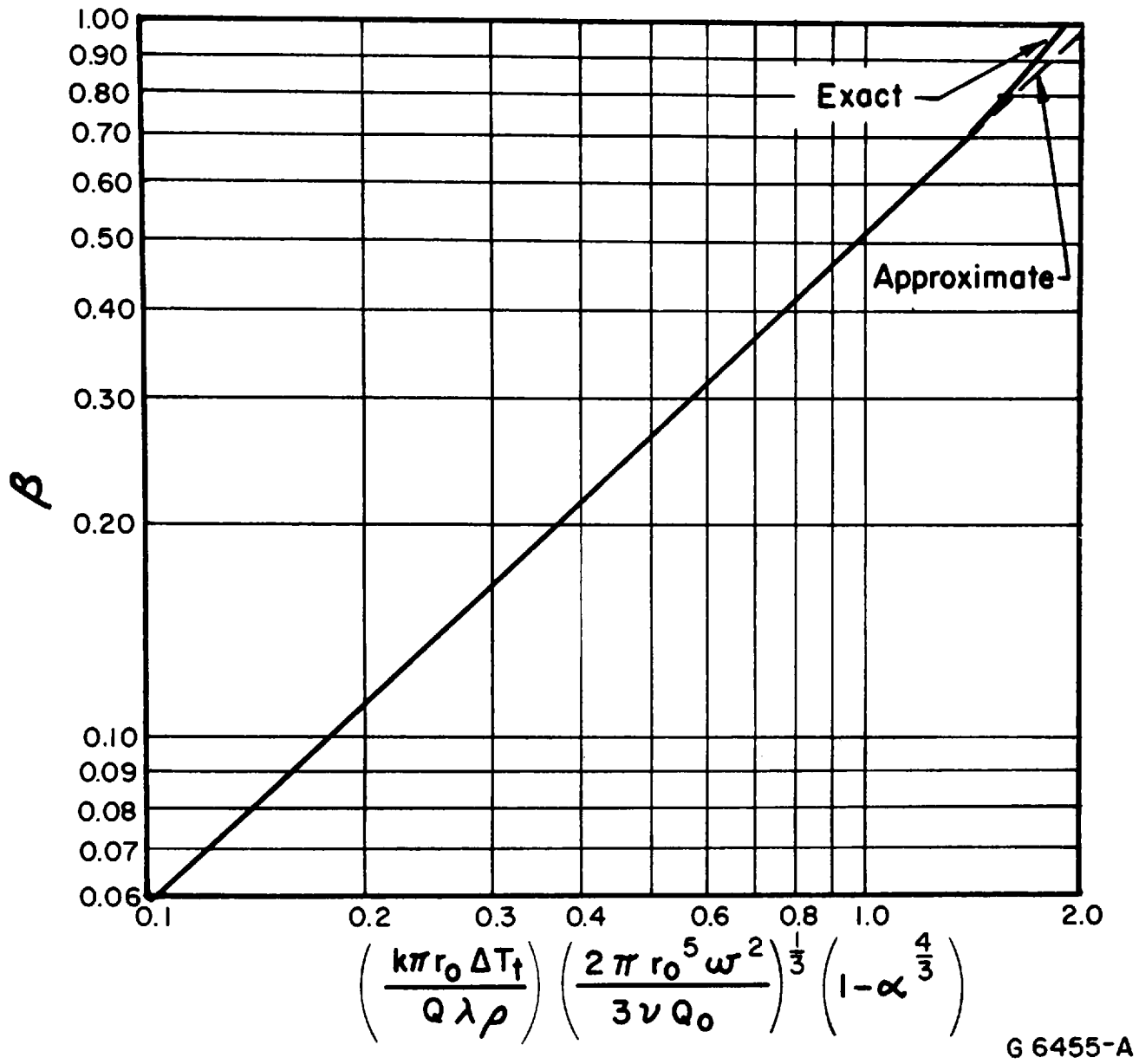

FIGURE A-4. OVER-ALL RATE OF EVAPORATION, β, OF A ROTATING DISK, FED EVENLY AT THE INNER RADIUS, AS A FUNCTION OF SYSTEM PARAMETERS WHERE DISK THICKNESS IS NOT CONSIDERED

For the range of interest, for $\alpha = 0$, it may be determined that:

$$Z \cong \frac{1}{3\sqrt{4}} W^{1/4} , \tag{A-34}$$

which reduces to:

$$\left(\frac{q\, r_o^2\, \pi}{Q_o\, \lambda \rho} \right) = \frac{1}{4^{1/3}} \left\{ \frac{r}{r_o} \right\}^{1/2} \left\{ \frac{k\, r_o\, \pi \Delta T_t}{Q_o\, \lambda \rho} \right\}^{15/16} \left\{ \frac{2\, \pi\, r_o^5\, \omega^2}{3\, \nu\, Q_o} \right\}^{5/16} \tag{A-35}$$

which represents the change in heat-transfer rate from the center to the circumference of the disk.

Returning to the problem of the rotating disk with a finite thickness, Equation (A-28) may be put in the form:

$$\int_{\gamma}^{W} Z\, dW = 1/2 \left\{ 1 \pm \frac{1}{3\sqrt{3}} (2P^3 + 1) \left(\frac{4}{P^3} - 1 \right)^{1/2} \right\} , \tag{A-36}$$

where

$$P = \left(\frac{1}{Z} - K \right) W^{1/3} .$$

It is convenient to make the substitution:

$$\xi = W^{1/3}/Z ,$$

and to use $W^{4/3}$ rather than W as the independent variable. Thus Equation (A-36) becomes:

$$\int_{\gamma^{4/3}}^{W^{4/3}} \left(\frac{1}{\xi} \right) d(W^{4/3}) = \frac{2}{3} \left\{ 1 \pm \frac{1}{3\sqrt{3}} (2P^3 + 1) \left(\frac{4}{P^3} - 1 \right)^{1/2} \right\} , \tag{A-37}$$

where

$$P = \xi - K(W^{4/3})^{1/4} .$$

Differentiating with respect to $W^{4/3}$:

$$\frac{1}{\xi} = \pm \frac{4}{3\sqrt{3}} \frac{(P^3 - 1)^2}{P^4 \left(\frac{4}{P^3} - 1 \right)^{1/2}} \left\{ \frac{d\xi}{d(W^{4/3})} - \frac{K}{4W} \right\} . \tag{A-38}$$

No exact integral of this equation was found, and therefore it was decided to proceed with a numerical evaluation of Y as a function of X.

Equation (A-28) is therefore put in the form:

$$P = \xi - KW^{1/3} = \left(\int_{\gamma}^{W} Z\, dW \right)^{1/3} + \left(1 - \int_{\gamma}^{W} Z\, dW \right)^{1/3} = \left(\frac{3}{4} \int_{\gamma^{4/3}}^{W^{4/3}} \frac{1}{\xi}\, d(W^{4/3}) \right)^{1/3}$$

$$+ \left(1 - \frac{3}{4} \int_{\gamma^{4/3}}^{W^{4/3}} \frac{1}{\xi}\, d(W^{4/3}) \right)^{1/3} . \qquad \text{(A-39)}$$

Figure A-5 presents a plot of P as a function of $\int_{\gamma}^{W} Z\, dW$.

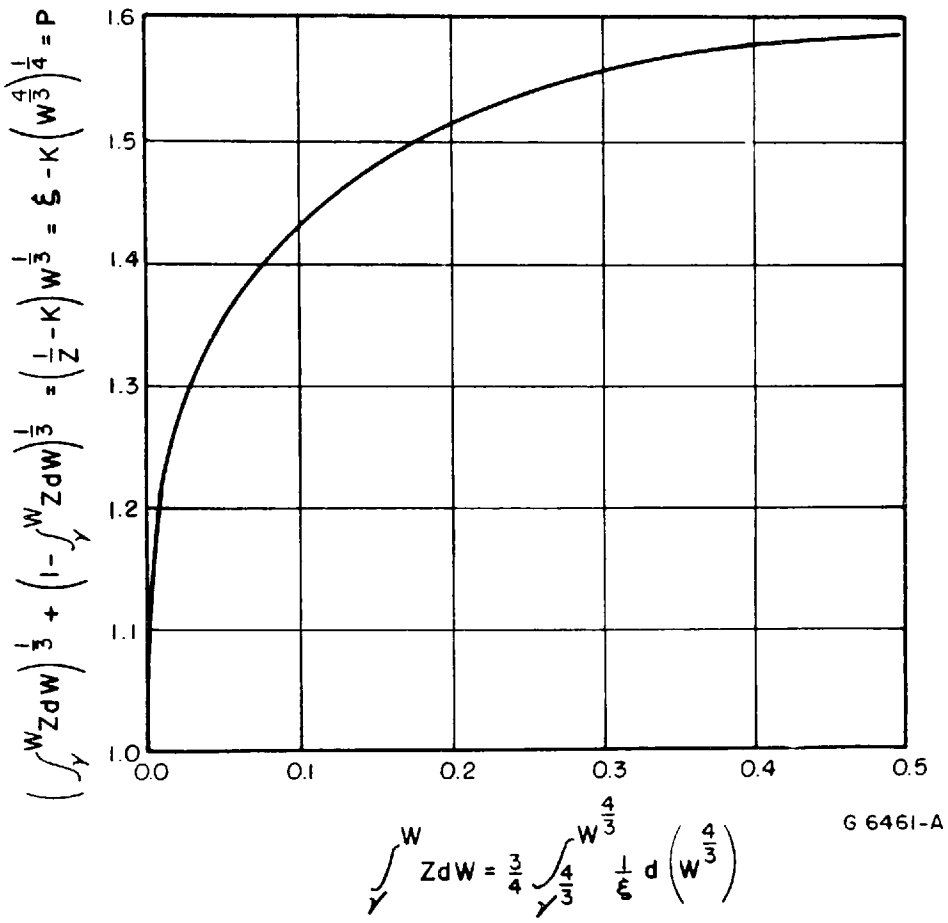

FIGURE A-5. P AS A FUNCTION OF $\int_{\gamma}^{W} Z\, dW$

The computational procedure is as follows. For a series of values of $\left[\int_{\gamma}^{W^{4/3}} \frac{1}{\xi}\, d(W^{4/3}) \right]_i$, the values of P_i are computed using Equation (A-39). If K is now selected, and a series of W_{ie} assumed (method to be indicated later), ξ_i can be computed from $P_i + K\, W_{ie}^{1/3}$, and thus $\frac{1}{\xi_i}$. The approximation,

$$\frac{1}{2}\left(\frac{1}{\xi_i}+\frac{1}{\xi_{i-1}}\right)\left(W_i^{4/3}-W_{i-1}^{4/3}\right)\cong\int_{\gamma^{4/3}}^{W_i^{4/3}}\frac{1}{\xi}\,d(W^{4/3})-\int_{\gamma^{4/3}}^{W_{i-1}^{4/3}}\frac{1}{\xi}\,d(W^{4/3}) \quad , \tag{A-40}$$

is now used to compute $W_i^{4/3} - W_{i-1}^{4/3}$. Since it is known that $W_o = \gamma$, the values of W_i corresponding to ξ_i are now available. W_{ie} can be checked against W_i; for a first selection of W_{ie}; the values of W_i for the next small value of K and the same value of γ can be used. Z_i is computed from $W_i^{1/3}/\xi_i$, as are γ/W_i and $\left(\int_\gamma^{W_i} Z\,dW\right)\Big/ W_i^{4/3}$ for later use.

Figures A-6a through A-6e present the set of curves, one for each value of K, for Z as a function of W for various values of γ. Each curve starts at an initial value of W corresponding to its γ, at some value of Z higher than the curve for $\gamma = 0$. The loss in output caused by a central hole is indicated by the different area under the corresponding curves. Comparing the curves for different values of K, it is seen that Z decreases somewhat with an increase in K. Since K is proportional to disk thickness, this indicates a decrease in performance with increasing disk thickness.

Figure A-7 shows β as a function of $W^{4/3} = \left(\frac{k\,\pi\,r_o\,\Delta T_t}{Q\,\lambda\rho}\right)\left(\frac{2\,\pi\,r_o^5\,\omega^2}{3\,\nu\,Q_o}\right)^{1/3}$ for various values of K and α, the curves for K = 0 correspond to those of Figure A-5. These curves are obtained by recognizing that β is equal to $\int^{W_1} Z\,dW$, where W_1 is the value of W at X = 1, or $\left(\frac{k\,\pi\,r_o\,\Delta T_t}{Q\,\lambda\rho}\right)^{3/4}\left(\frac{2\,\pi\,r_o^5\,\omega^2}{3\,\nu\,Q_o}\right)^{1/4}$ and recognizing that $\gamma/W_i = \alpha/X_i = \alpha$ at $X_i = 1$. Cross plots are then made from the curves of $W^{4/3}$ as a function of α, for various values of β and K.

Figure A-7 shows that, for constant α, β decreases with increasing K; for constant K, β decreases with increasing α. These curves may be used for computing the average U, by using the definition of W in the nomenclature and obtaining the value of β from the figures.

Evaporating Film Only

If an ideal sling arrangement is included on the condensing side, or if the condensation is dropwise, followed by detachment of the condensate, then ΔT_c is zero or close thereto, and Equation (A-28) is replaced by:

$$1 = Z\left[K+\left(\frac{1-\int_\gamma^W Z\,dW}{W}\right)^{1/3}\right] \quad . \tag{A-41}$$

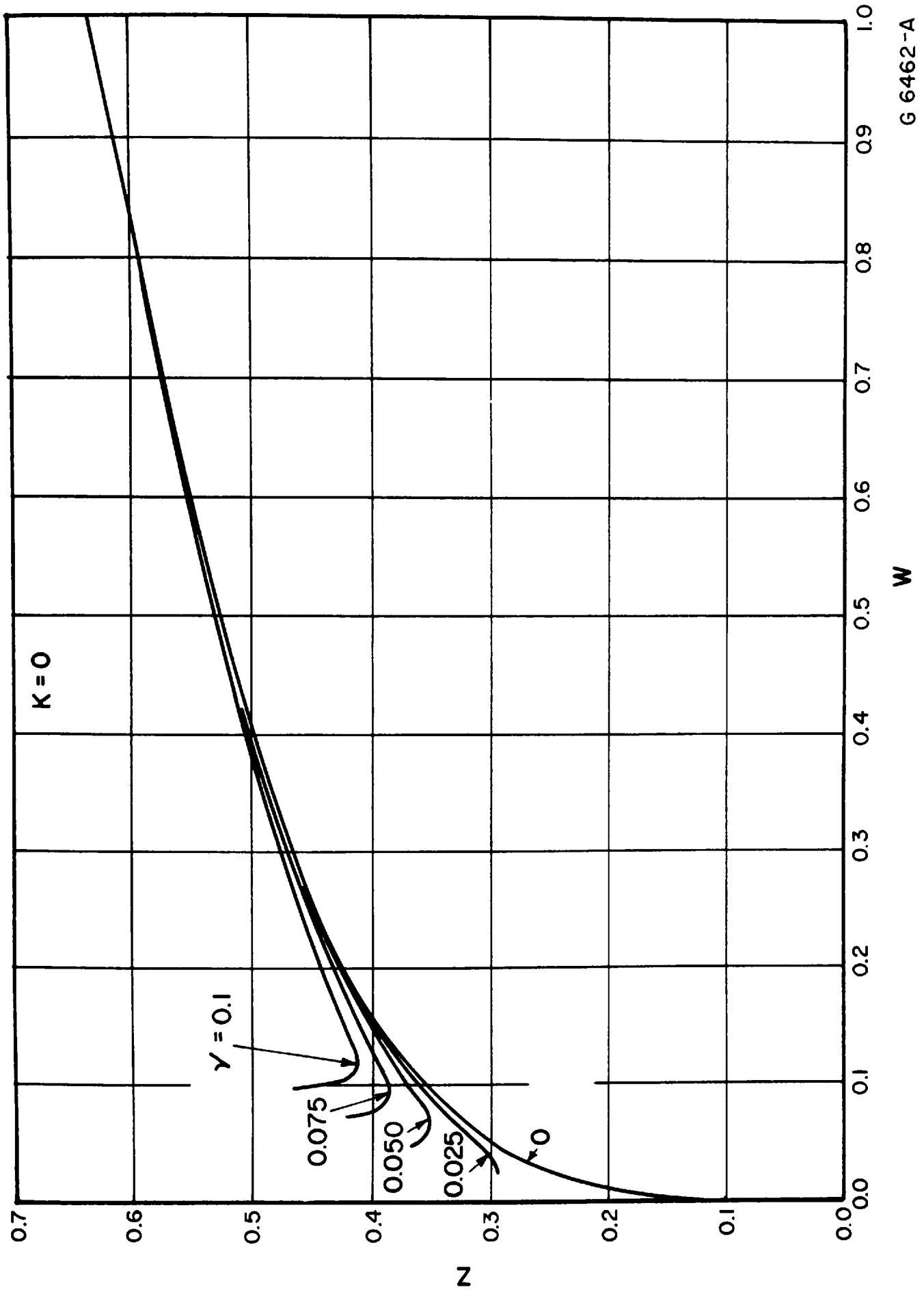

FIGURE A-6a. Z AS A FUNCTION OF W FOR VARIOUS VALUES OF γ WHEN K = 0

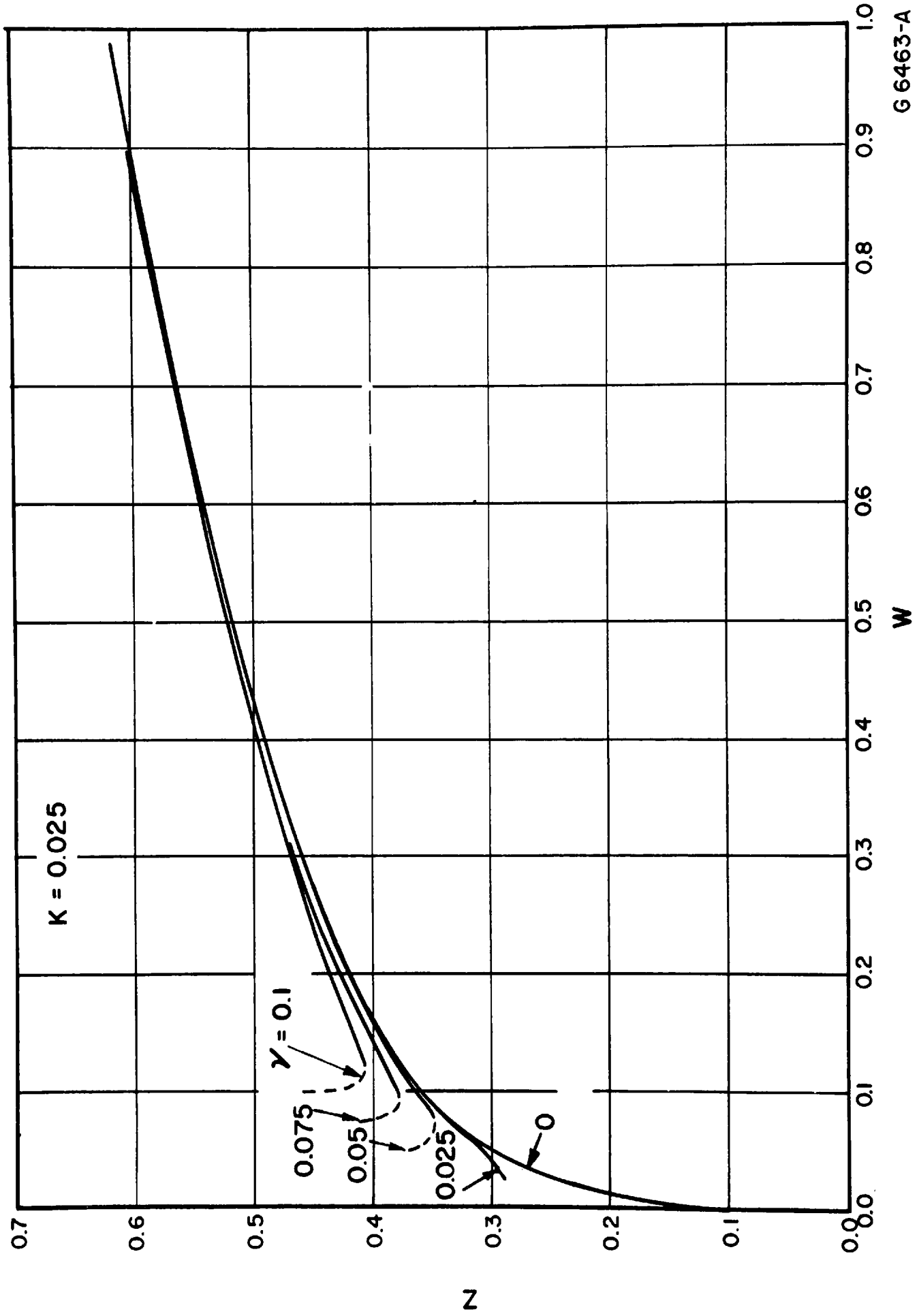

FIGURE A-6b. Z AS A FUNCTION OF W FOR VARIOUS VALUES OF γ WHEN K = 0.025

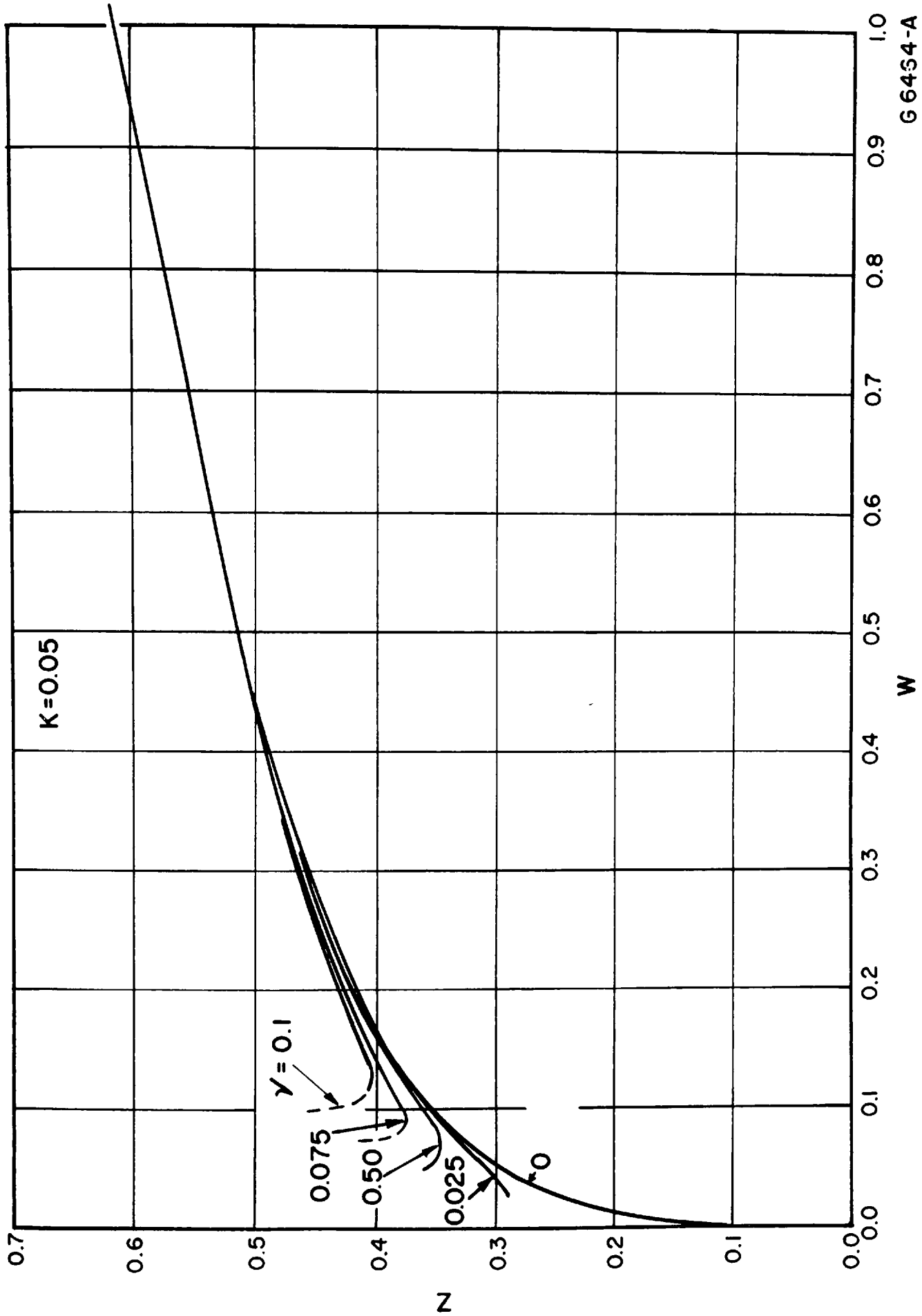

FIGURE A-6c. Z AS A FUNCTION OF W FOR VARIOUS VALUES OF γ WHEN K = 0.05

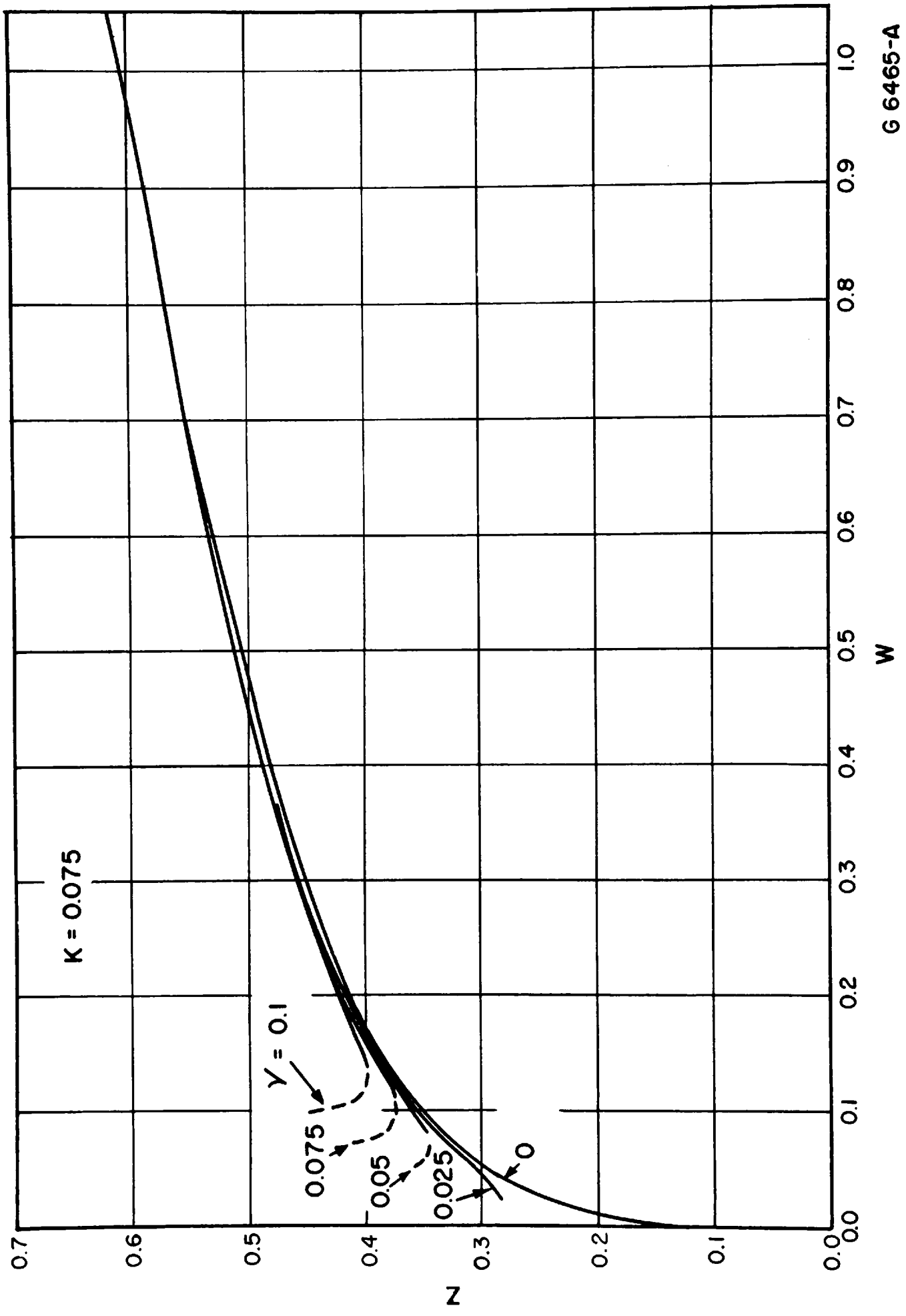

FIGURE A-6d. Z AS A FUNCTION OF W FOR VARIOUS VALUES OF γ WHEN K = 0.075

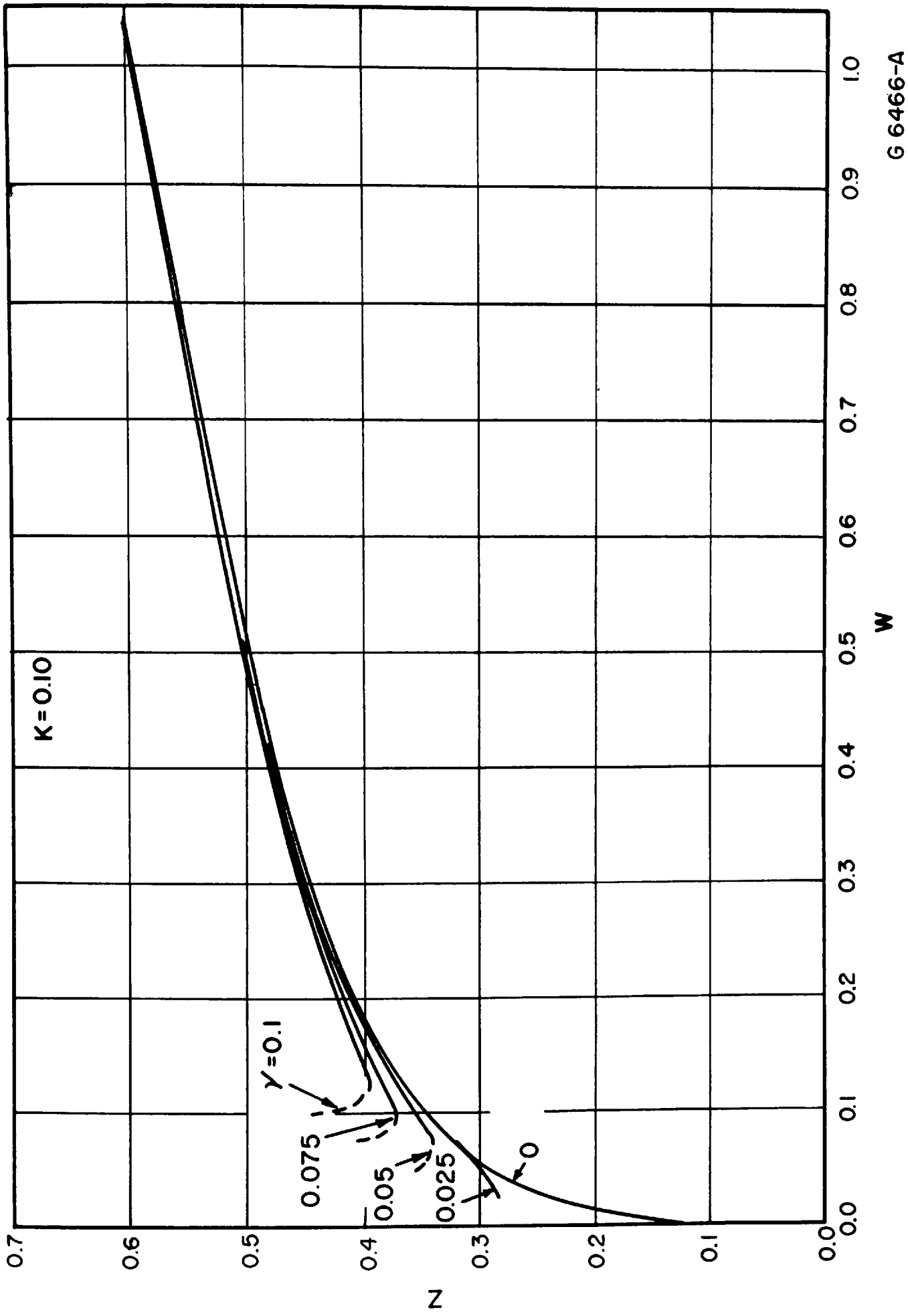

FIGURE A-6e. Z AS A FUNCTION OF W FOR VARIOUS VALUES OF γ WHEN K = 0.1

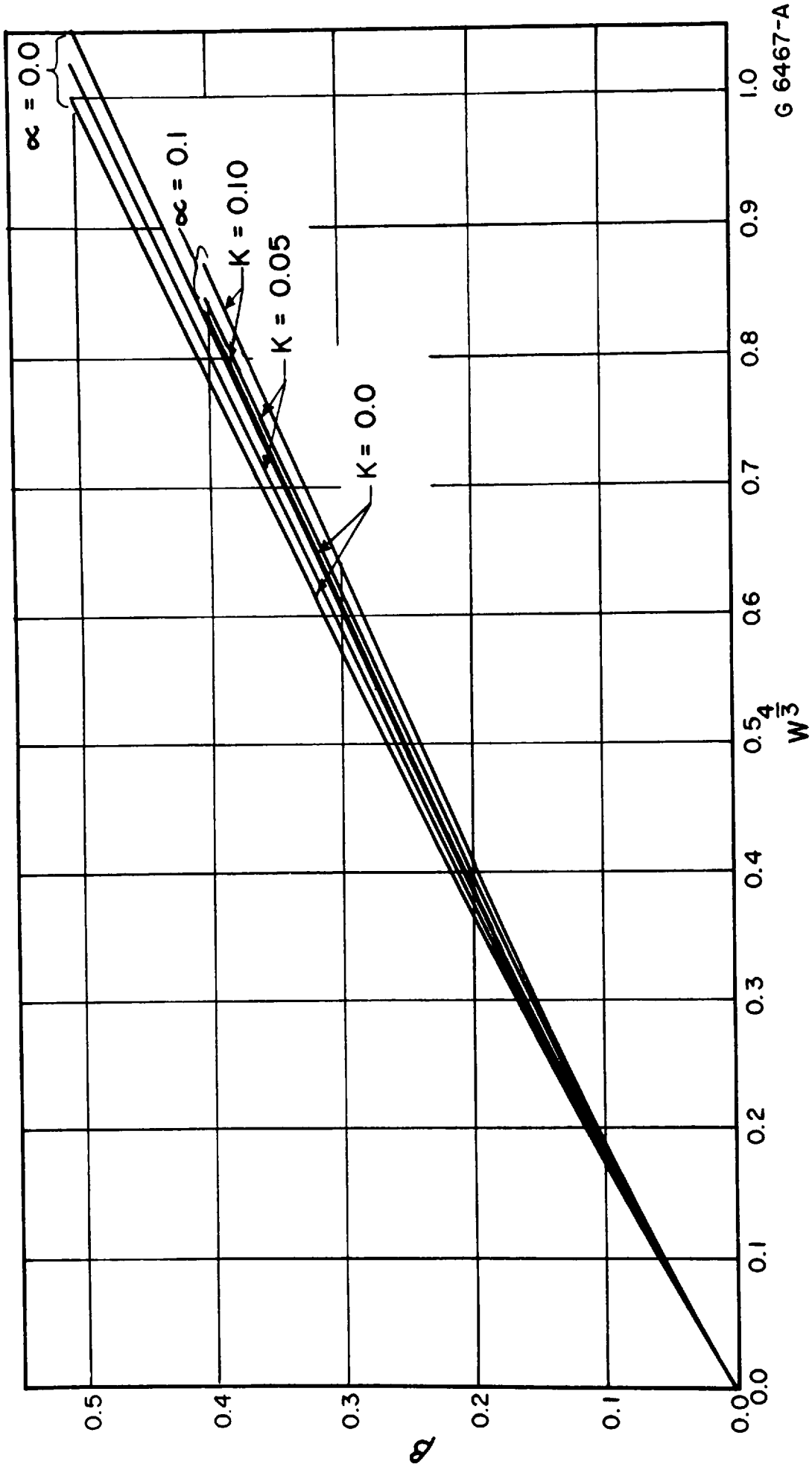

FIGURE A-7. β AS A FUNCTION OF THE GROUP $W^{4/3}$ WHEN X = 1 FOR DIFFERENT VALUES OF K AND α

For K = 0:

$$1 - \left(1 - \int_{\gamma}^{W} Z \, dW \right)^{4/3} = W^{4/3} - \gamma^{4/3} \quad . \tag{A-42}$$

Using Equation (A-20):

$$1 - (1 - \beta')^{4/3} = \left(\frac{k \pi r_o \Delta T_t}{Q_o \lambda \rho} \right) \left(\frac{2 \pi r_o^5 \omega^2}{3 \nu Q_o} \right)^{1/3} (1 - \alpha^{4/3}) \quad . \tag{A-43}$$

This can be solved exactly for β' as:

$$\beta' = 1 - \left\{ 1 - \left(\frac{k \pi r_o \Delta T_t}{Q_o \lambda \rho} \right) \left(\frac{2 \pi r_o^5 \omega^2}{3 \nu Q_o} \right)^{1/3} (1 - \alpha^{4/3}) \right\}^{3/4} \quad . \tag{A-44}$$

This can be approximated in the region of interest by:

$$\beta' \cong 0.85 \left\{ \left(\frac{k \pi r_o \Delta T_t}{Q_o \lambda \rho} \right) \left(\frac{2 \pi r_o^5 \omega^2}{3 \nu Q_o} \right)^{1/3} (1 - \alpha^{4/3}) \right\}^{\frac{21}{20}} \quad . \tag{A-45}$$

The ratio of β'/β, using Equations (A-45) and (A-31), is:

$$\beta'/\beta \cong 1.69 \left\{ \left(\frac{k \pi r_o \Delta T_t}{Q_o \lambda \rho} \right) \left(\frac{2 \pi r_o^5 \omega^2}{3 \nu Q_o} \right)^{1/3} (1 - \alpha^{4/3}) \right\}^{\frac{9}{80}} \quad .$$

Returning to Equation (A-41), this equation could be evaluated using numerical integration in the same manner as Equation (A-28). Figure A-8 gives the value of the function P′ which is used to replace P in the computational procedure. It might be kept in mind, in later discussions of the use of the fresh-water curves to compute the salt-water condition, that the procedure is much simpler in the case where no condensing film is considered.

The Evaporation of Sea Water

If, rather than fresh water, sea water or brackish water is fed to the evaporating side, there is an increase in salt concentration in the film as it moves outward from the center of the rotor. At the same time, the temperature at which evaporation occurs for a given pressure is increased and the effective temperature difference is reduced. Thus, the heat flux through the two films and the metal is decreased. The problem could be set up analytically, but would be even more cumbersome to handle than the problem just considered; therefore, it is of interest to consider how the results obtained thus far may be used to study this more practical problem.

The procedure is as follows: The rotating disk is divided into annuli of equal area. From the pressure difference, ΔT_p is computed, and, in turn, using the initial salt concentration, ΔT_t is determined. Then Y is plotted against X out to the first value of X_1, where X_1 is the first value of an equal series of ΔX out to X = 1. From the area under this curve, the value of flow rate at X_1 can be computed as well as a new concentration of salt, and a new temperature difference. The new temperature difference can be

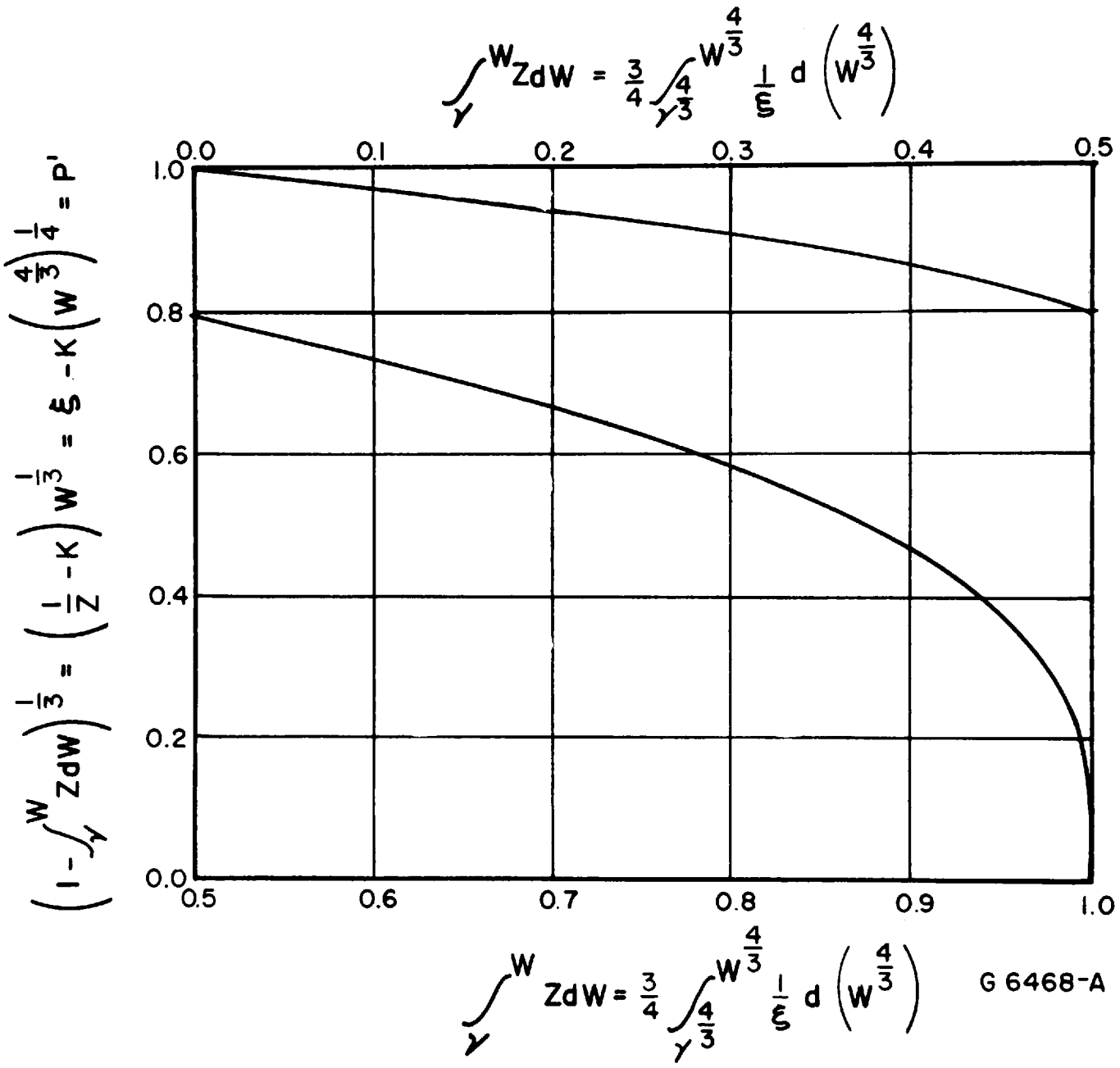

FIGURE A-8. P' AS A FUNCTION OF $\int_{\gamma}^{W} Z\, d\, W$

averaged with the initial value to recompute the amounts of evaporation to X_1, the value of ΔT, and the flow rate. For the same value of X_1, the same amount of evaporation (and of condensation), the same flow rate, but a different ΔT_t and a different α, a new curve of Y as a function of X is followed out to X_2. The temperature at this point is computed and used as before to obtain an average temperature, and recompute to X_2. The curve of Y against X to X_2 can then be integrated to obtain the evaporation rate. This process is continued until X = 1.

Maximum Performance of a Rotating Heat-Transfer Surface

In order that progress, in terms of heat-transfer coefficient, U_o, in the experimental phase of the program may be judged, it is desirable to compare the values of U_o obtained experimentally with those which are considered the theoretical maximum. In this section the analytical methods for determining the maximum U_o of different rotor or disk configurations are presented.

It is assumed that, for maximum performance, the salt concentration of the water on the disk surface should be maintained constant over the entire disk surface on the evaporating side. When this is the case, the rate of evaporation at any radius must be a constant fraction of the rate at which feed water is sprayed on the evaporating side at that radius. Furthermore, this ratio is equal numerically to the entire weight rate of fluid evaporation divided by the weight rate of the fluid spraying on the entire rotor. In addition, the amount evaporated per unit area is directly related to heat flux, q*. Therefore, the weight flow rate on the surface at radius, r, is given by:

$$M = \int_{r_i}^{r} \left\{ \text{(weight rate of spraying/unit area)} - \text{(weight rate of evaporation/unit area)} \right\}$$

$$2\pi r\, dr = \int_{\alpha}^{X} A_o \left(\frac{\text{weight rate of evaporation}}{\text{unit area}} \right) \left(\frac{1}{\bar{\beta}} - 1 \right) dX$$

$$= \int_{\alpha}^{X} \frac{A_o\, q}{\lambda} \left(\frac{1 - \bar{\beta}}{\bar{\beta}} \right) dX \quad . \qquad \text{(A-46)}$$

It may be noted that the initial salt concentration divided by the final salt concentration is equal to $(1 - \bar{\beta})$.

If the condensate is detached immediately upon formation, as in the case with ideal dropwise condensation, then

$$\Delta T_c = 0 \quad ,$$

and

$$\Delta T_t = \Delta T_m + \Delta T_e \quad .$$

*Nomenclature for this section is given at the end of this appendix.

Since

$$\Delta T_m = \frac{q\,\delta_m}{k_m} \quad , \tag{A-7}$$

and for flat rotors,

$$\Delta T_e = \frac{q\,\delta_e}{k_e} = \frac{q}{k_e}\left(\frac{3\,Q\,\nu}{2\,\pi\,\omega^2\,r^2}\right)^{1/3} \quad ,$$

by substitution of Equation (A-46),

$$\Delta T_e = \frac{q}{k_e}\left[\frac{3\,\nu}{2\,A_o\,X\,\omega^2\,\rho}\int_\alpha^X \frac{A_o\,q}{\lambda}\left(\frac{1-\bar{\beta}}{\bar{\beta}}\right)dX\right]^{1/3}$$

$$= \frac{q}{k_e}\left[\frac{3\,\nu\,(1-\bar{\beta})}{2\,\omega^2\,\lambda\rho\,\bar{\beta}\,X}\int_\alpha^X q\,dX\right]^{1/3} \quad . \tag{A-47}$$

Therefore, the temperature difference, ΔT_t, is given by:

$$\Delta T_t = \frac{q\,\delta_m}{k_m} + \frac{q}{k_e}\left[\frac{3\,\nu\,(1-\bar{\beta})}{2\,\omega^2\,\lambda\rho\,\bar{\beta}\,X}\int_\alpha^X q\,dX\right]^{1/3} \quad .$$

Disk Without Central Opening

The case of a disk without a central opening results from a simplification of Equation (A-47). This simplification is made for the purpose of facilitating a solution. First, q is assumed constant, giving:

$$\Delta T_t = \frac{q\,\delta_m}{k_m} + \frac{q}{k}\left(\frac{3\,\nu\,(1-\bar{\beta})\,q\,(X-\alpha)}{2\,\omega^2\,\lambda\rho\,\bar{\beta}\,X}\right)^{1/3} \quad .$$

If $\alpha = 0$, then

$$\Delta T_t = \frac{q\,\delta_m}{k_m} + \frac{q}{k}\left(\frac{3\,\nu\,(1-\bar{\beta})\,q}{2\,\omega^2\,\lambda\rho\,\bar{\beta}}\right)^{1/3} \quad , \tag{A-48}$$

and ΔT_t becomes independent of X. Thus, this equation is now compatible with the initial assumptions of q constant; therefore, for $\alpha = 0$, the solution for q is that it is a constant given by Equation (A-48). Putting this in terms of the dimensionless groups to be used subsequently:

$$(1-\bar{Y})^3/\bar{Y}^4 = \bar{C}\left(\frac{1-\bar{\beta}}{\bar{\beta}}\right) = R \quad , \tag{A-49}$$

where

$$\bar{Y} = \frac{q\,\delta_m}{k_m\,\Delta T_t} \quad ,$$

and

$$\overline{C} = \frac{3\,\nu\,k_m^4\,\Delta T_t}{2\,\omega^2\,\lambda\rho\,k^3\,\delta_m^4} \quad .$$

For the above case, with $\alpha = 0$, the optimum value of evaporation rate may be obtained rather easily. It is noted that

$$\frac{\Delta T_o - \Delta T_t}{\Delta T_o} = \left(\frac{c_f}{c_o} - 1\right)\overline{\gamma} \approx \left(\frac{\overline{\beta}}{1 - \overline{\beta}}\right) \quad , \qquad \text{(A-50)}$$

to a sufficient degree of accuracy for this study where ΔT_o is the effective temperature difference at the initial pressure difference and salt concentrate, c_o is the initial salt concentrate, c_f is the final salt concentrate, and $\overline{\gamma}$ is an experimentally evaluated coefficient. $\overline{\gamma}$ can be obtained by evaluating from published data $\Delta T_b/\Delta c$ in the relation $\overline{\gamma} \approx -\frac{c_o}{\Delta T_o}\left(\frac{\Delta T_b}{\Delta c}\right)$. It follows that $\Delta T_o\,\overline{\gamma}/c_o$ is approximately constant. It might also be noted that ΔT_t is not only the total temperature difference but is simultaneously the temperature difference based on pressure minus the boiling-point elevation at c_f. If U_o is evaluated on the basis of ΔT_o, then:

$$U = U_o\,(\Delta T_o/\Delta T_t) \quad .$$

Furthermore:

$$\overline{C} = \overline{C}_o\,(\Delta T_t/\Delta T_o) \quad .$$

Making these substitutions into Equation (A-49):

$$\left(\frac{\Delta T_t}{\Delta T_o} - \frac{U_o\,\delta_m}{k_m}\right)^3\left(1 - \frac{\Delta T_t}{\Delta T_o}\right) = \left(\frac{U_o\,\delta_m}{k_m}\right)^4 \overline{\gamma}\,\overline{C}_o \quad . \qquad \text{(A-51)}$$

This may be differentiated to obtain the maximum value of $U_o\,\delta_m/k_m)$ as a function of $(\Delta T_t/\Delta T_o)$, for constant $\overline{\gamma}\,\overline{C}_o$. The result is:

$$\frac{\Delta T_t}{\Delta T_o} = \frac{3}{4} + \frac{U_o\,\delta_m}{4\,k_m} \quad . \qquad \text{(A-52)}$$

Combining Equations (A-51) and (A-52) to eliminate $\frac{U_o\,\delta_m}{k_m}$:

$$\frac{\Delta T_t}{\Delta T_o} = \frac{1 + 3\left(\frac{\overline{\gamma}\,\overline{C}_o}{27}\right)^{1/4}}{1 + 4\left(\frac{\overline{\gamma}\,\overline{C}_o}{27}\right)^{1/4}} \quad . \qquad \text{(A-53)}$$

On the other hand, eliminating $\Delta T_t/\Delta T_o$:

$$\frac{U_o\,\delta_m}{k_m} = \frac{1}{1 + 4\left(\frac{\overline{\gamma}\,\overline{C}_o}{27}\right)^{1/4}} \quad . \tag{A-54}$$

For the expected range of values of $\overline{\gamma}\,\overline{C}_o$, U_o will vary approximately with $\omega^{1/2}$.

General Equation for Disk With Central Opening

Returning to the general case, $\alpha \neq 0$, the equation for temperature difference, Equation (A-47), may be put in the form:

$$\left(\frac{k_m \Delta T_t}{q\,\delta_m} - 1\right)^3 = \left(\frac{k_m{}^4\,\Delta T_t\,3\,\nu\,(1-\overline{\beta})}{\delta_m{}^4\,k^3\,2\,\omega^2\,\lambda\rho\,\overline{\beta}\,X}\int_\alpha^X \left(\frac{\delta_m\,q}{k_m \Delta T_t}\right) dX\right) \quad . \tag{A-55}$$

Defining $\overline{Y}$ and $\overline{C}$ as before:

$$\left(\frac{1}{\overline{Y}} - 1\right)^3 = \left(\frac{1-\overline{\beta}}{\overline{\beta}}\right)\frac{\overline{C}}{X}\int_\alpha^X \overline{Y}\,dX \quad . \tag{A-56}$$

Differentiating:

$$3\left(\frac{1}{\overline{Y}} - 1\right)^2\left(-\frac{1}{\overline{Y}^2}\right)\frac{d\overline{Y}}{dX} = \left(\frac{1-\overline{\beta}}{\overline{\beta}}\right)\overline{C}\left\{-\frac{1}{X^2}\int_\alpha^X \overline{Y}\,dX + \frac{\overline{Y}}{X}\right\} \quad ,$$

or

$$3\left(\frac{1}{\overline{Y}} - 1\right)^2\left(\frac{1}{\overline{Y}^2}\right)\frac{d\overline{Y}}{dX} = +\frac{1}{X}\left(\frac{1}{\overline{Y}} - 1\right)^3 - \left(\frac{1-\overline{\beta}}{\overline{\beta}}\right)\frac{\overline{CY}}{X} \quad .$$

This leads to:

$$\frac{3\,(1-\overline{Y})^2}{\overline{Y}\left\{(1-\overline{Y})^3 - \left(\frac{1-\overline{\beta}}{\overline{\beta}}\right)\overline{C}\,\overline{Y}^4\right\}}\,d\overline{Y} = d\,(\ln X) \quad . \tag{A-57}$$

It will be noted [cf. Equation (A-46)] that since

$$\int_\alpha^1 \overline{Y}\,dX = \frac{\lambda\,M_o\,\overline{\beta}\,\delta_m}{A_o\,k_m\,\Delta T_t} = \frac{U\,(1-\alpha)\,\delta_m}{k_m} \quad , \tag{A-58}$$

from Equation (A-56),

$$\left(\frac{1}{\overline{Y}_o} - 1\right)^3 = \frac{3\,\nu\,k_m^3\,A_o\,(1-\overline{\beta})}{2\,\omega^2\,k^3\,\delta_m^3\,A_o\,\rho} \equiv \overline{C}\left(\frac{M_o\,(1-\overline{\beta})\,\lambda\,\delta_m}{A_o\,\Delta T_t\,k_m}\right) = \overline{C}\,\frac{(1-\overline{\beta})}{(\overline{\beta})}\cdot\frac{U\,\delta_m}{k_m}\,(1-\alpha)\ . \tag{A-59}$$

It will also be noted that $\overline{Y} = 1$ at $X = \alpha$, and decreases for $X > \alpha$.

Solution of General Equations

Before a satisfactory method of solution was developed, several different methods of solution to Equation (A-57) were investigated and found unsatisfactory for one reason or another in the range of condition of interest in this study. This method is outlined below; the other methods studied are outlined in Laboratory Record Book No. 15741-A, since they could be of use in other ranges of operating conditions.

It is noted that, by using Equation (A-57),

$$\ln\frac{X}{\alpha} = \int_1^{\overline{Y}}\frac{d\,(\ln X/\alpha)}{d\,\overline{Y}}\,d\,\overline{Y} = \int_{\overline{Y}}^{1}\frac{3\,(1-\overline{Y})^2\,d\,\overline{Y}}{\overline{Y}\left\{R\,\overline{Y}^4 - (1-\overline{Y})^3\right\}}\ . \tag{A-60}$$

Defining:

$$\xi = \frac{(1-\overline{Y})^3}{R\,\overline{Y}^4}\ ,$$

where

$$0 \leq \xi < 1\ ,$$

and substituting into Equation (A-60):

$$\ln\frac{X}{\alpha} = \int_o^{\xi}\left(\frac{3}{4-\overline{Y}}\right)\frac{d\,\xi}{1-\xi}\ . \tag{A-61}$$

Figure A-9 shows $3/(4-\overline{Y})$ as a function of $\overline{Y}$, and Figure A-10 shows $R\,\xi$ as a function of $3/(4-\overline{Y})$; using these figures, the general form of $\ln X/\alpha$ as a function of $\overline{Y}$ may be ascertained. It is noted that for values of R and α in the range of interest, $\overline{Y}$ is sufficiently small over a large enough portion of the range of X/α that the approximation,

$$\frac{X}{\alpha} = \left(\frac{1}{1-\xi}\right)^{3/4} = \left\{1 - \frac{(1-\overline{Y})^3}{R\,\overline{Y}^4}\right\}^{-3/4}\ , \tag{A-62}$$

can be used.

Figures A-11a, A-11b, and A-11c present the results of using this approximation in the form of $\overline{Y}$ as a function of X/α for various values of R. This set of curves was

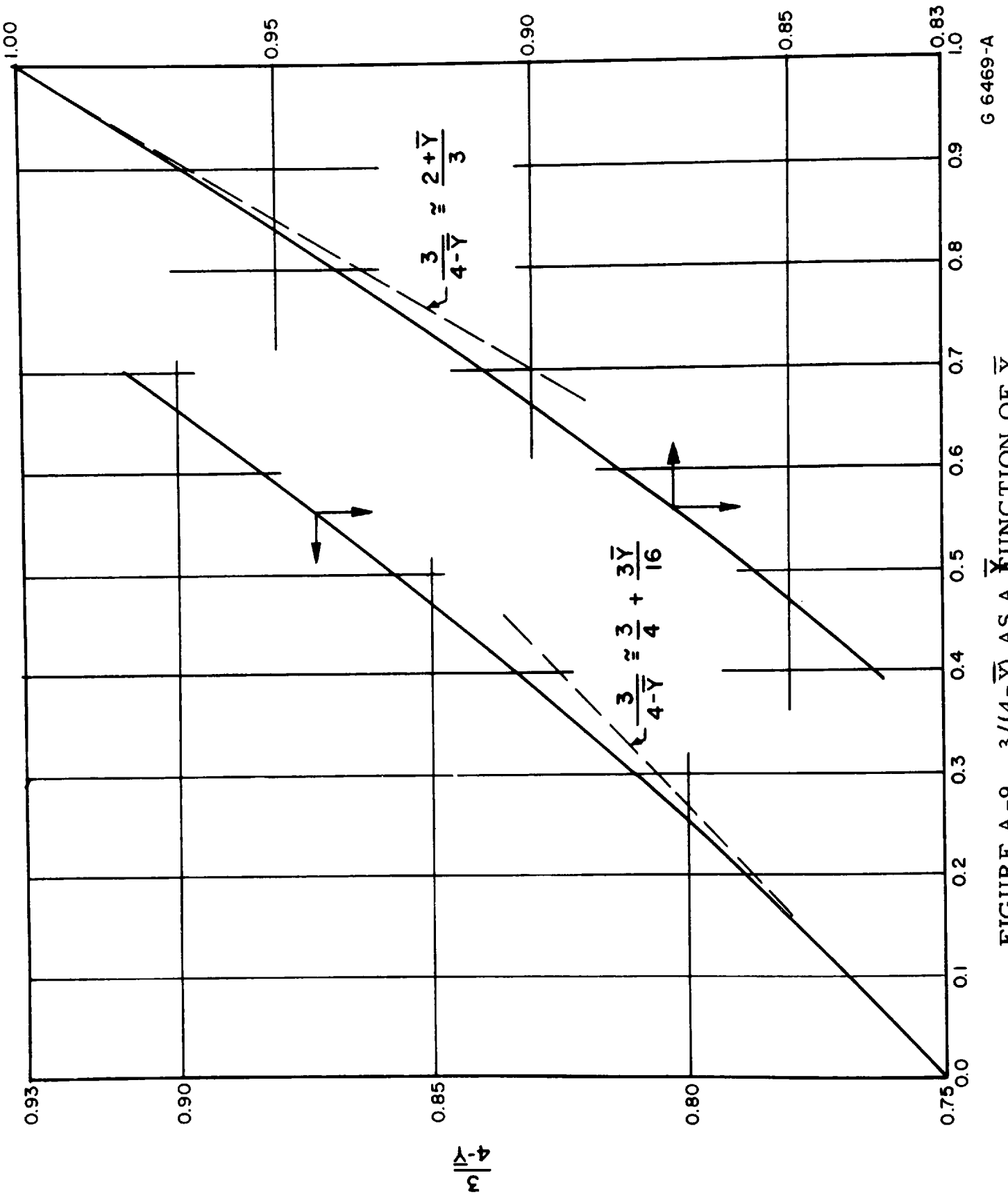

FIGURE A-9. $3/(4-\overline{Y})$ AS A $\overline{Y}$ FUNCTION OF $\overline{Y}$

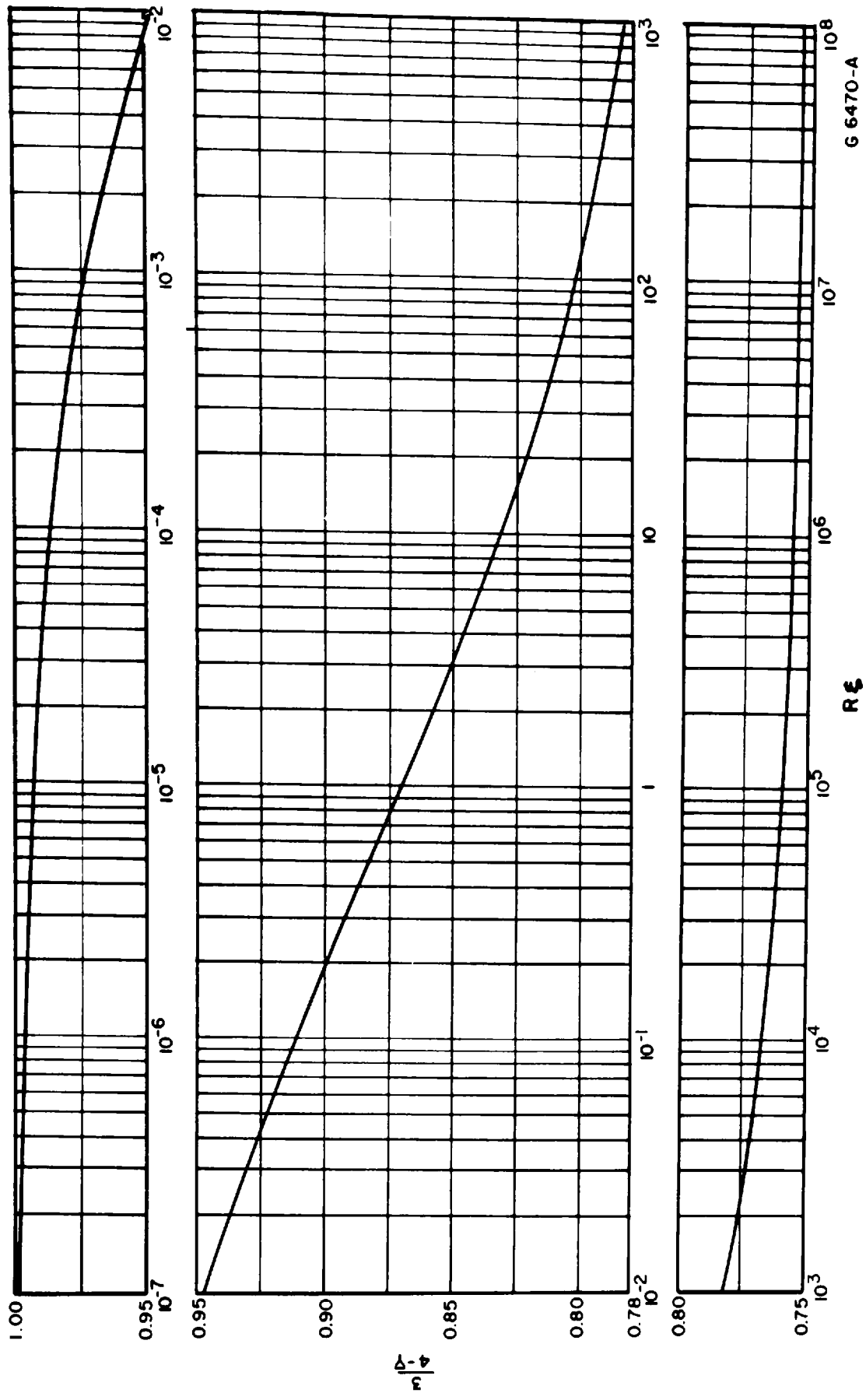

FIGURE A-10. THE GROUP $R\xi$ AS A FUNCTION OF $3/(4-\bar{Y})$

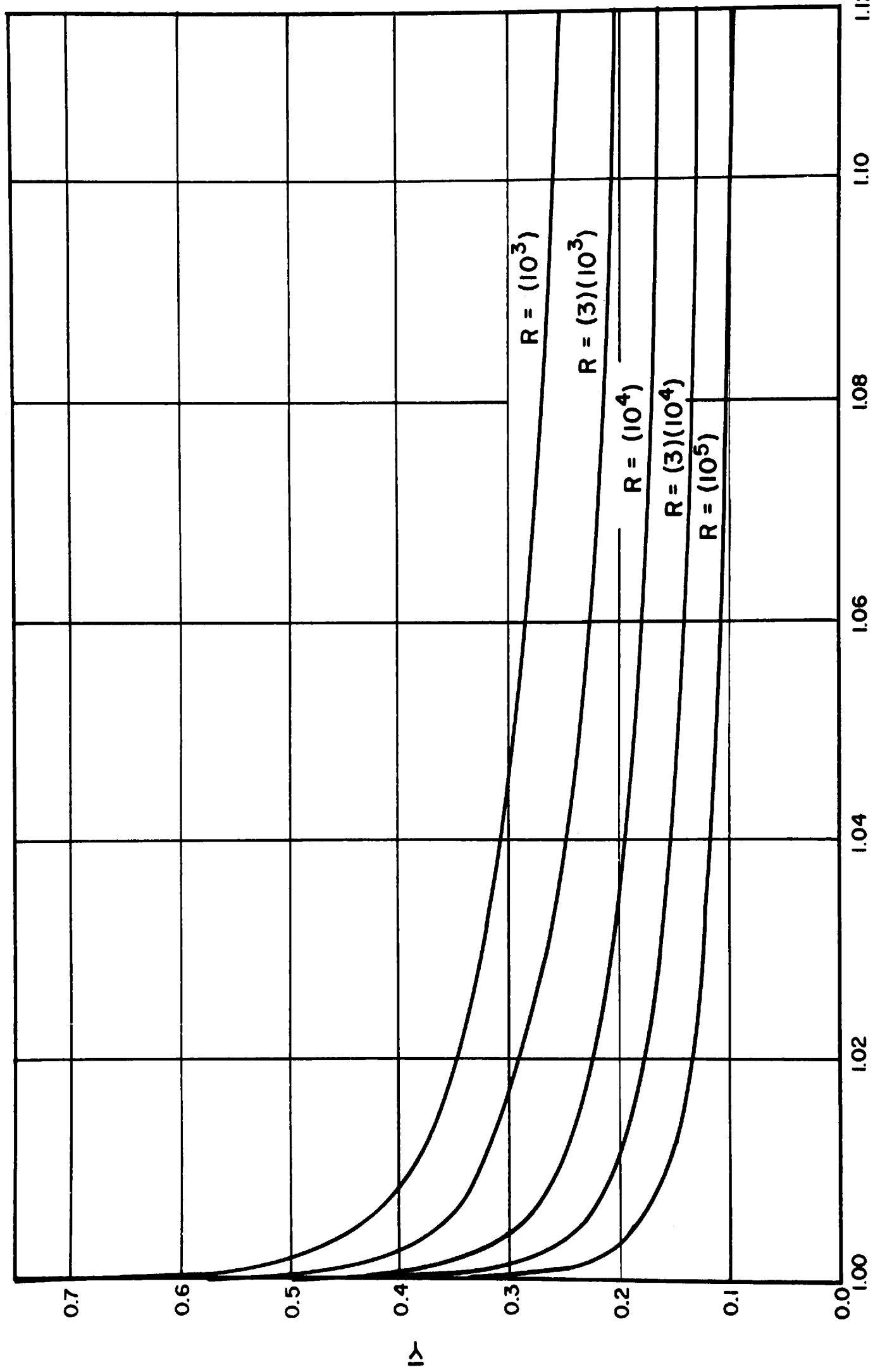

FIGURE A-11a. $\overline{Y}$ AS A FUNCTION OF X/α FOR FIVE VALUES OF R WHERE $1 \leq X/\alpha \leq 1.10$

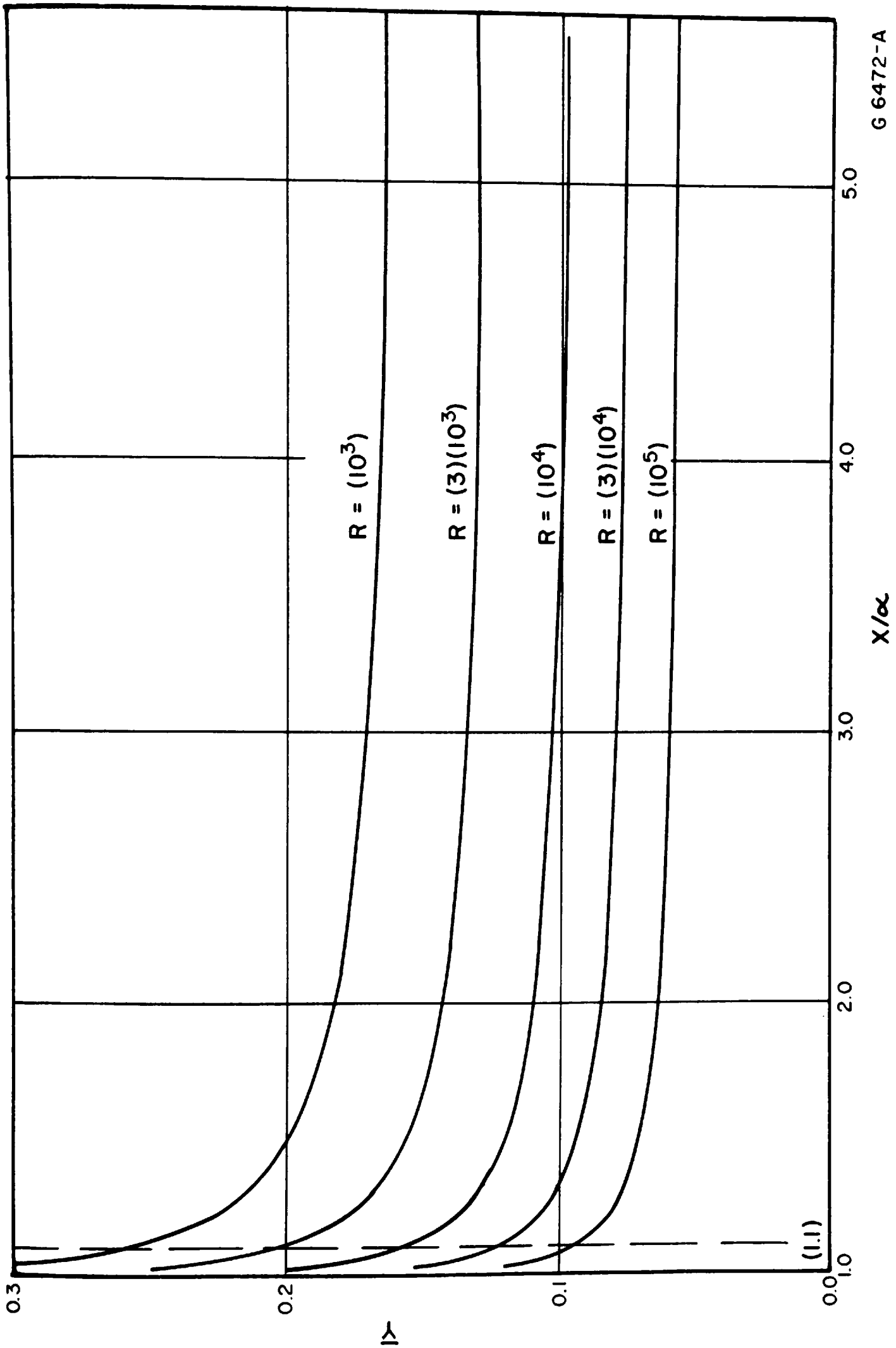

FIGURE A-11b. $\overline{Y}$ AS A FUNCTION OF X/α FOR FIVE VALUES OF R WHERE $1.1 \leq X/\alpha \leq 5.0$

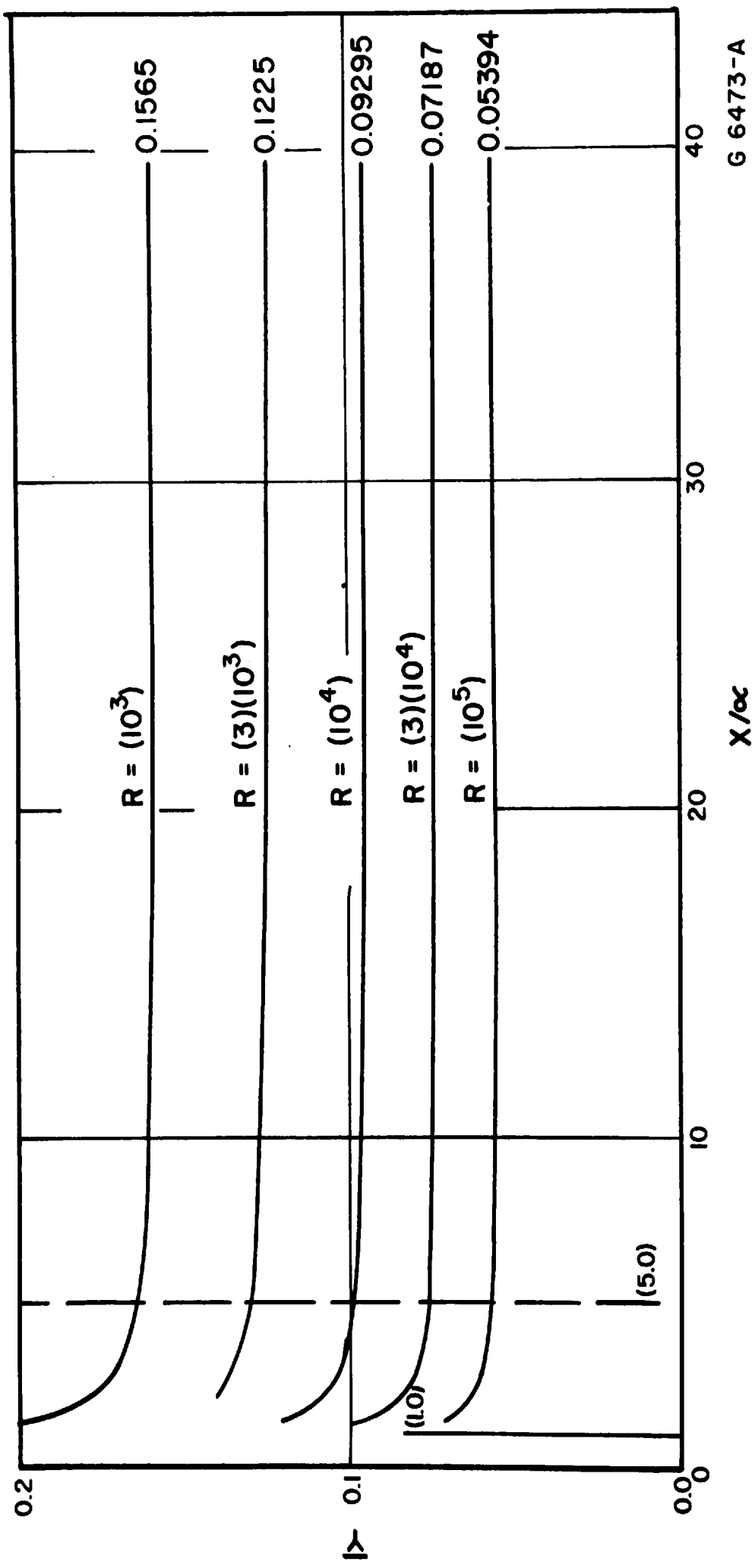

FIGURE A-11c. $\bar{Y}$ AS A FUNCTION OF X/α FOR FIVE VALUES OF R WHERE $5.0 \leq X/\alpha \leq 40$

integrated graphically to obtain $\frac{\lambda M_o \bar{\beta} \delta_m}{\alpha A_o k_m \Delta T_t}$ as a function of α and R.

Figure A-12 presents the results of the integration in the form of $\frac{\lambda M_o \bar{\beta} \delta_m}{A_o k_m \Delta T_t}$ which equals $\frac{U \delta_m (1 - \alpha)}{k_m}$ as a function of α for various values of R which equals $\left(\frac{3 \nu k_m^4 \Delta T_t (1 - \bar{\beta})}{2 \omega^2 \lambda \rho k^3 \delta_m^4 \bar{\beta}} \right)$. Unfortunately, a simple general expression for these curves was not found, although for a given value of α the expression:

$$\frac{k_m}{U \delta_m} = \bar{C}_1 + \bar{C}_2 R^{1/4} \quad , \tag{A-63}$$

fits the data quite well over the range of R of interest.

Optimization of Fraction Evaporated. Following the same procedure as outlined for $\alpha = 0$ to determine the optimum value of $\Delta T_t / \Delta T_o$ and the corresponding value of $U_o \delta_m / k_m$, Equation (A-63) is converted to:

$$\left(\frac{k_m}{\delta_m U_o} \right) \left(\frac{\Delta T_t}{\Delta T_o} \right) = \bar{C}_1 + \bar{C}_2 \bar{C}_o \left(\frac{\Delta T_t}{\Delta T_o} \right) \bar{\gamma} \Big/ \left(1 - \frac{\Delta T_t}{\Delta T_o} \right) \tag{A-64}$$

Differentiating and solving for $d\left(\frac{U_o \delta_m}{k_m} \right) \Big/ d\left(\frac{\Delta T_t}{\Delta T_o} \right) = 0$ gives:

$$\frac{\Delta T_t}{\Delta T_o} = \frac{1 + 3 \left(\frac{\bar{C}_2 \bar{\gamma}^{1/4} \bar{C}_o^{1/4}}{4 \bar{C}_1} \right) \left(\frac{\Delta T_t / \Delta T_o}{1 - \Delta T_t / \Delta T_o} \right)^{1/4}}{1 + 4 \left(\frac{\bar{C}_2 \bar{\gamma}^{1/4} \bar{C}_o^{1/4}}{4 \bar{C}_1} \right) \left(\frac{\Delta T_t / \Delta T_o}{1 + \Delta T_t / \Delta T_o} \right)^{1/4}} = \frac{1 + 3 \left(\frac{\bar{C}_2}{4 \bar{C}_1} \right) R^{1/4}}{1 + 4 \left(\frac{\bar{C}_2}{4 \bar{C}_1} \right) R^{1/4}} . \tag{A-65}$$

Thus, again $\Delta T_t / \Delta T_o$ varies from 3/4 to 1 for the maximizing $U_o \delta_m / k_m$; and for the range of values of R of interest, $\Delta T_t / \Delta T_o$ is very close to 3/4.

A plot of $U_o \delta_m / k_m$ as a function of $\bar{\gamma} \bar{C}_o$ for various values of $\Delta T_t / \Delta T_o$ for a given value of α shows that the value of $U_o \delta_m / k_m$ near the maximum is not sensitive to the value of $\Delta T_t / \Delta T_o$. Thus, for computational purposes in determining the maximum value of U_o, $\Delta T_t / \Delta T_o$ of 3/4 may be used. This will also determine the value of $\bar{\beta}$.

Discussion of Results

Figure A-13 presents, therefore, $U_o \delta_m / k_m$ as a function of $\frac{\delta_m}{k_m} \left\{ \frac{\omega^2 \lambda \rho k^3}{\nu c_o} \left(- \frac{\Delta c}{\Delta T_b} \right) \right\}^{1/4}$ for several values of α, for maximum efficiency. It will be noted that

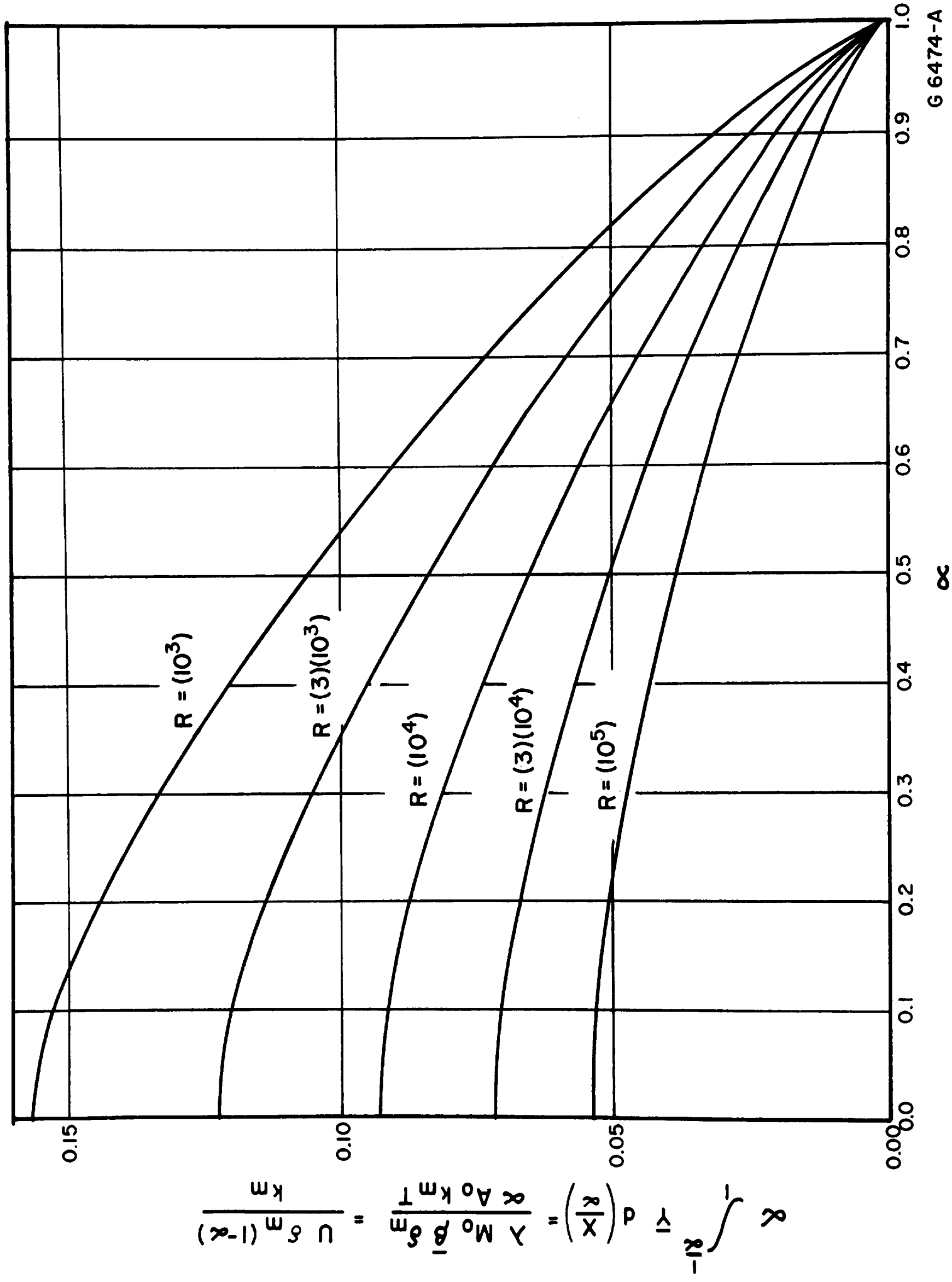

FIGURE A-12. THE GROUP $\frac{U\delta_m(1-\alpha)}{k_m}$ AS A FUNCTION OF α FOR THE VARIOUS VALUES OF THE GROUP R

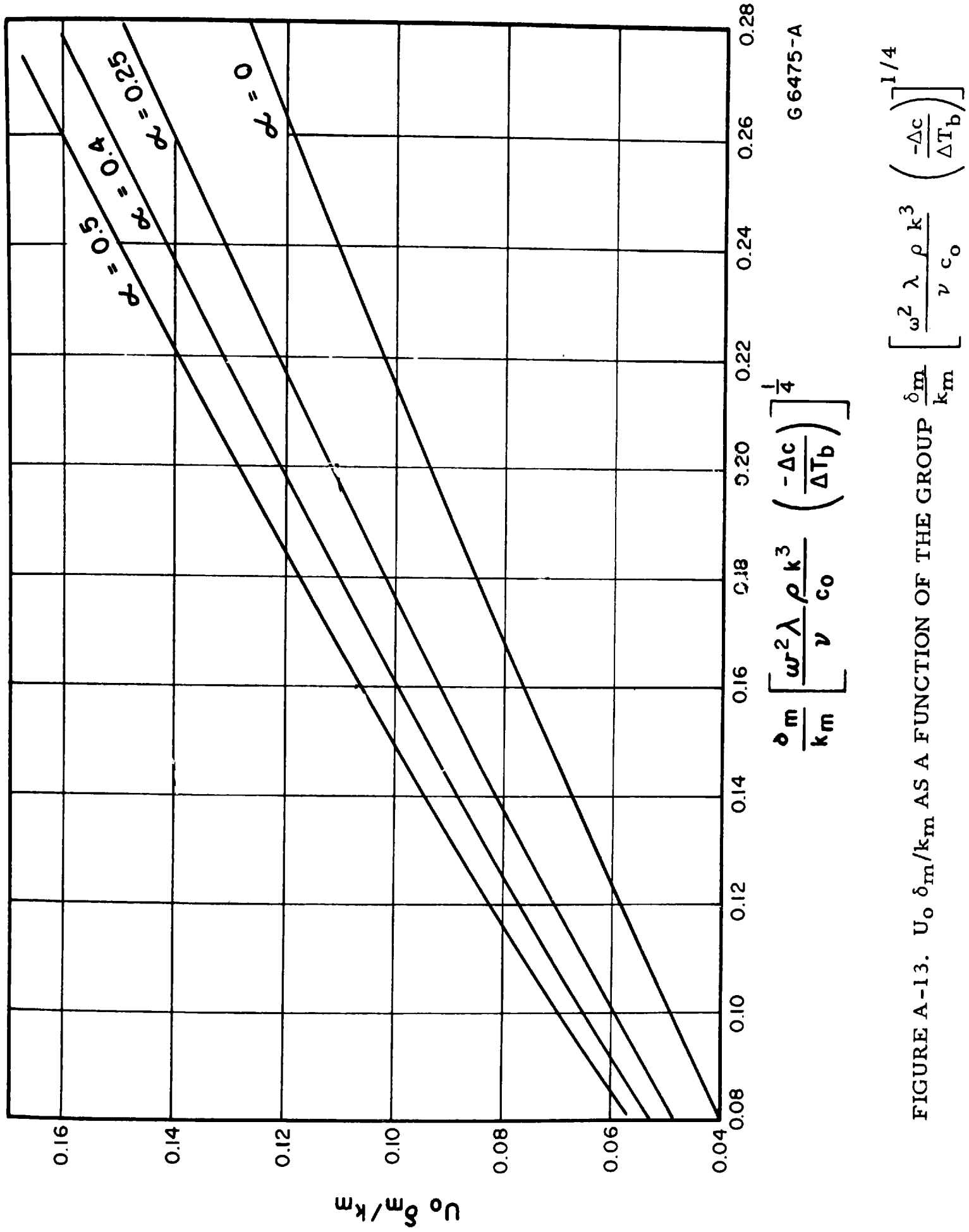

FIGURE A-13. $U_o\ \delta_m/k_m$ AS A FUNCTION OF THE GROUP $\frac{\delta_m}{k_m}\left[\frac{\omega^2\lambda\rho k^3}{\nu c_o}\left(\frac{-\Delta c}{\Delta T_b}\right)\right]^{1/4}$

the relation is nearly linear. Furthermore, increasing the value of α increases the value of U_o. This, of course, presumes that the liquid is sprayed on at the correct rate, which is higher toward the center when $\alpha \neq 0$.

If the comparison of U_o is to be based on the gross area within the outer radius, as might be dictated by space limitation, rather than the net area, U_o should be multiplied by $1 - \alpha$. In this case, increasing α is not beneficial. One therefore must reach a balance between surface efficiency and space requirements.

Comparison of Experimental and Theoretical Values of Heat-Transfer Coefficient

The variation in heat transfer with rotor radius was determined experimentally with the No. 4 still. To do this, annular areas of the rotor were insulated starting at the rim and working inward. The thickness of the insulating material, epoxy resin, averaged about 1/8 inch. The adherence of the resin to the copper rotor is considered to have been excellent as witnessed by the difficulty encountered in removing it at the completion of the experiment. Each run, regardless of the evaporating area, was conducted under nearly the same operating conditions.

Table A-1 gives the data obtained with a single flat rotor and a central feed system. As inspection of U column shows, there is considerable scatter. This undoubtedly was due to the necessity of opening the still to the atmosphere between each run. However, the data are sufficiently accurate to show both a trend of increasing heat-transfer coefficient, U, with increasing radii and a fall-off in U at the rim of the rotor.

TABLE A-1. EXPERIMENTAL MEASUREMENT OF HEAT-TRANSFER COEFFICIENT AT DIFFERENT RADII

Area No.	Outer Radius, in.	Mean Radius, in.	Surface Area, ft^2	Corrected Yield of Each Area, lb/hr	Local U for ΔT = 4F, $\frac{Btu}{(hr)(ft^2)(F)}$
0	0	--	0	0	--
1	13	9.2	3.52	17.8	1302
2	17	15.1	2.61	26.0	2570
3	21	19.1	3.37	33.5	2560
4	25	23.1	3.90	50.1	3310
5	27.5	26.2	3.10	6.0	500

Note: Operating Conditions
Central feed system
Fresh-water feed
Feed rate = 320-370 lb/hr
Rotor speed = 300 rpm
Evaporating temperature = 112 F
ΔT = 4 degrees F.

Theoretical values for U at different rotor radii may be obtained using Figures A-6 through A-6e in this appendix. Considering the operating conditions listed in Table A-1, the following may be determined (nomenclature used is given at the end of this appendix):

Feed rate ≈ 340 lb/hr = 5.5 ft^3/hr

ω = 300 rpm = (3.6)(π)(10^4) radian/hr

δ_m = 0.066 in. = 0.0055 ft

k_m = 222 Btu/(hr)(ft^2)(F)/(ft)

λ = 1029 Btu/lb

k = 0.363 Btu/(hr)(ft^2)(F)/(ft)

ν = 0.0236 ft^2/hr

ρ = 61.8 lb/ft^3

K = 0.101 ≈ 0.1

α = 0

$W = (0.1521)(r^2)$

$Z = (q)(5.91)(10^{-5})$

The theoretical and experimental values of the heat-transfer coefficient for this particular set of conditions are shown in Figure 33 in the text.

Possible Reasons for Lower Heat-Transfer Coefficients With Salt-Water Feed

Diffusion of Salt in the Evaporating Film

This short study is directed toward determining whether the diffusion of salt (sodium chloride) from the surface of the evaporating film is slow enough to appreciably affect the boiling-point elevation of salt water. For the purposes of this first approximation, the flow problem on the rotor surface will be greatly oversimplified, making use of the following assumptions:

(1) The moving evaporating film is a stationary layer of salt solution.

(2) The concentration gradient in the evaporating film is linear.

(3) Only one "average" point on the rotor need be considered. This point is located on the mean radius, that is, half way out on the 56-inch-diameter rotor in terms of area (r ≈ 20 inches).

(4) Fick's first law applies:

$$\frac{\partial m}{\partial t} = - DA \frac{\partial c}{\partial x} \quad , \tag{A-66}$$

where:

$\frac{\partial m}{\partial t}$ = mass transfer rate of solute

D = diffusion coefficient

A = cross-sectional area

$\frac{\partial c}{\partial x}$ = concentration gradient.

The operating conditions and heat-transfer characteristics of the following example will be the same as shown in Figure 27 of the text. Of course, ΔT_p would have to be increased to about 4.8 degrees F to compensate for boiling-point elevation. As may be seen from Figure 27, the thickness of the evaporating film at r = 20 inches is about 0.001 inch or 0.00254 cm. Using both Figure 27 in the text and Figure A-3 of this appendix, it has been estimated that roughly 15 per cent of the feed water is evaporated from the area inside the mean radius.

As water is evaporated from the surface of the film, the salt is left behind. If it were not for diffusion, the feed-water film would soon become covered with a thin layer of salt and distillation would stop. As this does not happen, there must be a balance between the salt being "deposited" by the evaporating liquid and the diffusion rate of this salt into the film. The theoretical salt-deposition rate at the operating conditions listed in Figure 27 is:

$$R_s = \frac{(U)\ (\Delta T_t)\ (C)}{(h_{fg})} \quad , \tag{A-67}$$

where:

R_s = addition rate, lb/(hr)(ft^2) or gm/(sec)(cm^2)

U = heat-transfer coefficient Btu/(hr)(ft^2)(F)

ΔT_t = effective temperature difference, degrees F

C = concentration of salt solution, g/g, lb/lb

h_{fg} = latent heat of evaporation, Btu/lb

$$R_s = \frac{(2900)(4.3)(0.04)}{1030} = 0.485 \text{ lb/(hr)(ft}^2\text{)}$$

$$= (6.58)(10^{-5}) \text{ g/(sec)(cm}^2\text{)}.$$

On the basis of 15 per cent evaporation, the average salt concentration on the rotor is calculated to be 4.1 per cent. From data given in the International Critical Tables, the diffusion coefficient of salt (sodium chloride) in salt solution, for the conditions of interest, has been estimated at 1.76 (10^{-5}) cm^2/sec. Substituting into Equation (A-66), the concentration gradient necessary to maintain equilibrium is:

$$(6.58)(10^{-5})\ g/(sec) = -(1.76)(10^{-5})cm^2/sec\ (1)\ cm^2\ \frac{\partial c}{\partial x}\ ,$$

or

$$\frac{\partial c}{\partial x} = -3.74\ \frac{g/cm^3}{cm}$$

When this concentration gradient is applied to the 0.00254-cm-thick evaporating film which has an average concentration of 0.041 g/cm^3, the influence of diffusion may be determined. For the first trial the salt concentration next to the metal rotor will be taken at 3.5 per cent. Using the aforementioned values, the concentration at the surface becomes $(3.74)(0.00254) + 0.035 = 0.0445 \approx 4.5$ per cent. The average of 4.5 and 3.5 is 4.0, which indicates that the first choice of 3.5 per cent was slightly low, but perhaps close enough for the purposes of this discussion.

The boiling-point elevation (bpe) based on the average concentration of 4.1 per cent, is 0.68 degree F; the bpe based on the 4.5 per cent concentration at the surface is 0.76 degree F. This difference in bpe introduces an error in the calculation of over-all ΔT_t and in turn the over-all U. The error in this example is about (0.76-0.68)/(4.8-0.68) or 2 per cent.

As mentioned previously, the above calculations, which are based on a gross oversimplification of the problem, were made not for the purpose of obtaining direct answers but rather for the purpose of trying to detect a condition. On this basis only may the above calculations be considered useful. Intuitively one would say that the higher the ΔT_t the more pronounced the effect caused by a concentration gradient in the evaporating film; also, the thinner the film, the less the effect.

Difference in Physical Properties of Fresh Water and Salt Water

The thickness and thermal conductivity of the evaporating film, when dropwise condensation is used, offers the controlling thermal resistance. Thus, the higher the term k/δ for the evaporating film, the higher the over-all U. The letters k and δ denote thermal conductivity and film thickness, respectively. In the following calculations of film thickness, factors other than the physical properties of the feed water are held constant. To simplify the conditions, equal mass flow rates are used and an average salt-water concentration of 5 per cent is assumed. The film thickness is defined by:

$$\delta = \left(\frac{3\ Q_o\ \nu}{2\ \pi\ \omega^2\ r^2\ \cos\ \phi} \right)^{1/3} \qquad \text{(Reference 4)}$$

The terms are defined in the nomenclature. In the following example, the subscript F will refer to fresh-water feed and the subscript S will refer to salt-water feed.

Operating temperature = 112 F

Q_o = 200 lb/hr, Q_F = 3.24 ft^3/hr, Q_S = 3.13 ft^3/hr

$\nu_F = (2.36)(10^{-2})$ ft^2/hr, $\nu_S = (2.525)(10^{-2})$ ft^2/hr

k_F = 0.3626 Btu/(hr)(ft)(F), k_S = 0.358 Btu/(hr)(ft)(F)

$\delta_F = [(3.24)(2.36)(10^{-2})(A)]^{1/3} = 0.425\ (A)^{1/3}$

$\delta_S = [(3.13)(2.525)(10^{-2})(A)]^{1/3} = 0.429\ (A)^{1/3}$

By dropping the constant $(A)^{1/3}$:

$k_F/\delta_F = 0.3624/0.425 = 0.853$,

and

$k_S/\delta_S = 0.358/0.429 = 0.835$.

From these figures it appears that for at least one condition, sea-water feed offers about (100) (0.853-0.835)/0.853 = 2.1 per cent more resistance to heat flow.

Also of general interest may be a comparison of the effect on heat transfer of the differences in the physical properties of fresh water at 110 F and at 150 F. Again in this instance, a feed rate of 200 lb/hr is assumed with the result:

Q_{o1} = 3.235 ft^3/hr Q_{o5} = 3.267 ft^3/hr

ν_1 = 0.0241 ft^2/hr ν_5 = 0.0172 ft^2/hr

k_1 = 0.3615 Btu/(hr)(ft^2)(F) k_5 = 0.383 Btu/(hr)(ft^2)(F)

$\delta_1 = [(3.235)(0.0241)(A)]^{1/3} = 0.445\ (A)^{1/3}$

$\delta_5 = [(3.267)(0.0172)(A)]^{1/3} = 0.379\ (A)^{1/3}$

dropping the constant $(A)^{1/3}$

$k_1/\delta_1 = 0.3615/0.445 = 0.812$

$k_5/\delta_5 = 0.383/0.379 = 1.001$

(Subscripts 1 and 5 denote the 110 F and 150 F conditions respectively.)

The per cent difference is (100)(1.001-0.812) 0.812 = 23.3 or about 6 per cent per 10 degrees F.

The Flow Characteristics and Possible Sources of Noncondensable Gas in the Hickman Still

Presented in this section are calculations of the flow of noncondensable gas relative to a rotating heat-transfer surface. Also presented are air-leak data from the No. 5 still.

Study of Diffusion Rate of Noncondensable Gas in Steam

In determining the diffusion rate of noncondensable gas (air) in steam, it is assumed that the steam flow inside a rotor is laminar and radial in direction. Using half the rotor cavity width as the characteristic length for calculating the Reynolds number of the radial flow inside the rotor cavity of the No. 4 still, one finds that the assumption of laminar flow may be valid only in the region near the rim of the rotor. Also, intuitively, one would think that steam inside the rotor does not flow exactly radially, but rather in a spiral path. Thus, the calculation to follow represents only a first step.

Figure A-14 shows how the concentration of noncondensable gas and steam velocity may vary with rotor radius for a given rotor. The steam that first enters the rotor is assigned a noncondensable-gas contamination of 0.001 per cent by weight. This value is considered to be about the same concentration as would be found in a production unit of the Hickman still. The size and shape of the rotor used in the following example is described in Figure A-14.

As the steam and noncondensable gas travel radially outward in the condensing cavity, more and more of the steam condenses on the rotor surface and the noncondensable gas becomes more concentrated as the mixture approaches the rotor rim. Also, the rate of change of concentration (concentration gradient) increases as the rim is approached. For the following calculation, the most severe case is used, namely, the average concentration gradient between the radii of 27.8 inches and 28 inches. The diffusion equation is:

$$-\frac{dn}{dx} D = \Gamma = v\rho \quad , \tag{A-68}$$

where

D = diffusion coefficient of air in steam, ft^2/sec

$\frac{dn}{dx}$ = concentration gradient of air, lb/ft^3 per ft

Γ = net rate of mass transfer toward the region of low concentration per unit area, lb/ft^2-sec

v = average radial diffusion velocity of air, ft/sec

ρ = density of air, lb/ft^3.

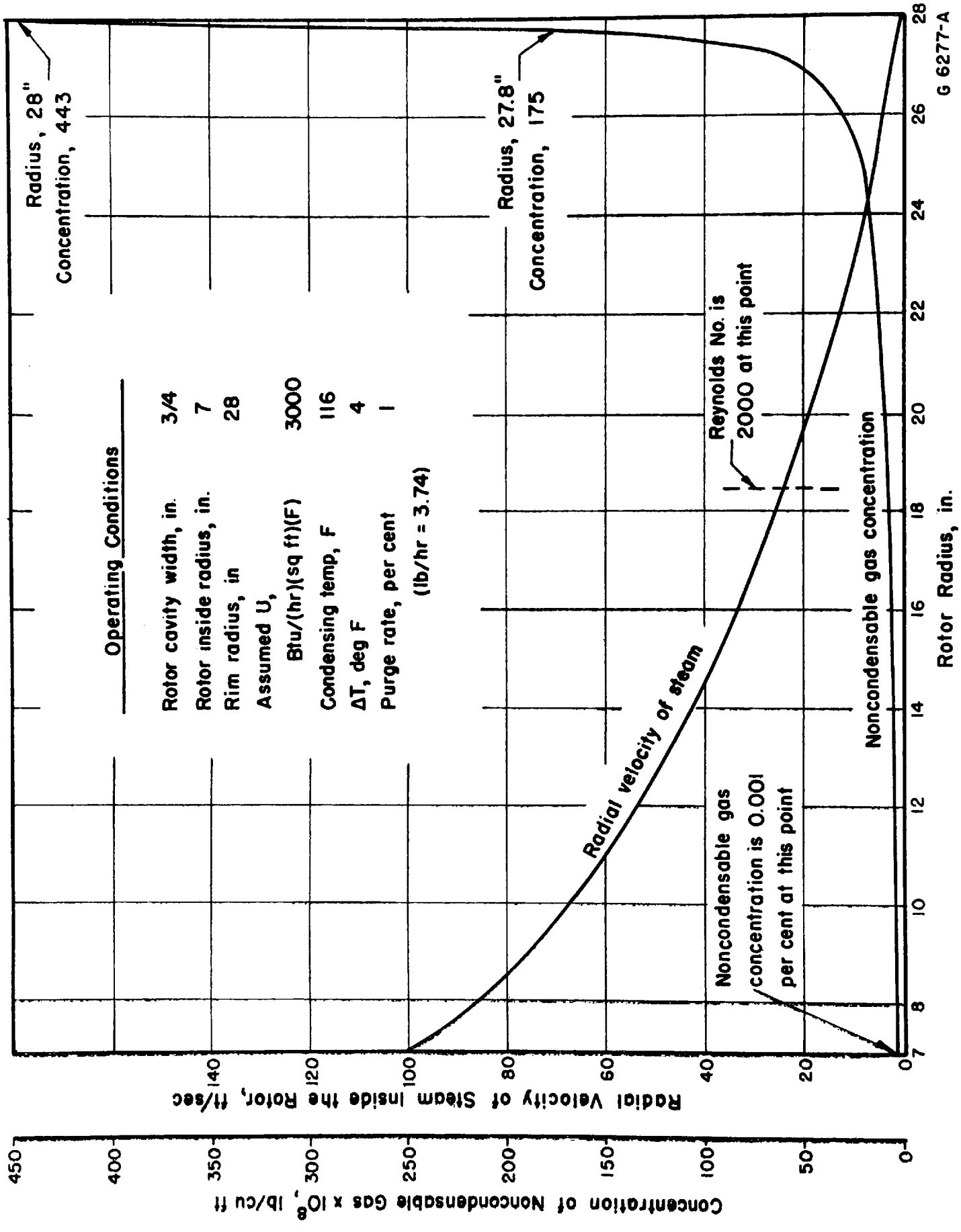

FIGURE A-14. STEAM FLOW AND NONCONDENSABLE-GAS CONCENTRATION INSIDE A SAMPLE ROTOR

When the standard diffusion coefficient for air in steam is corrected for the temperature and pressure of the condensing steam, it is found to have a value of 3.40 $(10)^{-3}$ ft^2/sec. Using Equation (A-68), the average diffusion velocity at a radius of 27.9 inches is calculated to be about 0.3 ft/sec. This velocity is about equal and opposite to the steam flow at this point. It is interesting to note that the average velocity of the condensing steam in a direction perpendicular to the rotor surface is about 0.7 ft/sec. On the basis of this calculation, it appears that purge rates from the rotor in the order of 1 per cent or slightly larger will be necessary in order to prevent a build-up of noncondensable gas at the rim of the rotor. Experimental data obtained with the No. 4 still indicate that over-all purge rates as low as 0.1 per cent may be possible. However, these data were influenced by partial condensation of the purge steam in the rim-purge tube. The variations in noncondensable-gas concentration shown in Figure A-14 and the above calculation suggest that noncondensable gas may tend to build up between purge points. Thus, it appears desirable to purge uniformly around the rim of the rotor.

Method of Estimating Noncondensable-Gas Contamination

Noncondensable gas can arise from three sources in the No. 5 Badger-Hickman evaporator during operation with sea-water feed: (1) leaks in the housing and adjoining pipes, (2) carbon dioxide liberated during evaporation, and (3) dissolved gases in the feed water.

Calculation of Leak Rate. The leak rate for the housing is determined from measurements of temperature and pressure at the beginning and end of a definite interval of time. Mathematically:

$$\text{Leak rate} = \frac{V_n \, T_{std} \, D_{std}}{P_{std}} \left(\frac{P_2}{T_2} - \frac{P_1}{T_1} \right) \Bigg/ \Delta\Theta \; \frac{lb}{hr} \quad , \tag{A-69}$$

where

V_n = 1225 ft^3 is the total volume of housing at T_{std}, D_{std}, P_{std}

T_{std}, D_{std}, P_{std} = standard conditions for air temperature, 528 R; density, 7.52 x 10^{-2} lb/ft^3; and pressure 29.92 in. of Hg

P_1, P_2 = partial pressure of air in housing at beginning and end of test, in. of Hg

T_1, T_2 = temperature at beginning and end of test, R

$\Delta\Theta$ = duration of test, hr.

The partial pressure of the air is the total absolute pressure in the system less the pressure of saturated steam at the respective temperatures. Typical leak rates determined by this method are as follows:

Date	Air Leak Rate, lb/hr
4-1-58	0.56
4-8-58	0.39
5-14-58	0.45
5-16-58	0.33
5-22-58	0.25
6-4-58	0.39
6-6-58	0.58
6-22-58	0.23
7-6-58	0.60
9-4-58	0.59
10-9-58	0.65
10-15-58	0.34
Average	0.45

Determination of Carbon Dioxide Liberated During Evaporation. As sea water boils and becomes more concentrated, the calcium bicarbonate [$Ca(HCO_3)_2$] breaks down to form calcium carbonate [$CaCO_3$], carbon dioxide [CO_2], and water [H_2O], as follows: $Ca^{++} + 2HCO_3^- \rightarrow CaCO_3\downarrow + CO_2\uparrow + H_2O$. The amount of CO_2 liberated in this manner can be determined by first measuring the amount of $Ca(HCO_3)_2$ in the feed water and residue, correcting the residue measurement by using the feed-residue ratio, and then determining the total change in calcium bicarbonate.

The carbon dioxide liberated during evaporation is directly proportional to the change in calcium bicarbonate content between the feed and the residue corrected to feed concentration. That is,

$$CO_2 \text{ liberated} = \text{change in calcium bicarbonate} \times \frac{\text{Molecular wt. } CO_2}{\text{Molecular wt. } Ca(HCO_3)_2} .$$

The following analysis, performed by E. A. Cadwallader, Office of Saline Water, was made for Reading 36 in Table B-1 of Appendix B for which the condensing temperature is 125.5 F and the feed-to-residue ratio is 1.45/1:

Calcium bicarbonate in feed	0.188 g/liter
Calcium bicarbonate in residue	0.274 g/liter
Calcium bicarbonate in residue corrected to feed concentration	0.190 g/liter

Thus, within the accuracy of the analysis there is effectively no breakdown of the bicarbonate. It can be concluded that the amount of carbon dioxide liberated during evaporation at 125 F is not detectable with the above method.

Dissolved Gas in Sea Water and Efficiency of the Degasser. The efficiency of the packed feed-water degasser was tested with the still operating at a condensing temperature of 130 F and a feed rate of 30 gal/min (15,500 lb/hr) and with the degasser functioning in a normal manner. Samples of feed water upstream of the degasser, of feed water downstream of the degasser, and of the residue were analyzed for dissolved oxygen. The results of the analyses are as follows:

	Analysis, ppm	
	Test 1	Test 2
Dissolved Oxygen in Sea Water	7.0-8.0	7.0-8.0
Dissolved Oxygen in Feed Water Before Entering Degasser	2.04	2.18
Dissolved Oxygen in Feed Water After Leaving Degasser	No trace	No trace
Dissolved Oxygen in Residue	No trace	No trace

The "Nonreferee Method A" procedure described in the 1955 ASTM Standards, Part 7, page 1365, was used for these analyses and is regarded as accurate to the nearest 0.02 ppm. Sea water contains several dissolved gases, the most abundant being oxygen and nitrogen at a total concentration of approximately 20 ppm. Thus, with no degassing the total amount of dissolved oxygen and nitrogen that can enter the system at, for example, a feed rate of 18,000 lb/hr is about 0.35 lb/hr. Assuming the dissolved nitrogen to be released in the same ratio as oxygen, total gas in the feed water is reduced by a factor of at least 350 in the degasser. Thus, the dissolved gas remaining in 18,000 pounds of feed water is only 0.001 pound.

In addition to this analysis, the effect on degassing of varying the amount of steam passing through the degasser, and of varying the operating pressure of the degasser were checked. These changes were found to have no effect on the over-all performance of the still. It can be concluded that the degasser performs efficiently and no unusual control measures are required.

Total Noncondensable Gas. By adding the amount of noncondensable gas that enters the still from the above three sources the following is obtained for the operating conditions of 125 F condensing temperature and a feed rate of 35 gal/min (18,000 lb/hr):

Average air-leak rate	0.45 lb/hr
Dissolved gases in feed water	0.001 lb/hr
Carbon dioxide formation	Nil
	0.451 lb/hr

By combining the noncondensable gas-rate value of 0.45 lb/hr with an average steam flow in the No. 5 still of 5000 lb/hr, the noncondensable gas contamination is found to be $(10^6)(0.45)/5000 = 90$ ppm. This figure of 90 ppm is true only when the noncondensable gas in the system is not allowed to recirculate. As the No. 5 still had a poor purge arrangement, the influence of noncondensable gas is undoubtedly far greater than is indicated by curves shown in Figure 26 of the text.

NOMENCLATURE

A	area within radius r, (πr^2)	ft^2
A_i	area within radius r_i	ft^2
A_o	area within radius r_o	ft^2
A_t	total rotor area	ft^2
B	$\left(\frac{k \pi r_o \Delta T_t}{Q_o \lambda \rho}\right)\left(\frac{2 \pi r_o^5 \omega^2}{3 Q_o \nu}\right)^{1/3}$	--
b	constant	--
C	$\left(\frac{k \delta_m}{r_o k_m}\right)\left(\frac{2 \pi r_o^5 \omega^2}{3 Q_o \nu}\right)^{1/3}$	--
$\overline{C}$	$\left(\frac{3 k_m^4 \Delta T_t \nu}{2 \omega^2 \lambda \rho k^3 \delta_m^4}\right)$	--
$\overline{C}_o$	$\overline{C}$ evaluated at $T = T_o$	--
c_f	final salt concentration	$\frac{\text{lb salt}}{\text{lb solution}}$
c_o	initial salt concentration	$\frac{\text{lb salt}}{\text{lb solution}}$
c_p	specific heat of liquid	$\frac{\text{Btu}}{(\text{lb})(\text{F})}$
Δc	difference in concentration generally between c_f and c_o	$\frac{\text{lb salt}}{\text{lb solution}}$
h_{fg}	enthalpy of evaporation or condensation (λ)	Btu/lb
J	total heat flow through area A	$\frac{\text{Btu}}{\text{hr}}$
K	$\left(\frac{k \delta_m}{r_o k_m}\right)\left(\frac{2 \lambda \rho r_o^4 \omega^2}{3 k \Delta T_t \nu}\right)^{1/4}$	--
k	thermal conductivity of liquid	$\frac{\text{Btu}}{(\text{hr})(\text{ft}^2)(\text{F/ft})}$
k_m	thermal conductivity of metal rotor	$\frac{\text{Btu}}{(\text{hr})(\text{ft}^2)(\text{F/ft})}$
M	weight flow rate at radius r	lb/hr
M_o	total weight flow rate of liquid supplied to rotor	lb/hr
N_{pr}	Prandtl number for liquid $(c_p \mu/k)$	--
P	$\left(\frac{1}{Z} - K\right) W^{1/3}$	--
Q	volume flow rate on evaporating side at radius r	ft^3/hr
$\overline{Q}$	flow rate	ft^3/hr
Q_o	initial volume flow rate	ft^3/hr
q	local heat flux	$Btu/(ft^2)(hr)$
R	$\overline{C}(1 - \overline{\beta})/\overline{\beta}$	--
r	rotor radius	ft
r_i	inner radius of rotor	ft
r_o	outer radius of rotor	ft
ΔT_b	difference in boiling point elevation between c_f and c_o, i.e., Δc	°F
ΔT_c	temperature drop through the condensing film	°F
ΔT_e	temperature drop through the evaporating film	°F
ΔT_m	temperature drop through the metal rotor	°F
ΔT_o	temperature difference based on vapor pressure difference minus the bpe at the initial salt concentration	°F
ΔT_p	over-all temperature difference based on vapor pressure ($\Delta T_t = \Delta T_p$ when fresh water is evaporated)	°F
ΔT_t	total temperature drop	°F
U	average over-all heat-transfer coefficient $U = \left(\frac{\beta Q_o \lambda \rho}{\Delta T_t A_o (1 - \alpha)}\right) = \left(\frac{\overline{\beta} M_o \lambda}{\Delta T_t A_o (1 - \alpha)}\right)$	$\frac{\text{Btu}}{(\text{hr})(\text{ft}^2)(\text{F})}$
U_l	local heat-transfer coefficient	$\frac{\text{Btu}}{(\text{hr})(\text{ft}^2)(\text{F})}$
U_a	assumed value of heat-transfer coefficient	$\frac{\text{Btu}}{(\text{hr})(\text{ft}^2)(\text{F})}$
U_o	over-all heat-transfer coefficient based on T_o rather than T	$\frac{\text{Btu}}{(\text{hr})(\text{ft}^2)(\text{F})}$
V_m	mean radial velocity of film	ft/hr
W	$(X)\left(\frac{k \pi r_o \Delta T_t}{Q_o \lambda \rho}\right)^{3/4}\left(\frac{2 \pi r_o^5 \omega^2}{3 Q_o \nu}\right)^{1/4}$	--
X	$\pi r^2/A_o = A/A_o$	--
Y	$q A_o/Q_o \lambda \rho$	--
$\overline{Y}$	$q \delta_m/k_m \Delta T_t$	--
$\overline{Y}_a$	limiting value of $\overline{Y}$ under specified conditions	--
$\overline{Y}_o$	value of $\overline{Y}$ at rim or rotor	--
Z	$(Y)\left(\frac{k \pi r_o \Delta T_t}{Q_o \lambda \rho}\right)^{-3/4}\left(\frac{2 \pi r_o^5 \omega^2}{3 Q_o \nu}\right)^{-1/4}$	--
α	A_i/A_o	--
β	fraction of liquid volume input that is evaporated for central feed and film condensation	--
β'	fraction of liquid volume input that is evaporated for central feed and dropwise condensation	--
βQ_o	over-all rate of evaporation	ft^3/hr
$\overline{\beta}$	weight fraction of feed liquid which is evaporated	--
γ	$(\alpha)\left(\frac{k \pi r_o \Delta T_t}{Q_o \lambda \rho}\right)^{3/4}\left(\frac{2 \pi r_o^5 \omega^2}{3 \nu Q_o}\right)^{1/4}$	--
$\overline{\gamma}$	about $\left[-\frac{c_o}{\Delta T_o}\left(\frac{\Delta T_b}{\Delta c}\right)\right]$	--
δ_c	thickness of condensing film	ft
δ_e	thickness of evaporating film	ft
δ_m	thickness of metal rotor	ft
λ	enthalpy of evaporation or condensation (h_{fg})	Btu/lb
μ	dynamic viscosity of liquid	lb/(hr)(ft)
ν	kinematic viscosity of liquid (μ/ρ)	ft^2/hr
ξ	$(1 - \overline{Y})^3/R \overline{Y}^4$	--
ρ	density of liquid	lb/ft^3
φ	slope of rotor surface (for flat rotor, $\varphi = 0$)	degrees
ω	angular speed of rotor	radian/hr

APPENDIX B

EXPERIMENTAL DATA, NOTES ON MECHANICAL RELIABILITY, AND A DISCUSSION OF FEED-WATER-JET INTERRUPTION WITH REGARD TO THE NO. 5 STILL

This appendix contains detailed data of selected runs that were made with the No. 5 still. Several of the more important mechanical difficulties encountered with the No. 5 still during the 1-year program are discussed. In addition, the practical problems associated with supplying feed water to the evaporating surface are treated.

Experimental Data Obtained With the No. 5 Still

Tables B-1 and B-2 show recorded data and calculated values, respectively, that were obtained with the No. 5 still.

Evaluation of Modifications of The Feed Distribution System

Table B-3 gives the results of an experimental evaluation of a number of modifications of the feed-distribution system for the No. 5 still. The tests were made at a condensing temperature of 130 F and an effective feed rate of 30 gal/min (14,000 lb/hr). The term "effective feed rate" is used because in several instances the actual feed rate was reduced to compensate for blocked feed nozzles which were used in some of the runs.

Columns 1 and 2 of Table B-3 show the results of two runs that were made with the still essentially as it was assembled when first erected at Harbor Island. The data in Column 1 were taken before acid washing of the rotor surfaces, and may be compared with the data in Column 2 which were taken just after acid washing. The increase in yield shown in Column 2 indicates a slight accumulation of scale or corrosion products on the rotor surfaces. The remainder of the columns in Table B-3 show the results obtained from various design modifications. Data obtained when the circumferential central-feed sparger was evaluated are presented in Columns 3 and 4. These data may be compared with data listed in Columns 1 and 2. Although a minute reduction in collection rate is indicated by the data, this loss is considered to lie within the range of experimental error for the system. Accordingly, it was concluded that the sparger offered no advantage over the nozzle feed system. In Columns 1 through 5, the low collection rate from the No. 6 rotor was found to be attributable to damaged feed nozzles. This was discovered during the changeover from the single- to the double-nozzle feed system. Later, when the single-nozzle feed system was reinstalled, all of the nozzles were checked to insure that they were functioning properly.

Columns 5 and 6 of Table B-3 show the effect of changing from a single-nozzle feed system to a double-nozzle feed system with the still operating at a rotor speed of 306 rpm. The increase in yield resulting from this feed change appeared quite encouraging. However, when the still was operated at 400 rpm, the double-nozzle feed system

actually gave a lower yield than did the single-nozzle feed system. This may be seen if Column 7 is compared with Column 4. As mentioned earlier, the reason for this inversion in characteristics of the double-nozzle feed system with increasing speed has not been determined. It is significant that the double-nozzle feed system shifts the output of the separate rotors so that the upper four rotors produce a higher percentage of the total yield than they do with the single-nozzle feed system. Evidently, this shift is due to the fact that the feed nozzles of the double system are 1/8 inch in diameter for the top four rotors and 7/64 inch in diameter for the lower four rotors, thus partially compensating for the change in liquid head along the rotor feed column. To compensate more thoroughly for the pressure gradient along the feed column, a set of graduated feed nozzles was installed on September 4, 1958. Unfortunately, prior to installation of these nozzles the first model of the distillate sampler was removed from the still. As a result, it was not possible to evaluate each rotor individually. However, the yield of the entire still was found to be about 6 per cent higher when the graduated single-nozzle feed system was used.

Columns 8 and 9 of Table B-3 show the results obtained during identical base-line runs which are used as a reference for the data given in the next four columns. Three modifications are evaluated in Column 10. The first of these, reversing the direction of one of the nozzles for the No. 3 rotor, resulted in no detectable change in collection rate. A second modification consisted of blocking all four nozzles of the No. 5 rotor in order to determine the background flow of the sampling system. Results of the third modification, blocked feed nozzles for the upper half of the No. 7 rotor, should be compared with those obtained with the same rotor for which the lower nozzles were blocked (Column 12). In both cases the yield is more than one-half of the yield with feed supplied simultaneously to both the upper and lower rotor halves, as shown in Column 9. This result verifies that the interchange of water between the rotor halves observed earlier on the No. 4 still also occurs in the No. 5 still. Columns 12 and 13 show the effect of orienting the feed nozzles in a number of different directions as indicated in the modification code.

The first distillate sampler that was used for the above runs was found to be limited to collection rates of about 8.5 cm/min. This collection rate was exceeded by the No. 7 rotor when the over-all output of the still was 5600 pounds of distillate per hour. Thus, it became clear that if the performance of the still were to improve greatly, the collector would be of little use. Theoretical calculations made during the design of a new deep-channel-type collector led to the conclusion that the original sampler may have been collecting not only water from the rotor but also water drops which bounce from the housing wall. The degree, if any, to which the bounce water affected the data is unknown. A new sampler, which was installed prior to the making of the December runs, incorporates splash guards.

Mechanical Reliability of the No. 5 Still

Although no long runs were made with the No. 5 still, some mechanical difficulties were experienced. These are reviewed in this section of the report so that there will be a record of them for consideration in future research.

During the tests conducted to determine the heat loss through the evaporator shell, a muffled knock became noticeable in the upper rotor bearing. Upon examination of the

TABLE B-1. EXPERIMENTAL DATA FOR THE NO. 5 BADGER-HICKMAN STILL

Reading Number	Date	Type of Feed	Barometric Pressure, in. Hg	Liquid Flow, lb/hr			Trim Steam, lb/hr	Pressure Difference, in. H_2O	Temperatures, F																			Power, kw		
										Feed Water							Distillate			Residue										
										Vent Cond.		F/R Exch.	F/D Exch.	Degasser		Evap.	Evap.	F/D Exch.		Evap.	F/R Exch.		Cond.	Wall Temp		Seal			
				Feed	Distillate	Residue			Ambient	In, T-1	Out, T-2	Out, T-3	Out, T-4	In, T-5	Out, T-106	In, T-6	Out, T-107	In, T-7	Out, T-8	Out, T-109	In, T-9	Out, T-10	Temp, T-11	East, T-31	West, T-32	Water, T-34	System	Compressor	Rotor
8, 9	4-10-58	Sea	29.81	14,470	4617	9,850	107.4	5.62	59	59.0	61.0	113.5	108.0	113.0	110.5	112.0	121.5	119.0	74.8	123.5	120.0	67.0	120.5	78	80	102	41.0	26.6	8.8
14, 15	4-12-58	Sea	29.92	9,510	4225	5,285	71.7	7.56	55	59.6	62.0	115.3	116.5	116.3	119.0	117.4	131.2	129.0	76.8	132.8	130.0	73.3	130.2	--	79	116	40.5	28.5	6.8
16, 17	4-12-58	Sea	29.98	13,443	4813	8,630	54.0	7.50	66	59.7	60.2	116.5	115.5	116.2	119.5	118.0	130.7	128.5	74.5	132.0	129.5	70.0	130.0	92	95	118	42.7	29.1	8.2
18, 19	4-12-58	Sea	29.98	13,130	5246	7,880	105.5	9.64	64	60.0	61.2	124.2	125.5	124.8	127.5	126.0	141.3	138.5	78.0	142.0	139.0	72.0	140.0	92	91	119	48.6	34.0	8.7
1, 2	5-23-58	Sea	30.00	14,050	4200	9,850	55.6	4.47	84	79.0	82.0	109.5	109.5	105.5	106.0	104.5	112.7	111.0	83.0	115.3	112.0	89.4	110.5	89	94	105	36.0	23.0	7.6
3, 4	5-23-58	Sea	29.98	15,540	5340	10,200	94.2	7.75	80	81.5	84.2	127.5	117.0	122.2	125.0	124.2	133.2	130.6	88.0	134.2	132.0	96.0	130.0	94	104	120	46.0	31.1	8.9
5	5-23-58	Sea	--	15,480	5440	10,150	--	7.75	--	77.5	83.5	--	--	122.5	125.2	--	--	--	--	--	--	--	130.5	--	--	--	46.0	31.2	8.9
6, 7	5-23-58	Sea	30.00	15,517	5532	9,985	84.7	7.63	75	79.2	83.2	125.3	118.5	122.5	125.0	124.2	133.2	130.3	88.0	134.2	132.0	91.7	130.0	92	93	119	46.2	31.8	8.8
1, 2	5-29-58	Sea	29.96	15,470	5614	9,860	73.4	7.57	82	78.7	81.2	124.0	118.5	122.2	126.0	124.5	133.2	130.0	88.0	134.2	132.0	89.5	130.0	96	96	121	46.0	31.8	8.8
3	5-29-58	Sea	29.96	20,760	5600	15,160	--	7.62	76	76.5	78.0	123.0	119.5	122.0	126.2	124.5	132.5	130.0	86.8	134.2	--	85.5	129.5	92	124	--	48.2	32.0	11.0
1, 2	6-5-58	Sea	30.18	15,515	5165	10,350	92.7	7.75	80	76.0	79.5	123.0	119.5	122.2	126.0	124.0	130.8	130.0	86.8	--	132.0	86.0	130.0	92	116	120	45.1	30.5	9.2
1, 2	6-10-58	Sea	29.97	15,626	4746	10,880	109.3	7.94	84	81.5	85.5	125.2	119.5	123.2	126.0	124.5	131.5	130.8	92.0	--	132.0	93.8	130.5	94	123	121	41.2	30.5	5.5
1, 2	6-16-58	Sea	29.75	15,540	5235	10,300	95.4	7.87	82	83.5	86.0	127.2	117.0	122.7	126.0	125.0	131.0	130.8	90.0	--	132.0	97.2	130.5	98	108	122	43.0	31.8	5.4
1, 2	6-19-58	Sea	29.99	15,420	5140	10,280	72.5	7.87	86	82.6	86.2	125.8	117.5	123.2	126.0	124.5	131.0	130.8	90.0	--	132.0	95.7	130.0	100	109	122	46.0	31.0	8.9
1, 2	6-23-58	Sea	29.71	15,440	5235	10,200	100.7	7.78	68	75.2	78.0	120.8	120.5	121.7	125.5	124.5	131.0	130.2	89.0	--	132.0	85.2	130.0	97	--	120	46.6	31.7	9.2
2, 3	6-23-58	Sea	29.72	15,490	5188	10,300	99.4	7.81	69	74.5	77.6	121.3	121.5	122.0	125.8	125.0	131.0	130.8	91.0	--	132.0	84.5	130.0	97	94	122	46.5	31.8	9.0
1, 2	6-26-58	Sea	30.12	12,730	4530	8,200	47.8	7.75	81	83.5	86.2	125.5	120.6	122.5	126.0	125.6	130.5	130.2	89.5	--	132.0	98.0	130.0	98	105	119	43.3	29.5	8.0
4	6-26-58	Sea	Distillate sampler measurements only				--	--	--	--	--	--	--	--	--	--	--	--	--	--	--	--	--	--	--	--	--	--	--	--
1, 2	6-30-58	Sea	30.20	14,720	5370	9,350	59.5	7.81	85	80.6	84.2	120.0	125.8	122.2	125.8	124.8	125.8	130.8	100.0	--	132.2	88.5	130.8	92	98	122	46.2	31.2	8.4
1	7-2-58	Sea	--	13,710	5060	8,650	--	7.94	--	--	--	--	--	--	--	124.5	--	--	--	--	--	--	131.2	--	--	--	45.8	31.4	8.5
2	7-2-58	Sea	--	14,340	5285	9,050	--	8.00	--	--	--	--	--	--	--	125.0	--	--	--	--	--	--	131.2	--	--	--	48.2	27.5	15.8
3, 4	5-16-58	Sea	30.01	15,570	5120	10,450	105.0	7.75	73	66.0	67.0	121.2	118.5	120.2	126.0	124.5	132.0	130.5	77.8	134.5	132	78.0	130	93	95	118	45.0	30.2	8.9
2, 3	7-10-58	Sea	30.19	15,530	5366	10,160	95.2	7.88	86	84.5	87.2	128.2	116.0	122.2	126.0	124.5	131.0	130.5	91.0	--	132.5	99.0	130.5	97	112	123	45.0	27.5	11.7
4	9-8-58	Sea	29.95	17,960	5625	12,340	125.0	6.69	82	83.8	85.0	125.5	107.5	116.2	121.2	120.0	125.0	126.5	85.1	--	127.5	99.5	125.5	102	106	116.0	43.5	29.0	8.4
29	9-9-58	Sea	30.06	18,020	5586	12,430	124.0	6.75	77	81.7	83.2	123.8	108.0	116.2	121.2	120.0	--	126.0	84.8	126.8	127.5	96.0	125.2	92	92.5	113.5	44.0	28.7	8.5
36	9-10-58	Sea	30.05	18,070	5610	12,460	100.0	6.75	78.5	82.5	83.2	123.5	108.0	116.2	121.8	120.0	--	125.8	84.8	126.8	128.0	96.5	125.5	120+	99	117.0	43.2	28.7	8.4
43	9-11-58	Sea	29.97	18,100	5531	12,570	89.0	6.31	75	78.2	81.0	120.5	111.5	116.8	121.2	120.0	--	125.0	86.5	125.0	126.0	93.2	124.5	94.5	90	114	43.0	28.3	8.6
1	10-14-58	Sea	30.42	18,580	5880	12,700	Est. 118	7.0	72	72.5	74.8	--	--	116.5	121.2	120.0	--	--	--	126.2	--	85.8	125.5	95	92	--	42.0	25.1	10.0
1-A	10-14-58	Sea		18,610	5930	12,680	Est. 118	-	--	--	--	--	--	--	--	--	--	--	--	--	--	--	--	--	--	--	--	-	-	-
2	10-14-58	Sea	30.40	18,380	5860	12,520	118	7.0	75	72.5	75.2	--	--	116.2	121.2	120.0	--	--	--	125.8	--	85.0	125.5	100	94	--	41.2	25.1	10.0
2-A	10-14-58	Sea		18,400	5890	12,510	Est. 110	-	--	-	--	-	--	--	--	--	--	--	--	--	--	--	--	--	--	--	--	--	--	--
3	10-14-58	Sea	30.39	18,300	5860	12,440	99	7.0	75	73.5	76.2	--	--	117.2	121.2	120.0	--	--	--	126.2	--	87.5	125.5	97.5	97.5	--	41.2	25.1	10.0
3-A	10-14-58	Sea		18,550	5920	12,630	Est. 119	-	--	--	--	--	--	--	--	--	--	--	--	--	--	--	--	--	--	--	--	-	--	--
4	10-14-58	Sea	30.38	18,490	5840	12,650	138	7.0	74	73.5	77.2	--	--	117.2	121.2	120.0	--	--	--	127.0	--	87.5	125.5	92.5	102	--	41.2	25.1	10.0
4-A	10-14-58	Sea		18,620	5810	12,810	Est. 131	--	--	--	--	--	--	--	--	--	--	--	--	--	--	--	--	--	--	--	--	--	--	--
5	10-14-58	Sea	30.38	18,565	5825	12,740	124	7.0	73	73.5	76.2	--	--	117.2	121.2	120.0	--	--	--	127.0	--	87.5	125.5	90	113.5	--	41.2	25.1	10.0
6	10-14-58	Sea	--	18,695	5875	12,820	Est. 124	-	-	--	--	--	--	--	--	--	--	--	--	--	--	--	125.5	--	--	--	-	--	--
7	10-14-58	Sea	--	18,940[a]	5620	13,320[a]	Est. 137		-	--	--	--	--	--	--	--	--	--	--	--	--	--	125.5	--	--	--	--	--	--
8	10-14-58	Sea	--	18,750	5610	13,140	Est. 130		-	--	--	--	--	--	--	--	--	--	--	--	--	--	125.5	--	--	--	--	--	--
1	10-17-58	Sea	30.01	18,390	5274	13,120	Est. 146	7.13	75	76.2	80.2	123.2	107.5	118.2	121.2	120.0	--	125.8	85.0	126.5	127.8	89.5	125.5	91	97	--	39.8	23.5	10.0
2	10-17-58	Sea	--	18,400	5230[b]	13,170	Est. 146	--	--	--	--	--	--	--	--	--	--	--	--	--	--	--	--	--	--	--	--	--	--
3	10-17-58	Sea	30.02	18,340	5280	13,100	146	7.06	72	76.2	79.2	122.5	107.5	116.8	120.8	120.0	--	127.0	80.5	126.2	127.5	92	126.0	90	91.5	--	40.0	23.5	10.1
4	10-17-58	Sea	30.03	18,620	5286	13,330	164	7.06	72	76.2	78.5	123.2	107.5	116.5	120.8	120.0	--	127.0	80.0	126.8	127.5	91.2	126.0	90	89.5	--	40.1	24.0	10.3
5	10-17-58	Sea	30.03	18,680	5274	13,400	146	7.06	70	76.2	79.0	122.8	108.5	116.8	120.8	120.0	--	127.0	80.8	127.0	128.0	92.2	126.0	--	89	--	40.1	24.0	10.5
6	10-17-58	Sea	30.03	18,565	5265	13,300	145	7.12	69	76.0	78.5	123.0	108.5	116.8	121.2	119.7	--	127.0	79.8	127.0	128.0	91.8	126.2	90	89	--	40.1	24.0	10.1
1, 2 (Packed degasser)	10-21-58	Sea	29.82	18,740	5460	13,280	90	6.94	65	65.0	67.5	115.5	110.5	115.8	120.0	118.5	--	125.6	77.6	125.8	127.0	76.8	125.5	90	81	--	40.0	23.6	10.1
3, 4 (Both degassers)	10-21-58	Sea	29.79	18,335	5310	13,025	204	6.81	64	66.3	71.0	115.2	112.5	115.5	118.5	116.1	--	--	79.2	125.4	126.0	80.2	125.0	87	79	--	40.0	23.6	10.1

TABLE B-1. (Continued)

Reading Number	Date	Type of Feed	Barometric Pressure, in. Hg	Liquid Flow, lb/hr: Feed	Distillate	Residue	Trim Steam, lb/hr	Pressure Difference, in. H_2O	Temperatures, F: Ambient	Feed Water: Vent Cond. In, T-1	Vent Cond. Out, T-2	F/R Exch. Out, T-3	F/D Exch. Out, T-4	Degasser In, T-5	Degasser Out, T-106	Evap. In, T-6	Distillate: Evap. Out, T-107	F/D Exch. In, T-7	F/D Exch. Out, T-8	Residue: Evap. Out, T-109	F/R Exch. In, T-9	F/R Exch. Out, T-10	Cond. Temp, T-11	Wall Temp: East, T-31	Wall Temp: West, T-32	Seal Water, T-34	Power, kw: System	Compressor	Roto
5, 6 (Flash degasser)	10-21-58	Sea	29.78	18,290	5080	13,210	390	6.50	62	66.2	72.6	113.2	112.5	113.8	115.0	112.2	--	--	82.4	122.6	124.0	80.2	123.5	84	75	--	40.0	21.0	10.2
1, 2 (Packed degasser)	10-24-58	Sea	29.90	18,290	5353	12,940	105	7	77	71.3	73.2	119.2	106.0	116.8	121.2	120.0	--	--	78.5	125.8	127.0	84.0	125.2	110	96	--	39.8	24.0	10.0
3, 4 (No degasser)	10-24-58	Sea	29.86	18,340	5160	13,180	150	7	77	70.8	75.3	116.8	116.0	117.2	116.2	117.0	--	--	85.2	125.8	127.0	83.5	125.2	100	98.5	--	39.8	23.5	10.0
1, 2 (Baffle evaluation)	10-9-58	Sea	29.95	15,920	5550	10,370	101	7.90	80	73.5	77.2	--	--	122.2	125.5	125.0	--	--	--	131.5	--	--	130.5	108	101	120	43.0	29.1	7.6
4, 5 (New nozzle evaluation)	10-9-58	Sea	29.94	18,370	5230	13,140	120	6.75	73	74.2	76.8	--	--	117.2	121.2	120.0	--	--	--	125.5	--	--	125.0	90	94	112	42.0	27.9	8.5
1, 2 (Vains)	10-30-58	Sea	30.22	18,460	5474	12,860	166	6.88	66	66.5	69.2	110.3	112.5	116.3	119.8	118.5	--	--	79.3	126.0	127.0	78.5	125.5	94	95	--	40.8	24.5	9.9
1, 2	12-9-58	Sea	30.16	20,090	4490	15,600	170	5.19	53	57.3	59.3	105	104	106.5	110.0	108	--	114.8	69	115.5	116.5	67	115.2	87	73	96	37.7	21.0	11.0
3, 4	12-9-58	Sea	30.12	20,700	5140	15,560	210	6.91	58	56.8	59.0	113.8	112.5	113.8	118.5	117.2	--	124.8	72.6	125.5	127.0	70.2	125.2	86	86	105	41.3	23.6	11.8
5, 6	12-9-58	Sea	30.16	21,150	5690	15,460	Est. 300	8.75	54	57.4	60.0	122.3	121.5	122.5	127.2	126.0	--	134.8	75.8	135.5	135.8	73	135	84	81	111	45.0	27.2	12.2
7, 8	12-9-58	Sea	30.21	21,370	5840	15,530	Est. 370	10.0	48	56.8	59.2	126.3	127	127.0	131.8	131.0	--	142.0	75.8	142.0	141.8	73.5	140.2	84	79	114	46.7	27.8	12.8
1, 2	12-15-58	Dist	30.28	21,040	5820	15,215	Est. 120	5.03	33	84.0	86.5	112.8	101	107.2	109.0	107.2	--	113.0	88.0	113.8	115.0	96.5	115.0	64	56	88	42.0	24.5	11.2
3, 4	12-15-58	Dist	30.32	22,020	6980	15,045	130	6.94	31	87.0	89.2	121.8	101.5	117.0	120.0	119.0	--	123.8	94.0	125.2	126	100.5	125.5	68	56	97	46.4	28.3	11.9
5	12-15-58	Dist	30.33	22,930	7850	15,080	Est. 140	9.00	29	88.2	90.7	129.8	130	126.2	129.2	128.8	--	135.0	93.2	135	136	102.7	135.2	71.5	58	104	52.1	33.4	12.9
6	12-15-58	Dist	30.35	23,240	8770	14,470	Est. 140	9.25	28	91.7	96.2	129.5	125	128.2	129.5	129.0	--	135.0	100.8	135	135.5	104.7	135.2	72.5	59	--	54.1	36.0	12.4
1, 2	12-17-58	Dist	30.10	22,200	7076	15,120	164	6.62	55	87.8	91.0	120.2	117.5	118.5	121.0	120.0	--	125.5	95	124.2	125.5	95.5	125.0	86	87	109	46.9	29.0	12.0
3	12-17-58	Dist	30.08	23,380	8235	15,140	Est. 185	8.75	51	93.5	96.0	131.8	122	127.8	130.0	129.0	--	135.2	99	135.0	135.2	106.2	135.0	81.5	84	115.5	52.1	33.4	12.5
4, 5	12-17-58	Dist	30.09	23,680	8686	14,990	194	10.19	48	92.0	97.2	136.0	127	132.2	135.0	134.0	--	140.8	100	140.0	140.8	107.8	140.5	84	78	119	55.9	36.5	13.2
6	12-17-58	Dist	30.10	23,970	8970	15,000	Est. 210	11.06	46	97.0	102.5	141.5	132.5	136.2	139.5	139.0	--	144.8	106.0	144.5	144.8	111.8	144.8	84	81.5	122	58.0	38.1	13.4
7	12-17-58	Sea	30.11	21,890	6600	15,290	Est. 260	9.88	46	48.8	50.5	124.8	124.5	124.5	131.5	130.2	--	139.8	70.0	141.0	141.5	65.8	140.0	83	77.5	119	48.0	28.9	13.1
1	12-19-58	Sea	30.09	22,140	6540	15,600	Est. 260	10.00	54	49.0	52.0	127.2	121.5	125.8	131.5	130.2	--	139.8	65.0	141.2	141.2	67.2	140.0	94	85	116	50.2	31.4	13.2

(a) Includes the 280 lb/hr of 5% NaOH solution (14 lb NaOH/hr).
(b) Does not include the 343 lb/hr of NaOH solution (10 lb NaOH/hr).

TABLE B-2. CALCULATED PERFORMANCE DATA

Column No.:	1	2	3	4	5	6	7	8	9	10	11	12	13	14
Date:	7/10/58	5/23/58	4/10/58	5/23/58	4/12/58	4/12/58	4/12/58	5/23/58	5/29/58	6/5/58	6/10/58	10/21/58	10/21/58	10/21/58
Reading Number:	1	1, 2	8, 9	3, 4	18, 19	14, 15	16, 17	3, 4	3	1, 2	1, 2	1, 2	3, 4	5, 6
Condensing Temperature, F	105.0	110.5	120.5	130.0	140.0	130.0	130.0	130.0	129.5	130.0	130.5	125.5	125.0	123.5
Rotor Speed, rpm	400	400	400	400	400	400	400	400	400	400	300	400	400	400
Type of Water	Sea	Sea	Sea	Sea	Sea	Sea	Sea	Sea	Sea	Sea	Sea	Sea	Sea	Sea
Feed, lb/hr	16, 230	14, 050	14, 467	15, 540	13, 130	9, 510	13, 443	15, 540	20, 760	15, 515	15, 626	18, 740	18, 335	18, 290
Residue, lb/hr	12, 520	9, 849	9, 850	10, 200	7, 884	5, 285	8, 630	10, 200	15, 160	10, 350	10, 880	13, 280	13, 025	13, 210
Distillate, lb/hr	3, 710	4, 201	4, 617	5, 340	5, 246	4, 225	4, 813	5, 340	5, 600	5, 165	4, 746	5, 460	5, 310	5, 080
F/D Ratio	4.38	3.35	3.13	2.91	2.51	2.25	2.80	2.91	3.71	3.00	3.30	3.43	3.45	3.60
Trim Steam, lb/hr	80	56	108	94	106	61	54	94	128	93	109	90	204	390
Purge Withdrawal, lb/hr	141	54	42	100	52	46	46	100	117	104	105	118	123	68
Temperature Difference (Corrected for BPE), F	3.74	3.84	3.67	4.08	3.96	3.79	3.88	4.08	4.14	4.12	4.20	4.11	4.09	4.05
Net Coefficient of Heat Transfer, U, Btu/(hr)(ft^2)(F)	1, 600	1, 725	2, 010	2, 050	2, 090	1, 760	1, 950	2, 050	2, 075	1, 970	1, 780	2, 100	2, 070	2, 000
Power, kw														
Rotor	9.7	7.7	8.6	8.9	8.7	6.8	8.2	8.9	11.0	9.2	5.5	10.1	10.1	10.2
Blower	20.5	23.1	26.5	31.0	34.0	28.5	29.1	31.0	32.0	30.3	30.5	23.6	23.6	21.0
System	35.5	36.2	41.0	46.0	48.6	40.5	42.6	46.0	48.2	45.1	41.2	40.0	40.0	40.0
Auxiliaries (By Difference)	5.3	5.4	5.9	6.1	5.9	5.2	5.3	6.1	5.2	5.6	5.2	6.3	6.3	8.8
KW/1000 Gal Distillate	84.0	75.8	77.0	76.0	79.5	82.0	75.7	76.0	75.4	75.5	75.4	64.5	66.3	69.3
Lb Dist/Blower, kw	181.0	182.0	174.5	172.0	154.3	148.2	165.4	172.0	175.0	170.4	155.7	232	225	242

FOR THE NO. 5 BADGER-HICKMAN STILL

15 10/24/58 1, 2	16 10/24/58 3, 4	17 12/9/58 1, 2	18 12/9/58 3, 4	19 12/9/58 5, 6	20 12/9/58 7, 8	21 12/15/58 1, 2	22 12/15/58 3, 4	23 12/15/58 5	24 12/15/58 6	25 12/17/58 1, 2	26 12/17/58 3	27 12/17/58 4, 5	28 12/17/58 6	29 12/17/58 7	30 12/19/58 1
125.2	125.2	115.2	125.2	135	140.2	115.0	125.5	135.2	135.2	125.0	135.0	140.5	144.8	140.0	140.0
400	400	400	400	400	400	400	400	400	400	400	400	400	400	400	400
Sea	Sea	Sea	Sea	Sea	Sea	Fresh	Fresh	Fresh	Fresh	Fresh	Fresh	Fresh	Fresh	Sea	Sea
18, 290	18, 340	20, 090	20, 700	21, 150	21, 370	21, 040	22, 020	22, 930	23, 240	22, 200	23, 380	23, 680	23, 970	21, 890	22, 140
12, 940	13, 180	15, 600	15, 560	15, 460	15, 530	15, 215	15, 045	15, 080	14, 470	15, 120	15, 140	14, 990	15, 000	15, 290	15, 600
5, 353	5, 160	4, 490	5, 140	5, 690	5, 840	5, 820	6, 980	7, 850	8, 770	7, 076	8, 235	8, 686	8, 970	6, 600	6, 540
3.42	3.56	4.48	4.03	3.72	3.66	3.62	3.16	2.92	2.65	3.14	2.84	2.73	2.67	3.32	3.39
105	150	170	210	300	370	120	130	140	140	164	185	194	210	260	260
111	77	105	130	140	143	83.2	105	117	124	112	102	176	194	170	174
4.20	4.21	3.96	4.16	4.18	4.24	4.55	4.88	5.09	5.23	4.70	4.96	5.11	5.06	4.18	4.25
2, 000	1, 940	1, 820	1, 970	2, 170	2, 200	2, 020	2, 240	2, 400	2, 610	2, 350	2, 570	2, 640	2, 780	2, 510	2, 440
10.0	10.0	11.0	11.8	12.2	12.8	11.2	11.9	12.9	12.4	12.0	12.5	13.2	13.4	13.1	13.2
24.0	23.5	21.0	23.6	27.2	27.8	24.5	28.3	33.4	36.0	29.0	33.4	36.5	38.1	28.9	31.4
39.8	39.8	37.7	41.3	45.0	46.7	42.0	46.4	52.1	54.1	46.9	52.1	55.9	58.0	48.0	52.0
5.8	6.3	5.7	5.9	5.6	6.1	6.3	6.2	5.8	5.7	5.9	6.2	6.2	6.5	6.0	7.4
65.4	67.8	74.5	71.0	69.6	70.1	60.0	55.4	55.4	51.4	55.2	52.7	53.6	53.9	64.0	67.1
223	220	214	218	209	210	238	247	235	244	244	246	238	236	228	208

TABLE B-3. EVALUATION OF MODIFICATIONS OF THE FEED-DISTRIBUTION SYSTEM FOR THE NO. 5 BADGER-HICKMAN STILL

Column No.:	1	2	3	4	5	6	7	8	9	10	11	12	13	14	15	16
Date:	5/23	5/23	5/29	6/5	6/10	6/16	6/19	6/23	6/23	6/26	6/26	6/30	7/2	7/9	12/17	12/19
Reading No.:	3,4	6,7	1,2	1,2	1,2	1,2	1,2	1,2	2,3	1,2	4	1,2	1	4	7	1
Condensing Temp, F	130	130	130	130	130.5	130.5	130	130	130	130	130	130.5	131.2	146.4	140	140
Effective Feed Rate, gpm	30	30	30	30	30	30	30	30	30	30	40	30	30	30	42.5	42.5
Distillate, lb/hr	5340	5532	5614	5165	4746	5235	5140	5235	5188	4530	--	5370	5060	7580	6860	6800
Rotor Speed, rpm	400	400	400	400	306	306	400	400	400	400	400	400	400	400	400	400
Rotor Number (Counting From Top)	Distillate Sample Collected, cm/min															
1	4.07[a]	4.21[a]	4.29[a]	4.46[a]	5.10[a]	5.62[e]	5.92[e]	6.35[e]	6.25[e]	6.30[e]	6.51[e]	6.45[e]	6.46[e]	6.64[a]	1.53[o]	1.52[o]
2	6.09[a]	6.22[a]	5.92[b]	5.94[b]	5.93[b]	6.62[e,b]	7.00[e,b]	6.97[e]	7.09[e]	7.24[e]	7.54[e]	7.66[e,j]	7.45[e,j]	-- [a]	1.78[o]	1.71[o]
3	6.42[a]	6.43[a]	6.92[a]	6.49[a]	6.21[a]	6.81[c]	6.76[e]	7.17[e]	6.86[e]	7.09[e,f]	7.27[e,f]	7.15[e,k]	7.09[e,l]	7.15[a]	1.69[o]	1.64[o]
4	7.50[a]	7.86[a]	7.82[a]	7.70[a]	7.80[a]	7.94[e]	7.88[e]	7.98[e]	7.70[e]	8.04[e]	7.84[e]	8.09[e,l]	8.32[e,n]	-- [a]	1.94[o]	1.90[o]
5	7.73[a]	7.82[a]	7.93[c]	7.86[c]	7.96[c]	7.99[e,c]	7.72[e,c]	7.81[e,c]	7.81[e,c]	(0.58)[e,g]	-- [e,g]	8.04[e]	8.05[e,k]	8.33[a]	1.88[o]	2.00[o,p]
6	6.00[a]	6.00[a]	6.20[a]	6.23[a,d]	6.20[a,d]	6.50[e,d]	6.22[e,d]	8.11[e]	8.07[e]	8.14[e,h]	7.98[e,h]	8.04[h,d]	8.38[e,k]	--	2.10[o]	2.10[o,p]
7	8.37[a]	8.50[a]	8.71[a]	8.40[a]	7.78[a]	9.14[e]	8.25[e]	8.19[e]	8.13[e]	5.76[e,i]	6.49[e,i]	6.35[e,m]	(0.76)[e,g]	8.57[a]	1.90[o]	1.89[o]
8	3.05[a]	2.80[a]	2.91[a]	2.37[a]	2.96[a]	3.52[e]	2.46[e]	2.58[e]	2.46[e]	2.68[e]	2.84[e]	2.81[e]	2.33[e]	2.64[a]	--	--
Total (1 through 7)	46.18	47.04	47.80	47.08	46.99	50.62	49.75	52.58	51.91	43.15	--	51.78	46.71	33.33	12.82	12.76

(a) Single nozzle per rotor half, reference feed system.
(b) Circumferential central feed sparger.
(c) One-quarter-inch-diameter purge holes at root of rotor.
(d) One nozzle directed at transition from 30° to 15° slope of rotor surface.
(e) Two nozzles per rotor half.
(f) One nozzle directed with rotation, one nozzle directed against rotation.
(g) All nozzles blocked, no feed supply.
(h) One nozzle directed midway between center and rim.
(i) Nozzles for upper rotor half blocked.
(j) Nozzles for lower rotor half directed against rotation.
(k) Nozzles directed against rotation.
(l) Nozzles for upper rotor half directed against rotation.
(m) Nozzles for lower rotor half blocked.
(n) Nozzles directed radially in.
(o) Graduated feed nozzles.
(p) Twenty-four purge holes at root of rotor.

bearing and housing it was found that the copper bearing sleeve was loose within its housing and also that the bearing proper had been rotating in the sleeve. The copper bearing sleeve was replaced with a modified bronze sleeve. The bronze sleeve was made with an interference fit on the inside diameter and a 0.005-inch increase in outside diameter. The changes caused reduction but not removal of the bearing knock. The above condition exists because the thermal expansion of the dissimilar metals apparently was not taken into consideration in the original design.

At about the same time that the bearing failure occurred, a crack was detected in the central feed column. The source of this trouble was found to be corrosion failure of the ball bearing at the lower end of the feed column; a torsion load consequently was placed on the feed column. Rather than redesign this bearing, it was decided to replace the bearing every 6 months. The bearing is most susceptible to failure during down periods because then it is submerged in water each time the feed system is tested. Accordingly, this bearing evidently would be satisfactory during runs of long duration.

Ruptures occurred in both the shell and the tube sides of the feed-residue heat exchangers. These ruptures are thought to have been caused by water freezing in the exchangers during the unusually cold weather in February, 1958. In an effort to drain the system, all valves were opened prior to the freeze. It was not realized at that time that, because of the manner in which the heat exchangers were mounted, they could be drained completely only by blowing compressed air through the tubes. Still unexplained is the fact that the feed-distillate heat exchanger did not rupture, as it, too, was only partly drained. It is suspected that corrosion may have contributed to the failure of the residue exchanger. Regardless of the exact reason for the rupture, the important point to be made here is that, in future work in northern localities, each component of the system should be so designed that it can be completely drained by gravity.

The compressor seal shown in Figure B-1 failed several times during the experimental program. The first failure led to air leakage and occurred because (1) the water connections to the seal had been reversed during assembly, (2) foreign matter entered the seal (principally rust from the seal-water supply lines), and (3) the lower carbon ring was badly eroded probably as a result of (1) and (2). The seal components were cleaned, the piping was corrected, and the seal was reassembled with new carbon rings. Also later, filters capable of filtering out particles larger than 20 microns in the seal water were installed. Because of the need to continue immediately with the program, the compressor was operated several times before the filters were installed. On July 31, 1958, the compressor seal was again considered to have failed. However, in this instance, the seal was not leaking air but rather was leaking an excessive amount of water into the condensing space: about 1000 lb/hr as compared with the previous rate of less than 400 lb/hr. With the assistance of Dr. T. P. May of the International Nickel Company Test Station, an investigation was conducted to determine the cause of the failure. A detailed description of the results is given below. In general, it may be concluded that the seal should function properly for long periods of time if the seal water is chemically and physically clean. The present procedure is simply to use filtered distillate produced by the still.

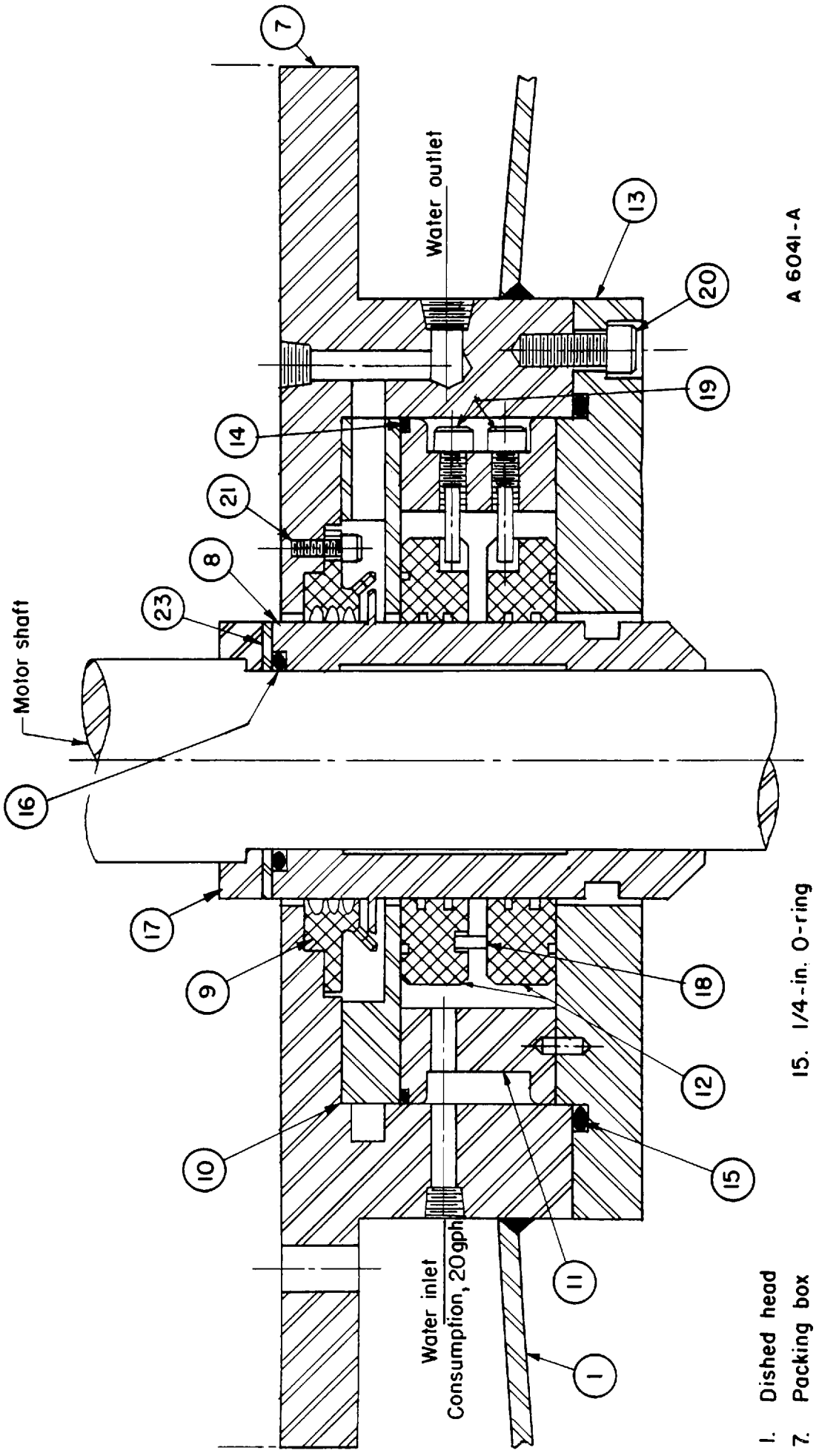

1. Dished head
7. Packing box
8. Shaft sleeve
9. Seal ring
10. Outboard retaining ring
11. Spacer
12. Carbon ring
13. Inboard retaining ring
14. 1/8-in. O-ring
15. 1/4-in. O-ring
16. 3/16-in. O-ring
17. Shaft sleeve retaining ring
18. Spacer spring
19. Carbon ring stops
20. Cap screw 1/2 in. - 13 knurled socket head
21. Cap screw 1/4 in. - 20 knurled socket head
23. Spacer sleeve

FIGURE B-1. ROTATING SEAL FOR THE ELLIOTT COMPRESSOR

Compressor-Seal Maintenance

Figures B-1 and B-2 are reproductions of drawings for the compressor shaft seal and the rotor shaft seal of the No. 5 still. The compressor seal shown in Figure B-1 was disassembled on July 31, 1958, after approximately 70 hours of operation. The following conditions were found:

(1) All exposed surfaces in the seal were covered with a heavy mineral film.

(2) At the point where the outside diameter of the lower carbon ring made contact with the Monel inboard retaining ring, crevice corrosion had developed. This was caused by the electrolytic action between the carbon and the Monel rings in an electrolyte (city water). The wire-drawing effect (a groove caused by high-speed fluid) was found on both the lower face of the bottom carbon ring and its mating surface. No doubt, small particles of dirt helped start the erosion and high-velocity water continued the action.

(3) The motor shaft sleeve and the inside diameter of the lower carbon ring had excessive clearance. The wear on the carbon ring may have been caused by dirt in the seal water.

(4) The outboard retaining ring showed slight effects of crevise corrosion where the outside diameter of the upper carbon ring mated with it. However, in this area denickelification (removal of nickel from the Monel) took place to a depth of 0.010 inch.

(5) The split aluminum seal ring had a noticeable coat of corrosion products on it.

The action taken in response to each of these conditions and the planned corrective measures are listed below. Briefly, the seal parts were either cleaned or replaced and distillate from the still was used as seal water in place of the high-salt-content city water.

(1) The film caused by minerals in the city water was removed by scrubbing with a commercial cleanser. By using distillate for seal water, further formation of mineral film should be eliminated.

(2) Crevice corrosion in this case was caused by two different conducting materials in an electrolyte. This situation caused what is called metal-ion-concentration-cell. For the time being, this cell action will be reduced by replacing the electrolyte (city water) with distillate. For the long run, an effort will be made either to replace the carbon ring with Teflon rings or to protect the Monel with a Hastelloy-C coating. At present the only attempt to reduce the wire-drawing effect will be to continue to use filtered seal water. Also, the possibility of inserting an O-ring in the groove on the face of the carbon rings has been suggested.

(3) Filtered seal water should reduce the wear between the motor shaft sleeve and the inside diameter of the carbon rings.

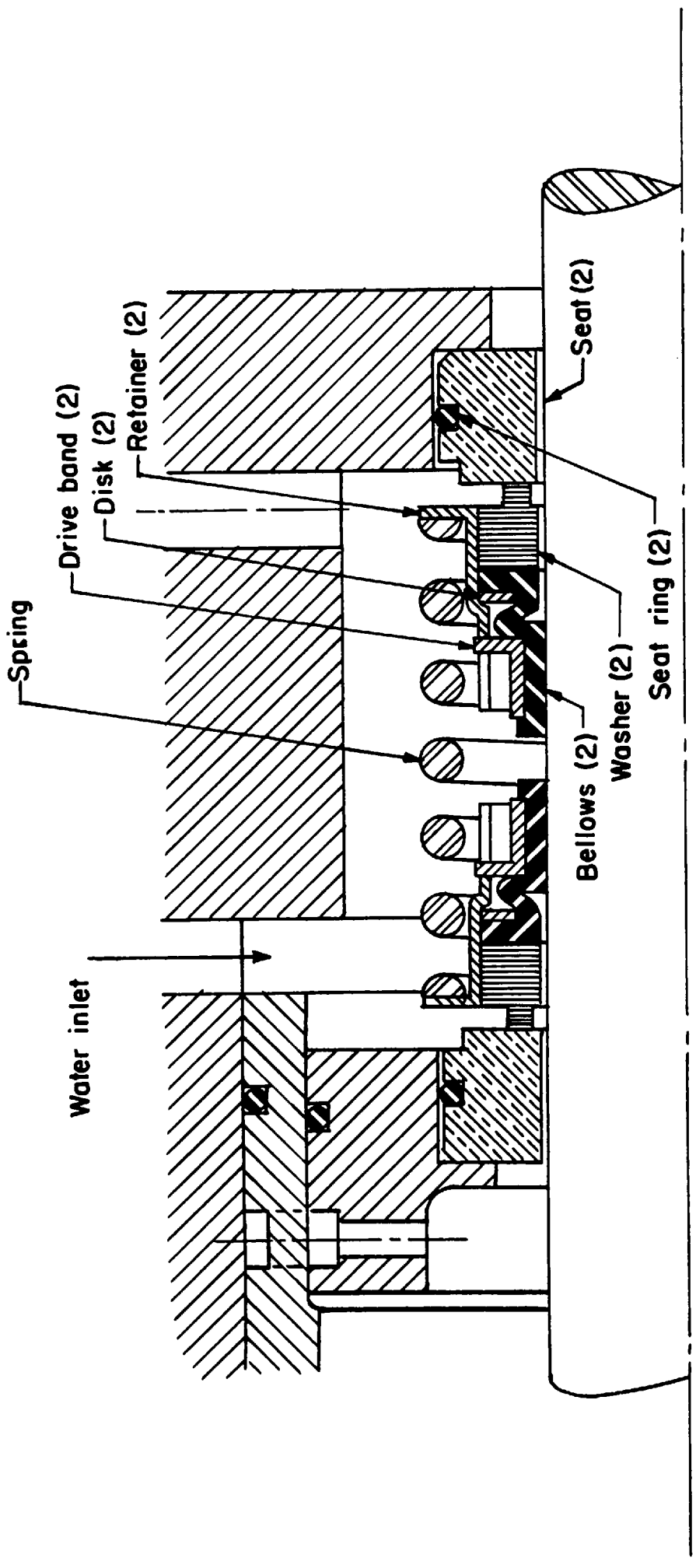

Notes :

Before completing the seal installation, wipe the lapping sealing faces of the seat and washer perfectly clean, then oil both faces with clean light oil

Oil bellows in seal assembly before installing unit

Oil seat ring in seat assembly before installing unit

Circulate one gallon per minute of clear water at 25 psi above the pressure against inboard seal. Inlet at bottom, outlet at top. Cool if necessary to maintain 200 F temp (max)

A 6042-A

FIGURE B-2. "JOHN CRANE" SEAL FOR ROTOR DRIVE SHAFT

(4) Denickelification should be reduced by using distillate in place of city water.

(5) An effort was made to reduce the corrosion on the aluminum seal ring by painting the split ring with two coats of zinc chromate primer.

Figure B-2 shows the rotor drive shaft seal, i. e. , the other rotating vacuum seal on the No. 5 still. For all practical purposes, this seal has given trouble-free service in operation. The one minor difficulty that developed was a water leak past one of the O-rings in the steal housing. This leak was caused by corrosion of the O-ring groove. The use of a corrosion-resistant material for the O-ring seat would eliminate this difficulty.

Interruption of the Feed-Water Jet by the Rotor-Support Cage

In order to meet structural strength requirements, the No. 5 still was built with each copper rotor bolted to a steel cage consisting of eight equispaced spokes. Because of this method of construction, during a single revolution of the rotor, the feed stream is interrupted by each of the eight spokes of the support cage. Previously it had been assumed that the amount of feed water that was prevented from reaching the surface by the spokes was about 6 per cent of the total flow, or the same as the ratio of the circumference of the cage to eight times the spoke diameter. Originally, the feed jets were mounted with an incident angle of about 35 degrees. The incident angle was kept as small as practical so that the feed-water jet would be traveling at a speed and direction comparable to that of the rotation of the rotor surface. The following analysis shows that the amount of water interruption depends on the orientation of the feed nozzles as well as on the speed of the spokes. In the analysis no attempt is made to define the spray pattern resulting from the interruption. The following assumptions are made: (1) the amount of water interrupted is only that which is in the path of the spoke, (2) the direction of motion of the spoke is a straight line (the spokes actually travel in a path of 21. 5-inch radius), and (3) the discharge coefficient of the feed nozzles is unity. The spoke diameter is taken as 1 inch for the calculations.

Figure B-3a shows the method of determining the relative velocity between the spoke and the water jet. The problem may be considered on the basis of a spoke moving at velocity V_{BA} passing through a fixed "wire" of water having the same direction as V_A. As shown in Figure B-3b, in order to minimize the interruption of the feed stream, the enclosed angle between V_{BA} and V_A should be 90 degrees.

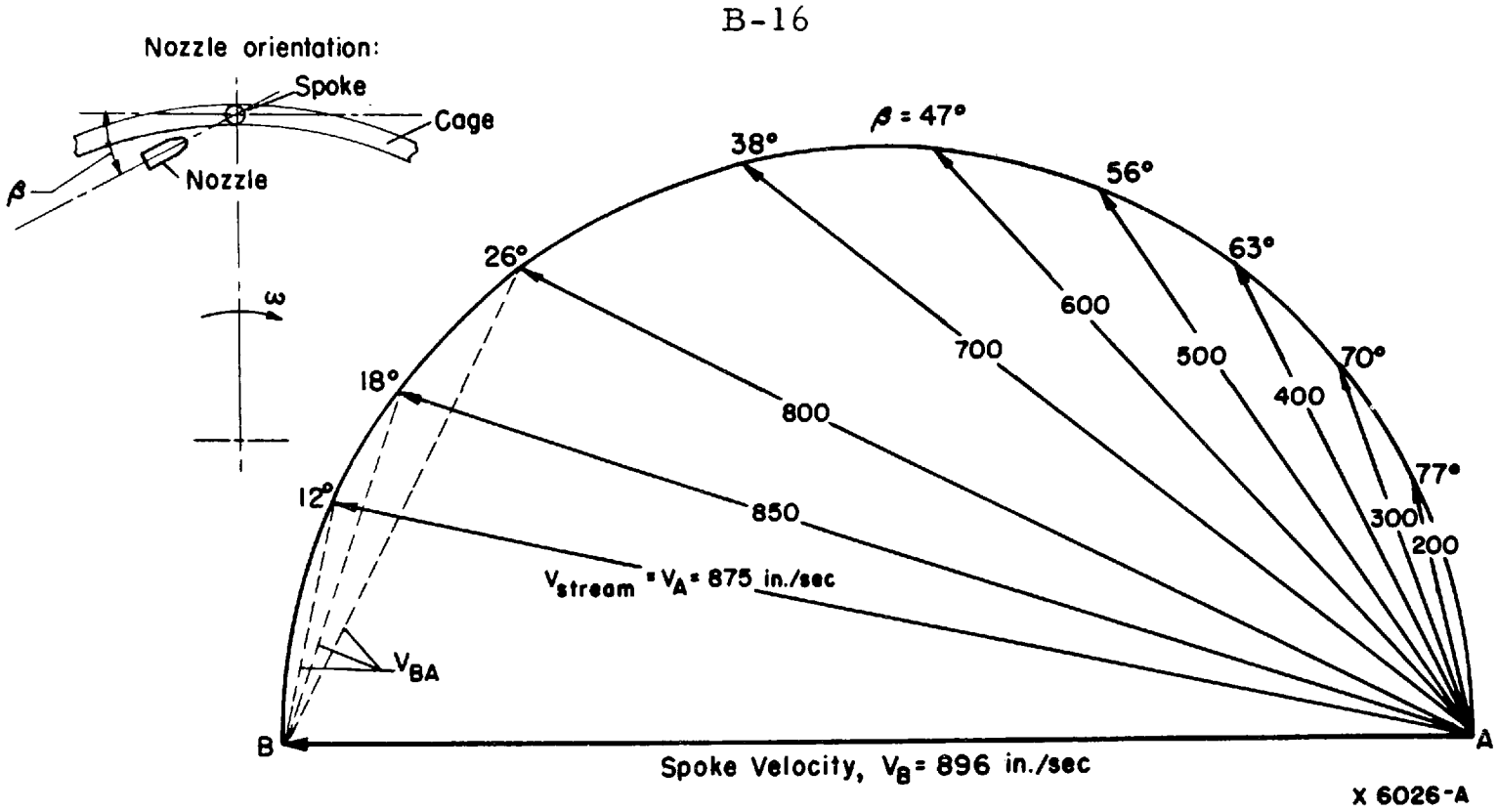

FIGURE B-3. INTERRUPTION OF FEED STREAM BY ROTOR SUPPORT CAGE

Figure B-4 shows a graphical solution for determining the optimum nozzle angle for various jet velocities up to 875 in./sec. Essentially the solution consists of constructing a semicircle on a vector which represents the absolute spoke velocity. Chords, whose lengths represent particular water-jet velocities, are then drawn. Because an enclosed angle in a circle is equal to one-half the enclosed arc, this establishes the angle, β, for which the enclosed angle between V_{BA} and V_A is 90 degrees. A basically similar solution can be made for jet velocities higher than the spoke velocity.

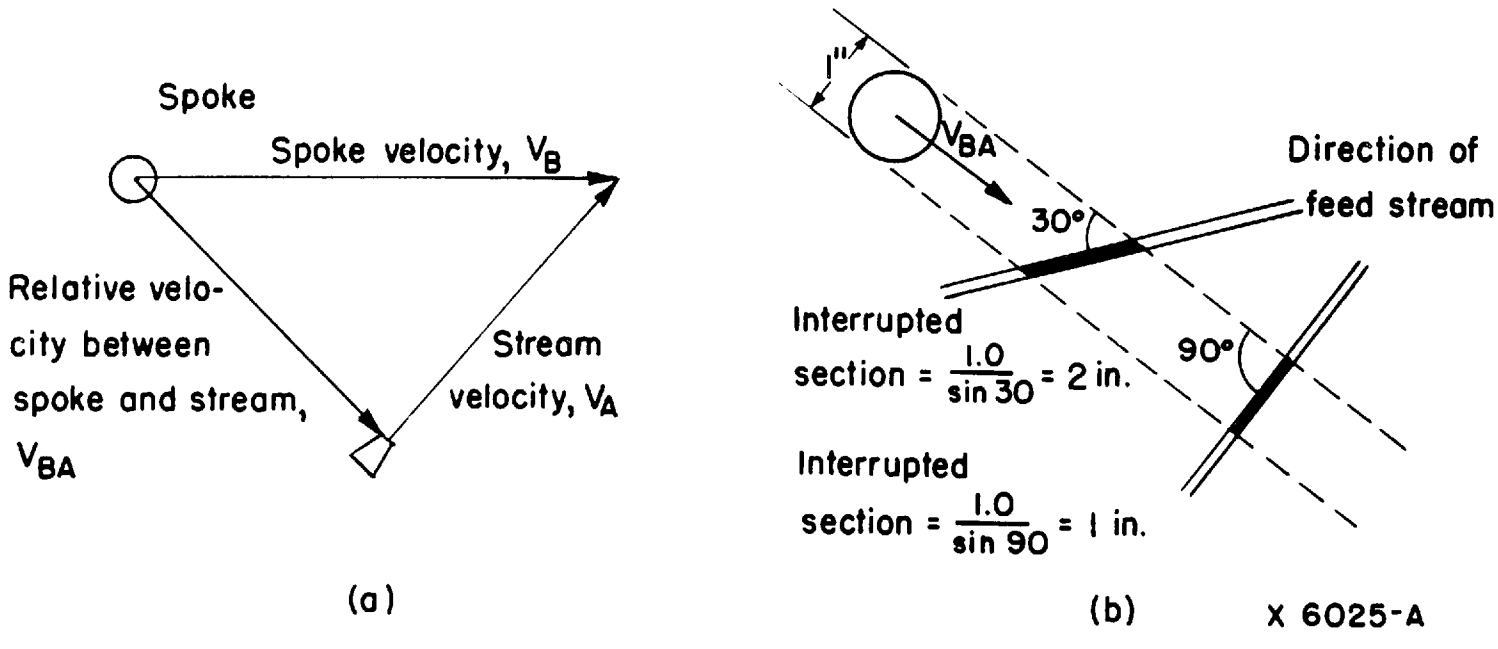

FIGURE B-4. DETERMINATION OF THE OPTIMUM NOZZLE ANGLE, β, FOR THE CONDITION WHEN FEED-JET VELOCITY IS BELOW THE SPOKE VELOCITY

Figure B-5 shows the minimum interruption that results from using nozzle angles as determined by the method of Figure B-4. Thus, it may be seen that for the present feed-stream velocities of 300 to 500 in./sec, the least interruption is about 10 per cent, not the originally assumed 6 per cent. The theoretical interruption for the original feed system where no effort was made to optimize feed nozzle angles ranged from 13.5 to 22 per cent.

Figure B-6 shows photographs of the fifth rotor of the No. 5 still after the 72-hour run. The photographs were taken at 45-degree intervals proceeding clockwise. The light areas represent thin scale deposits. The saw-tooth shape shown in each picture is an unwetted area resulting from interruption of the feed stream by the spokes of the rotor-support cage. The dark regions beginning about halfway out on the upper rotor surface suggest that the feed water detaches from the upper surface. It is believed that the erratic flow patterns, some with and some opposite the direction of rotation, may have been caused by disturbances of the feed water resulting from vibration in the rotor or feed column. The reason for other shades or discoloration is not known.

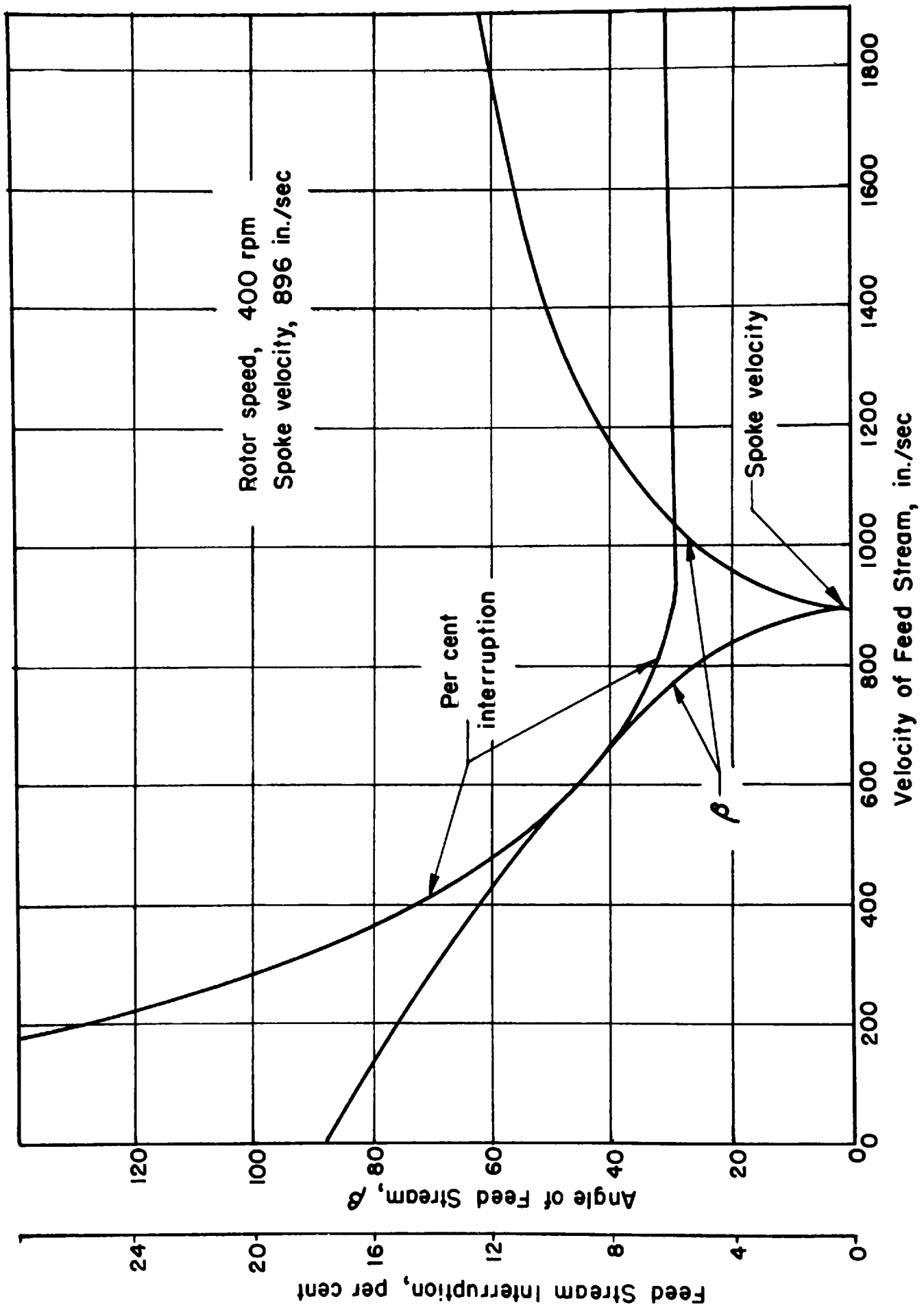

FIGURE B-5. NOZZLE DIRECTION REQUIRED FOR MINIMUM INTERRUPTION

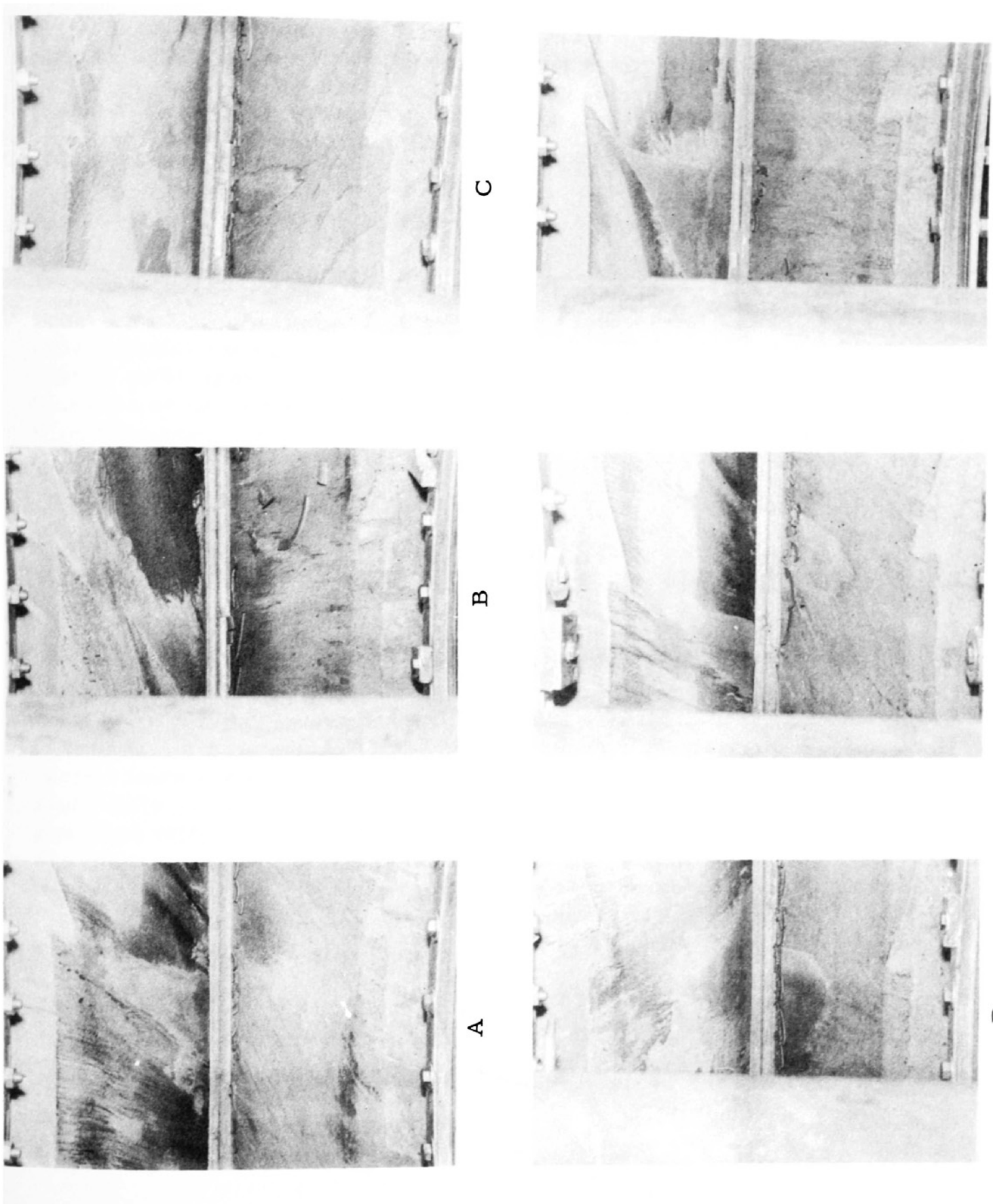

FIGURE B-6. PHOTOGRAPHS OF THE FIFTH ROTOR OF THE NO. 5 BADGER-HICKMAN STILL AT THE CONCLUSION OF THE 72-HOUR RUN

APPENDIX C

COST ANALYSIS OF THE HICKMAN STILL

In determining the operating costs for the Hickman still, it was necessary to select the heat-transfer coefficient and the rotor size and speed, define the energy losses in the system, and select the auxillary components. The reasons for making the various choices and the method of analyzing costs are described in this appendix.

Heat-Transfer Coefficient

A basic heat-transfer coefficient, U, of 3000 Btu/(hr)(ft^2)(F) was assumed for a rotor speed of 400 rpm and an evaporating temperature of 110 F. On the basis of the experimental work, the coefficient was assumed to vary proportionally with the square root of rotor speed and to increase or decrease 5 per cent for each 10 degrees F increase or decrease in evaporating temperature. The relationship between speed and U is discussed in the historical section of this report. Variation in U with changes in evaporating temperature is discussed in the heat-transfer section.

Still Size

The selection of rotors 8 feet in outside diameter and 4 feet in inside diameter was somewhat arbitrary. Optimization of rotor size would require an extensive analysis and was not attempted during this study. The inside diameter should be large, to keep vapor velocities at reasonable levels. The outside diameter should also be large, to maintain a reasonable number of rotors for a given capacity. On the other hand, large rotors require more power to accelerate the water to the rotor tip speed; are more difficult to handle during assembly; are more likely to deform because of pressure differences in the still; and, since they are larger than standard mill sizes, are more expensive to build. In view of the conflicting requirements, the selection of 8-foot-OD by 4-foot-ID rotors seemed to be a reasonable compromise. With rotors of this size mounted on a 1-foot-diameter shaft, critical-speed considerations limit the number of rotors per still to approximately 60 at 400 rpm.

Maximum Permissible Rotor Diameter or Rotor Speed

The equation giving the maximum tangential stress in thin disks of uniform thickness is

$$S_t = \frac{w\omega^2}{8g} \left\{(3 + \sigma)(R_1^2 + 2R_2^2) - (1 + 3\sigma)R_1^2\right\} * \qquad (C\text{-}1)$$

*See, for example, Timoshenko, S., "Theory of Elasticity", First Edition, McGraw-Hill Book Co., Inc., New York, N. Y. (1934).

where

w = specific weight of material, lb/in^3 (w_{Cu} = 0.322)
ω = angular speed, radians/sec
R_1 and R_2 = inner and outer radii, in.
σ = Poisson's ratio (approximately 0.3)

In using this equation to calculate the maximum outside diameter permissible for a given speed, the working or design stress for the rotor material is defined by $S_d = S_y/FS$, where S_y is the yield strength for the material, which in this instance is taken at 45,000 psi, and FS is the factor of safety. According to standard design practice, the factor of safety is composed of the product of a shock factor and the over-all margin of safety desired. These are taken as 1.5 and 2, respectively, for this application. In order to develop a conservative design criterion, an additional multiplying factor of 2 is introduced to account for stress concentrations which may arise as the result of sea-water corrosion. Thus FS = 1.5 x 2 x 2 = 6.

Figure C-1 shows the maximum permissible diameters for rotors as a function of speed using an FS of 6. Each combination of speed and diameter is equivalent to a maximum rim velocity of about 550 ft/sec. The band includes copper and most of the common alloys of copper shown in Figure 30 of the text. Most other materials, such as aluminum or stainless steel, would fall above the band shown for copper because of either their lighter unit weight or higher yield strength. In making the calculations it was found that the allowable outside diameter was insensitive to the internal diameter so that the latter is not included as an additional variable. Also, it should be pointed out that the results are independent of the thickness of the metal.

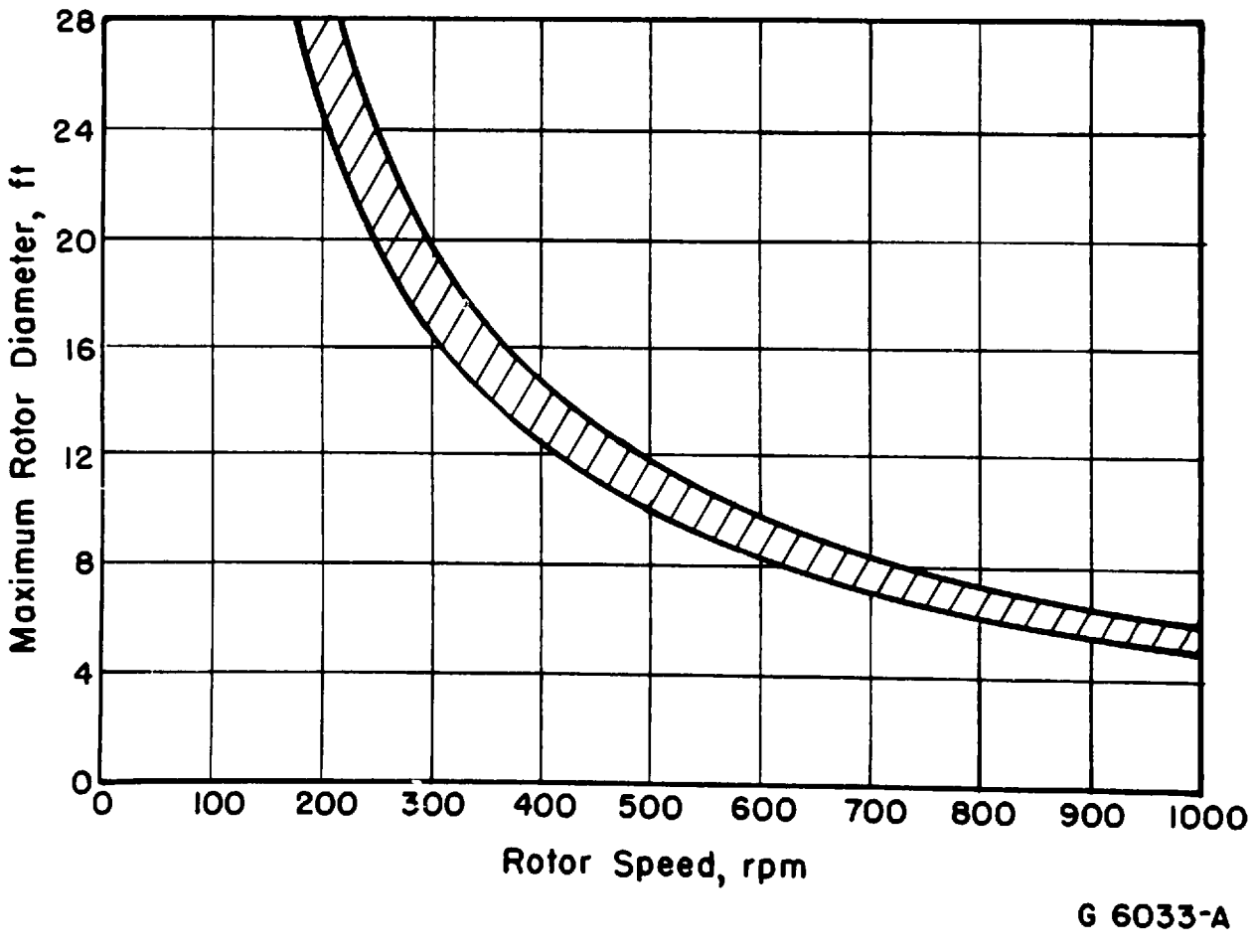

FIGURE C-1. STRESS LIMITS ON ROTOR DIAMETER

Rotor Core

In a multiple-rotor assembly the maximum velocity of the vapor in the core of the rotor assembly occurs at a point nearest the compressor inlet duct. Assuming no other losses in the system, the pressure head, ΔP, required to develop this velocity is approximately

$$\Delta P = \frac{V^2}{10.4gv} = \frac{(Q/A_i)^2}{10.4gv} = \frac{(U)^2(\Delta t)^2(2n)^2(k^2-1)^2(v)}{(135)(10^6)(g)(h_{fg})^2} \text{ inches of water} \qquad (C-2)$$

where

V = velocity of vapor, ft/sec
Q = volume flow of vapor, ft^3/sec
A_i = total opening area, ft^2
U = coefficient of heat transfer, $Btu/(hr)(ft^2)(F)$
Δt = temperature difference, F
n = number of rotors
k = ratio of outside to core diameters, D_o/D_i
v = specific volume of vapor, ft^3/lb
h_{fg} = latent heat of vaporization, Btu/lb

Actually, because of frictional losses, a somewhat higher pressure would be required. However, the additional pressure would be partially compensated by the recovery of the velocity head through diffusion on the downstream side of the orifice. Therefore, the above equation, without correcting coefficients, is considered sufficiently accurate for the following analysis.

Figure C-2 shows the capacity and pressure loss for a range of rotor dimensions and three evaporation temperatures. The two sets of curves are tied together by the product $U\Delta tn$, which with D_o (outside rotor diameter) and k determines a particular capacity. Consider the design of a 100,000 gpd still based on a coefficient of heat transfer of 3000 $Btu/(hr)(ft^2)(F)$ and an effective temperature difference of 4 F. Then, for a 10-foot-diameter rotor, the product $U\Delta tn$ is in the range of 240,000 to 300,000 depending on the value chosen for k. For a U of 3000 and a Δt of 4, the number of rotor pairs required becomes 20 for $k = 5$, and the inside diameter is 2 feet. If $k = 2$, the number of rotor pairs increases to 25 and the internal diameter becomes 5 feet.

The pressure-loss curves place additional restrictions on the over-all dimensions. Assume for instance that the power loss is to be limited to 10 per cent for a still having a 10-ft rotor diameter and operating with $U = 3000$ and $\Delta t = 4$. Pressure drops equivalent to a 10 per cent power loss are indicated on Figure C-2 for three evaporating temperatures. At 130 F evaporating temperature, $k = 3.5$ would be marginally acceptable for a 100,000 gal/day unit, resulting in an internal diameter of 3 ft and 21 rotor pairs. At temperatures below 130 F, k must be progressively decreased to meet the pressure-loss limitation so that, for example, a 5-foot core diameter with 25 rotor pairs would be needed for operation with 90 F evaporating temperature. The rapid enlargement of the core diameter as the evaporation temperature is lowered results from a combination of increasing power requirement per unit pressure rise and increasing specific volume of the vapor.

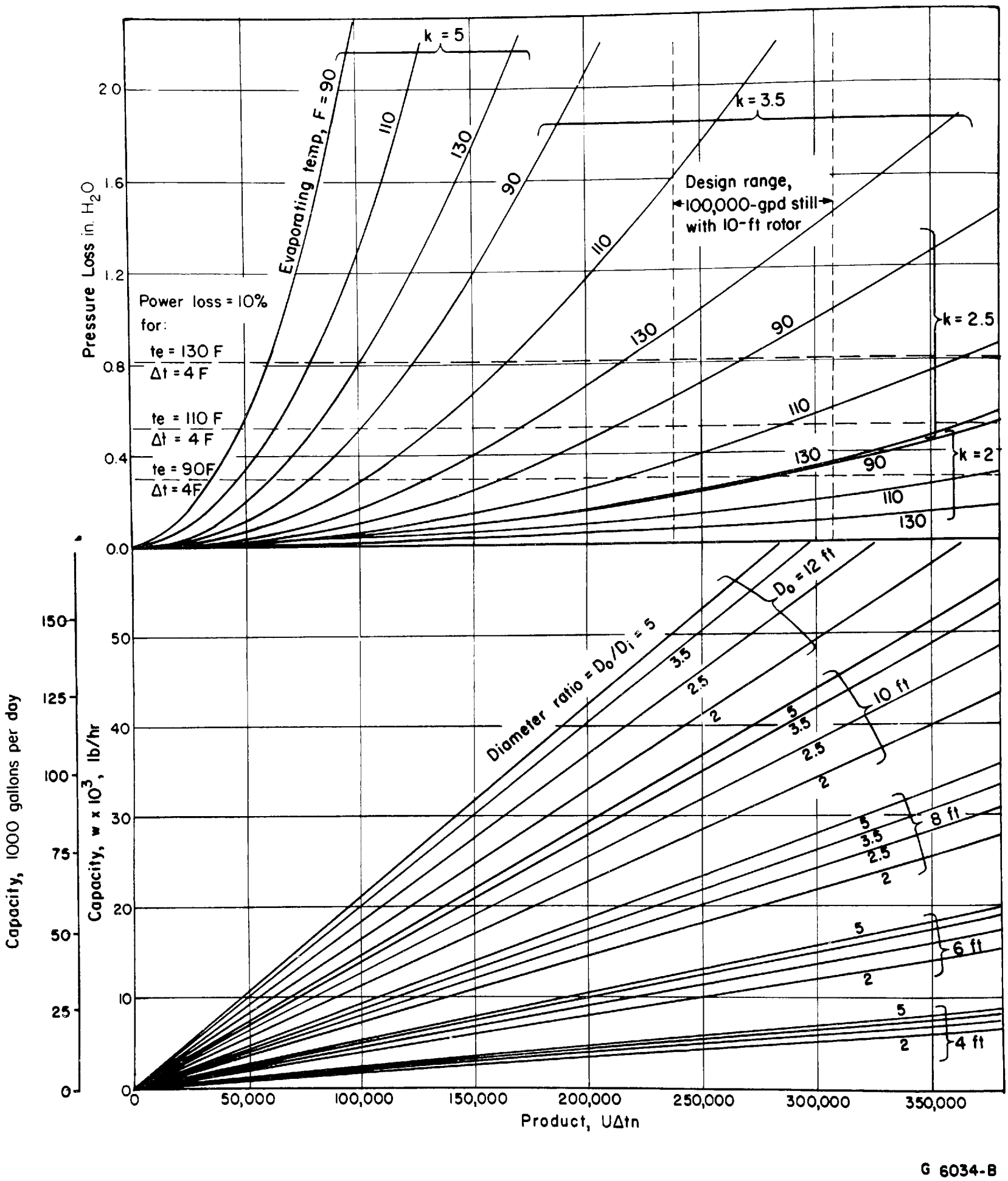

FIGURE C-2. RELATION OF DIMENSIONS OF ROTARY EVAPORATOR TO CAPACITY AND PRESSURE LOSS

For the design conditions of the No. 5 still, $U\Delta tn = 3500 \times 4.2 \times 8 = 117,000$ and $k = 2.3$, for which values the design capacity of 25,000 gallons per day checks in Figure C-2. At a design evaporating temperature of 125 F, the pressure loss is seen to be approximately 0.1 inch of water and remains less than 0.2 inch of water at evaporating temperatures down to 90 F. Thus, the No. 5 unit is sized adequately on this score. For the same pressure loss, a second method would be to graduate the core diameter along the column, that is, reduce the area of successive cores by 1/n times the entrance core area.

Evaporator Cost

Table C-1 lists the cost estimates for the various parts of the sample evaporator which is shown in Figure 20 of the text. These estimates are based on a production of ten units. For large evaporators, the costs of those items, which are influenced by the number of rotors, were modified in proportion to the number of rotors used. The resulting installed cost of the evaporator, without the drive motor, ranged from approximately $18 per square foot of evaporator surface for a 60-rotor evaporator to $23 per square foot for a 20-rotor evaporator.

Blower

The blower was assumed to be an axial flow compressor, with a discharge area equal to the area of the central passage through the rotor column, a limiting tip speed of 1100 feet per second and a blade discharge angle of 25 degrees. The head-versus-capacity characteristics were determined by the method of Stepanoff[7]. An efficiency of 85 per cent based on total head was assumed, and the axial component of discharge velocity was assumed to be lost in friction and turbulence, without any pressure recovery. With these assumptions, the blower was found to operate efficiently under all conditions except in the case of the 100,000-gallons-per-day still operating at 90 F evaporating temperature with apparent temperature differences of 7 degrees F and 8 degrees F. Because of the combination of large capacity and large head under these conditions, the assumed efficiency was reduced 5 per cent and 10 per cent at these two points. This assumption accounts for the sharp increase in cost for the 90 F evaporating condition at the large temperature differences.

Considering the axial velocity head as a loss accounts for the relatively high cost of operating at an evaporating temperature of 90 F. As evaporating temperature is reduced, the specific volume of saturated water vapor increases rapidly. Consequently, the velocity through the rotor column also increases rapidly, with a resultant increase in blower power.

In estimating the cost and power requirements of the blower, it was assumed that the blower would be made of stainless steel and that the drive motor would be 85 per cent efficient. The cost of the blower was taken from the curve for "Fans and Blowers" in the Office of Saline Water standardized cost procedure.[3]

TABLE C-1. COST ESTIMATES OF A 20-ROTOR 8-FOOT-DIAMETER HICKMAN EVAPORATOR

Item	Estimated Cost, dollars				
	Material	Labor	Burden	Total	Tooling
Evaporator Shell					
Bottom support skirt	280.00			280.00	
Bottom Ring	45.00			45.00	
Lugs	14.40			14.40	
Port rim	1.25			1.25	
Fabricate and assemble above parts		57.50	172.50	230.00	
Bottom of evaporator shell	188.00	9.60	28.80	226.40	
Jack screw assembly (three required)	39.33			39.33	
Bearing housing, lower	21.30	3.20	9.60	34.10	150.00
Motor mount	33.90	3.00	9.00	45.90	
Assemble: Bottom, jacks, housing, and mount		57.50	172.50	230.00	
Evaporator shell and fittings	1,340.40	56.00	168.00	1,564.40	
Weld shell to bottom support skirt		76.80	230.40	307.20	
Catwalk (on outside of tank)	64.00	19.20	57.60	140.80	
Ladder assembly	52.00	4.80	14.40	71.20	
Insulation (on outside of tank)	350.00	215.00	430.00	995.00	
Miscellaneous labor		60.00	180.00	240.00	
Subtotal	2,429.58	562.60	1,472.80	4,464.98	150.00
Compressor Housing					
Evaporator cap	870.00				
Rotating seal	500.00				
Subtotal	1,370.00			1,370.00	
Drive System					
Main shaft	788.00	63.00	189.00	1040.00	
Support spider (2)	350.00	4.80	14.40	369.20	400.00
Bottom drive wheel	68.40	7.20	19.60	95.20	400.00
Bottom plate	10.50	1.80	5.40	17.70	
Upper drive wheel	504.00	4.80	14.40	523.20	400.00
Labyrinth seal	75.00			75.00	
Rotor bolts (12)	54.00			54.00	
Rotor clamp rings and spacers (20 sets required)	2,040.00	20.00	60.00	2,120.00	
Assemble and balance rotor		288.00	1,064.00	1,352.00	2,500.00
Seal, lower bearing	9.10			9.10	
Plate, lower bearing	18.80	7.20	21.60	47.60	250.00
Spacer, lower bearing	12.00			12.00	150.00

TABLE C-1. (Continued)

Item	Estimated Cost, dollars				
	Material	Labor	Burden	Total	Tooling
Drive System (Continued)					
Lower bearing, SKF No. 29430	342.00			342.00	
Drive wheel	38.00			38.00	
Assemble lower bearing		75.00	225.00	300.00	700.00
Upper bearing housing cover	15.00			15.00	
Upper bearing housing bottom	11.00			11.00	
Spacer, upper bearing	10.00			10.00	
Spider tubing	6.45			6.45	
Stationary duct	15.20	3.60	10.80	29.60	
Bearing support, upper	8.00			8.00	
Upper bearing housing	20.00			20.00	
Upper bearing SKF No. 22216	35.00			35.00	
Assemble upper bearing housing		220.00	660.00	880.00	500.00
Miscellaneous labor		75.00	225.00	300.00	
Miscellaneous items (bolts, nuts, hangers, etc.)	300.00			300.00	
Subtotal	4,730.45	770.40	2,509.20	8,010.05	5,300.00
Working Surface					
Rotor (20 required)	6,840.00	180.00	540.00	7,560.00	1,200.00
Purge and distillate duct	185.85			185.85	
Feed system	116.00	57.60	172.80	346.40	
Miscellaneous labor		165.00	495.00	660.00	
Subtotal	7,141.85	402.60	1,207.80	8,752.25	1,200.00
Totals	15,671.88	1,735.60	5,189.80	22,597.28	6,650.00
Profit (17 per cent)				3,840.00	
Proportionate share of tooling cost				665.00	
Total cost of each unit, f.o.b. factory				27,102.28	

Heat Exchangers

In determining the cost of the heat exchangers, the economic water velocity through the exchangers was determined for each condition by the method of Drew, Hottel, and McAdams[8]. After the water velocity had been determined, heat-transfer coefficients were calculated. For simplification, heat-exchanger areas were calculated by assuming that the two fluids had equal specific heats, which were obtained by averaging the true specific heats. The heat-exchanger area was selected to provide an economic balance between the cost of the heat exchanger and the cost of trim steam required for make-up heat. For those operating conditions which required no trim heat, the size of the feed-to-distillate heat exchanger was reduced to provide a heat balance. The heat-exchanger material chosen was cupronickel.

Pumps

The feed, residue, and distillate pumps were sized to provide the power required to pump water through the heat exchangers at the required economic velocity and to supply feed water to the feed nozzles at 25 psig. Pump costs were estimated for stainless steel construction. Drive-motor efficiencies were assumed to be 85 per cent and the pumps were assigned an efficiency of 60 per cent.

The vacuum pump was sized to withdraw all of the gas dissolved in the sea-water feed plus a small quantity of air present because of system leaks. Considering a feed-to-distillate ratio of 2.5 to 1, the noncondensable gas pumped from the system was calculated to be equivalent to 60 ppm of the distillate. For a 100,000-gallons-per-day still, the flow rate of noncondensable gas is about 2.1 lb/hr. The required pumping capacity for removing this gas from a pressure of 0.7 psi, assuming an equal weight of steam, is 24 cfm.

Rotor Power

The power to drive the rotating assembly includes the energy necessary (1) to move the water across the rotor surface and bring it to the rotor tip speed, and (2) to overcome the windage and friction losses of the rotor column.

The power required to accelerate the water has been found, both analytically and experimentally, to be equal to MV^2, where M is the mass flow rate of the water and V is the tip speed of the rotor. Analysis indicates that this power is made up of the kinetic energy of the water, $1/2\ MV^2$, and a friction loss due to the water passing over the rotor surface which is also equal to $1/2\ MV^2$. Data from operation of the No. 4 still confirmed the analytical results.

Bearing friction losses were calculated from considerations of the weight of the rotor column and an assumed coefficient of rolling friction of 0.001. At 400 rpm, the power loss for the two shaft bearings was calculated as 0.25 hp for a 20-rotor unit and 0.75 hp for a 60-rotor unit.

Based on manufacturers' data, seal friction losses were calculated as 0.37 hp at 400 rpm, independent of the number of rotors.

The rotor windage loss was calculated by treating the rotor column and the tank wall as flat plates. With this simplification, windage was calculated for 400-rpm operation at 120 F evaporating temperature as 0.6 hp for a 20-rotor column and 1.8 hp for a 60-rotor column. For other temperatures and rotation speeds, windage was assumed to vary directly with the density of the surrounding atmosphere and as the cube of the speed of rotation.

Rotor-drive-motor efficiency was assumed to be 85 per cent.

Energy Balance

To calculate the energy balance for the still, the heat losses were assumed to be:

(1) Heat lost in distillate stream

(2) Heat lost in residue stream

(3) Heat lost to the atmosphere through the walls of the evaporator tank

(4) Heat lost to the atmosphere through the piping outside the evaporator tank

(5) Heat lost in the purge system

The energy added to the still was assumed to include:

(1) The blower work

(2) The pump work

(3) The work added to the water by the rotors, and the windage and friction losses of the rotor column

(4) Make-up heat supplied by trim steam, as required to complete the heat balance.

Feed water was assumed to enter the system at 60 F. Losses in the distillate and residue streams were then defined as the heat content of these streams relative to a 60 F base temperature. The discharge temperatures were determined by the optimization of heat-exchanger sizes.

The heat lost from the evaporator tank was calculated on the basis of experience with the No. 5 still which was approximately the same size as the stills presently considered. Experimental data established this loss in Btu/hr as 710 times (condensing temperature – outside air temperature). Outside air temperature was assumed to be 70 F for the present study.

The heat lost from the piping outside of the evaporator tank was arbitrarily assumed to be 20 per cent of that lost from the tank.

The heat lost in the purge system was assumed to be equal to 0.1 per cent of the heat transferred across the rotor. The energy gained in the system includes heat resulting from all the work done on the fluids by the blower, rotor, and pumps, plus the friction losses of the rotor column. The losses of the various drive motors because of less than 100 per cent efficient operation were not included, since it was assumed that all the motors would be mounted outside the still.

The difference between the heat lost from the system and the heat added to the system was supplied by trim steam, purchased at a price of $.55 per 1,000,000 Btu[3]. For those conditions under which a surplus of heat was shown, such as the low-evaporating-temperature and high-temperature-difference conditions, the size of the feed-to-distillate heat exchanger was reduced to effect a heat balance.

Numerical Example

An example of the method of analysis will be presented based on a 100,000-gallons-per-day still operating at an evaporating temperature of 150 F.

Size of Still

To determine the size of the still, the evaporating area was found from the relationship:

$$J = UA_t \Delta T$$

where

J = total heat flux, Btu/hr
A_t = evaporation area, ft^2
U = over-all heat-transfer coefficient, $Btu/(hr)(ft^2)(F)$
ΔT = actual temperature difference between evaporating and condensing regions of still, degrees F

For this example

$J = (34,700 \text{ lbs/hr})(1008.2 \text{ Btu/lb}) = 34.9 \times 10^6 \text{ Btu/hr}$
$U = 3600 \text{ Btu/(hr)(ft}^2\text{)(F)}$, based on $U = 3000 \text{ Btu/(hr)(ft}^2\text{)(F)}$ at 110 F.

For convenience, the calculated results are tabulated as functions of apparent temperature difference, where apparent temperature difference is the actual temperature difference plus the average boiling-point elevation of the water on the evaporating surface. At 150 F, the average boiling-point elevation with a feed-to-distillate ratio of 2.5 is 0.865 F. For apparent temperature differences of 4, 5, 6, 7, and 8 F, the evaporator area, number of rotors, evaporator cost, and cost of the rotating assembly alone were found to be as follows:

ΔT apparent	4	5	6	7	8
Evaporator area, ft^2	3,100	2,350	1,890	1,600	1,360
No. of rotors	41	31	25	21	18
Evaporator cost, dollars	58,900	47,600	40,700	36,150	32,770
Rotating assembly cost, dollars	45,300	35,850	30,200	26,400	23,600

Heat Exchangers

To select the heat-exchanger size required, the optimum heat-exchanger velocity was determined[8]:

$$G_{opt} = \frac{2n}{(3 - m - n)} \left(\frac{g_c \rho^2 b'}{a' f B_1} \right)^{1/3}$$

where

G_{opt} = optimum mass velocity, $lbs/(hr)(ft^2)$

n = coefficient describing dependence of heat-transfer coefficient on velocity, $h = \alpha G^n$

$n = 0.8$ for forced convection

m = coefficient describing dependence of friction on velocity, $f = a\left(\frac{\mu}{DG}\right)^m$

$m = 0$ for the range of Reynolds numbers of interest

g_c = conversion factor = 4.18×10^8 ft/hr^2

ρ = fluid density, assumed to be 62.4 lbs/ft^3

b' = heat exchanger amortized cost $\$/(ft^2)(hr)$

a' = cost of pumping power delivered to fluid, $\$/(ft)(lb)$

B_1 = ratio of equivalent tube length to actual tube length

f = coefficient of friction = 0.0054

For cupronickel heat exchangers,

$b' = .001115$ $\$/(ft^2)(hr)$ for 100 ft^2 exchanger

$b' = .000428$ $\$/(ft^2)(hr)$ for 1000 ft^2 exchanger

$b' = .000321$ $\$/(ft^2)(hr)$ for 2000 ft^2 exchanger

Assuming 60 per cent pump efficiency and 85 per cent motor efficiency,

$$a' = \frac{0.007}{(.60)(.85)} = 0.0097 \text{ \$/kw hr} = 5.18 \times 10^{-9} \text{ \$/(ft)(lb)}$$

Assuming $B_1 = 1.1$,

G opt = 2.83×10^6 lb/(hr)(ft^2) for 100 ft^2 exchanger

= 2.06×10^6 lb/(hr)(ft^2) for 1000 ft^2 exchanger

= 1.58×10^6 lb/(hr)(ft^2) for 2000 ft^2 exchanger

Optimum velocity,

V opt = 12.6 ft/sec for 100 ft^2 exchanger

= 9.2 ft/sec for 1000 ft^2 exchanger

= 8.3 ft/sec for 2000 ft^2 exchanger

Assuming 1-inch-diameter heat-exchanger tubes with 0.049-inch wall thickness, equal velocity for both fluids and, for simplification, equal temperature changes for both fluids, a trial and error solution indicated that the minimum combined cost of the heat exchanger and trim steam for the feed-to-distillate exchanger occurred with a heat exchanger area of 408 ft^2, costing $10,100. The optimum water velocity was 10.5 ft/sec.

The heating-side coefficient was found from:

$$\frac{hD}{k} = .023 \left(\frac{\rho V D}{\mu}\right)^{0.8} \left(\frac{3600\,\mu c_p}{k}\right)^{0.4} = 2050 ,$$

and the cooling-side coefficient from

$$\frac{hD}{k} = .023 \left(\frac{\rho V D}{\mu}\right)^{0.8} \left(\frac{3600\,\mu c_p}{k}\right)^{0.3} = 1900 ,$$

where

h = heat-transfer coefficient Btu/hr ft^2 F
D = tube diameter, ft
k = fluid thermal conductivity, Btu/hr ft F
μ = viscosity, lb/ft sec
c_p = specific heat, Btu/lb F.

With a metal conductivity of 312 Btu/(hr)(ft^2)(F)/in., the tube conductivity = 6370 Btu/(hr)(ft^2)(F).

The over-all coefficient $U = \dfrac{1}{\frac{1}{2050} + \frac{1}{1900} + \frac{1}{6370}} = 845$ Btu/(hr)(ft^2)(F).

Heat transfer in the exchanger,

$$J = U A_t \overline{\Delta T_m}$$

where $\overline{\Delta T_m}$ = mean fluid temperature difference.

The selection of heat-exchanger size was then accomplished by comparing total costs for the heat exchanger and make-up heat to bring the water to any given temperature, as in the following tabulation. Assume that feed water enters at 60 F and distillate at 149.1 F.

Heat-exchanger effectiveness	0.92	0.91	0.90
Fluid temperature change, F	82.0	81.1	80.2
$\overline{\Delta T_m}$, F	7.1	8.0	8.9
J, Btu/1000 gallons of distillate	669,000	662,000	654,000
Area required for 1000 gallons of distillate per hour, ft^2	111	98	87
Area required for 100,000 gallons per day, ft^2	462	408	362
Heat-exchanger cost, dollars	10,950	10,100	9,500
Heat-exchanger cost per 1000 gallons of distillate, dollars	0.0664	0.0612	0.0576
Make-up heat to 150 F, Btu/1000 gal	64,100	71,100	78,400
Make-up heat cost per 1000 gal, dollars	0.0352	0.0391	0.0431
Total, heat-exchanger cost plus make-up heat, dollars	0.1016	0.1003	0.1007

Therefore, the economical heat-exchanger size is that which results in the lowest total cost (408 ft^2 in this example). Similarly, the feed-residue heat exchanger was found to require 644 ft^2 and to cost $13.100.

Blower

The blower power required is that to produce the static head and the velocity head. The static head is defined as:

$$H_s = \frac{\gamma}{\gamma - 1} P_1 v_1 \left[\left(\frac{P_2}{P_1} \right)^{\frac{\gamma - 1}{\gamma}} - 1 \right]$$

where

γ = ratio of specific heats
P_1 = supply pressure, lb/ft^2
P_2 = discharge pressure, lb/ft^2
v_1 = inlet specific volume, ft^3/lb

The axial discharge velocity was determined by the discharge volume flow and the discharge area. The velocity head is then defined as:

$$H_v = \frac{Va^2}{2g} ,$$

where

Va = velocity in axial direction, ft/sec
g = 32.2 ft/sec^2.

The blower-motor power required is:

$$HP = \frac{(H_s + H_v)\,\dot{w}}{60 \times 33{,}000 \times \text{blower efficiency} \times \text{motor efficiency}} ,$$

where

$\dot{w}$ = flow rate, lb/hour.

The head, power, blower cost, and power cost are summarized in the following tabulation:

ΔT apparent	4	5	6	7	8
Static head, ft	5,130	6,400	7,700	8,960	10,280
Axial velocity, ft/sec	68	67	65	64	62
Velocity head, ft	72	70	66	64	60
Blower-motor power, hp	126	157	189	218	250
Blower cost, dollars	16,500	19,200	22,400	24,300	27,000
Blower power cost, $/1000 gallons	0.158	0.197	0.236	0.274	0.314

Rotor Drive

The rotor-drive-motor size was determined by the power required to accelerate the water and the windage and friction losses. The power required to accelerate 250,000 gallons per day of feed water to the tip speed of the 8-foot rotor is 38 hp. The windage and friction losses are relatively small, approximately 1.5 to 3.5 hp. With 85 per cent motor efficiency, the motor input power required is just under 50 hp. A 50-hp motor costs $2900.

Pumps

The power required to pump fluid through the heat exchangers was found from Reference 8, which expresses the pumping power cost for the optimum exchanger size as:

$$X_c = \frac{n}{3 - m - n} \; X_{fc} ,$$

where

X_c = pumping-power cost
X_{fc} = heat-exchanger fixed charges
m and n = coefficients used in determining heat-exchanger optimum velocity.

This power cost is divided between three pumps for the feed, distillate, and residue. An additional 2.5 hp was provided in the feed pump to produce the head required for the rotor feed system. The pumps for this example then cost approximately $7000, including $800 for the vacuum pump.

Degasser

The degasser cost was obtained from a vendor's estimate.

Energy Balance

After the heat-exchanger operating temperatures, the blower power, the rotor power, and the pump power had been determined, an energy balance was made which showed that trim steam requirements ranged from 332 lb/hr at 4 degrees F apparent temperature difference to 60 lb/hr at 8 degrees F apparent temperature difference.

The heat-exchanger analysis showed that both the distillate and residue were discharged at 68.1 F. The system heat losses in Btu/hr can then be summarized as follows:

Heat lost in residue,	392,000
Heat lost in distillate	281,000
Tank wall losses	56,800
Piping and miscellaneous losses	11,400
Purge loss	35,000
Total heat losses	776,200

The heat added to the system as a result of work performed by the rotor, pumps, and blower, and the heat required in the form of trim steam, were as follows:

Apparent ΔT	4	5	6	7	8
Blower heat added, Btu/hr	273,000	340,000	409,000	472,000	541,000
Pump heat added, Btu/hr	75,000	75,000	75,000	75,000	75,000
Rotor heat added, Btu/hr	106,000	104,000	103,000	102,000	100,000
Subtotal	454,000	519,000	587,000	649,000	716,000
Trim heat required, Btu/hr	322,000	257,000	189,000	127,000	60,000
Trim steam rate, lb/hr	322	257	189	127	60
Trim steam cost, $/1000 gal	0.042	0.034	0.025	0.017	0.008

The total operating costs were then determined by the standard OSW procedure[3], as summarized in Table C-2.

TABLE C-2. SUMMARY OF OPERATING COSTS (DOLLARS) FOR 100,000-GALLONS-PER-DAY HICKMAN STILL[a]

	Apparent ΔT				
	4	5	6	7	8
Capital Costs					
Essential Plant Costs					
(1) Special Equipment					
Evaporator	58,900	47,600	40,700	36,150	32,770
Degasser	1,000	1,000	1,000	1,000	1,000
(2) Standard Equipment					
Heat exchanger	23,200	23,200	23,200	23,200	23,200
Blower	16,500	19,200	22,400	24,300	27,000
Rotor drive motor	2,900	2,900	2,900	2,900	2,900
Pumps	7,000	7,000	7,000	7,000	7,000
Total PIE	109,500	100,900	97,200	94,550	93,870
(3) Erection and Assembly	32,850	30,270	29,160	28,360	28,160
(4) Instruments	4,380	4,040	3,890	3,780	3,750
Total Essential Plant Costs	146,730	135,210	130,250	126,690	125,780
Other Plant Costs					
(5) Raw-Water Supply	1,250	1,250	1,250	1,250	1,250
(6) Product Water Storage	1,000	1,000	1,000	1,000	1,000
(7) Service Facilities	--	--	--	--	--
(8) Contingencies	14,900	13,750	13,250	12,890	12,800
(9) Engineering	16,390	15,120	14,580	14,180	14,080
(10) Interest	7,210	6,650	6,410	6,240	6,200
(11) Site	300	300	300	300	300
Total Plant Investment	187,780	173,280	167,040	162,550	161,410
Working Capital	8,550	7,960	6,710	7,640	7,680
Total Capital Costs	196,330	181,240	173,750	170,190	169,090
Capital Cost per gallon per day	1.96	1.81	1.74	1.70	1.69
Operating Costs – dollars per stream day					
Essential Operating Costs					
(1) Fuel	--	--	--	--	--
(2) Electric Power					
Blower	15.80	19.70	23.60	27.40	31.40
Other	11.20	11.10	11.00	11.00	10.90
(3) Steam	4.20	3.40	2.50	1.70	0.80
(4) Other raw materials	--	--	--	--	--
(5) Supplies and Maintenance Material	2.81	2.60	2.50	2.44	2.42
(6) Operating Labor	10.96	10.22	9.90	9.83	9.90
(7) Maintenance Labor	2.81	2.60	2.50	2.44	2.42
(8) Payroll Extras	2.07	1.92	1.86	1.84	1.85
Total Essential Operating Costs	49.85	51.54	53.86	56.65	59.69
Other Operating Costs					
(9) General and Administration Overhead	4.75	4.41	4.28	4.23	4.25
(10) Amortization					
20-year-life items	24.90	25.30	25.80	26.40	27.20
5-year-life items	51.10	40.50	34.10	29.80	26.70
(11) Taxes and Insurance	11.25	10.40	10.00	9.75	9.69
(12) Interest on working capital	1.03	0.95	0.92	0.92	0.92
Total Operating Costs for One Stream Day	142.88	133.10	128.96	127.75	128.45
Cost per 1000 Gallons of Product Water	1.43	1.33	1.29	1.28	1.28

(a) Evaporating temperature = 150 F
Feed-to-distillate ratio = 2.5
Rotor speed = 400 rpm
Rotor diameter = 8 feet
U = 3600 Btu/(hr)(ft^2)(F).

Alternative Blower Drives

Costs included in the present study were based on utilization of an electric motor-driven compressor. Two other drive systems were considered, steam-turbine and diesel-engine drive.

With electric power purchased at $0.007 per kw-hr, and an assumed motor efficiency of 85 per cent, shaft power for an electric motor costs $0.00615 per hp-hr.

A diesel engine with a specific fuel consumption of 0.4 pound per hp-hr, using fuel purchased in large quantities at about $0.11 per gallon, produces power at a fuel cost of $0.0063 per hp-hr.

A steam turbine with a steam rate of 15 pounds per hp-hr, using steam purchased at $0.55 per 1000 pounds, has a steam cost of $0.00825 per hp-hr. In maximum sizes of Hickman stills, the steam rate may decrease to about 11 pounds per hp-hr, resulting in a steam cost of $0.00605 per hp-hr.

If product water from the still must be used as boiler feed water to produce steam, the steam-turbine drive appears less attractive. The quantity of steam required is approximately 10 per cent of the output of the still, so that the net cost of the product water would increase approximately 10 per cent. However, part of this increase could be offset by a reduction in heat-exchanger size.

Equipment costs for an electric motor, a steam turbine, and a diesel engine of the same power are roughly the same in the power range of interest. Since the energy costs appear to be very nearly the same, the choice of driver can be made on the basis of reliability, size, weight, or convenience, in which case the electric-motor drive appears to be the best choice. In a given installation, the cost of steam, diesel fuel, or electric power may be different from the values used in this comparison; accordingly, a different choice may be indicated.

Various System Arrangements for Utilizing the Hickman Principle

A rotating heat-transfer surface has two important advantages: (1) it gives high evaporation-condensation heat-transfer coefficients, and (2) the high heat-transfer coefficients are obtainable while operating with relatively low temperature differences. Thus, any evaporation – condensation process which may benefit from these two features is a potential application of the Hickman principle.

Vapor Compression

Figure C-3a shows a simplified sketch of the familiar single-effect vapor-compression still which uses an electrically driven compressor. With such a unit it is possible to produce at least 100,000 gallons of water per day per "can". The cost comparison figures presented in Figure 21 of the text are based upon a unit of this size. It is encouraging to note that this is in the capacity range that Koerig[9] shows to be promising for sea-water conversion in comparison with natural water sources.

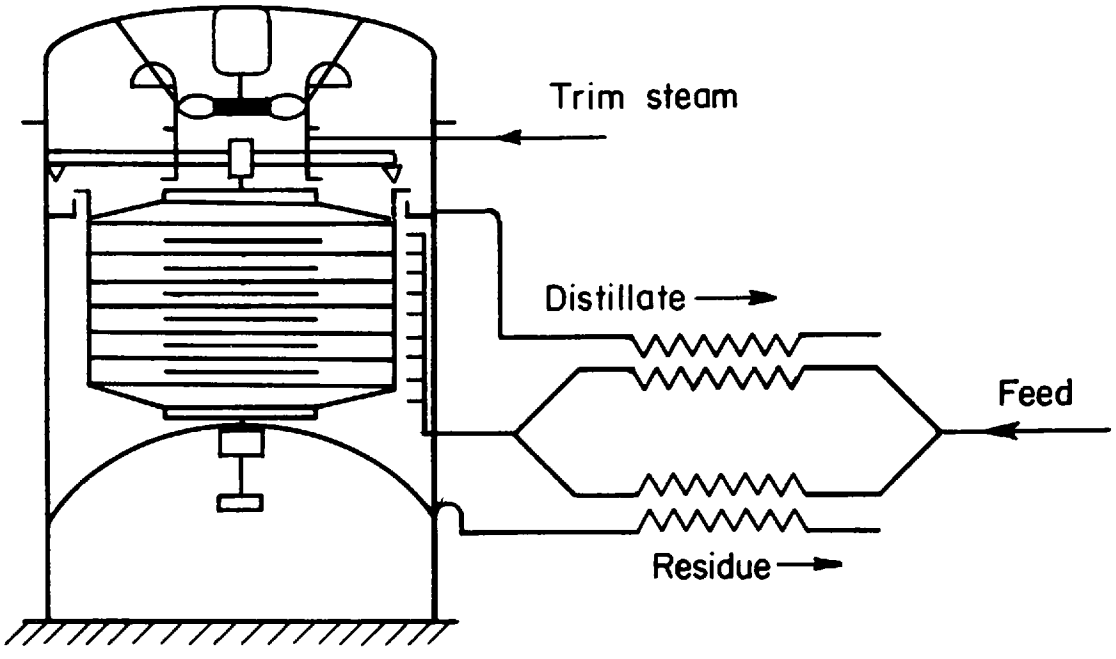

a. Single-Effect Vapor-Compression Hickman Still

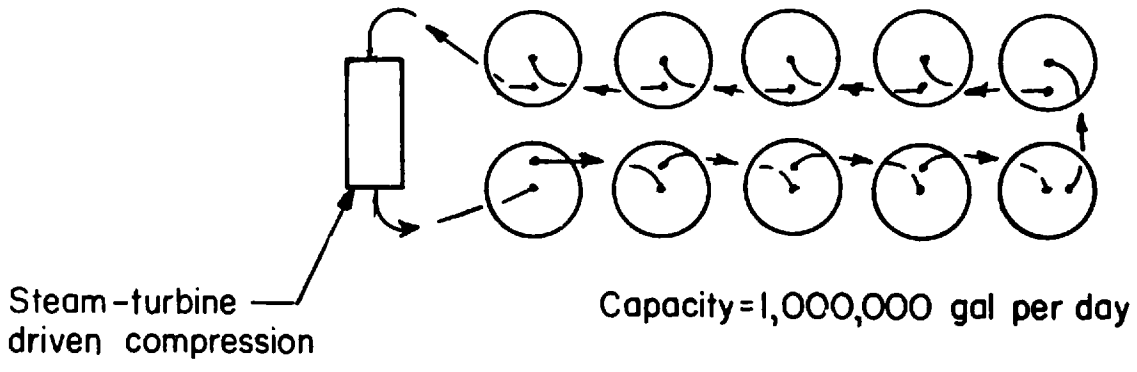

b. 10-Stage Multiple-Effect Vapor-Compression Hickman Still A-34336

FIGURE C-3. POSSIBLE USES FOR THE HICKMAN PRINCIPLE

Multiple-Effect Vapor Compression

Although, for structural reasons, the Hickman principle is presently best suited for applications which involve a relatively small pressure difference between the evaporating and condensing sides, this does not mean that the use of rotating heat-transfer surfaces is restricted to the vapor-compression cycle. The Hickman principle is readily adaptable to a multiple-effect cycle or to a combination multiple-effect vapor-compression cycle. This may be done simply by replacing the compressor with a steam duct from the next highest effect. The evaporator section of each effect would be the same as shown in Figure C-3a.

Figure C-3b shows a schematic of a ten-stage multiple-effect vapor-compression still which utilizes a turbine-driven compressor. This cycle has been mentioned here only for the purpose of illustrating the versatility of the Hickman principle. With such a cycle it may be possible to produce between 20 and 30 pounds of water per pound of high-pressure steam. The average capacity of each "can" again would be about 100,000 gallons per day. Thus, a bank of ten cans, connected to a single compressor would constitute a 1-million-gallons-per-day plant.

The next logical refinement, from a thermodynamic point of view, would be that of replacing the feed-residue heat exchangers, not shown in Figure C-3b, with multi-flash distillation units. The economic desirability of combining the three common distillation cycles into a single system is, of course, a matter for detailed study.

☆ U. S. GOVERNMENT PRINTING OFFICE : 1963 O - 705-370